Vol. 12 2019 No. 01

GEOGRAPHY ENVIRONMENT SUSTAINABILITY

EDITORIAL BOARD

CONTENTS

CONTENTS

Gleb E. Glazirin[1] and Eleonora R. Semakova[2*]
[1] Faculty of Geography, National University of Uzbekistan, Tashkent, Uzbekistan
[2] Department of Applied Space Technologies, Ulugh Beg Astronomical Institute, Tashkent, Uzbekistan
***Corresponding author:** ella9sem@gmail.com

ESTIMATION OF DISPERSED GLACIATION SHRINKAGE UNDER CLIMATE CHANGE

ABSTRACT. We propose a new method of estimating the shrinkage of glaciers over a wide area under conditions of changed climate. The method can be also used to quantitatively estimate the presence of glaciers under past climatic conditions, in mountainous areas where they are currently absent. The method is based on the use of statistical parameters of the distribution of glaciers by altitude zones, according to vertical distance from the climatic equilibrium line altitude (CELA). The method was used for the Pskem River basin (tributary of the Chirchik River, Western Tien-Shan) where glaciation has been extensively studied. Data are available for several glacier inventories for the basin for different time periods from 1957 to 2010. The number of glaciers for the part of the basin considered in the studies decreased by 16 percent during that period. Mean summer air temperature and annual precipitation were used as climate indicators characterizing ablation and accumulation on glaciers. Data of several meteorological stations located in the Pskem River basin were used to document these climatic characteristics. We estimated shrinkage of glaciers over the area for increases of summer air temperature of 0.5 - 2°C.

KEY WORDS: glaciers distribution, glaciation shrinkage, climate change

CITATION: Gleb E. Glazirin, Eleonora R. Semakova (2018) Estimation of Dispersed Glaciation Shrinkage Under Climate Change. Geography, Environment, Sustainability, Vol.12, No 1, p. 5-12
DOI-10.24057/2071-9388-2018-42

INTRODUCTION

Estimation of the change in characteristics of mountain glaciation under climate change is an important scientific and practical problem that has been solved for different mountainous regions around the world. In those past studies, however, the estimation of change was made either for individual large glaciers or for the total area of glaciation, in the respective regions.

The objective of our present work is to estimate the change in dispersed glaciation, using a different approach based on the use of statistical characteristics of glaciers (Glazirin 1991). By the term *glaciation* we denote an area of mountainous territory occupied by glaciers. *Dispersed* type of glaciation was identified by Khodakov (1978) and used to name a set of small glaciers that do not form a single massif but rather form a distributed or scattered array of glaciers, with possible concentrations or groups in sub-areas of the territory. Such glaciation is widespread in the peripheries of mountainous regions and is the only type of glaciation in some regions (for example, the Northern Ural, Kuznetsk Alatau). A method similar to the one we propose in the present paper has been used to assess the potential presence and viability of glaciers in some regions where they are currently absent or where they are critically endangered (Glazirin et al. 2000; Glazirin, Escher-Vetter 1998).

STUDY AREA

We show here how the proposed method can be applied to the example of glaciation of the left side of the Pskem River valley (Fig. 1). This area is located on the western periphery of the Tien-Shan. Currently it has about one hundred small glaciers having one accumulation area in most cases. According to the Catalogue of Glaciers (1968), their total area in 1957 was 63.6 km2. The climatic and orographic conditions for the existence of glaciation in the basin have been studied quite well (Schetinnikov 1976). In addition, real changes in glaciation have been identified in recent decades through several repeated glacier inventories (Narama et al. 2010; Semakova et al. 2016; Semakova and Semakov 2017; etc.), the last one done in 2010.

Typical glaciers of the region are shown in Fig. 2.

INPUT DATA

As mentioned, the proposed method is based on the use of statistical characteristics of glacier distribution. Thus, the inventories containing data suitable for our purposes were those containing information on the elevation and the area of each glacier. This criterion is satisfied, firstly, by the Catalogue of Glaciers (1968), prepared by Schetinnikov and reflecting the state of glaciers in 1957; secondly, by the inventory carried out by Schetinnikov based on the materials of the spatial survey from 1978 (unpublished data of Schetinnikov); and, thirdly, for the inventory carried out by Semakova et al. (2016).

In our work we only consider glaciers with an area more than or equal to 0.1 km2. This was done for two reasons. Firstly, this is the size limit used in the Catalogue of Glaciers of USSR (1968). Secondly, the possibility of errors in identifying and determining the size of smaller glaciers increases dramatically (Catalogue 1968; Semakova et al. 2016).

There are several meteorological stations in the Pskem River basin, but the longest and most reliable data series, starting with 1937, is available from Pskem station, located at an altitude of 1,260 m in the middle part of the valley. This station serves as a base for all hydrological and glaciological calculations in the Pskem River basin. The relationships between its data and expeditionary observation data in the glacial zone of the basin verify its representativeness for the basin (Borovikova et al. 1972; Schetinnikov 1976; etc.).

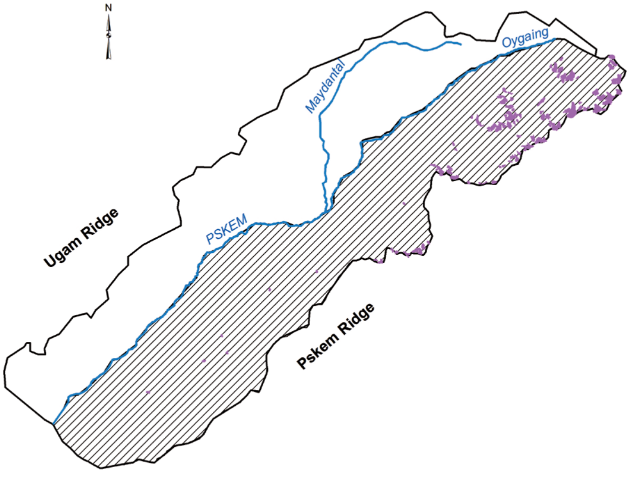

Fig. 1. Filled is the study area in the Pskem River basin

The main climatic parameters that affect the size and regime of glaciers are known to be solid atmospheric precipitation and air temperature. In the study area the main amount of precipitation falls in the winter-spring season (according to Pskem

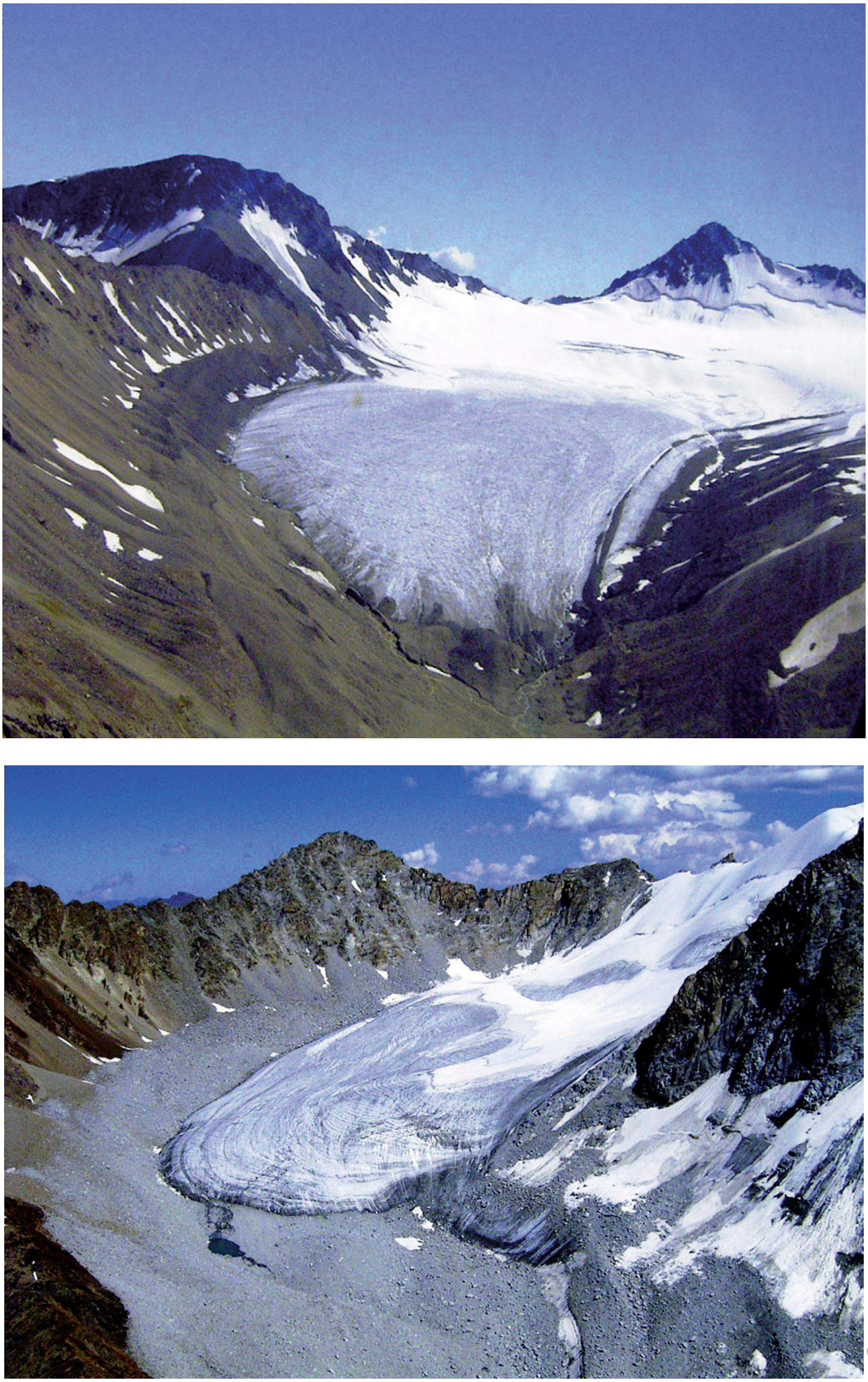

(a)

(b)

Fig. 2. Typical glaciers in the Pskem River basin

station observations about 90.5% of precipitation falls during the period from October to May), so it can be assumed that the annual solid precipitation at glaciation altitudes is equal to the total annual precipitation.

METHODOLOGY

The main idea of the method is as follows: the possible number of glaciers is estimated under given climatic conditions and the climatic equilibrium line altitude (*CELA*) is considered to be an integral indicator of these climatic conditions.

In regions with developed mountain glaciation *CELA* can be found from the relation of *CELA* and the area of glaciers present (Severskiy 1978). Successful application of the method requires, however, a large set of glaciers, including big ones. There are no big glaciers in the basin, so application of the method is unacceptable for our task solution. *CELA* was calculated by Glazirin (1991) on the basis of glaciation data from 1957, yielding a value for *CELA* of 3.93 km for the selected part of the basin. To characterize the climatic conditions of the basin for the time period the values of annual precipitation and the mean summer air temperature at Pskem station were taken for the preceding eleven years (1947-1957).

The next step is to calculate a possible number of glaciers under given climatic conditions (evaluated *CELA*). Glazirin (1991) proposes a formula for calculating a probability of the existence of glaciers in an altitude zone with an average Z elevation, depending on how far Z is from *CELA*. We estimated this dependence directly for the studied area (Fig. 3). The input data were the areas of the altitude zones evaluated from SRTM v.4 (Farr et al., 2007) and the number of glaciers in each altitude zone in 1957. The total number of glaciers is equal to the sum of the numbers of glaciers in each of the altitude zones.

Now it is necessary to determine the change in *CELA* under possible climate changes.

Let us assume that *Xa(CELA)*, which is the mean long-term annual precipitation on *CELA* position, is equal to *ab(CELA)*, which is the mean long-term annual ablation. We are able to calculate *ab(CELA)* using the Krenke-Khodakov formula (1982):

$$ab(CELA) = 1.33 \cdot (9.66 + Ts(CELA))^{2.85} \qquad (1)$$

Here, *Ts(CELA)* is the mean summer air temperature at *CELA* altitude. This temperature can be calculated using a simple formula,

$$Ts(CELA) = Ts(Zst) + y(CELA - Zst) \qquad (2)$$

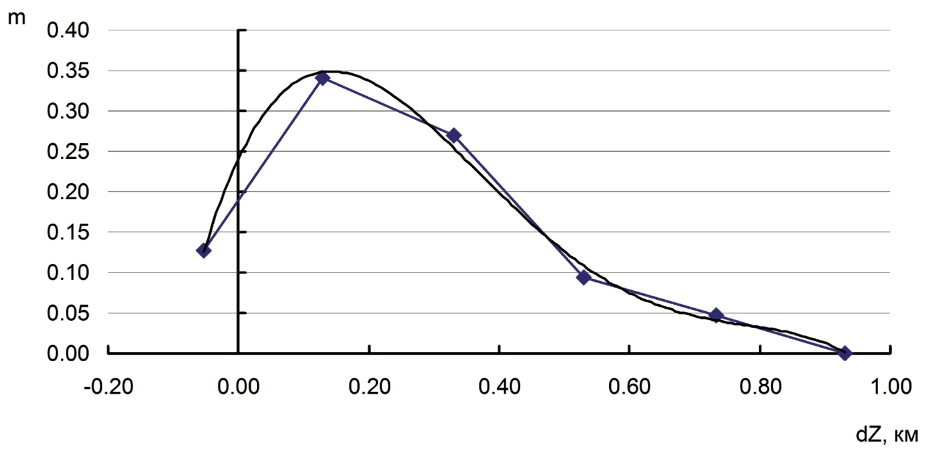

Fig. 3. Dependence of *m* (the number of glaciers per 1 km² of the altitude zone) on the difference between *CELA* and the average altitude of the corresponding zone *(dZ = CELA - Z)*

where γ is the vertical gradient of the mean summer air temperature. It was determined from the data of meteorological stations located in this basin and adjacent ones and turned out to be equal to -7.3^{0}C per 1 km. We used data from four weather stations (Chimgan, Oygaing, Maydantal, and Pskem, located at altitudes ranging from 1.26 to 2.16 km), as well as data gathered during several summer expeditions to glaciers in the basin. Thus, it is assumed that the change in air temperature is the same at all altitudes.

We will assume that the change in the annual precipitation *(Xa)* according to altitude, including ridges, is also linear (Getker 1987), and is determined by the following formula developed by Borovikova et al. (1972):

$$Xa(CELA) = Xa(Zst) \cdot (1 + k(CELA - Zst)) \quad (3)$$

The coefficient k can be calculated if we know the mean long-term precipitation at Pskem station *Xa(Zst)* and the precipitation sum at *CELA*, taken as equal to the mean long-term annual ablation. The coefficient k calculated for the period of 1947-1957 is equal to 0.09. So, the precipitation varies identically at all altitudes in a percentage ratio. The vertical temperature gradient γ and the coefficient k are assumed constant for subsequent periods.

We can find a new value of *CELA* by the equality of the calculated ab and Xa using formulas (1 - 3) if we specify a change in temperature at Pskem station. Further, it is possible to calculate a new number of glaciers in the altitude zones and in the study area overall using the new *CELA* and Fig 3.

Calculations were performed under the assumption that the annual precipitation was constant (this assumption is acceptable since according to observations at Pskem station for the period from 1937 to 2014 the mean change in annual precipitation is only 0.35 mm per year, the mean precipitation being 861 mm per year) while the mean summer air temperature increased.

We are also interested in finding the total area of glaciers. This area can be calculated in the following way. Let us assume that, under conditions of shrinkage of glaciation, the size distribution of glaciers remains the same (Glazirin 1991). The integral distribution of glaciers according to the inventory of 2010 (Semakova et al. 2016) is shown in Fig. 4. Taking into consideration the shrinkage of total glacial area and decrease in number of glaciers, the upper part of this distribution is cut off, so the remaining maximum value of the distribution is its new area.

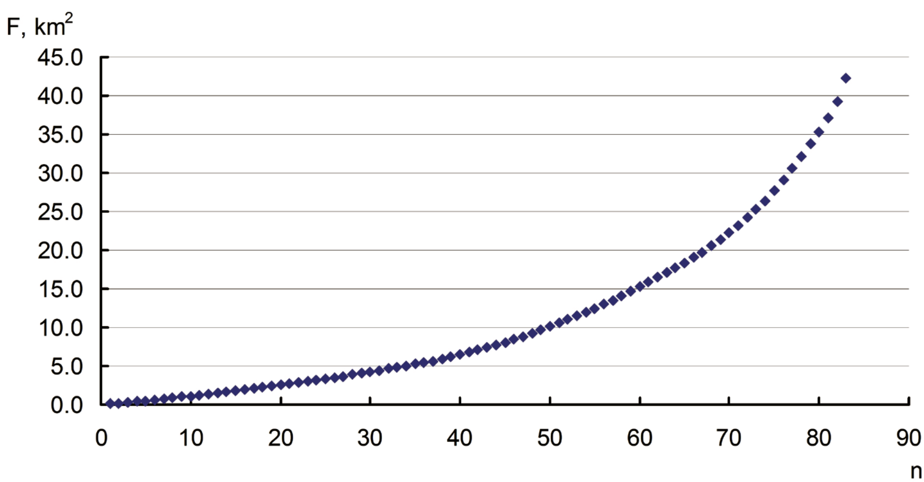

Fig. 4. Integral distribution of the glaciers in the study area according to the inventory data from 2010; n - numbers of glaciers, ranked by the increase of their area

We tried to estimate the reliability of the method by comparing the actual and calculated number of glaciers obtained in the result of the second and third inventories (1978 and 2010) using *k* and *m(dZ)* parameters found from the first catalogue of data (1957).

The calculated number of glaciers (95) at the time of the second inventory almost coincided with the actual number (94 glaciers with a total area of 52.6 km^2). For the third inventory, the calculated number of glaciers (91) slightly exceeded its actual number (83, with a total area of 42.2 km^2). This information allows us to judge the reliability of the methodology. Unfortunately, it is not possible to assess this reliability more generally because for the period between the first, second, and third inventories the climate has not changed significantly. The mean summer air temperature at Pskem station for the period of 1947-1957 was equal to 20.5°C, for the period of 1968-1978 it was 20.7°C, and for the period of 2000-2010 it was 20.9°C. The mean annual precipitation sums for the respective periods were 868, 885 and 892 mm per year. Given that the method is based on reliable and proven regularities we hope that the accuracy will be quite satisfactory, at least in the case of an insignificant deviation from modern climatic conditions.

RESULTS

The estimation was done on the assumption that the mean summer air temperature (ΔT) would rise by 0.5, 1.0, 1.5, and 2.0°C, which are appropriate values according to long-term climate change forecasts (Nikulina, Spectorman 1998). The change in the parameters of glaciation was determined according to the latest glacier inventory (2010). The table shows the values of *CELA*, the number of glaciers (N), and their total area (F) under possible air temperature increases.

As we see, with a temperature increase of 0.5°C *CELA* increases by 60-70 m. The number of glaciers decreases on average by 11 glaciers and glaciation area decreases significantly. We should note that glaciation persists in the study area even under such a significant air temperature increase.

It should be mentioned that the calculation allows us only to estimate stationary glaciation, i. e., when it has fully adapted to new climatic conditions. The period of adaptation is not expected to be a long one, given the small size of the glaciers. We assume that it should be equal to 11 years.

DISCUSSION AND CONCLUSION

We propose a method for estimating the change in the parameters of dispersed glaciation under conditions of climate change. It should be noted that the method can be used even when no direct data are available on the relationship between the climate and the area of glaciation of a certain region, i.e., when only meteorological data from the nearest meteorological stations and a single glacier inventory are available.

The relationship presented in Fig. 3 will apparently differ in other mountainous regions, because the specifics of orography, and various vertical gradients of air temperature and precipitation, are different. It is desirable to find an individual relation for each region, and also the relation be-

Table 1. Characteristics of the study area glaciation under given changes in the mean summer air temperature

	ΔT, ^{0}C				
	0	0,5	1	1,5	2
CELA, km	3.98	4.05	4.11	4.18	4.24
N	83	79	64	51	40
F, km^2	42.2	33.7	17.7	10.6	6.5

tween the calculated number of glaciers and their total area. In the interest of improving accuracy the proposed method, namely, that of using integral distribution of glaciers, has to be improved in the future. It should be noted that the method can even be used for areas where there are only single glaciers, or where only their traces are preserved (Glazirin and Escher-Vetter 1998; Glazirin et al. 2000).

We emphasize that this method is only suitable for calculating the reduction of glaciation in situations and terrains where the style of glaciation may properly be described as dispersed. And, it may not be suitable for calculating the increase in glaciation when new, small glaciers are forming, and existing glaciers are growing in size, or when glaciers are merging so as to lead to formation of large, complex glaciers: it can happen that the area of glaciation increases but the number of glaciers decreases. It is obvious that statistical regularities in the numbers of glaciers, as they are distributed by altitude zones, may change, and the relationships of the type shown in Fig. 3 may change as well.

ACKNOWLEDGEMENTS

We would like to thank Dr. L.N. Borovikova and Dr. Todd K. Hinkley for valuable advice and suggestions made during preparation of the paper.

REFERENCES

Borovikova L., Denisov Yu., Trofimova E. and Shentsis I. (1972). Mathematical modeling of the flow process of mountain rivers. Leningrad: Gidrometeoizdat. (In Russian).

Catalogue of Glaciers of USSR (1968). 14(1). Part 1. The Pskem River. Leningrad: Gidrometeoizdat. (In Russian).

Farr T.G., Rosen P.A., Caro E., Crippen R., Duren R., Hensley S., Kobrick M., Paller M., Rodriguez E., Roth L., Seal D., Shaffer S., Shimada J., Umland J., Werner M., Oskin M., Burbank D., Alsdorf D. (2007). The Shuttle Radar Topography Mission. Rev. Geophys. 45, RG2004, doi: 10.1029/2005RG000183.

Getker M. (1987). Snow resources of Central Asia. Moscow, Doctoral thesis abstract. (In Russian).

Glazirin G. (1991). Mountain glacier systems, their structure and evolution. Leningrad: Gidrometeoizdat. (In Russian).

Glazirin G. and Escher-Vetter H. (1998). The existence of glaciers in Bavaria, demonstrating climatic limitations of mountain glaciation. Zeitschrift fur Gletcherkunde und Glacialgeologie, 34(1), pp. 47–56.

Glazirin G., Glazirina E., and Trofimov G. (2000). The possibility of the existence of glaciation on the northern slopes of the Karatepe ridge in the Late Pleistocene and Holocene. SANIGMI, 153(234), pp. 179-187. (In Russian).

Khodakov V. (1978). Water-ice balance of the regions of the modern and ancient glaciation of the USSR. Moscow: Nauka. (In Russian).

Krenke A. (1982). Mass transfer in glacier systems in the territory of the USSR. Leningrad: Gidrometeoizdat. (In Russian).

Narama C., Kääb A., Duishonakunov M., Abdrakhmatov K. (2010). Spatial variability of recent glacier area changes in the Tien Shan Mountains, Central Asia, using Corona (~1970), Landsat (~2000), and ALOS (~2007) satellite data. Global and Planetary Change, 71, pp. 42-54.

Nikulina S., Spectorman T. (1998). Using scenarios of changes in global air temperature for assessing the thermal regime of Uzbekistan. SANIGMI, 156(237), pp. 103-108. (In Russian).

Schetinnikov A. (1976). Glaciers of the Pskem River basin. Leningrad: Gidrometeoizdat. (In Russian).

Severskiy I. (1978). To the method of calculating the mean annual solid precipitation sums at the glacier feeding boundary. Vestnik of the Kazakhstan Academy of Sciences, 11, pp. 43-50. (In Russian).

Semakova E., Gunasekara K., Semakov D. (2016). Identification of the glaciers and mountain naturally dammed lakes in Uzbekistan using ALOS satellite data. Geomatics, Natural Hazards and Risk, 7(3), pp. 1–18, doi: 10.1080/19475705.2015.1023852.

Semakova E. and Semakov D. (2017). On a possibility to use the remote sensing techniques for glaciological analysis in mountain regions of Uzbekistan. Ice and Snow, 57 (2), pp. 185–199. (In Russian), doi:10.15356/2076-6734-2017-2-185-199.

Received on August 16th, 2018 Accepted on February 20th, 2019

Igor I. Zveryaev[1*] and Alexey V. Arkhipkin[1]
[1] Shirshov Institute of Oceanology, Russian Academy of Sciences, Moscow, Russia
***Corresponding author:** igorz@sail.msk.ru

VARIABILITY AND CHANGES OF THE GROWING SEASON LENGTH AND FROST DAYS NUMBER IN RUSSIAN SUB-ARCTIC

ABSTRACT. Observational data from the Russian sub-Arctic stations are used to investigate long-term variability of the growing season length (GSL) and the number of frost days (FD) in 1949-2013. Consistent with the global warming pattern we find a trend-like increase (decrease) of GSL (FD) which is evident since early 1970th of the last century. These trend-like changes are best pronounced at Western stations (i.e. in European Russia and western Siberia) and they are essentially smaller to the East. Although we find some significant links to regional teleconnections (such as Scandinavian, East Atlantic and West Pacific teleconnections), in general our results imply rather weak impact of large scale atmospheric dynamics on interannual variability of GSL and FD. Further analysis of correlations between GSL and FD on the one side and snow cover on the other side revealed generally stronger links to snow cover compared to teleconnections. However, revealed links to regional atmospheric teleconnections and snow cover are significantly impacted by the linear trends. In general, our results imply that compared to large scale atmospheric dynamics impacting interannual variability, snow cover (being a result of wintertime synoptic activity) plays a more important role in decadal-interdecadal variations of GSL and FD in Russian sub-Arctic, which may have some value regarding predictability of the summer climate in the region.

KEY WORDS: Growing season, frost days, snow cover, teleconnections, northern Eurasia, climate variability and change

CITATION: Igor I. Zveryaev and Alexey V. Arkhipkin (2018) Variability and Changes of the Growing Season Length and Frost Days Number in Russian sub-Arctic . Geography, Environment, Sustainability, Vol.12, No 1, p. 13-22
DOI-10.24057/2071-9388-2018-55

INTRODUCTION

The growing season length (GSL) and number of frost days (FD) are among the most important climate indices (e.g., Zhang et al. 2011; Donat et al. 2013). Recent studies demonstrate increasing evidences of changes in air temperature and thus the GSL particularly in the Northern Hemisphere (Frich et al. 2002; Song et al. 2010). An increase in GSL have been noted in the late twentieth century through analysis of satellite data and phonological and meteorological observations (Linderholm 2006). The GSL variability appears as an important indicator of climate change. Myneni et al. (1997) showed that increases in the photosynthetic activity of terrestrial vegetation, as seen from satellite data, have been associated with increase of the GSL. IPCC (2013) affirms that the projected climate change will further increase GSL.

Thus, in some areas, such as high northern latitudes, an increased GSL along with a warmer climate might have a positive effect on crop production and possibly increase the harvests and seasonal yields.

The occurrence of freezing conditions is an integral element of a regional ecosystem processes, recreational activities and economy. Several studies revealed a clear trend towards fewer low temperature extremes in the late twentieth century over all continents (e.g., Horton et al. 2001; Kunkel et al. 2004). The global analysis of climate extreme indices by Frich et al. (2002) revealed the evidence of fewer frost days in much of the middle and high latitudes of the Northern Hemisphere during the second half of the twentieth century. Alexander et al. (2006) found significant decrease in the annual number of frost days over Western Europe and large parts of Russia during the period 1951-2003. Bartoly and Pongrácz (2007) detected a decreasing number of cold nights, severe cold days and frost days between 1961 and 2001.

It should be noted however that characteristics of interannual variability of GSL and FD vary significantly from region to region. Thus, a large degree of uncertainty remains regarding GSL and FD variability in such under sampled region as Russian sub-Arctic during recent decades, a time period characterized by the most intensive climate warming. Recently available observational data sets provide a good opportunity to address this issue.

In the present study we therefore aim to examine variability and changes in GSL and FD in Russian sub-Arctic and investigate possible mechanisms driving (or impacting) these variability and changes. The data used and the analysis methods are described in Materials and Methods section. The major results of undertaken analysis are presented and briefly discussed in Results and Discussion. Finally, major conclusions of the study are formulated in Conclusions section.

MATERIALS AND METHODS

In this study we use the growing season length (GSL) and number of frost days (FD) data for 1949-2013 which are calculated basing on Global Historical Climatology Network (GHCN) daily station dataset. Both GSL and FD are among the key climate indices recommended by the Expert Team on Climate Change Detection and Indices (ETCCDI, e.g., Zhang et al. 2011). In essence GSL is an annual number of days between the first occurrence of 6 consecutive days with daily mean temperature exceeding 5ºC and first occurrence of 6 consecutive days with daily mean temperature below 5ºC. For the Northern Hemisphere this is calculated from January 1 to December 31. FD is annual number of days when minimum temperature is below 0ºC. These data are provided by the Climate Change Research Centre, University of New South Wales (e.g., Donat et al. 2013) and publicly available at www.climdex.org. Based on the criteria of time series length and absence of gaps, for our analysis, we selected 8 Russian sub-Arctic stations which are indicated in Fig. 1. It should be mentioned that, in general, Russian sub-Arctic is not well covered by observations (see e.g. Fig. 1 in Alexander et al. 2006). Nevertheless, the stations selected for present study, are relatively evenly distributed in west – east direction, though the number of stations in the eastern part of the region is obviously smaller.

To investigate possible links between interannual variability of GSL and FD in Russian sub-Arctic and regional atmospheric circulation we use indices of the major teleconnection patterns that have been documented and described by Barnston and Livezey (1987). The patterns and indices were obtained by applying rotated principal component analysis (e.g., Hannachi et al. 2007) to standardized 500hPa height anomalies in the Northern Hemisphere. The teleconnection patterns used here include the North Atlantic (NAO), East Atlantic (EA), East Atlantic – West Russia (EAWR), Polar – Eurasia (POL), West Pacific (WP) and the Scandinavian (SCA) patterns. Their regularly updated indices, covering

Fig. 1. Russian sub-Arctic stations under analysis

the period 1950 – present, are available from the NOAA Climate Prediction Centre (CPC) website (www.cpc.ncep.noaa.gov/data/teledoc/telecontents. html). Further details on the teleconnection pattern calculation procedures can be found in Barnston and Livezey (1987) and at the CPC website. These indices have been curtailed to match the period of our analysis. To briefly examine possible impact of snow cover on the GSL and FD variability, we make use of the snow water equivalent (SWE) data from the GlobSnow dataset (Takala et al. 2011) which are satellite data provided on the grid with 25km spatial resolution.

Long-term linear trends of GSL and FD were estimated by least squares (e.g., Wilks 1995) at each station. Statistical significance of trend estimates was assessed according to a Student t-test (Bendat and Piersol 1966). Conventional correlation analysis has been applied to study links to teleconnection patterns and snow cover. In this study we consider simultaneous connections between GSL and FD and major teleconnection patterns as well as snow cover. According to the Student t-test (Bendat and Piersol 1966), the minimum significant correlation coefficient between the time series analyzed is 0.24 for the 5% significance level. Since the significance level of the correlation coefficient might be reduced if the time series are influenced by autocorrelation, the potential impact of autocorrelation on the estimation of significance of correlation coefficients has been examined. Significant autocorrelations have not been found in analyzed time series which is expected since each value is separated by 1 year. It should be emphasized that statistical methods used in this study imply that only linear relationships between analyzed variables are addressed.

RESULTS AND DISCUSSION

The time series of GSL and FD calculated for 8 Russian sub-Arctic stations are shown respectively at Fig. 2 and 3. Obviously, both GSL and FD vary significantly at interannual and decadal - interdecadal time scales. The major feature in GSL variability is an upward trend starting from the early 70-ties which is best pronounced at the more westerly located stations (Fig. 2). In particular, the largest trends are found in Vytegra and Pechora reflecting an increase in GSL of 8.0 and 8.3 days per decade respectively (Table 1). In contrast, respective trends in easterly located Suntar (2.6 day/decade) and Sejmchan (2.4 day/decade) are not statistically significant. It is worth noting that decadal scale GSL variations in earlier (i.e., before 70-ties) period are also better pronounced at western stations of Russian sub-Arctic (Fig. 2). Although these results (i.e., increase in GSL) are broadly consistent with the global warming trend and its recent intensification (e.g., Bindoff et al. 2013; IPCC 2013), it should be noted that this intensification began in late 70-ties, somewhat later than above described trends in GSL.

Contrasting to GSL, the major feature in FD variability is a downward trend also starting in early 70-ties and also better pronounced at the more westerly located stations (Fig. 3). Particularly, the largest negative trends of FD are found in Arhangelsk and Kotlas reflecting a decrease in FD of 6.6 and 6.0 days per decade respectively (Table 1). Again, similar to GSL, negative trends of FD at the easterly located stations are relatively small and statistically insignificant (Fig. 3). Note however, that at Sejmchan a strong negative trend (-7.9 day/decade) of FD is evident starting from late 80-ties (Fig. 3h). This might indicate a different (compared to more westerly located stations) origin of this downward trend of FD. Although GSL and FD basically characterize different seasons, it should be stressed that these climate indices are not completely independent and demonstrate statistically significant negative correlations varying from -0.49 (-0.46) at Sejmchan to -0.77 (-0.74) at Aleksandrovskoe. Note, correlations between respective de-trended time series (shown in parentheses) are only slightly smaller.

We further briefly examine possible links between GSL and FD variability and some regional teleconnections (Barnston and Livezey 1987). In general, correlations between GSL and FD time series and seasonally averaged indices of regional teleconnections are not very large although in

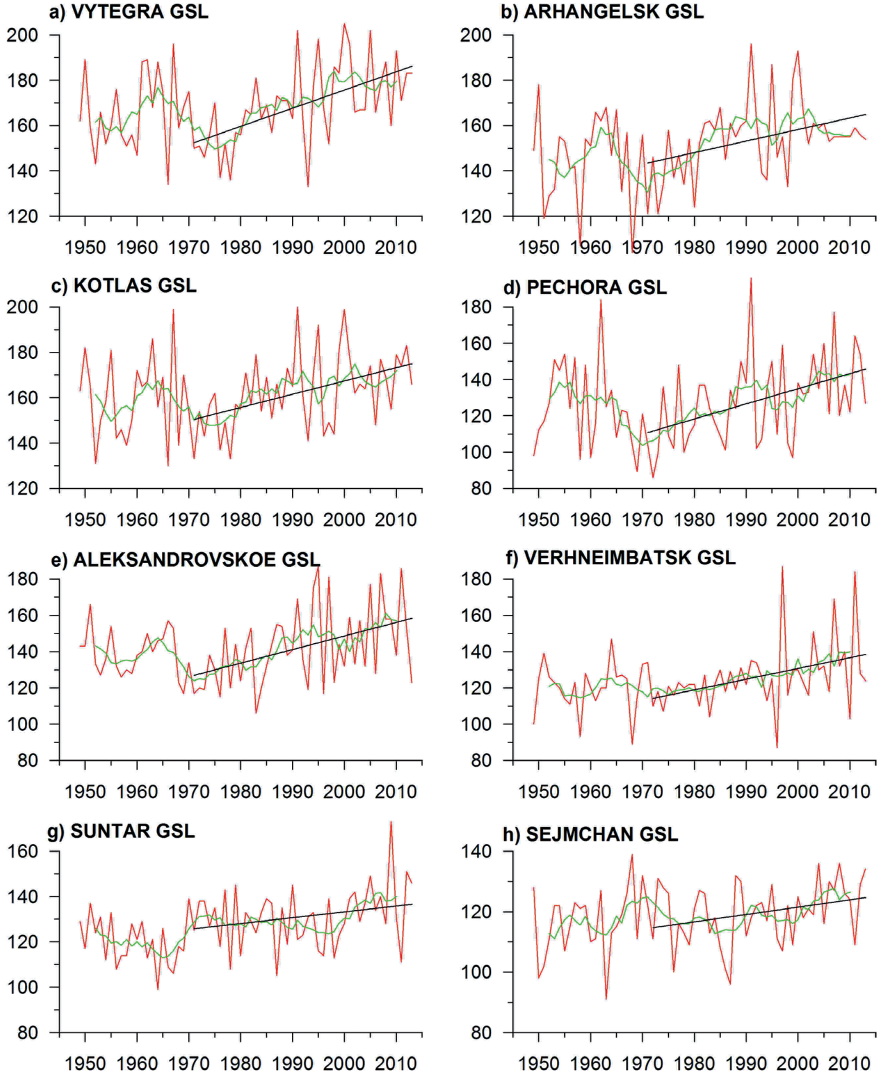

Fig. 2. Time series of GSL at Russian sub-Arctic stations. Green curves indicate running means (7-yr window). Black line indicates linear trend

many cases they are statistically significant at 5% significance level according to Student t-test (Bendat and Piersol 1966). Thus, we mention here only the largest among estimated correlations (Table 2). For GSL (i.e., for summer season) we found relatively large (-0.35) correlation between GSL at the most westerly located (see Fig. 1) Vytegra station and the SCA teleconnection index. Another relatively large (-0.37) detected correlation is that between GSL at the most easterly located Sejmchan station and the WP teleconnection index (Table 2). Note, we do not find large correlations for other stations located between Vytegra and Sejmchan. This basically means that interannual variability of GSL in Siberia is not impacted significantly by examined teleconnections that mostly active in the North Atlantic and Pacific sectors. For FD the largest correlations are found at Vytegra (-0.37) and Suntar (-0.38), in both cases with the EA teleconnection. At Suntar we also found relatively large (0.35) correlation between FD and the POL teleconnection.

It is obvious that considered correlations might be impacted by the linear trends revealed in original time series of GSL and FD

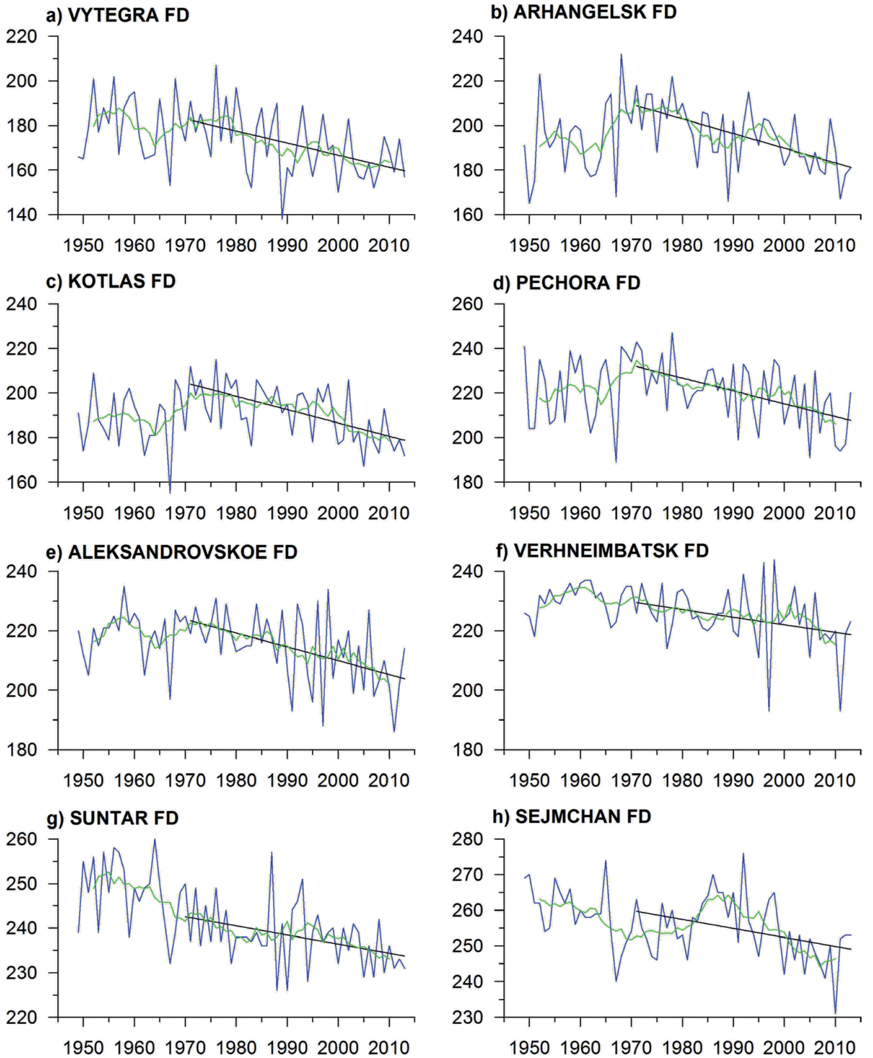

Fig. 3. Time series of FD at Russian sub-Arctic stations. Green curves indicate running means (7-yr window). Black line indicates linear trend

Table 1. Linear trends (in days per decade) in growing season length (GSL) and frost days (FD) number at Russian sub-Arctic stations for 1971-2013. The trends that statistically significant at 5% level are shown in *italics*

	VYT	ARH	KOT	PEC	ALE	VER	SUN	SEJ
GSL	*8.0*	*5.1*	*5.8*	*8.3*	*7.4*	*5.9*	2.6	2.4
FD	*-5.4*	*-6.6*	*-6.0*	*-5.7*	*-4.6*	*-2.6*	-2.1	-2.5

Table 2. Correlations between GSL and FD and indices of regional teleconnections. Correlations for de-trended time series are presented in parentheses. Correlations that statistically significant at 5% level are shown in *italics*

GSL	
VYTEGRA - SCA	*-0.35 (-0.30)*
SEJMCHAN - WP	*-0.37 (-0.29)*
FD	
VYTEGRA - EA	*-0.37* (-0.19)
SUNTAR - EA	*-0.38* (-0.11)
SUNTAR - POL	*0.35* (0.13)

(Fig. 2 and 3). To examine the role of linear trends, we removed the trends from original time series, and estimated correlations for de-trended time series. As expected, correlations for de-trended time series are generally lower than those for original time series (Table 2). It is important to note that correlations for de-trended GSL time series are only slightly smaller and remain statistically significant. In contrast, correlations for de-trended FD time series are very small and statistically insignificant. Thus, the trends revealed in time series of GSL and FD do indeed impact detected links to regional teleconnections, and this impact is stronger for FD time series.

Finally, we investigate links to SWE, which is the key characteristic of snow cover. To do this we examine correlations between GSL and FD indices at each station and gridded SWE field in northern Eurasia. As a general tendency, we note that for each station the largest correlations to SWE are detected (not shown) in the end of cold season, in March-April, when seasonal snow accumulation is the largest. This result is physically reasonable since anomalously large (small) snow cover at the end of cold season favors longer (shorter) winter season and thus, negative (positive) anomalies of GSL and opposite anomalies of FD. Another principal result is that correlations to SWE (especially in the nearby regions) are generally larger than above considered correlations to regional teleconnections. This implies relative importance of the local processes in interannual variability of GSL and FD in Russian sub-Arctic. As illustration in Fig. 4 we show some of the obtained correlation patterns. Rather high and significant negative correlations between GSL at Pechora station and SWE in April are revealed over extensive region of northern European Russia and western Siberia (Fig. 4a). As expected, the largest (reaching -0.6) correlations are detected in the area close to the station. Somewhat similar correlation pattern is obtained for GSL at Aleksandrovskoe (Fig. 4b), however, the correlations are generally larger and the region of largest correlations is more extensive. This might indicate increasing role of local interactions in more continental climate. Correlation pattern for FD at Arhangelsk reveals an extensive region of significant positive correlations over northern European Russia and northern part of western Siberia (Fig. 4c), which generally suggest that positive (negative) SWE anomalies result in increased (decreased) FD number. Very large (exceeding 0.7) positive correlations to SWE in northeastern part of Eurasia are also found for FD at Sejmchan station (Fig. 4d). We further examine links between de-trended time series of GSL, FD and SWE. As seen from Fig. 5, obtained correlation patterns differ significantly from respective patterns for original time series (Fig. 4). Correlations are not only significantly smaller (e.g. correlations between FD at Arhangelsk and SWE over northern part of western Siberia, Fig. 5c), but in many cases (regions) change sign. For example, large positive correlations between FD at Sejmchan and SWE detected in delta of the Ob river (Obskaya guba) and in Kolyma region (eastern Siberia, Fig. 4d), after de-trending change sign and become negative ones (Fig. 5d).

Thus, overall our results imply rather tight links between GSL and FD at Russian sub-Arctic stations and regional snow cover variations. These links, however, are

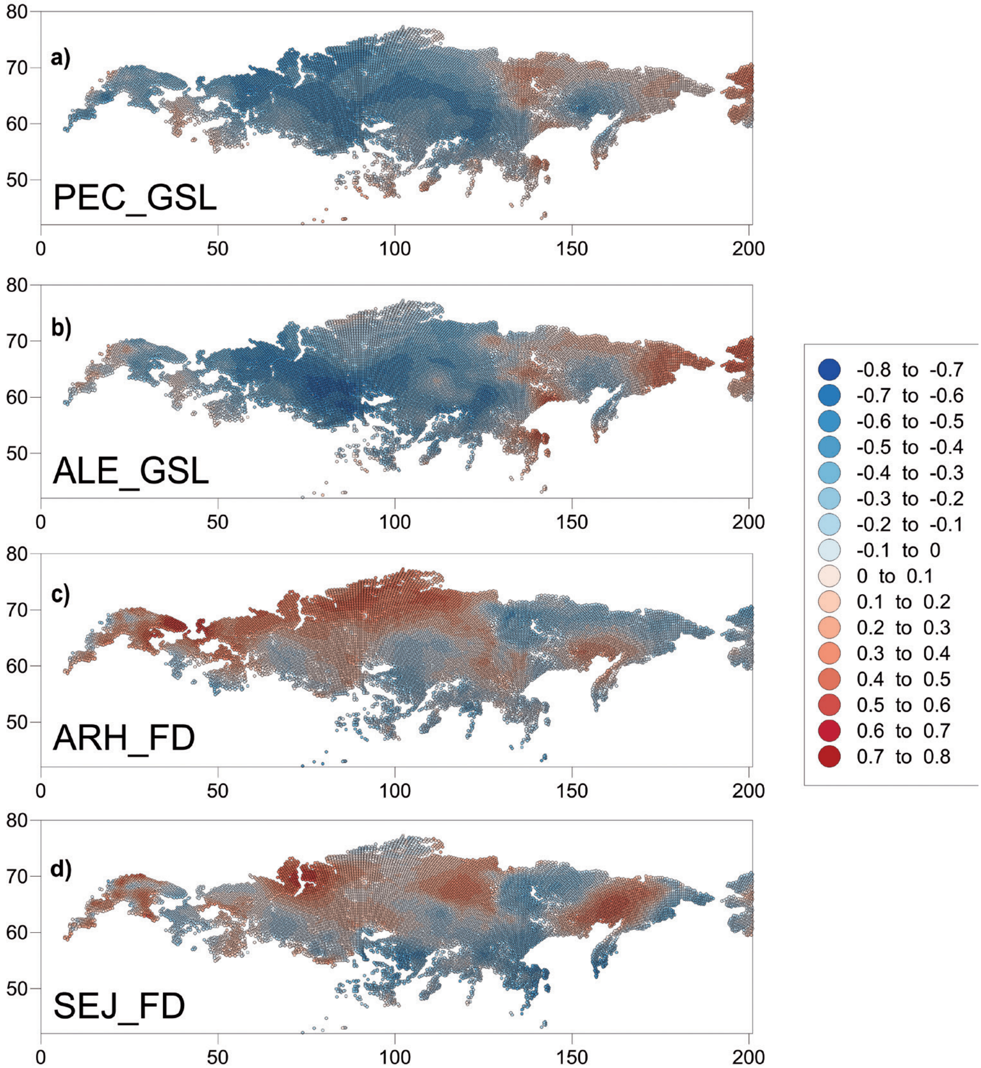

Fig. 4. Correlations between SWE in April and GSL at Pechora (a), GSL at Aleksandrovskoe (b), FD at Arhangelsk (c) and FD at Sejmchan (d). Red (blue) color indicates positive (negative) correlations

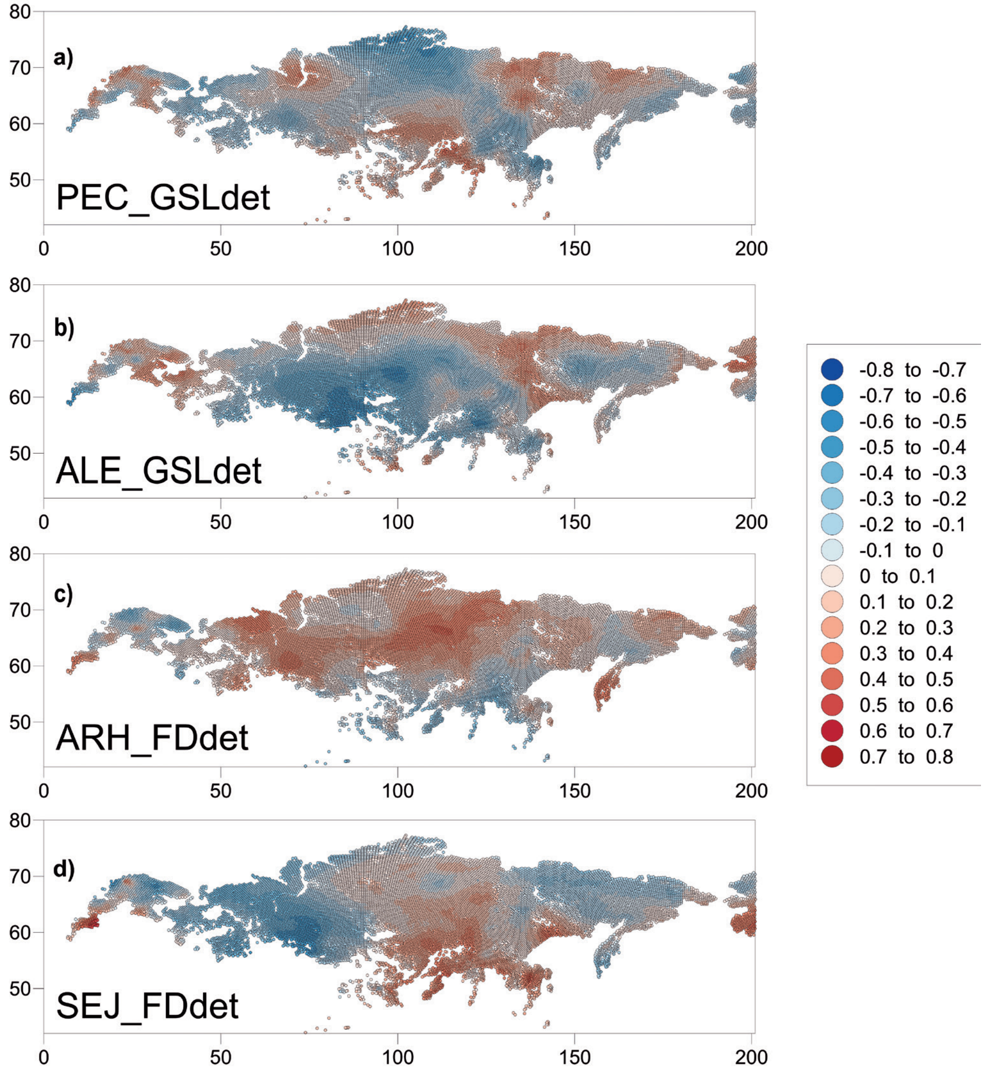

Fig. 5. Same as Fig. 4, but for de-trended time series

strongly impacted by linear trends revealed during recent decades. This is indeed indicative of differing character of interactions between considered parameters at different (i.e. interannual versus deacadal-interdecadal) time scales. Although impact of atmospheric dynamics (expressed by teleconnections) on GSL and FD is generally weaker (compared to snow cover), it should be stressed that it acts on the shorter (i.e. interannual) time scale while impact of snow cover is more pronounced at decadal-interdecadal time scales.

CONCLUSIONS

This study is an investigation of interannual variability of GSL and FD in Russian sub-Arctic in 1949-2013. We find significant upward and downward trends in GSL and FD respectively. Though these trends are broadly consistent with the global warming trend (e.g., Bindoff et al. 2013; IPCC 2013), it should be stressed that detected trends in GSL and FD are evident only since early 70-ties. Before that, at some stations even opposite trends can be observed. It is also important to emphasize that detected trends in GSL and

FD are stronger and more significant at western stations compared to easterly located stations.

Regarding interannual variability, we found rather moderate impact of the SCA teleconnection on GSL variability at Vytegra, and an impact of the WP teleconnection on GSL at Sejmchan station. During winter the EA teleconnection impacts FD variability at Vytegra and Suntar. Thus, GSL and FD variability at majority of considered stations (particularly in Siberia) is not significantly influenced by regional teleconnections (Barnston and Livezey 1987). Moreover, even significant correlations to teleconnections are impacted by linear trends. This impact is particularly strong for FD time series (Table 2).

We also explored links between GSL and FD variability at selected Russian sub-Arctic stations and snow cover (characterized by SWE) variations in northern Eurasia. While we leave in depth analysis of these links for the further study, it should be stressed that the present analysis reveals generally stronger links to SWE than that to teleconnections. As expected the largest correlations to SWE are detected in the areas around respective stations. Altogether these results imply that compared to large scale atmospheric dynamics (characterized by teleconnections) which impacts (in some regions) GSL and FD on interannual time scale, snow cover formed by winter synoptic activity, plays a more important role in longer-term (i.e., decadal-interdecadal) variability of GSL and FD in Russian sub-Arctic. Both links to regional teleconnections and links to SWE are greatly impacted by detected linear trends. In this regard, a detailed analysis of such links at different time scales is needed, and will be undertaken in our further studies.

ACKNOWLEDGMENTS

This study was supported by the Russian Science Foundation grant 14-37-00038. The present analysis was performed under the framework of the State Agreement № 0149-2018-0001. The study was also supported by the project 14.B25.31.0026 funded by the Ministry of Education and Science of the Russian Federation.

REFERENCES

Alexander L., Zhang X., Peterson T.C., Caesar J., Gleason B. et al. (2006). Global observed changes in daily climate extremes of temperature and precipitation, J. Geophys. Res., 111, D05109, doi: 10.1029/2005JD006290.

Barnston A. and Livezey R. (1987). Classification, seasonality and persistence of low-frequency atmospheric circulation patterns, Mon. Weather Rev., 115, pp. 1083-1126.

Bartoly J. and Pongrácz S. (2007). Regional analysis of extreme in worldwide temperature and precipitation indices for Carpathian Basin from 1946 to 2001. Global and Planetary Change, 57, pp. 83-95.

Bendat J. and Piersol A. (1966). Measurement and Analysis of Random Data, John Wiley, Hoboken, N. J.

Bindoff N., Stott P., AchutaRao K., Allen M., Gillett N. et al. (2013). Detection and Attribution of Climate Change: from Global to Regional. In: Climate Change 2013: The Physical Science Basis. Contribution of Working Group I to the Fifth Assessment Report of the Intergovernmental Panel on Climate Change [Stocker, T.F., Qin D., Plattner G.-K., Tignor M., Allen S.K., Boschung J., Nauels A., Xia Y., Bex V., and Midgley P.M. (eds.)]. Cambridge University Press, Cambridge, United Kingdom and New York, NY, USA.

Donat M., Alexander L., Yang H., Durre I., Vose R. et al. (2013). Global land-based datasets for monitoring climatic extremes, Bull. Amer. Met. Soc., 94, pp. 997-1006.

Frich P., Alexander L., Della-Marta P., Gleason B., Haylock M. et al. (2002). Observed coherent changes in climatic extremes during the second half of the twentieth century, Clim. Res., 19, pp.193-212.

Horton E., Folland C. and Parker D. (2001). The changing incidence of extremes in worldwide and Central England temperatures to the end of the twentieth century, Climatic Change, 50, pp. 267-295.

IPCC (2013). Summary for Policymakers. In: Climate Change 2013: The Physical Science Basis. Contribution of Working Group I to the Fifth Assessment Report of the Intergovernmental Panel on Climate Change [Stocker, T.F., Qin D., Plattner G.-K., Tignor M., Allen S.K., Boschung J., Nauels A., Xia Y., Bex V., and Midgley P.M. (eds.)]. Cambridge University Press, Cambridge, United Kingdom and New York, NY, USA.

Kunkel K., Easterling D., Hubbard K., and Redmond K. (2004). Temporal variations in frost-free season in the United States 1895-2000. Geophys Res Lett., 31, L03201, doi: 10.1029/2003GL018624.

Linderholm H. (2006). Growing season changes in the last century, Agricultural and forest meteorology, 137, pp.1-14.

Myneni R., Keeling C., Tucker C., Asrar G., and Nemani R. (1997). Increased plant growth in the northern high latitudes from 1981 to 1991, Nature, 386, pp. 698-702.

Song Y., Linderholm H., Chen D., and Walther A. (2010) Trends of the thermal growing season in China, 1951-2007. Int. J. Climatol., 30, pp. 33-43.

Takala M., Luojus K., Pulliainen J., Derksen C., Lemmetyinen J. et al. (2011). Estimating Northern Hemisphere snow water equivalent for climate research through assimilation of space-borne radiometer data and ground-based observations, Remote Sens. Environ., 115, pp. 3517-3529.

Wilks D. (1995). Statistical Methods in the Atmospheric Sciences. Academic Press, San Diego, CA, USA.

Zhang X., Alexander L., Hegerl G., Jones P., Tank A. et al. (2011). Indices for monitoring changes in extremes based on daily temperature and precipitation data, WIREs Clim. Change 2011, doi: 10.1002/wcc.147.

Received on October 23rd, 2018 Accepted on February 20th, 2019

Vladimir Konovalov[1*], Ekaterina Rets[2], Nina Pimankina[3]
[1] Institute of geography, Russian Academy of Science, Moscow, Russia,
[2] Institute of water problems, Russian Academy of Science, Moscow, Russia
[3] Institute of geography, Almaty, Kazakhstan
***Corresponding author:** vladgeo@gmail.com

INTERRELATION BETWEEN GLACIER SUMMER MASS BALANCE AND RUNOFF IN MOUNTAIN RIVER BASINS

ABSTRACT. Measurements of summer mass balance B_s, made over the period 1946-2016, on 56 continental glaciers, located in the basins of mountain rivers in 14 countries, were analysed for the purpose of resolving several tasks: (a) constructing physically based interrelations between river flow W_{bas} and B_s; (b) estimating the representativeness of local measurement of B_s for enhancement of hydrological computations and for control of modelled values W_{bas}; and (c) use of time series of B_s for the evaluation of norms and extrema of W_{bas}. Results of the study of the outlined problem serve as the basis for making the transition of local glaciological characteristics to the basin-wide level by using the relationship between runoff and summer balance of glaciers. It includes also analysis and conclusions on the spatial and temporal homogeneity of averaging glaciological mass balance data by the sampling method.

KEY WORDS: summer mass balance, glacier runoff, glaciers representativeness, extremes and norm, multi-year series, statistical averaging

CITATION: Vladimir Konovalov, Ekaterina Rets, Nina Pimankina (2019) Interrelation Between Glacier Summer Mass Balance And Runoff In Mountain River Basins. Geography, Environment, Sustainability, Vol.12, No 1, p. 23-33
DOI-10.24057/2071-9388-2018-26

INTRODUCTION AND OBJECTIVE OF THE STUDY

According to the definitions in Kotlyakov (1984), Kotlyakov and Smolyarova (1990), and Cogley et al. (2011), the summer balance B_s is equal to the change in the glacier's mass starting from the time of maximum of snow accumulation to the end of the ablation period. During this interval of time, it is possible to determine the integral value of B_s as a whole for the season, or for the specific ten days/months inside the year. As a result of applying the best methods and techniques of measurements, the obtained volume of B_s characterizes output of melt water from the area of a glacier, which is necessary to calculate and forecast the river's runoff formed by the melting snow and ice.

At present, the continuous measurements B_s with the minimal number $N_{min} \geq 10$ of yearly data during 1946-2016 are available (Dyurgerov and Meier 2005; Fluctuations of Glaciers Database 2017) on a 56 continental glaciers, which distributed extremely unevenly on the Earth, see Fig. 1. Similar spatio-temporal distributions of annual mass balance B_a for 144 glaciers illustrates Fig. 3a-b, prepared by data from (Mernild et al.

2013). For this figure, we used decadal averages of B_a during 1971-2008.

The list of 56 glaciers selected for B_s analysis is given in the Table A1. In this set of data, the adopted value of N_{min} satisfies more or less to statistical requirements for correct averaging. Principally, such empirical sample have to be equal to not less than 15 years. However, following known rules of statistic leads to diminishing the size of glacier sample. In particular, at $N_{min} \geq 15$ it will consist 45 instead of 56 glaciers with long-term asynchronous data of B_s. Zemp et al. (2015) concluded, that for climate change assessments with >30 observation years, the glaciological dataset currently contains 37 reference glaciers.

There are exist opinion (Dyurgerov and Meier 2005; Zemp et al. 2009; Fluctuations of Glaciers Database 2017, and many others), that glaciers, included in WGMS mass balance network are considered a priori as reference or representative for regional/global monitoring of changes in the annual mass balance B_a and its components (winter B_w and summer B_s balances) in glacier populations. Analysis (Kotlyakov et al. 1997; Braithwaite 2009; Fountain 2009; Konovalov 2015; Zemp et al. 2009) based on the 60-years information on B_a, B_w and B_s at such reference glaciers has revealed the following properties of the WGMS network for measurements the glacier mass balance. 1) Selection of the so-called "representative/benchmark" glaciers is often basing on the principle of lowest cost for fieldwork instead of previous analyzing the spatial distribution of area, altitude-morphological and other characteristics of glaciers in the corresponding population. 2) Predominance of European data leads to distortion of global average values of annual and summer mass balances of glaciers. The amount of distortion is unknown because averaging measurements on "reference" glaciers ignores regional accumulation and ablation patterns. 3) Completeness of the series and the timing of observations is very low, due to many omissions.

The other problem of using initial data on B_s (Dyurgerov and Meier 2005; Fluctuations of Glaciers Database 2017) for regional/global averaging is their significant asynchrony. Table 1 illustrates the asynchrony of B_s yearly data in ten-year periods during 1946-2015.

Currently, the vast majority of glaciological publications contain climatic, physical and dynamic characteristics on the regime of individual glaciers having local spatial and temporal distribution. The peculiarity of calculations and forecasts of runoff at the scale of mountain watersheds is the necessity of estimating the annual/seasonal volume of melt water $W_{bas}=W_{snow}+W_{gl}$ formed on the total area of F_{bas} river basin, above the outlet hydrologic station. Here W_{snow} is the volume of snowmelt and W_{gl} – is glacier runoff. In models (e.g. Borovikova et al. 1972; Rets et al. 2011, 2017,2018; WaSiM Model 2015) for rivers of snow-glacial type, the catchment area presented as a set of elementary sites having known plane and altitude coordinates, parameters of exposure and slope of the surface. The total volume of water formed at all elementary sites is using to transform it into a flow hydrograph. In order to assess the quality of modeled W_{bas} we may use the initial measurements of ablation/summer mass balance. Similar assessment the modeled values of W_{bas} can be performed by comparing the measured runoff and calculated one on

Table 1. Density of WGMS network for spatial and temporal averaging of total data on B_s

Index	Ten-year time intervals						
	1946-55	1956-65	1966-75	1976-85	1986-95	1996-2005	2006-2015
M	20	109	293	337	381	304	219
M_1 %	3.4	18.5	49.7	57.1	64.6	51.5	37.1

*M – is actual number of measurements B_s for ten-years, M_1 % – is percentage of M from possible maximum $M_0 = N_{gl}$*10, where N_{gl} is total number of selected glaciers in the each decade, i.e. 56 in our case.*

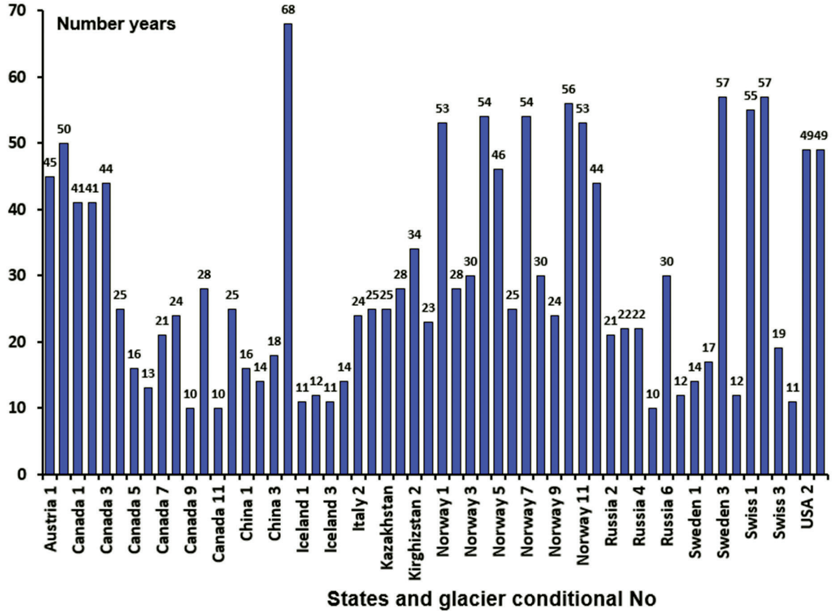

Fig. 1. Number of years with B_s data on glaciers in different states within 1946-2016. Reference on source of information see in the text

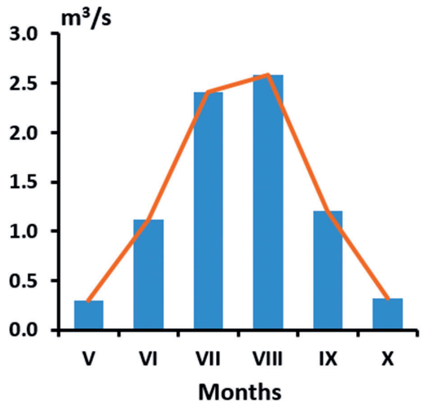

Fig. 2. Monthly runoff of Vernagtferner River in May-October. Reference on data source see in the text

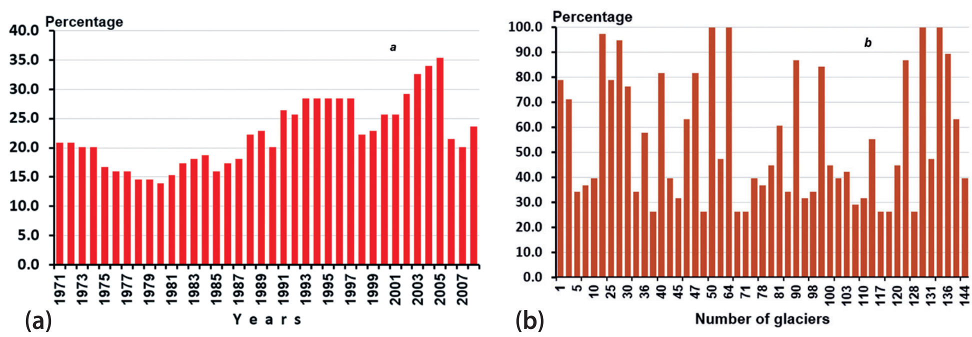

Fig. 3. Temporal distribution of B_a data (a), and spatial distribution of averaged B_a data (b) Reference on source of information for figures a-b see in the text

the basis of application the equation of the annual water balance (Konovalov 2014; Konovalov 2015; Konovalov and Pimankina 2016).

The objectives of our research are the following. a) To understand how suitable current B_s data in (Dyurgerov and Meier 2005; Fluctuations of Glaciers Database 2017) for statistically substantiated spatial and temporal averaging. It means that our assessment concerns only existence or absence of data and not of their quality. The last one characteristic needs rigorous analysis for each case, but not fulfilled yet, and one may discover not compatible data of B_s for the same glacier in different sources. (b) To study physically based relationships between W_{bas} and B_s for simplified verification of modelled values of W_{bas}. c) To use time series B_s to characterize the norms and extremes of W_{bas}. d) To verify the possibility of spatial extrapolation of B_s data, obtained on glaciers, which have been considered as representative/reference in the WGMS network.

STUDY REGION, OBJECTS AND METHODS

The regions of and subjects for the present study are continental glaciers of the Earth, contained in the system of WGMS - World Glaciers Monitoring Service (Dyurgerov and Meier 2005; Fluctuations of Glaciers Database 2017). Several glaciers suitable for our analysis are in the Table 2. Their number is mainly limited of extremely rare or inaccessible hydrological information at runoff measurement stations, have located near the glaciers with B_a, B_w and B_s data. Information on the runoff for the rivers of snow-glacial type are taken from the special glaciological editions and hydrological reference books such as the following: Glacier Aktru 1987; Bodo 2000; Dahlke et al. 2012; Glacier Djankuat 1978; Escher-Vetter and Reinwarth 1994; Kamnyanskiy 2001; Krimmel 2000; USGS Alaska Water Science Center; Vilesov and Uvarov 2001. At selecting the time interval for averaging the runoff and B_s data, took into account the interannual distribution of runoff at the hydrological stations near the glaciers. A typical example of such distribution presented in Fig. 2. Source of data is Escher-Vetter and Reinwarth (1994).

High level correlation dependences $Q=f(B_s)$, presented in the Table 2, serve as a basis for obtaining empirical functions of distribution for Q and B_s, building links between statistical probability (Prob) of flow and summer mass balance, and ultimately assessing the probability of extreme flow values.

Table 2. Studied glaciers and correlation between runoff Q and summer mass balance B_s

State	Glacier name	F_{bas}	F_{gl} 1	F_{gl} 2	N	R^2			
						Q_1	Q_2	Q_3	Q_4
Kyrgyzstan	Abramova	55.5	26.1	47.0	21	0.80	0.84	0.84	0.89
Austria	Vernagtferner	11.4	9.3	81.6	31	0.82	0.91	0.92	0.91
Russia	Djankuat	8.0	3.1	38.8	6	0.80	0.87	0.95	
Russia	Maly Aktru	36.0	2.5	6.9	7	0.56	0.85	0.85	
Kazakhstan	Centralny Tyuksu	21.0	2.9	13.7	22	0.36	0.22	0.31	0.22
USA	Wolverine	31.3	18.0	57.5	37	0.22	0.25	0.26	0.27
Sweden	Stor	19.6	3.1	15.9	16	0.15	0.15	0.15	0.12

Definition of symbols: R^2 is coefficient of determination; F_{bas} is area of basin above site of runoff measurement, km^2; F_{gl} 1 is area of reference glacier, km^2; $F_{gl}2 = F_{gl}1/F_{bas}$ in %. Hence, value F_{gl} 2 reflects significance of reference glacier in a area of basin; N is nimber of measurement years; Q_1 is average of Q(VI-VIII) as f(B_s), Q_2 is average of Q(VI-IX) as f(B_s), Q_3 is average of Q(VI-X) as f(B_s), Q_4 is average of Q(V-X) as f(B_s), V-X are the months May throuigh October.

Calculations of probabilities Q and B_s (empirical non-exceedance $X>x_i$) were done by the method from (Alexeev 1971):

$$p_i(x_i) = \frac{m(x_i) - 0.25}{N_i + 0.5} * 100 \qquad (1)$$

where $m(x_i)$ = 1, 2, ..., N_i - the sequence numbers of the values x_i after their arrangement in descending order.

Besides the determing empirical functions of distribution Q and B_s, there included selection of the most appropriate type of standard function of probability distribution (see parameter Freq B_s in the Table 3). The computer program in (Oosterbaan 1994) used for that purpose.

RESULTS AND DISCUSSION

In principle, the process of runoff formation from the glacier area and from the not glaciated surface measured on a point, located near the terminus of the glacier, includes such closely related characteristics as the intensity of melting, air temperature, solar radiation, clouds, and water vapor pressure in the air. This fact serves as a justification for the search for correlation $Q=f(B_s)$, which turned out to be quite successful on the example of four glaciers from seven in the Table 2. Variation in the coefficient R^2 for $Q = f(B_s)$ in the other three cases need further study, and they may be due to inaccuracies in determining the flow and/or summer balance B_s of glaciers, which was corrected (e.g. Dyurgerov and Meier 2005; Fluctuations of Glaciers Database 2017) and turned out to be not compatible in different sources of data.

Examples of subsequent use of dependencies $Q = f(B_s)$ on the Vernagtferner and Abramova glaciers, used to obtain equations Prob=$f(B_s)$, Freq Bs=$f(B_s)$, Prob $Y_1 \div Y_4$=f(Prob B_s), are presented in the table 3. Here Prob is statistical probability, and Freq B_s is the equation of the chosen standard function of probability distribution.

Forcing the line of dependences Prob $Y_1 \div Y_4$ = f(Prob B_s) through the origin of the coordinate axes in order to estimate the influence of the runoff from the non-glacial part of the basin leads to a slight decrease in the determination coefficient R^2. In this case, the values of R^2 for the glaciers Abramova and Hintereisferner in the order $Y_1 \div Y_4$, as

Table 3. Formulas for calculating the distribution functions of the mass balance B_s

Abramova Glacier			Vernagtferner Glacier		
Prob B_s / Freq B_s	Prob $Y_1 \div Y_4$= =f(Prob B_s); (Δ)	R^2	Prob B_s / Freq B_s	Prob $Y_1 \div Y_4$= f(Prob B_s) (Δ)	R^2
Prob B_s = -0.05B_s + 137.1 R^2 =0.97	Y_1 = 0.89 Prob B_s + +5.5; Δ=13.1	0.79	Prob B_s = -0.05 B_s +126.0 R^2= 0.98	Y_1 = 0.92 B_s+3.9; Δ=11.2	0.85
	Y_2 = 0.85 Prob B_s + +7.6; Δ=15.3	0.72		Y_2 = 0.93 B_s+3.5; Δ=10.6	0.86
Freq Bs = =1/{1+ +exp(A B_s+B)}	Y_3 = 0.86 Prob B_s + +6.9; Δ=14.6	0.74	Freq B_s = =1/{1+ +exp(A B_s^E+B)}	Y_3 = 0.95 B_s+2.5; Δ=9.0	0.90
A= -0.00246 B=4.6	Y_4= 0.85 Prob B_s + +7.5; Δ=15.2	0.72	E = 0.750 A= -2.29E-002 B=5.13	Y_4 = 0.94 B_s+2.9; Δ=9.6	0.89

Definition of symbols: B_s is summer mass balance, mm; Prob B_s is B_s statistical probability by formula (1), in %; Freq B_s is integral function of distribution, %; R^2 is coefficient of determination; Y_1 is equation to calculate Prob Q(Jun-Aug) as function of Prob B_s, Y_2 is equation to calculate Prob Q(Jun-Sep) as function of Prob B_s, Y_3 is equation to calculate Prob Q(Jun-Oct) as function of Prob B_s, Y_4 is equation to calculate Prob Q(May-Oct) as function of Prob B_s, Δ is RMS error of calculating Prob $Y_1 \div Y_4$, in %

in Table 3, are as follows: 0.78 (13.4), 0.70 (15.8), 0.73 (14.7), 0.70 (15.7) and 0.85 (11.3), 0.86 (10.8), 0.90 (9.1), 0.89 (9.7); the number in parentheses are the rms error of calculation Prob $Y_1 \div Y_4$, in%.

As an analogue of the glacial flow W_{gl}, it is also possible to use other known characteristics: data on the annual mass balance B_a, AAR, relationships between areas of accumulation and the entire glacier, and ELA, altitudinal boundary of equality between accumulation and ablation at the end of the ablation period. Annual information on the listed variables (except ELA) for 1971-2008 is contained in the work of Mernild et al. (2013). For glaciers in Table 3 it was not found to be useful to replace W_{gl} with B_a.

Spatial and temporal homogeneity of averaging mass balance data by sampling method

It is known, that the modern network of measurements of glacier mass balance components (B_a, B_s, B_w) includes several hundred objects (Dyurgerov and Meier 2005; Mernild et al. 2013; Zemp et al. 2015). Along with the diverse using of local time series on individual glaciers, the averaging of B_a and B_s is widely used on regional and global scales. For example, at averaging B_s over 10, 15, or 30 years during 1940-2016, in the sample remains unsynchronized spatial data only on consequently 56, 45, and 37 glaciers out of the total number of those in the WGMS network. Table 1 and Tables A1-2 present data density for decadal averaging of B_s for 56 glaciers and composition of the used sample. In addition to these, Tables 4-5 characterize the number of RGI 6 regions, where data of B_a are available for spatio-temporal averaging. After processing such information, Zemp et al. (2015) have determined decade-average B_a values for 19 regions of RGI 6 (RGI Consortium 2017).

As can be seen, the completeness and synchronicity of the time series B_a and B_s, presented in Fig. 1, 3, Tables 1, 4-5 and Tables A1-2, raise great doubts about the statistical validity of regional and global averages of B_a and B_s. Accordingly, this is reflected in the findings on the impact of these characteristics on the associated other natural processes, for example, relation to the climate change, changing the level of the ocean, etc.

Hydrological justification of the representativeness O_F B_s

Given the way in which was formed an empirical sample of 56 glaciers (see paragraph Introduction and Objectives of the

Table 4. Density of RGI 6 regions for spatial averaging of total data on B_a

Index	Ten-year time intervals						
	1941–50	1951–60	1961–70	1971–80	1981–90	1991–2000	2001–10
M	3	7	10	15	17	16	16
M_1 %	15.8	36.8	52.6	78.9	89.5	84.2	84.2

M – is actual number of RGI 6 regions, M_1 % – is percentage of M from possible maximum of RGI 6 regions, i.e. 19 in our case.

Table 5. Density of decades for temporal averaging of B_a at 19 regions of RGI 6

Index	Numbers of RGI 6 regions																		
	1	2	3	4	5	6	7	8	9	10	11	12	13	14	15	16	17	18	19
M	6	2	7	2	6	2	5	3	5	7	4	3	4	2	4	7	5	4	6
M_1 %	86	29	100	29	86	29	71	43	71	100	57	43	57	29	57	100	71	57	86

M – is actual number of decades in RGI 6 regions, M_1 % – is percentage of M from possible maximum of decades with B_a data in RGI 6 regions, i.e. 7 in our case.

research), it is evident that such a scanty sample cannot be representative regarding population of 215,547 (RGI Consortium 2017) continental glaciers on Earth. However, an estimate of the spatial representativeness of the summer mass balance measured on individual glaciers is of interest for the rationalization of methods for calculating and forecasting the flow of rivers fed by snow and ice melt.

The solution of this problem, obtained with the example of river basins in the Pamir-Alai and Central Caucasus (see Table 6), is based on an assessment of the effect of using local measurements of B_s as one of the main or additional arguments in the equations of multiple linear regression for calculation of the runoff for June-September and June-August. In this case we adopted model of river runoff W_{bas}, as a regression function of precipitation P and air temperature T, i.e. W_{bas}=f(P, T), where both arguments cover the certain characteristic intervals of time. In this combination of independent variables the seasonal air temperature is considered as the index of the thawed component of the river flow. The regression analysis also includes calculating, by means of Alekseev's method (1971), the relative contributions δ of independent variables T, P, and B_s for describing W_{bas} variance for VI-VIII, VI-IX, and IV-IX (June-August, June-September, and April-September) seasons. The expression in order to estimate δ for the independent variable no 1 has the general form:

$$\delta_1 = r_{01}^2 / (r_{01}^2 + r_{02}^2 + r_{03}^2) \tag{2}$$

where r_{01}^2 – is the square of paired correlation between the given function, labelled as 0, and independent variable no 1. And so on for the next variable in the numerator of (2) and the rest of the parameters δ.

Multi-year mass balance measurements, available on the Abramova and Dzhankuat reference glaciers (Dyurgerov and Meier 2005; Fluctuations of Glaciers Database 2017; Kamnyanskiy 2001), were used for modeling seasonal runoff W_{bas} in river basins of the Pamir-Alai and Central Caucasus, respectively. Local measurements of B_s on these glaciers might be considered representative at the basin scale, if it is true that B_s as an additional independent variable provides an increase in the coefficient of multiple linear correlation for equation W_{bas}=f(P, T). And also, if B_s can be used instead of T in the equation W_{bas}=f(P, T) for a certain basin.

After performing numerical experiments it is found out, that only in one catchment (the Akbura River) of six in the Pamir-Alai, the empirical equations W_{bas}=f(P, T) for calculating the river runoff for IV-IX, VI-IX and

Table 6. Glaciation in some watersheds of Pamir-Alai (P-A) and Central Caucasus (CC)

River basin	Outlet point	F_{bas}, km²	$\delta F_{gl}=F_{gl}/F_{bas}$, %	R1/R2
Isfara (P-A)	Tashkurgan	1560	8.3	0.78/0.73
Sokh (P-A)	Sarykanda	2480	10.2	0.91/0.79
Shahimardan (P-A)	Djidalik	1180	4.0	0.70/0.69
Isfayram-1 (P-A)	Uchkorgon	2200	4.6	0.72/0.56
Isfayram-2 (P-A)	Lyangar	697	14.6	0.76/0.60
Akbura (P-A)	Papan	2200	5.0	0.82/0.83
Baksan-1 (CC)	Zayukovo	2100	6.7	0.61/0.39
Baksan-2 (CC)	Tegenekly	210	27.1	0.58/0.73

R1 – coefficient of correlation for equation W_{bas}=f(P, T), R2 – the same parameter after using Bs instead of T in equation for W_{bas}

VI-VIII included data of the summer mass balance B_s on the Abramova glacier, located outside the Akbura basin. Here we used the next time averaging for the independent variables P, T, measured at meteorological stations: P(X-IV), T(VI-VIII).

As it seen from the Table 7, measurements of B_s on the Abramova glacier we may consider as basin-wide representative for calculating of seasonal runoff in the neighboring Akbura watershed by equation Wbas=f(P, T, B_s).

For estimating basin-wide applicability of the B_s frequency distributions obtained on the Abramova reference glacier (see Table 3), we used again W_{bas} data for the six Pamir-Alay river basins. After correlation analysis as of all basins, the highest R^2 coefficient between frequensies of W_{bas} and B_s for VI-IX and VI-VIII was in the Sokh river basin. There, the empirical equation for computing cumulative frequency distribution of Wbas(VI-VIII) by the corresponding of B_s data at the Abramova Glacier has coefficient of correlation, equal to 0.66. After that, for transition from the obtained frequency distribution value to the runoff data we should use equation W_{bas}(VI-VIII) =f(Freq W_{bas}(VI-VIII)), obtained earlier for the Sokh river basin. Consequently, this analysis also confirms limited basin-wide applicability of the B_s frequency distributions obtained on the Abramova reference glacier.

CONCLUSION

1. Research of the outlined problem, illustrated by the Tables 1-7 and Appendix A, (available at https://ges.rgo.ru) serves as the basis for the practically important transition from the local to the regional level of glaciological asessments by means of using the relationship between runoff and summer balance of glaciers. In this case, as repeatedly shown, the contribution of B_s in the formation of the river flow and, accordingly, the correlation Q=f(B_s) become weaker as the relative area of the glaciation decreases above the site of runoff measurement. However, it is still possible to use parameters (mean, extremums, coefficient of variation, etc.) of empirical functions of spatial and temporal distributions of B_s and Prob B_s, regardless of flow data and data from the World Glaciers Monitoring Service. The possible source of getting wide spread information about B_s is its determination (Davaze et al. 2018) as a function of the surface albedo of a glacier, measured by remote sensing at the end of ablation season.

2. The investigation has shown that the correlation coefficient between the total summer mass balance, characterizing the glacier's water output, and the river runoff W_{bas} at the hydrological outlet site for the time intervals: June-August, June-September, June-October, and May-October varies in a wide range: from 0.97 to 0.39 (Table 1). Study and understanding of this is still insufficient.

3. The hydrological representativeness of a glacier is a new characteristic, of practical importance for basin-wide tasks of hydrology and glaciology. For its evaluation, we propose to replace the seasonal air temperatures with the summer mass balance of glaciers B_s or to include B_s in the multi-

Table 7. Parameters of equations for calculating seasonal runoff W_{bas} in the Akbura river basin

Months	Mean W_{bas}, m^3/s	Equation for calculating W_{bas}	R^2	rmse	δ P	δ T	δ B_s
IV-IX	32.4	18.1-0.012B_s+5.77T+0.035P	0.70	3.0	0.41	0.21	0.38
VI-IX	38.7	23.8-0.016B_s+7.30T+0.038P	0.67	3.9	0.35	0.17	0.48
VI-VIII	44.3	27.2-0.012B_s+8.95T+0.044P	0.67	4.8	0.33	0.16	0.51

Definition of symbols: R^2 – coefficient of deternination; rmse – root mean square error of calculated W_{bas} in m^3/s; δ P, δ T, δ B_s – are consequntly relative contributions of precipitation P, air temeperature T, and B_s for describing W_{bas} variance.

ple regression equations for calculating the runoff of rivers fed by melting of snow and ice. This method can be recommended for at least of some glaciers in the existing network of the WGMS (World Glacier Monitoring Service).

ACKNOWLEDGMENTS

This research was supported from the budget of the Institute of Geography RAS in framework of scientific themes № 0148-2018-0008 and № 0148-2019-0004 and grants: RFBR № 16-35-60042, and MON RK: № AP05133077. These grants were accordingly used by E. Rets (Institute of Water Problems, RAS) and N. Pimankina (Institute of geography, Almaty, Kazakhstan).

REFERENCES

Aktru Glacier. (1987). Lednik Aktru. Leningrad: Gidrometeoizdat. (in Russian)

Alexeev G.A. (1971). Objective methods of smoothing and normalization of correlation dependencies. Leningrad: Hydrometeoizdat. (in Russian with English summary)

Bodo B.A. (2000). Monthly Discharges for 2400 Rivers and Streams of the former Soviet Union [FSU].

Borovikova L.N, Denisov Yu.M, Trofimova E.B. and Shentsis I.D. (1972). Mathematical modelling of mountain rivers runoff process. Leningrad: Hydrometeoizdat. (in Russian)

Braithwaite R.J. (2009). After six decades of monitoring glacier mass balance, we still need data but it should be richer data. Annals of Glaciology, 50, pp. 191-197.

Cogley J.G., Hock R., Rasmussen L.A., Arendt A.A., Bauder A, Braithwaite R.J., Jansson P., Kaser G., Möller M., Nicholson L. and Zemp M. (2011). Glossary of Glacier Mass Balance and Related Terms, IHP-VII Technical Documents in Hydrology No. 86, IACS Contribution No. 2, UNESCO-IHP, Paris.

Dahlke H.E., Lyon S.W., Stedinger J.R., Rosqvist G., and Jansson P. (2012). Contrasting trends in floods for two sub-arctic catchments in northern Sweden – does glacier presence matter? Hydrology and Earth System Sciences, 16, pp. 2123–2141. Available at: http://www.hydrol-earth-syst-sci.net/16/2123/2012/. doi:10.5194/hess-16-2123-2012

Davaze L., Rabatel A., Arnaud Y., Sirguey P., Six D., Letreguilly A., and Dumont M. (2018). Monitoring glacier albedo as a proxy to derive summer and annual surface mass balances from optical remote-sensing data. The Cryosphere, 12, pp. 271-286. doi: https://doi.org/10.5194/tc-12-271-2018

Dyurgerov M. and Meier M.F. (2005). Glaciers and the Changing Earth System: A 2004 Snapshot. Occasional Paper 58: Institute of Arctic and Alpine Research, University of Colorado, Boulder, CO.

Dzhankuat Glacier. (1978). Lednik Djankuat. Leningrad: Gidrometeoizdat. (in Russian)

Escher-Vetter H. and Reinwarth O. (1994). Two decades of runoff measurements (1974 to 1993) at the Pegelstation Vernagtbach/Oetztal Alps. Zeitschrift für Gletscherkunde und Glazialgeologie, Bd. 30 (1-2), pp. 53-98.

Fluctuations of Glaciers Database. (2017). World Glacier Monitoring Service, Zurich, Switzerland. DOI:10.5904/wgms-fog-2017-10. Available at: http://dx.doi.org/10.5904/wgms-fog-2017-10

Fountain A.G., Hoffman M.J., Granshaw F., and Riedel J. (2009). The 'benchmark glacier' concept – does it work? Lessons from the North Cascade Range, USA. Annals of Glaciology, 50, pp. 163-168.

Kamnyanskiy G.M. (2001). Total on measurement of mass balance on the Abramov Glacier in 1967-1988). Proceeding of SANIGMI, 161(242), pp. 122-131. (in Russian)

Konovalov V.G. (2014). Modelling and reconstruction the parameters of rivers runoff and glaciers mass balance on the Northern Caucasus. Ice and Snow. 3, pp. 16-30. (in Russian with English summary)

Konovalov V.G. (2015). New approach to estimate water output from regional populations of mountain glaciers in Asia. GES. Geography, Environment, Sustainability, 8(2), pp. 13-29.

Konovalov V.G. and Pimankina N.V. (2016). Spatial and temporal change the components of water balance on the Northern side of ZailiiskyAlatau. Ice and Snow, 56 (4), pp. 453-471. (in Russian with English summary)

Kotlyakov V.M., Osipova G.B., Popovnin V.V. and Cvetkov D.G. (1997). The last publications of the World Glaciers Monitoring Service: Traditions and Progress. MGI, 82, pp. 122-136. (in Russian)

Kotlyakov V.M. (ed). (1984). Glaciological Dictionary. Leningrad: Gidrometeoizdat. (in Russian)

Kotlyakov V.M., and Smolyarova N.A. (1990). Elsevier's Dictionary of Glaciology in Four Languages. Amsterdam: Elsevier.

Krimmel R.M. (2000). Water, Ice, and Meteorological Measurements at South Cascade Glacier, Washington, 1986-1991 Balance Years. U.S. GEOLOGICAL SURVEY Water-Resources Investigations Report 00-4006, 77 p.

Mernild S.H., Lipscomb W.H., Bahr D.B., Radić V. and Zemp M. (2013). Global glacier changes: a revised assessment of committed mass losses and sampling uncertainties. The Cryosphere, 7, pp. 1565-1577. DOI: https://doi.org/10.5194/tc-7-1565-2013

Oosterbaan R.J. (1994). Frequency and regression analysis of hydrologic data. Part I : Frequency analysis. Chapter 6 in: H.P.Ritzema (Ed.), Drainage Principles and Applications, Publication 16, second revised edition. International Institute for Land Reclamation and Improvement (ILRI), Wageningen, The Netherlands. ISBN 90 70754 3 39.

Rets E., Chizhova J., Budantseva N., Frolova N., Kireeva M., Loshakova N., Tokarev I., Vasil'chuk Y. (2017). Evaluation of glacier melt contribution to runoff in the north Caucasus alpine catchments using isotopic methods and energy balance modeling. GEOGRAPHY, ENVIRONMENT, SUSTAINABILITY 11, 3, pp. 4–19. https://doi.org/10.24057/2071-9388-2017-10-3-4-19

Rets E.P., Dzhamalov R.G., Kireeva M.B., Frolova N.L., Durmanov I.N., Telegina A.A., Telegina E.A., Grigoriev V.Y. (2018). RECENT TRENDS Of RIVER RUNOff IN THE NORTH CAUCASUS. GEOGRAPHY, ENVIRONMENT, SUSTAINABILITY, 11, 3, pp. 61-70. https://doi.org/10.24057/2071-9388-2018-11-3-61-70

Rets E.P., Frolova N.L. and Popovnin V.V. (2011). Modelling the melting of mountain glacier surface. Ice and Snow, 4, pp. 42-31.

RGI Consortium. (2017). A Dataset of Global Glacier Outlines: Version 6.0. DOI: https://doi.org/10.7265/N5-RGI-60.

NWIS Site Information for Alaska: Site Inventory Official Website. [online]

Available at: https://waterdata.usgs.gov/ak/nwis/inventory/?site_no=15478040&agency_cd=USGS [Accessed 29 Nov. 2018].

Vilesov E.N. and Uvarov V.N. (2001). Evolution of present day glaciation in Zailiisky Alatau over the 20 century. Almaty: Kazak University. (in Russian with English summary).

WaSiM-ETH. Official Website. [online] WaSiM model. (2015). Available at: http://www.wasim.ch/en/the_model.html [Accessed 06 June. 2018].

Zemp M., Hoelzle M. and Haeberli W. (2009). Six decades of glacier mass-balance observations: a review of the worldwide monitoring network. Annals of Glaciology, 50, pp. 101-111.

Zemp M., Frey H., Gärtner-Roer I., Nussbaumer S.U., Hoelzle M., Paul F., Haeberli W., Denzinger F., Ahlstrøm A.P., Anderson B., Bajracharya S., Baroni C., Braun L.N., Cáceres B.E., Casassa G., Cobos G., Dávila L.R., Delgado Granados H., Demuth M., Espizua L., Fischer A., Fujita K., Gadek B., Ghazanfar A., Hagen J.O., Holmlund P., Karimi N., Li Z., Pelto M., Pitte P., Popovnin V.V., Portocarrero C.A., Prinz R., Sangewar C.V., Severskiy I., Sigurðsson O., Soruco A., Usubaliev R., Vincent C. (2015). Historically unprecedented global glacier decline in the early 21st century. Journal of Glaciology, 61(228), pp. 745-761. DOI: 10.3189/2015JoG15J017

Received on June 30th, 2018 Accepted on November 15th, 2018

Pavel G. Panin[1*], Svetlana N. Timireva[1], Tatyana D. Morozova[1], Andrey A. Velichko[1 (†)]

[1] Institute of Geography, Russian Academy of Sciences, Moscow, Russia

***Corresponding author:** pgpanin@igras.ru

MICROMORPHOLOGY OF THE LATE AND MIDDLE PLEISTOCENE PALEOSOLS OF THE CENTRAL EAST EUROPEAN PLAIN

ABSTRACT. In this paper we focused on the micromorphology of the Late and Middle Pleistocene paleosols exposed in twelve loess-paleosol sequences sections in the central part of the East European Plain. Each studied paleosol complex known as Mesin (MIS 5), Kamenka (MIS 6 (8) - 7 (9)), and Inzhavino (MIS 8 (10) - 9 (11)) pedocomplexes (PCs) consists typically of two members, the earlier – main – phase of the soil development taking place during an interglacial, and the later one – at the subsequent interstadial time. Interglacial paleosols formation is associated with the thermal optimum of climatic macrocycles and corresponds to conditions close to modern in the territory under consideration. Interstadial paleosols formation characterizes the intervals within the glacial period, accompanied by an increase in heat and moisture. However, the heat supply of such intervals did not reach modern level in this region (Velichko and Morozova 2015). As follows from the analysis of the soil micromorphology over the studied area, the soil microstructure experienced notable changes under changing latitudinal zonality. During the interglacial periods clay coatings and Fe-Mn pedofeatures dominated the soil microfabric; in the south loess-paleosol sequences coatings are in negligible quantities, Fe-Mn pedofeatures decrease in amount, and carbonate pedofeatures appear instead. In the microfabric of the interstadial paleosols, Fe-Mn pedofeatures are abundant, but unlike interglacial paleosols, the coatings are rare. Basically, the coatings are humus-clayey in composition, but in the more southern sections coatings are absent.

KEY WORDS: Loess, loess-paleosol sequences, interglacial, interstadial, morphology, soil, climate

CITATION: Pavel G. Panin, Svetlana N. Timireva, Tatyana D. Morozova, Andrey A. Velichko (2019) Micromorphology of the Late and Middle Pleistocene paleosols of the central East European Plain. Geography, Environment, Sustainability, Vol.12, No 1, p. 34-62
DOI-10.24057/2071-9388-2018-32

INTRODUCTION

The central part of the East European Plain is known as one of the main loess regions (Velichko and Khalcheva 1982; Velichko et al. 1994, 2006; Haase et al. 2007). In the sequences loess alternate with paleosols. Principal phases of the paleosol formation fall in interglacials (MIS 5e; 7 (9); 9 (11)); later on, as the climate became cooler, vegetation changed accordingly and interstadial soils (MIS 5c (5); 6; 8) developed (Velichko et al. 2007). The soil formation process practically stopped during the ice ages, and the loess accumulated on the soil surface. So loess-paleosol sequences (LPS) record and keep information of the soils of past epochs (Velichko and Morozova 2015; Zykin and Zykina 2015; Sycheva and Khokhlova 2016; Sedov et al. 2016; Tabor et al. 2017; Costantini 2017; Panin et al. 2018). Quite a number of studies were aimed at the paleosol sequences on the East European Plain (Morozova 1981; Bolikhovskaya 1995; Velichko 2002; Rusakov and Korkka 2004; Dlussky 2007; Panin 2007; Glushankova 2008; Sycheva et al. 2017; a.o.). The multidisciplinary approach used in those studies (including analyses of the soil morphology and micromorphology, paleomagnetic characteristics, physical and chemical properties, pollen analysis, etc) provided a possibility of reconstructing landscapes and climates of the past. Attempts at reconstructing soils of the Mikulino, Kamenka, and Likhvin interglacials and of the Bryansk Interstadial were made by Morozova (1995), Velichko (2002) and Dlussky (2001, 2007). The authors, however, did not pay much attention to changes in paleosols under conditions of changing soil zonality in the interglacial and interstadial periods.

In paper we focus the attention on the micromorphology of the Late and Middle Pleistocene paleosols. The micromorphological studies of paleosols make it possible to recognize specific features of the soil structure at the micro-level (Matvishina 1982; Bronger and Heinkele 1989; Bronger et al. 1998; Nettleton et al. 2000; Kemp 1999; Kemp 2013; a.o.). In particular, that approach permits to identify pedofeatures of Ca, Fe and Mn, and also other features that may be interpreted as manifestations of certain soil-forming processes (Gerasimova et al. 1992; Fedoroff et al. 2010). Together with physical-chemical characteristics and description of the paleosol morphology, the study of the micromorphology provided an insight into the type of soil formation and made it possible to reconstruct the paleosols of the central East European Plain in the Late and Middle Pleistocene. The purpose of this work is to identify changes in the microstructure and other micromorphological features of paleosols in different latitudinal zones of the soil cover of the center of the East European Plain in the Late and Middle Pleistocene.

MATERIALS AND METHODS

The present work is based on the materials of the Middle and Late Pleistocene paleosols studied in comparison with today's soils existing in the central East European Plain. The sections considered here (Fig. 1) were analyzed by the authors of this paper and partly published in their earlier works. Among the sections, are Gololobovo (Panin 2007; Panin 2015; Little et al. 2002; Chizhikova et al. 2007), Ozherelye and Mikhnevo (Panin 2007), Suvorotino (Panin 2007), Bogolyubovo (Velichko et al. 1996), Likhvin (Little et al. 2002), Bryansk and Arapovichi (Velichko and Morozova 1963; Morozova 1981), Korostelyovo (Velichko 2002), Sebryakovo-Mikhailovka (Velichko et al., 2006), Gun'ki (Velichko et al. 1997) and Strelitsa-2017. In those sections the Late Pleistocene (Mezin paleosol complex, PC) and Middle Pleistocene (Kamenka PC and Inzhavino PC) paleosols were exposed together with the surface soils.

Here we use the latest variant of the chronostratigraphic scheme (Table 1) as suggested by A.A. Velichko and his colleagues (Velichko and Morozova 2015; Velichko et al. 2011). There exists, however, another variant of correlation between stratigraphic horizons and the marine isotope stages, also in wide use (Velichko and Morozova 2010). According to it, the Romny paleosol is correlated with MIS 7, and paleosols of Kamenka and Likhvin interglacials – with MIS 9 and MIS 11 respectively.

The sections are exposed in the brickyard quarries or cut in steep valley slopes where surface soils are present – Greyzemic Phaeozems, Haplic and Calcic Chernozems. The modern soils in many quarries have been stripped away; some sections in valley scarps are often devoid of the upper humus horizons (sections Bogolyubovo and Gololobovo).

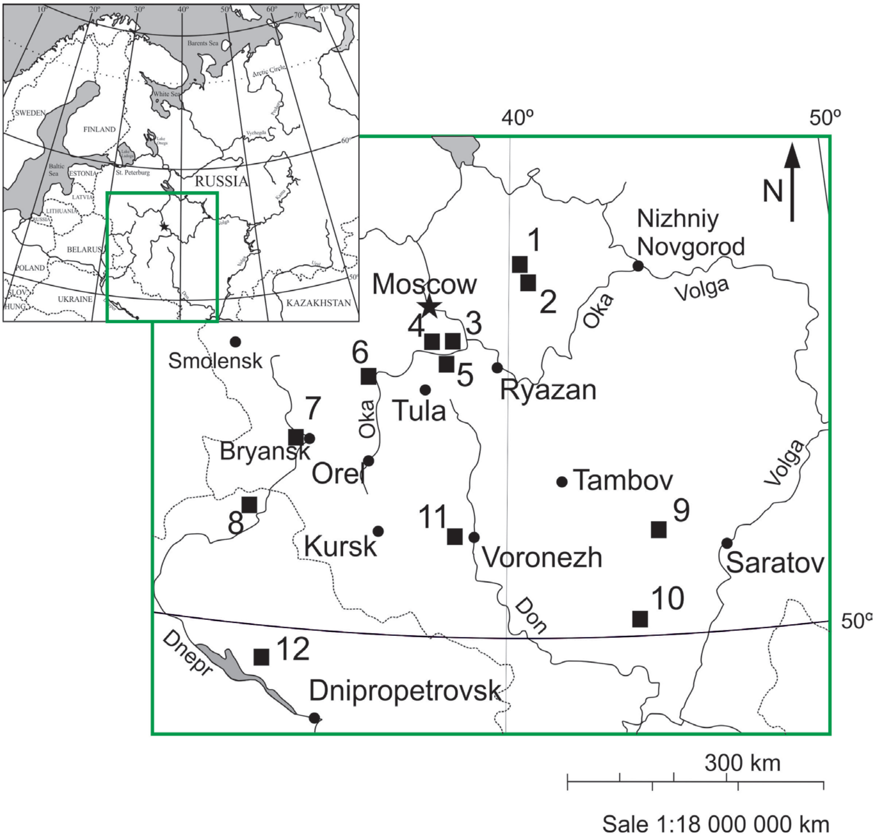

Fig. 1. Position of the studied sections

Table 1. Chronostratigraphic scheme of the East European Plain (Velichko and Morozova 2010; Velichko and Morozova 2015; Velichko et al. 2011)

Ice ages	East European loess region		MIS variant 1	MIS variant 2	Age of paleosol, ka
Holocene			1	1	~ 11.7
Valday Glaciation	Altynovo loess		2	2	-
	Trubchevsk paleosol				-
	Desna loess				-
	Bryansk paleosol		3	3	~ 25 - 32
	Khotylevo loess		4	4	-
	Mezin paleosol complex	Krutitsa interstadial paleosol	5c	5	~ 98 - 105
		Sevsk loess	5d		-
Mikulino Interglacial		Salyn interglacial paleosol	5e	5e	~ 117 - 135

<table>
<tr><td rowspan="7">Dnieper Glaciation</td><td colspan="2">Moscow loess</td><td rowspan="7">6</td><td rowspan="3">6</td><td>-</td></tr>
<tr><td colspan="2">Kursk interstadial paleosol</td><td>-</td></tr>
<tr><td rowspan="3">Dnieper loess</td><td>Loess</td><td>-</td></tr>
<tr><td>Romny (?) interstadial paleosol</td><td>7</td><td>-</td></tr>
<tr><td>Orchik (?) loess</td><td rowspan="3">8</td><td>-</td></tr>
<tr><td rowspan="3">Kamenka paleosol complex</td><td>Late Kamenka interstadial paleosol (?)</td><td>-</td></tr>
<tr><td>Loess</td><td>-</td></tr>
<tr><td>Kamenka (Chekalin) Interglacial</td><td>Early Kamenka interglacial paleosol</td><td>7</td><td>9</td><td>~ 200 - 250</td></tr>
<tr><td rowspan="3">Pechora Glaciation</td><td colspan="2">Borisoglebsk loess</td><td rowspan="3">8</td><td rowspan="3">10</td><td>-</td></tr>
<tr><td rowspan="3">Inzhavino paleosol complex</td><td>Late Inzhavino interstadial paleosol</td><td>-</td></tr>
<tr><td>Loess</td><td>-</td></tr>
<tr><td>Likhvin Interglacial</td><td>Early Inzhavino interglacial paleosol</td><td>9</td><td>11</td><td>~ 380 - 410</td></tr>
<tr><td>Oka Glaciation</td><td colspan="2">Oka loess</td><td>10
11
12</td><td>12</td><td>-</td></tr>
</table>

During the field survey a detailed morphological description (Rozanov 2004) of every section was performed along with sketching, taking photographs, and sampling. Samples for physical and chemical analyses and for micromorphological studies have been taken from every genetic horizon at 15–20 cm intervals. In order to properly interpret the fossil soil genesis, the surface soils were also sampled with the aim of a comparison with samples from paleosols.

Earlier investigations resulted in acquiring abundant materials on physical-chemical characteristics and micromorphological data that gave us an insight into the development, structure, and properties of paleosols, both interstadial and interglacial ones (Velichko and Morozova 1963; Velichko and Morozova 1972; Velichko and Morozova 2010; Velichko et al. 1985; Panin 2007; Panin 2015). It follows from the results obtained that the interstadial paleosols both of Late and Middle Pleistocene developed under grass steppe vegetation under conditions of lesser heat supply than those formed during interglacials. Typically, the interglacial paleosols formed under forests (Velichko and Morozova 2015).

The paleosol micromorphology was studied in thin sections (<30 μm thick) impregnated with polysynthetic resin. In describing thin sections and interpreting the soil formation processes we followed the techniques described in literature (Gerasimova et al. 1992; Gerasimova et al. 2011). Thin sections were photographed under a polarized-light microscope Motic BA310Pol at 4X/0.1 magnification. The paper includes descriptions of micromorphology and photographs for sections Gololobovo, Mikhnevo, Ozherelye and Sebryakovo-Mikhailovka, where both studied paleosols and surface soils.

Along with the investigation of the micromorpholology and morphology, the following components were determined in the paleosols: organic carbon, obtained using wet combustion technique developed by Tyurin (Rastvorova et al. 1995); amorphous iron compounds, by Tamm's method (Tamm 1922), and non-silicate iron compounds, by Mehra and Jackson (1960). All the analyses were performed in the Chemical Analytical Laboratory, Institute of Geography, Russian Academy of Sciences.

The genetic horizons in soil profiles are marked in accordance to the FAO (2006) (Table 2). The names of the surface soils and paleosols are given in according of the IUSS Working Group WRB 2014 (2015).

RESULTS

Table 2 presents the surface soils and buried paleosols and gives information on their thickness, contents of organic carbon and their soil profile. LPS include several PC of the Late and Middle Pleistocene age. The greatest assortment of paleosols (besides the surface soil) was found in the Strelitsa-2017 section. There have been recorded a well pronounced Bryansk (MIS 3) and Romny (MIS 6 or 7) paleosols, as well as Mezin, Kamenka, Inzhavino, and Voronskiy PCs (MIS

Table 2. Characteristics of the modern soils and paleosols studied in the LPS sections

Section number (see Fig. 1)	Names of sections (coordinates of the location of the sections)	Soil profile	Soil profile thickness, m	Organic carbon content in upper horizons max, %
Surface soil (Holocene) - MIS 1				
1	Suvorotino (56°13′08»N, 40°27′08″E)	A-EBt-Bt-BC	1.45	1.76
2	Bogolyubovo (56°12′22″N, 40°33′00″E)	Btp-Bt1-Bt2	1.50	no data
3	Gololobovo (55°2′49″N, 38°35′29″E)	Btp-Bt-BCt	2.75	0.30
4	Mikhnevo (55° 7′03″N, 37°59′06″E)	Ap-EBt-Bt-BCk	1.33	1.03
5	Ozherelye (54°48′37″N, 38°17′54″E)	Ap-AE-Bt	1.15	0.32
6	Likhvin (54° 6′19″N, 36°15′26″E)	Ap-ABt-Bt-BCk	3.12	2.38
7	Bryansk (53°13′14″N; 34°20′53″E)	A-Bt1-Bt2-Bt3-BC	1.25	2.03
8	Arapovichi (51°56′52″N, 33°19′01″E)	O-A-B-BC-C	1.50	0.70
9	Korostelyovo (51°50′28″N, 42°24′58″E)	O-A-ABk-Bk	1.68	3.92
10	Sebryakovo-Mikhailovka (50°07′02″N, 43°12′46″E)	A-AB-Bk-BCk	1.95	1.85
11	Strelitsa-2017 (51°37′15″N, 38°54′09″E)	Ap-Bk-BCk	0.84	no data
12	Gun′ki (49°14′32″N, 33°34′15″E)	A-Bk	0.40	1.16

Mezin paleosol complex (Late Pleistocene)				
Krutitsa interstadial paleosol – MIS 5c				
1	Suvorotino	A@	0.30	0.19
2	Bogolyubovo	ABg@	0.45	0.59
3	Gololobovo	A@	0.75	0.27
5	Ozherelye	A@	0.22	0.25
6	Likhvin	Al@-Bh	0.35	0.38
7	Bryansk	A@1-A@2-AE	0.20	0.37
8	Arapovichi	Ak@-A@	0.70	1.40
9	Korostelyovo	Aks@	0.65	0.59
10	Sebryakovo-Mikhailovka	A@	0.54	no data
11	Strelitsa-2017	Ak@-ABk	1.15	no data
12	Gun'ki	A@	0.80	0.70
Salyn interglacial paleosol – MIS 5e				
1	Suvorotino	E-Bt-BC	1.20	0.15
2	Bogolyubovo	E@-Bt	0.30	no data
3	Gololobovo	AE@-E-Bt	0.35	0.12
5	Ozherelye	ABt@-Bt	0.23	0.22
6	Likhvin	AE@-B1@-Bg	0.85	0.50
7	Bryansk	EB-Bt@-Bt-BC	2.40	0.04
8	Arapovichi	EBt@-Btk1-Btk2-BCt	2.20	0.45
9	Korostelyovo	ABk-BCk	0.99	0.43
10	Sebryakovo-Mikhailovka	Ay@-By	1.88	0.58
11	Strelitsa-2017	Ak@-Bk	1.62	no data
12	Gun'ki	Bk	1.10	0.46
Kamenka paleosol complex (Middle Pleistocene)				
Late Kamenka interstadial paleosol – MIS 6 (8)				
3	Gololobovo	A@	0.35	0.21
5	Ozherelye	A@	0.22	0.10

4	Mikhnevo	A@	<0.10	no data
9	Korostelyovo	A@	1.10	0.55
10	Sebryakovo-Mikhailovka	A@	0.81	0.25
11	Strelitsa-2017	A@	0.12	no data
12	Gun'ki	A@	0.90	0.29
Early Kamenka interglacial paleosol – MIS 7 (9)				
3	Gololobovo	EBt-Bt	1.40	0.11
4	Mikhnevo	Bt@	0.78	0.25
5	Ozherelye	EBt-Bt	2.30	0.09
6	Likhvin	Btg-BCg1-BCg2	0.85	0.27
9	Korostelyovo	A-Bk	0.77	0.43
10	Sebryakovo-Mikhailovka	B-BC	1.27	0.17
11	Strelitsa-2017	A@-AB-Bk-BCk-BC	2.03	no data
12	Gun'ki	Bk	1.20	0.07
Inzhavino paleosol complex (Middle Pleistocene)				
Late Inzhavino interstadial paleosol – MIS 8 (10)				
3	Gololobovo	A@	0.37	0.16
5	Ozherelye	A@	0.35	0.17
9	Korostelyovo	Ak@1-Ak@2	0.94	0.39
10	Sebryakovo-Mikhailovka	Ak@	1.04	0.38
11	Strelitsa-2017	Ak@	0.14	no data
Early Inzhavino interglacial paleosol – MIS 9 (11)				
3	Gololobovo	E@-Bt1-Bt2	1.95	0.05
5	Ozherelye	EBt-Bt	0.60	0.10
6	Likhvin	Et@-Bt@-BC-BCg	1.95	0.27
9	Korostelyovo	Bk1-Bk2	0.90	0.25
10	Sebryakovo-Mikhailovka	Bk	0.42	0.17
11	Strelitsa-2017	A@-E-Bg	0.30	no data

Surface soils (MIS 1)

13-15). In the Bogolyubovo section (northern part of the loess zone) there are found the Bryansk paleosol and Mezin PC only.

The majority of studied sections – Suvorotino, Bogolyubovo, Gololobovo, Mikhnevo, Ozherelye, Likhvin, Bryansk and Arapovichi – are within the limits of the latitudinal zone of Greyzemic Phaeozems soils, while a few other localities feature Haplic and Calcic Chernozems. As seen in Table 2, in Greyzemic Phaeozems the maximum content of organic carbon is 2.03%, in the latitudinal zone of Haplic and Calcic Chernozems the maximum is 3.92%.

In the Mikhnevo section coatings are extremely rare in the humus horizon of Greyzemic Phaeozems. The micromorphology of horizons Bt abounds typically in clayey and humus-clayey coatings (Fig. 2a, b), both the coating size and organic carbon content increasing downwards. Pedofeatures of Fe-Mn composition are seen in horizon EBt (Fig. 2c, d). In the Sebryakovo-Mikhailovka section Chernozems the groundmass of the humus horizon is well aggregated. Thin sections of horizon Bk display pale yellowish - brown color, aggregate structure; there are carbonate nodules (Fig. 2e, f). Horizon BCk is noted for carbonate nodules increasing sharply in number (Fig. 2g, h).

The Late Pleistocene Mezin paleosol complex

There are two paleosols in the sequence representing the Mezin PC: the Krutitsa interstadial and Salyn interglacial ones. The Krutitsa interstadial soil consists mostly of humus horizons (A and AB) and is no more than 1 m thick. The soil thickness is slightly greater in the south of the East European Plain (0.54 to 0.80 m in sections Korostelyovo, Sebryakovo-Mikhailovka, Gun'ki) and does not exceed 0.70 m farther north (see Table 2). The paleosol is mostly described as brownish-gray loam of crumby structure. The Salyn interglacial paleosol consists of horizons AB, AE, E, and Bt, the total thickness of the soil reaching 2.4 m (Bryansk section). The Salyn soil is mostly composed of loam and sandy loam with crumby and angular to subangular blocky structure, brown and bright-brown in color. Albic horizon is present as separate whitish lenses of sandy loam. The Krutitsa paleosol is distinguished for a high organic carbon content (up to 1.40%). In the Salyn interglacial paleosol the organic carbon content is less than in the Krutitsa one and does not exceed 0.58%.

In the interstadial Krutitsa paleosol of Ozherelye section hypo-coatings and coatings located in pores are mostly humus-clay in composition (Fig. 3a, b) and large granular aggregates (Fig. 3c, d). In Sebryakovo-Mikhailovka section there are no coatings, while Fe and Fe-Mn nodules appear instead (Fig. 3e). The humus horizon microstructure is well aggregated. Similar granular aggregates are seen as in the interstadial paleosol of the Gololobovo section, only of a smaller size (Fig. 3f). Large diamond-shaped and ungeometrical crystals (Fig. 3g, h) are distinctly seen, which is typical for gypsum pedofeatures (Kubiena 1938; Gerasimova et al. 1992; Poch et al. 2010). The transitional horizon between the interstadial and interglacial paleosols is free of gypsum. Gypsum pedofeatures are characteristic for paleosols of the Mezin PC in the southern sections of the Azov Sea (Panin et al. 2018).

The microstructure of the Salyn interglacial paleosol sampled in the Gololobovo section (horizon AE@) features large grains of quartz (Fig. 4a) and the appearance of granular aggregates (Fig. 4b). B-fabric of the groundmass is speckled and crystallitic. Albic horizons contain Fe nodules. In the horizon Bt the coatings are mostly of humus-clay composition (Fig. 4c). They are usually of compact structure, dark brown or yellow color, are mostly confined to pores. In the Sebryakovo-Mikhailovka section small-size Fe-Mn nodules occur in horizon Ay@ (Fig. 4d, e). Pedofeatures of gypsum (Fig. 4f, g) and carbonate (Fig. 4h) were recorded in the horizons Ay and By of the interglacial paleosol.

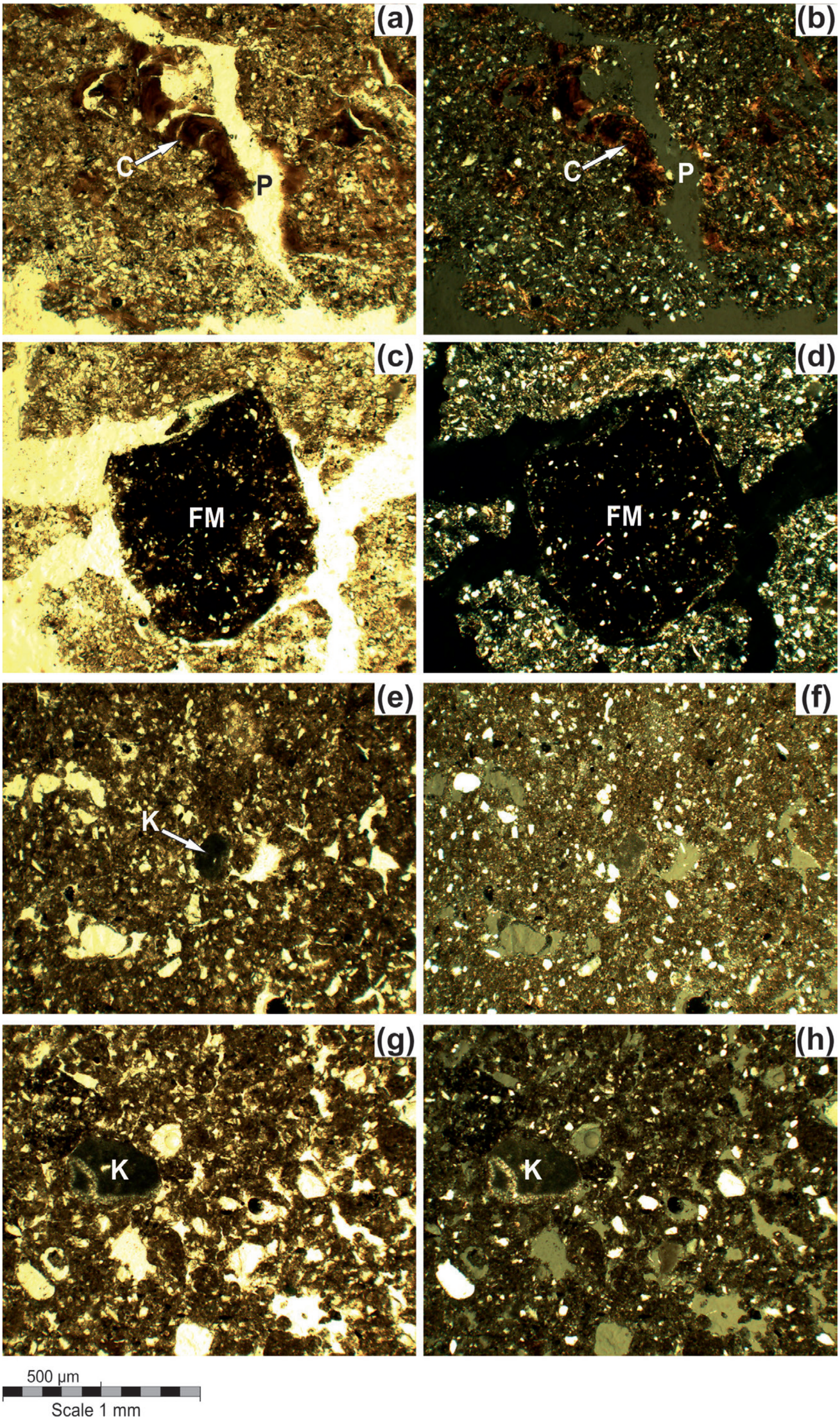

Fig. 2. Micromorphology of the surface soil: a – the horizon Bt, Mikhnevo section (PPL); b – the same (XPL); c – the horizon EBt, Mikhnevo section (XPL); d – the same (XPL); e – the horizon Bk, Sebryakovo-Mikhailovka section (PPL); f – the same (XPL); g - the horizon BCk, Sebryakovo-Mikhailovka section (PPL); h – the same (XPL). Symbols in the figures: C – coating, P – plane, FM – Fe-Mn pedofeatures, K - carbonate nodule

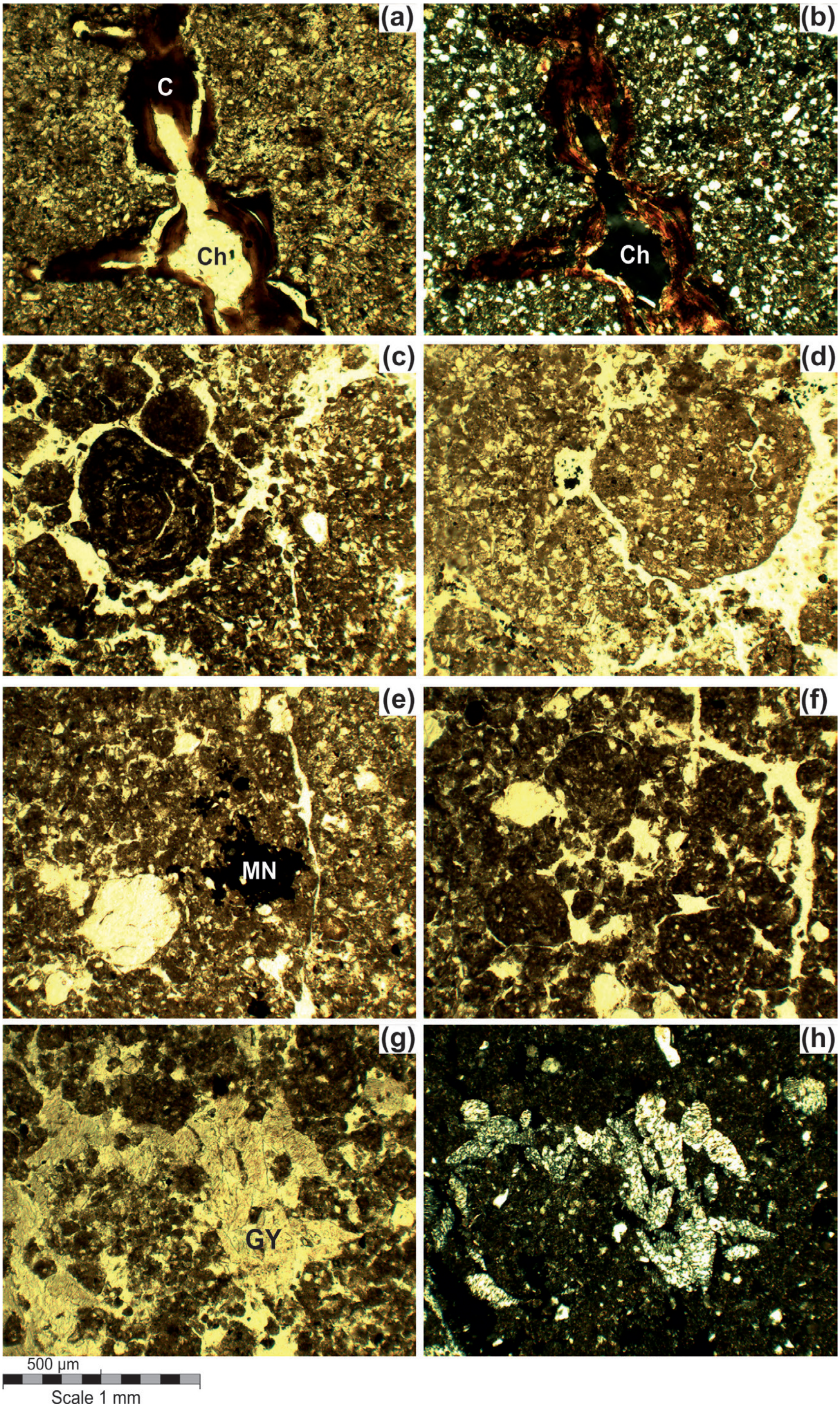

Fig. 3. Micromorphology of the Krutitsa interstadial paleosol: a – the horizon A@, Ozherelye section (PPL); b – the same (XPL); c, d - the horizon A@, Gololobovo section (PPL); e, f, g – the horizon A@, Sebryakovo-Mikhailovka section (PPL); h – the horizon A@, Sebryakovo-Mikhailovka section (XPL). Symbols in the figures: C – coating, Ch – channel, MN – Mn pedofeatures, GY - gypsum pedofeatures

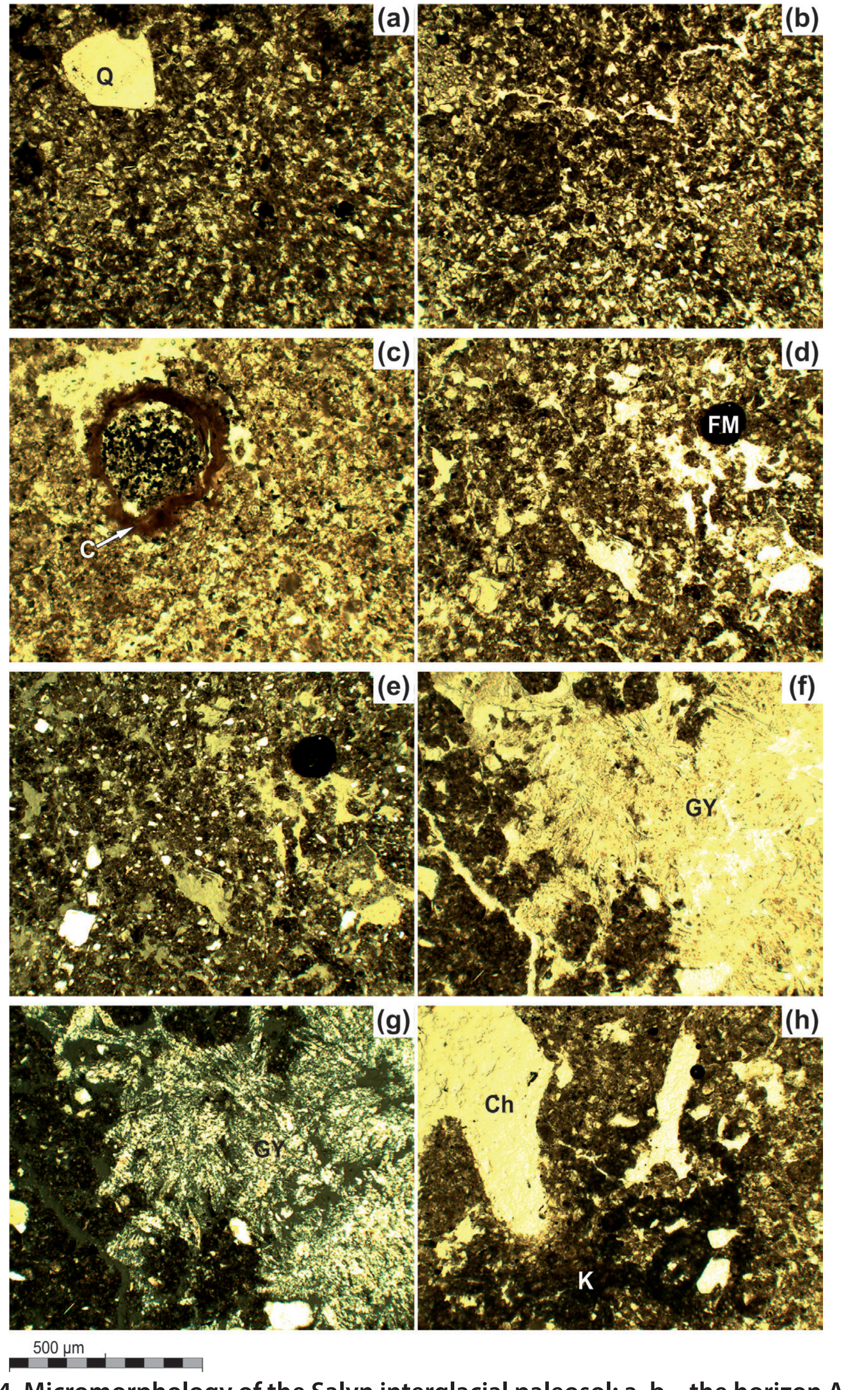

Fig. 4. Micromorphology of the Salyn interglacial paleosol: a, b – the horizon AE@, Gololobovo section (PPL); c – the horizon Bt, Gololobovo section (PPL); d – the horizon Ay@, Sebryakovo-Mikhailovka section (PPL); e – the same (XPL); f - the horizon By, Sebryakovo-Mikhailovka section (PPL); g – the same (XPL); h - the horizon By, Sebryakovo-Mikhailovka section (PPL). Symbols in the figures: Q – quartz, C – coating, Ch – channel, FM – Fe-Mn pedofeatures, K - carbonate nodule, GY - gypsum pedofeatures

The Middle Pleistocene Kamenka paleosol complex

The Middle Pleistocene Kamenka PC includes two paleosols – late Kamenka interstadial paleosol and early Kamenka interglacial one (Table 2). According to morphological descriptions, the interstadial paleosol consists of a humus horizon 0.22 m (Ozherelye section) to 1.10 m (Korostelyovo section) thick. As is seen in Fig. 5, the Kamenka PC in sections Mikhnevo (Fig. 5a) and Strelitsa-2017 (Fig. 5b) is heavily cryoturbated. Horizon A@ of the late Kamenka interstadial paleosol is present in the cryogenic wedge-like structures penetrating into the early Kamenka interglacial paleosol.

The maximum organic carbon content in the interstadial paleosol is 0.55% (Korostelyovo section). The interglacial paleosol profile shows lesser proportions of organic carbon (0.43%) as compared with the interstadial soil. In common with the interstadial paleosol, the maximum content of both is found in the Korostelyovo section.

The late Kamenka interstadial paleosols are mostly characterized by gray-brown groundmass of humus-clay composition. The paleosol described in Ozherelye section is noted for a predominance of humus-clay coatings around channels (Fig. 6a, b). There is also Fe-Mn nodules present in the soil. The groundmass is penetrated by cracks, which led to the destruction of the coatings (Fig. 6c, d). In terms of micromorphology, the humus horizon in the Sebryakovo-Mikhailovka section is characterized by brownish-gray color and aggregate structure (Fig. 6e, f). The groundmass is silty-clay. The b-fabric is striated and speckled.

The early Kamenka interglacial paleosols differ noticeably from the interstadial ones in the coating quantity and variability of their composition. In the horizon EBt dominant are laminated light brown and brown coatings, mostly clayey (Fig. 7a) in composition (Ozherelye section). There are Fe-Mn pedofeatures present here (Fig. 7b, c). In the horizon Bt the clayey coatings are confined to ancient pores (Fig. 7d). The groundmass

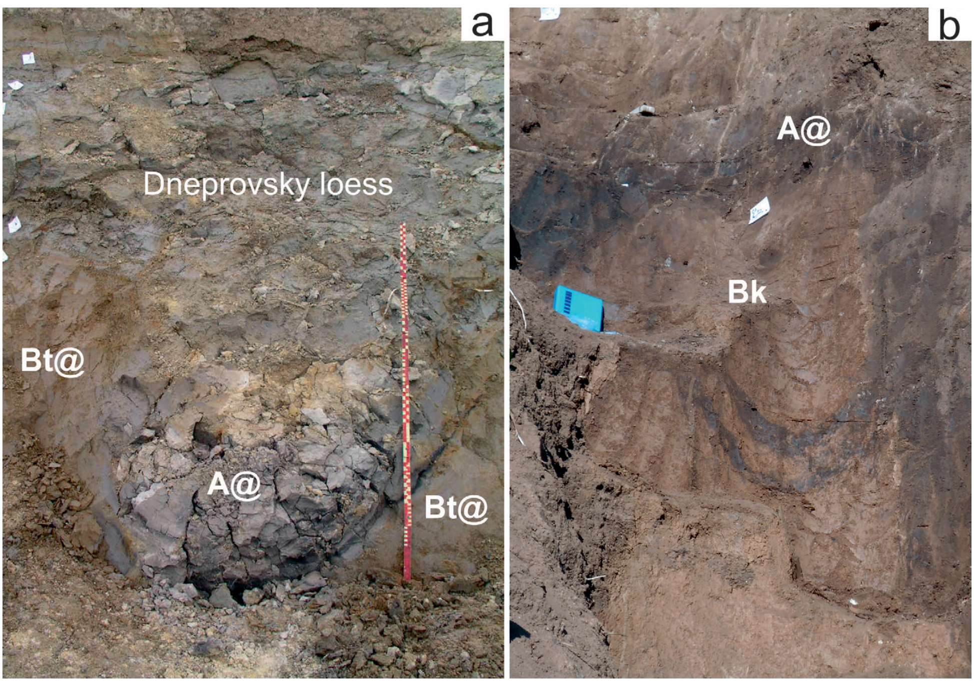

Fig. 5. Morphology of the Kamenka PC: a) Mikhnevo and b) Strelitsa-2017 sections. Symbols in the figures: horizon A@ of the interstadial paleosol, horizons Bt@ and Bk of the interglacial paleosol

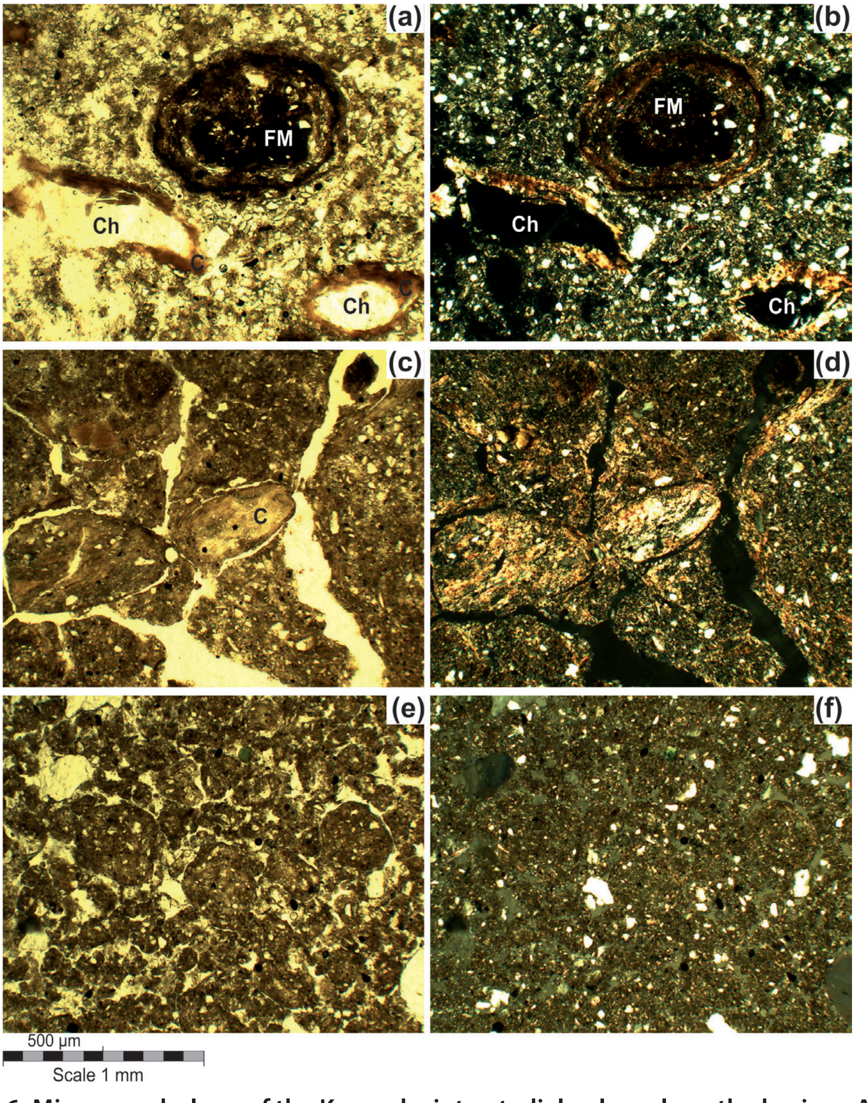

Fig. 6. Micromorphology of the Kamenka interstadial paleosol: a – the horizon A@, Ozherelye section (PPL); b - the same (XPL); c - the horizon A@, Ozherelye section (PPL); d - the same (XPL); e –- the horizon A@, Sebryakovo-Mikhailovka section (PPL); f – the same (XPL). Symbols in the figures: C – coating, Ch – channel, FM – Fe-Mn pedofeatures

both in upper and lower parts of the interglacial soil profile is light-brown. In the Sebryakovo-Mikhailovka section the interglacial paleosol microstructure is typically well aggregated (Fig. 7e). The soil in thin section is brownish. Carbonate and Fe-Mn nodules occurs over the entire interglacial soil profile (Fig. 7f, g, h).

The Middle Pleistocene Inzhavino paleosol complex

The Inzhavino PC lies stratigraphically below Kamenka PC; in common with the latter it consists of two paleosols: the late Inzhavino interstadial paleosol and the early Inzhavino interglacial one. Cryoturbations are clearly distinguishable in the Inzhavino PC in all the sections (Gololobovo section, see Fig. 8). Interstadial pa-

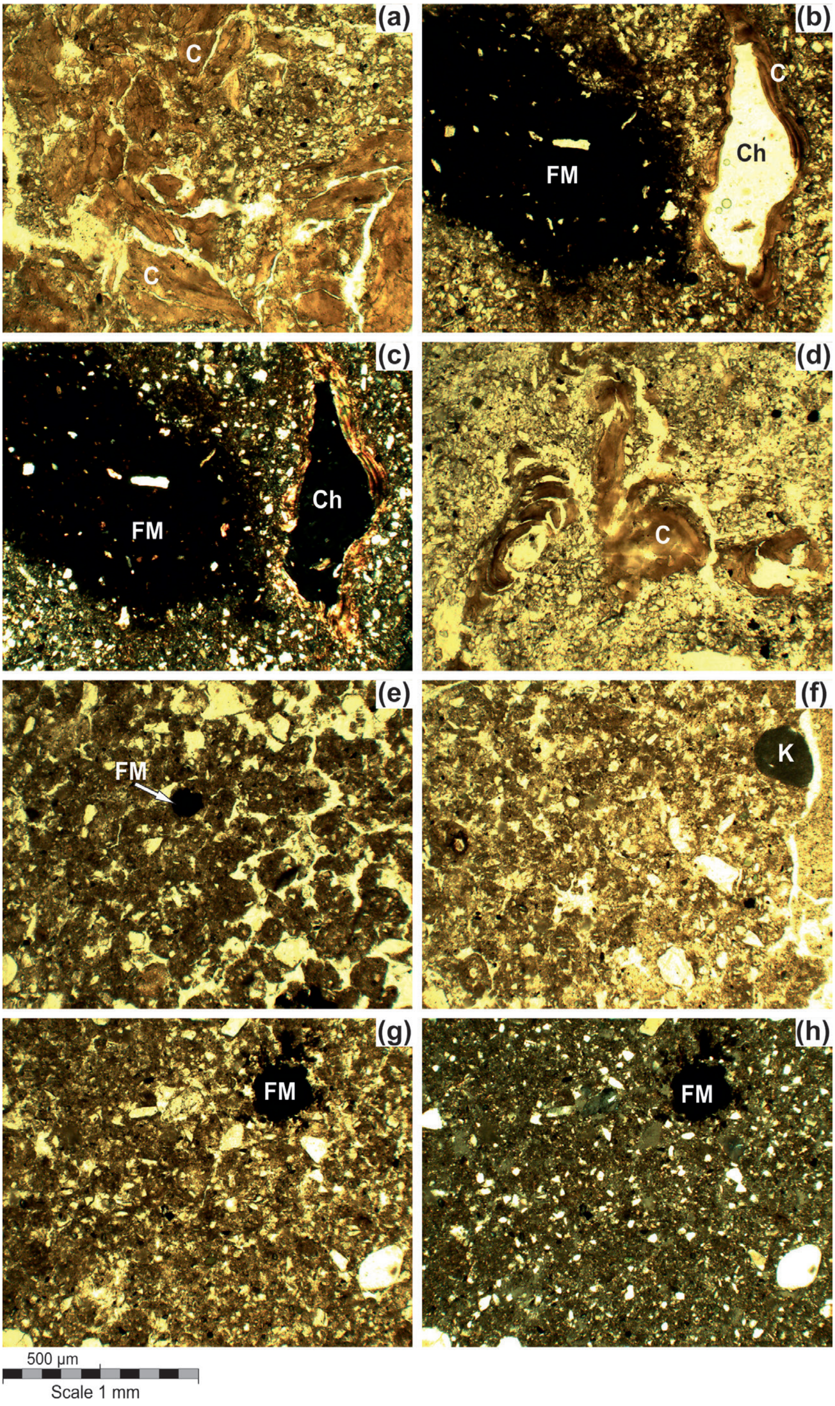

Fig. 7. Micromorphology of the Kamenka interglacial paleosol: a, b – the horizon EBt, Ozherelye section (PPL); c – the horizon EBt, Ozherelye section (XPL); d – the horizon Bt, Ozherelye section (PPL); e, f - the horizon B, Sebryakovo-Mikhailovka section (PPL); g – the horizon BC, Sebryakovo-Mikhailovka section (PPL); h - the same (XPL). Symbols in the figures: C – coating, Ch – channel, FM – Fe-Mn pedofeatures, K - carbonate nodule

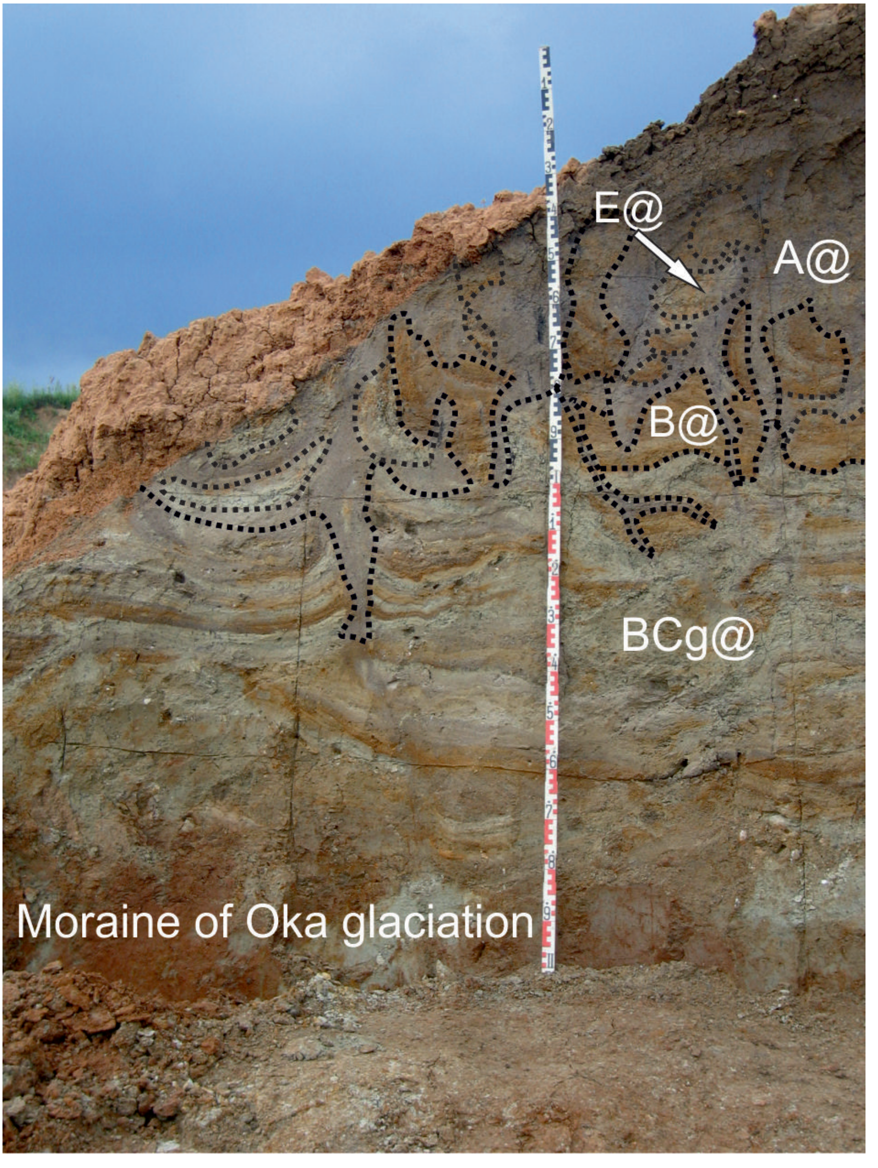

Fig. 8. Morphology of the Inzhavino PC: horizon A@ of the interstadial paleosol, horizons E@ and B@, BCg@ of the interglacial paleosol

leosols have brownish-gray humus horizon composed of clay loam. The thickness of the paleosols varies from 0.14 to 1.04 m (Table 2). The maximum organic carbon content in the interstadial paleosol is 0.39% (Korostelyovo section).

The albic horizon is present in the profile of interglacial paleosols studied in sections Gololobovo, Ozherelye, Strelitsa-2017 and Likhvin. In the interglacial paleosols the dominant colors are dark and bright-brown argic horizons; albic horizons composed of sandy loam are whitish. In sections Korostelyovo and Sebryakovo-Mikhailovka there is no albic horizon in the soil and the profile consists of argic horizons only.

In the interglacial paleosol studied in the Gololobovo section there is a distinctly pronounced albic horizon where iron

Table 3. Physical and chemical characteristics of the Inzhavino PC soils

Genetic horizons	pH	Iron fractions, %	
		Fe_o	Fe_d
A@	8.05	0.18	0.98
E@	8.40	0.14	0.34
Bt1	8.20	0.21	0.93
Bt2	8.25	0.17	1.05

content – both of oxalate extractable iron (Feo) and dithionite extractable iron (Fed) - drops noticeably (Table 3).

The microstructure of the interstadial paleosols sampled in the Gololobovo section displays granular aggregates in horizon A@ (Fig. 9a, b). Coatings of humus-clay and clay composition are recognizable in thin sections under microscope, together with Fe pedofeatures (Fig. 9c, d). Coatings located in pores up to 1 mm in diameter are composed of humus and clay particles, laminated. In the Sebryakovo-Mikhailovka section the interstadial paleosol is characterized by brown coloration in thin section, granular aggregate microstructure, silty-clayey groundmass with admixture of coarse sand (Fig. 9e, f). Packing voids are well pronounced, as well as chambers.

The interglacial paleosol exposed in the Gololobovo section (horizon E) contains large Fe-Mn nodules (Fig. 10a, b), though no coatings. Lower in the profile, in horizon Bt, coatings, mostly clayey, appear and increase in number downwards (Fig. 10c, d). The b-fabric is speckled. The groundmass of the interglacial paleosol shows a silty-clay composition in the Sebryakovo-Mikhailovka section (Fig. 10e, f). There are also large (more than 1 mm in diameter) carbonate concretions and Fe-Mn nodules (Fig. 10g, h).

DISCUSSION

Synthesis of paleoenvironmental data obtained as a result of integrated studies of the loess-soil sequences in the central East European Plain made possible to trace the principal stages in the soil evolution in the region over ~400 000 years, that is, since the Middle Pleistocene to the present days. Table 4 summarizes the results of the micromorphological studies of the Loess-Paleosol Sequences. A relative abundance (Stoops 2003) of Fe-Mn, carbonate, and gypsum pedofeatures, as well as coatings is given.

According to Urusevskaya (2011), the main processes in the Albic Retisols (latitudinal zone I) are lessivage, humus accumulation and mineral acid hydrolysis. The leading soil-forming processes in the Greyzemic Phaeozems (latitudinal zone II) are ground leaf litter formation, humus accumulation, acid hydrolysis of minerals and lessivage. The microstructure of both Greyzemic Phaeozems and Albic Retisols are distinguished by an abundance of Fe and Mn pedofeatures (Table 3), indicative of wetting (Gerasimova et al. 1992; Zaidel'man and Nikiforova 2010; Lindbo et al. 2010). In the Chernozems (III latitudinal zone) development the leading processes were as follows: ground leaf litter formation, humus accumulation, active structuring due to biogenic processes and flocculation, and carbonate redistribution due to eluvial and illuvial processes (Chernova 2011). The microstructure of Chernozems is noted, besides Fe-Mn pedofeatures, for carbonate nodules present in abundance.

The Late Pleistocene Mezin paleosol complex

The presence of humus-clayey coatings, together with a relatively high humus content in the Krutitsa interstadial paleosol (exposed in Suvorotino, Bogolyubovo, Gololobovo, Mikhnevo, Ozherelye, Likhvin, Bryansk, Arapovichi sections), suggests a

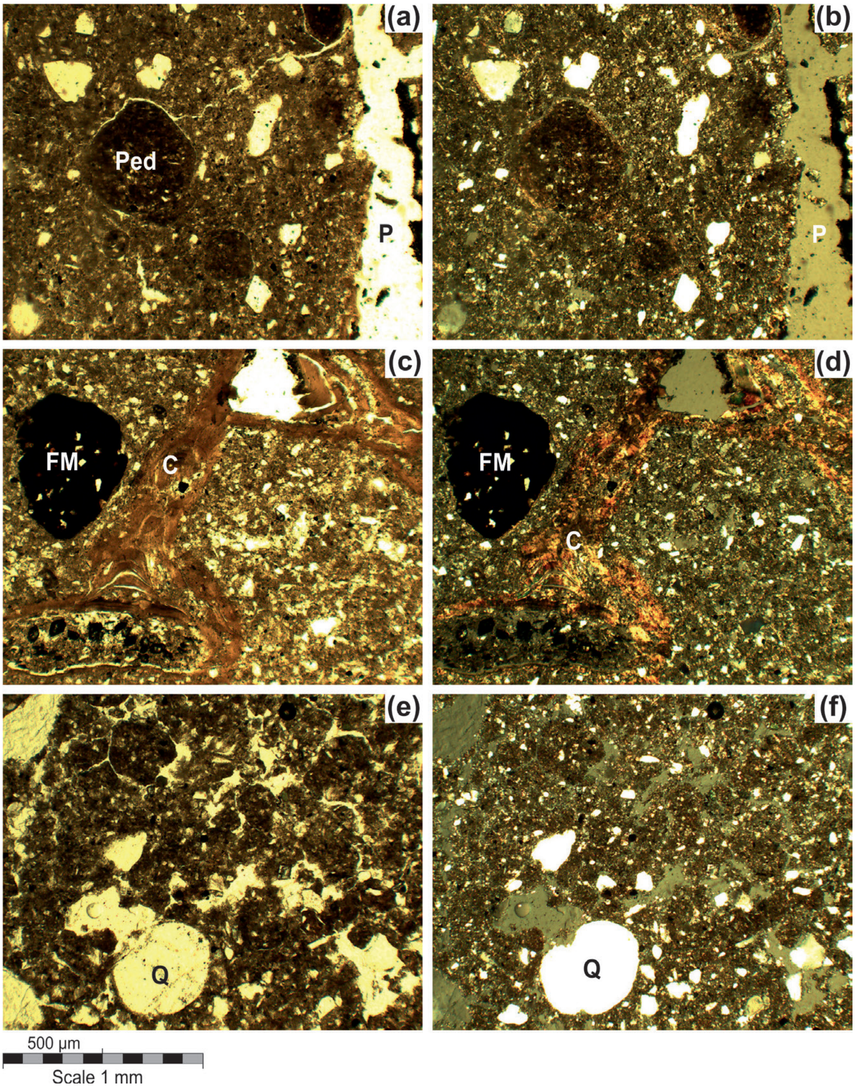

Fig. 9. Micromorphology of the Inzhavino interstadial paleosol: a – the horizon A@, Gololobovo section (PPL); b - the same (XPL); c – the horizon A@, Gololobovo section (PPL); d – the same (XPL); e – the horizon A@, Sebryakovo-Mikhailovka section (XPL); f - the same (XPL). Symbols in the figures: Ped - soil aggregate, C – coating, P – plane, FM – Fe-Mn pedofeatures, Q – quartz

leading role of humus accumulation processes. Large granular aggregates and were formed in the paleosols as a result of cryogenic processes (Van Vliet-Lanoë 1998; Van Vliet-Lanoë 2010; Todisco and Bhiry 2008; Villagran et al. 2013), in the Russian literature, these aggregates are called «ooid aggregates» (Morozova 1965; Gerasimova et al. 1992). The influence of cryogenic processes on the soil profile is also well expressed at the macro level. In the morphological description, large permafrost wedges are distinguished in the soil profile, as for example in horizons A@ Kamenka (Fig. 5) or Inzhavino (Fig. 8) PC. Taking into consideration the small thickness of their profile (0.42 m), the listed characteristics suggest a certain similarity of those paleosols to modern imperfectly developed Gleyic Chernozems (Panin 2007; Panin 2015; Velichko and Morozova 2015) formed under steppe vegetation (Novenko et al. 2008). In

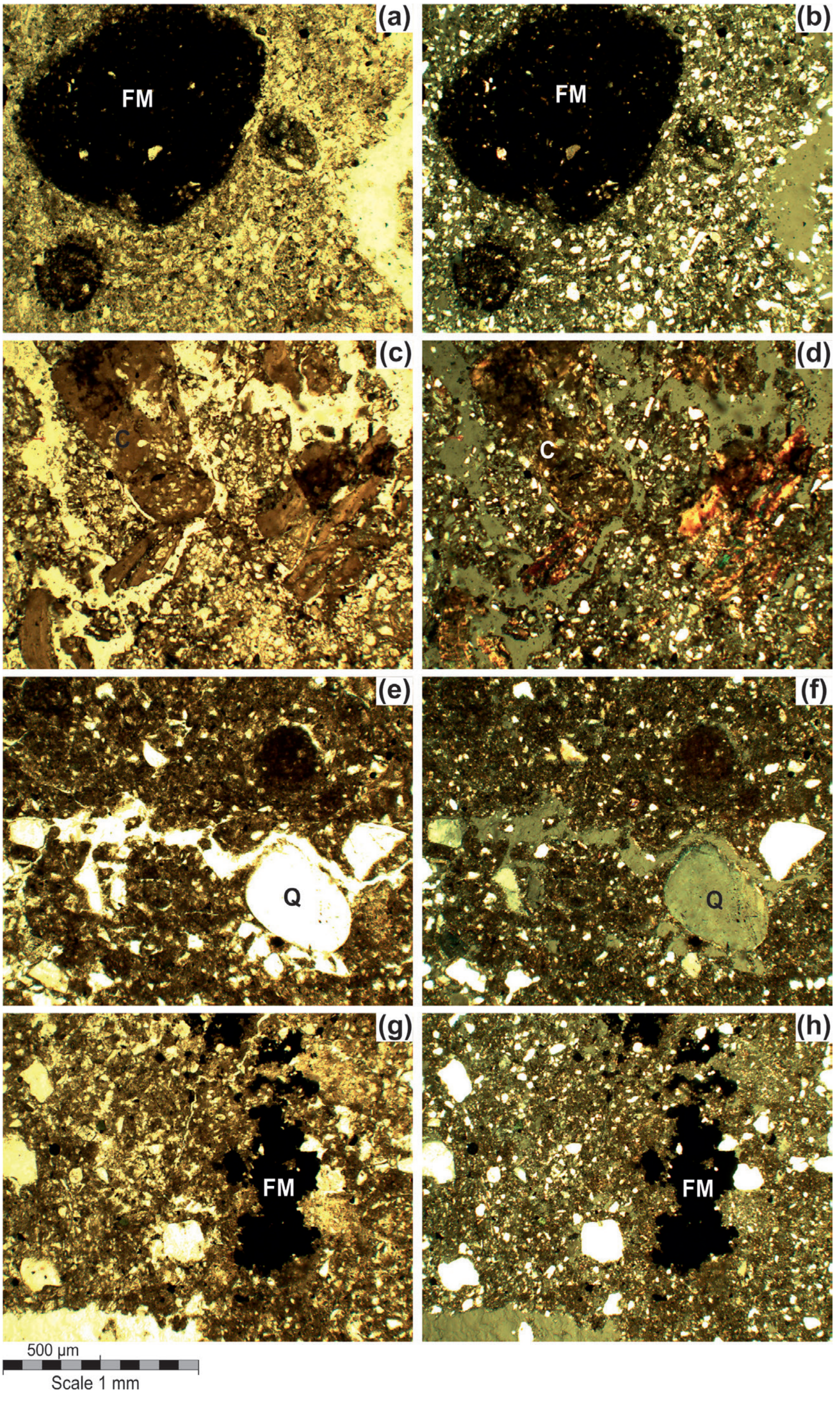

Fig.10. Micromorphology of the Inzhavino interglacial paleosol: a – the horizon E@, Gololobovo section (PPL); b - the same (XPL); c – the horizon Bt, Gololobovo section (PPL); d – the same (XPL); e – the horizon Bk, Sebryakovo-Mikhailovka section (PPL); f - the same (XPL); g – the horizon Bk, Sebryakovo-Mikhailovka section (PPL); h - the same (XPL). Symbols in the figures: FM – Fe-Mn pedofeatures, C – coating, Q – quartz

Table 4. Comparison between characteristics of the surface soil and paleosols microstructure (– = absent; + = very few, ++ = common, +++ = frequent, ++++ = dominant)

Latitudinal zone (see Fig. 11)	Names of sections	Pedofeatures			
		Fe and Mn	Clay coating	Carbonate	Gypsum
Surface soil (Holocene) (Fig. 11A)					
I (Albic Retisols)	-	+++	+++	-	-
II (Greyzemic Phaeozems)	Suvorotino, Bogolyubovo, Gololobovo, Mikhnevo, Ozherelye, Likhvin, Bryansk, Arapovichi	+++	++++	-	-
III (Chernozems)	Korostelyovo, Sebryakovo-Mikhailovka, Strelitsa-2017, Gun'ki	+	-	+++	-
Salyn interglacial paleosol (Fig. 11B)					
I (Albic Retisols)	Suvorotino, Bogolyubovo	++++	++	-	-
II (Greyzemic Phaeozems and Retisols)	Gololobovo, Mikhnevo, Ozherelye, Likhvin, Bryansk, Arapovichi	++	+++	+	-
III (Gypsic Chernozems or Gypsic Kastanozems)	Korostelyovo, Sebryakovo-Mikhailovka, Strelitsa-2017, Gun'ki	+	+	+++	++++
Early Kamenka interglacial paleosol (Fig. 11C)					
I (Cambisols)	Suvorotino, Bogolyubovo, Gololobovo, Mikhnevo, Ozherelye, Likhvin, Bryansk, Arapovichi, Strelitsa-2017, Gun'ki	+++	++++	-	-
II (Chernozems)	Korostelyovo, Sebryakovo-Mikhailovka	++	-	+++	-
Early Inzhavino interglacial paleosol (Fig. 11D)					
I (Albic Retisols and Greyzemic Phaeozems)	Gololobovo, Mikhnevo, Ozherelye, Likhvin, Bryansk, Arapovichi, Strelitsa-2017	++++	++++	-	-
II (Chernozems)	Korostelyovo, Sebryakovo-Mikhailovka, Gun'ki	+++	-	++	-

sections Korostelyovo, Sebryakovo-Mikhailovka, Gun'ki and Strelitsa-2017 the microstructure of interstadial paleosols is distinct for large regularly shaped gypsum crystals; according to Gerasimova et al. (1992), such crystals may develop under conditions of continuous, or long-term, presence of water in the soil, which makes possible the crystal growth. Most likely gypsum was introduced by eolian processes and formed crystals of rhomboid forms in the process of soil-formation. The considered soils may be classified with Gypsic Chernozems.

In the Salyn paleosol microstructure there is a clearly traceable albic horizon that contains Fe-Mn nodules, clayey coatings are present in the argic horizon (Suvorotino, Bogolyubovo sections). The described characteristics permit the soil to be classified as texture-differentiated soils. In the Gololobovo, Ozherelye, Likhvin, Bryansk, Arapovichi sections Fe-Mn nodules become less pronounced in the Salyn paleosol microstructure, while the coatings gain in abundance. There are clayey coatings of illuviation, undoubtedly indicative of lessivage (transportation of clay matter). According to Novenko et al. (2008), at the beginning of the Mikulino Interglacial the studied region was dominated by spruce communities, pine and birch-pine forests; later on, oak forests appeared with elm, ash, and maple. As suggested by the pollen analysis data, that time was marked by an increase in moisture supply and the stagnant water persisting on the land surface. The considered Salyn paleosol described in Suvorotino and Bogolyubovo sections may be classified as Albic Retisols, in the Gololobovo, Ozherelye, Likhvin, Bryansk, Arapovichi sections the paleosol is assigned to Greyzemic Phaeozems. The results obtained are in a good agreement with conclusions by Sycheva (1998) on Retisols being also formed near the Aleksandrovsky Quarry (51°36'09"N, 36°06'51"E) in the Interglacial.

In Sebryakovo-Mikhailovka, Korostelyovo, and Gun'ki sections the Salyn soil micromorphology studies revealed the presence of large rhomb-shaped pedofeatures of gypsum and carbonates. Similar forms of gypsum were described in the Salyn paleosol in the Azov Sea region (Velichko et al. 2017a; Velichko et al. 2017b; Panin et al. 2018); that gives ground for suggestion on a similarity in the soil-forming processes all over the south of the East European Plain. Gypsum is present in the soil as a concentration of small and larger crystals. Presumably, it could be related to fluctuations of the humidity, when the soil profile was repeatedly dried up (Minashina and Shishov 2002; Poch et al. 2010). As compared with northern regions, the soil profile is richer in organic carbon (0.49%), its thickness is 1.32 m. Taking into consideration the presence of gypsum and carbonates in the soil and well aggregated groundmass, one may suggest that the paleosol development followed the Chernozem type. The considered soils may be compared, therefore, with modern Gypsic Chernozems or Gypsic Kastanozems. According to Glushankova (2012), soils at the Korostelyovo section vicinities at the Mikulino Interglacial were represented by a combination of forest and meadow-chernozem soils.

The Middle Pleistocene Kamenka paleosol complex

The interstadial paleosol known as late Kamenka has much in common in its genesis with the Krutitsa interstadial paleosol. In the northern sections (Gololobovo, Ozherelye, Mikhnevo) studies of the soil microstructure revealed humus-clayey coatings, along with Fe nodules and carbonate pedofeatures. There are traces of cryoturbations recognizable in the paleosol profile. It may be concluded that the Kamenka interstadial paleosols are practically identical to those of Krutitsa in their characteristic. In the Gololobovo, Mikhnevo, Ozherelye sections in the studied region the paleosols are comparable with imperfectly developed modern Gleyic Phaeozems (Panin 2007, 2015; Velichko and Morozova 2015). Paleosols of the Korostelyovo, Sebryakovo-Mikhailovka, Strelitsa-2017 and Gun'ki sections are attributed to imperfectly developed Kastanozems and Haplic Kastanozems, or to imperfectly developed Haplic Chernozems.

Studied in sections Gololobovo, Ozherelye, Mikhnevo, and Likhvin, the Kamenka interglacial is typically noted for a thick profile (1.33 m, on average) and bright brown color. The interglacial soil profile consists primarily of horizons AB, EBt and Bt. The microstructure displays Fe-Mn pedofeatures and Fe nodules indicative of abundant wetting of the upper horizons. The whitish albic horizon does not stand out morphologically; at the level of microstructure the groundmass is brown or light brown in color. It may be attributed to the presence of clayey coatings; the latter filling completely pores and preventing iron compounds from penetrating deeper, so that the albic horizon turns brown due to the iron presence (Bronnikova and Targulyan 2005). The main soil-forming processes that took part in the paleosol profile development are lessivage, clayization, humus accumulation and illuviation. As follows from the micro-biomorphic analysis, the early Kamenka interglacial paleosol developed under broadleaf forests. Those paleosols may be classified as Cambisols, developed under broadleaf forests (Glushankova and Agadjanian 2015). The modern analogs of those soils are found in Central Europe, in particular, in the Vistula River basin (Świtoniak and Charzyński 2014).

In the Sebryakovo-Mikhailovka and Korostelyovo sections, the early Kamenka interglacial paleosol is aggregated in microstructure; there are pedofeatures of carbonates and Fe nodules, indicative of warm and wet climate at the time of soil development (Kovda et al. 2016). The groundmass is well aggregated, with granular structure, the soil profile thickness is 1.08 on average, organic carbon content is 0.25%. Based on those characteristics, the soil may be placed in the group of Chernozems.

The Middle Pleistocene Inzhavino paleosol complex

The microstructure studies performed on the late Inzhavino interstadial paleosol exposed in Gololobovo and Ozherelye sections revealed the dominance of humus-clayey coatings, and the presence of Fe nodules. The entire paleosol profile is 0.36 m thick on the average, organic carbon content amounts to 0.17%. The main soil-forming processes that account for the soil appearance are humus accumulation, lessivage, and surficial gleying. Hence the interstadial paleosols may be classified as Gleyic Phaeozems. There are morphologically distinct humus horizons in the interstadial paleosols of the Korostelyovo and Sebryakovo-Mikhailovka sections bearing recognizable traces of cryogenic processes. Granular aggregates are seen in their microstructure, along with carbonate pedofeatures. The average thickness of the paleosol profiles amounts to 0.99 m, organic carbon content is 0.39%. Unlike interstadial paleosols of the Mezin and Kamenka PC, gypsum pedofeatures are practically absent from the paleosol, which suggests a wetter climate than that of the subsequent interstadials. Calcic Chernozems developed under meadow steppe now may be taken as modern analogs of that paleosol.

The early Inzhavino paleosol is dated to the Likhvin Interglacial. Its profile is 1.5 m thick on the average, organic carbon is 0.17%. A whitish albic horizon is clearly seen in the soil profile. In common with other interglacial paleosols, there are numerous coatings (clayey and silty-clayey ones) in the Inzhavino paleosol microstructure. Our data gave grounds to assign the soil to texture-differentiated group, under coniferous-broadleaf forests (Glushankova and Agadjanian 2015). Among the modern soils Albic Retisols in combination with Greyzemic Phaeozems may be considered as their analogs.

In the Korostelyovo and Sebryakovo-Mikhailovka sections the early Inzhavino soil profile is, on average, 0.66 m thick, organic carbon content is 0.21%. The microstructure features carbonates, the groundmass is well aggregated, silty-clayey in composition, contains Fe-Mn nodules. The Likhvin interglacial paleosols in the region may be classed with Chernozem ones. The present-day analogs of the paleosols are Chernozems under meadow steppe (Glushankova and Agadjanian 2015).

The studies performed on the paleosol series revealed the latitudinal zone typical of the regional soils during that interval: chernozemic soils of the southern arid regions changed northward into humid texturally-differentiated soils. In the interglacial periods the soil zonation resembled closely the modern latitudinal zone. At interstadials, poorly developed Chernozems were most widespread under meadow-steppe vegetation. Fig. 11 shows the geographic distribution of present-day soils of the central East European Plain and reconstructed paleosols attributed to the Mikulino, Kamenka, and Likhvin interglacials. In addition, some data used in the reconstructions were taken from published materials on LPS studied in the sections: Aleksandrovsky Quarry (Sycheva 1998; Sycheva and Sedov 2012; Sycheva et al. 2017), Mikhailovka (Agadjanian and Glushankova 2017), Afonino (Dlussky 2007), Likhvin (Lazukov and Chebotareva 1977), as well as sections published by Dlussky (2001), Markov (1977), Yakimenko (1995), Dodonov and Velichko (2003), Glushankova (2008, 2012), Glushankova and Agadjanian (2015), Bolikhovskaya and Molodkov (2006), Virina et al. (2000), a.o.

As can be seen from Table 4, the quantity of Fe-Mn pedofeatures and coatings decreases from north to south, while the quantity of carbonates increases to the south. First of all, this could be due to a change in the amount of precipitation. So for surface soils of I and II (Fig. 11) zones, the average annual precipitation is 540 - 650 mm, and for III zone is 300 - 560 mm per year. The same

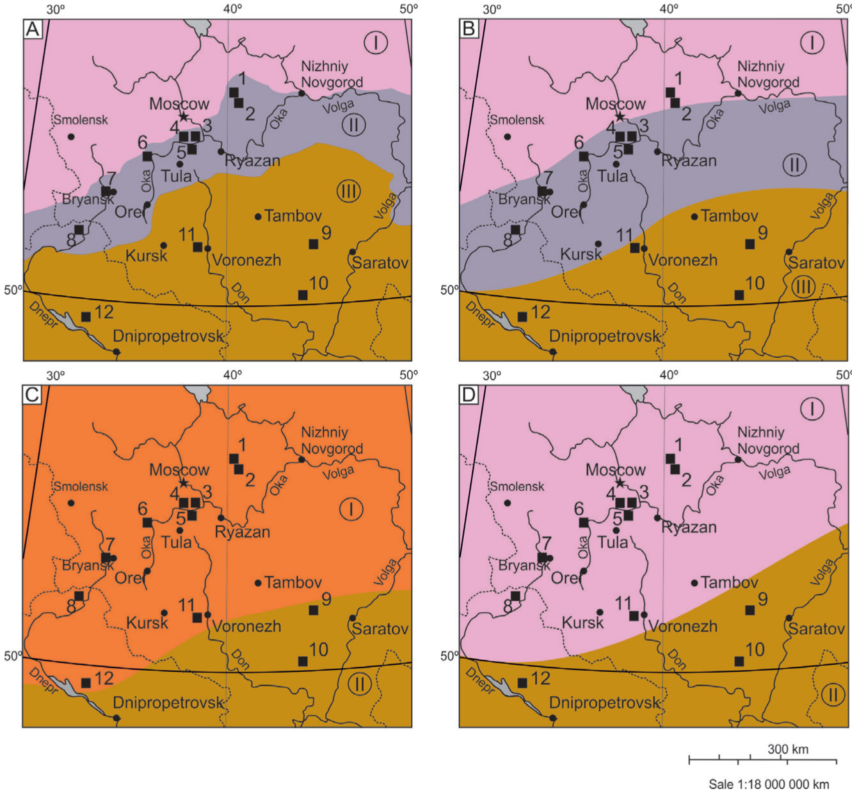

Fig. 11. Reconstructions of the geographic distribution of the paleosols of the interglacials and the surface soils (numbers on the maps correspond to those in Fig. 1):
A – surface soils (Urusevskaya et al. 2011): I – Albic Retisols zone; II – Greyzemic Phaeozems zone in combination with Retisols; III – Chernozems zone;
B – reconstructed paleosols of the Mikulino interglacial: I – Albic Retisols zone; II – Greyzemic Phaeozems zone in combination with Albic Retisols; III – Gypsic Chernozems or Gypsic Kastanozems zone;
C – paleosols of the Kamenka Interglacial: I – Cambisols zone; II – Chernozems zone;
D – paleosols of the Likhvin interglacial: I – Albic Retisols and Greyzemic Phaeozems zone; II –Chernozems zone

trend is typical for the Salyn paleosol (MIS 5e), where in more southern sections, in addition to carbonates, gypsum appears. According to Velichko et al. (2004) during the Mikulino interglacial the paleosols of the I and II zones (Table 4, Fig. 11) developed at an average annual precipitation of 600 - 650 mm per year, while the paleosols of the III zone (Table 4, Fig. 11) developed at 580 mm per year (Ryskov et al., 2008). The average annual precipitation in Kamenka (MIS 7 (9) and Likhvin (MIS 9 (11)) interglacials varies between 600 and 750 mm, but the greatest amount of precipitation is typical for the Likhvin interglacial (Velichko et al., 2004; Ryskov et al., 2008). As can be seen from Table 4, the maximum content of Fe-Mn pedofeatures and coatings is limited to the Inzhavino paleosol of the Likhvin interglacial, which confirms the degree of moistening of the paleosols of this period. Therefore, according to the microfabric of paleosols, it can be seen that in the territory of the center of the East European Plain the most humid conditions are characteristic for the Likhvin interglacial (MIS 9 (11)) with their gradual decrease towards the Holocene period.

According to Velichko et al. (2004) during the interstadial periods of the Late and Middle Pleistocene the amount of precipitation was 220 - 450 mm per year. In the microfabric of interstadial paleosols, there are Fe-Mn pedofeatures and coatings, and in more southern sections carbonate and gypsum nodules, but their quantity does not change significantly during the considered Pleistocene periods, which suggests similar pedogenic conditions for their formation. In the interstadials periods, considered soil complexes, the climate did not vary greatly from the Middle to Late Pleistocene, but the soil cover during these periods had latitudinal zonality, which consisted of two zones.

CONCLUSION

1. As follows from the data on micromorphology, the interstadial and interglacial paleosols permit tracing the changes in climate of the time intervals when the paleosols developed in the center of the East European Plain. The soil microstructure dominated by Fe-Mn nodules and coatings is typical of the soil formation in humid climate, while the presence of carbonate pedofeatures and gypsum suggests the climate aridity.

2. In the northern part of the East European Plain interglacial paleosols of the Mikulino and Inzhavino age had a texture-differentiated profile, while paleosols dated to the Kamenka interglacial lacked of albic horizon. In the southern regions the profile of the interglacial paleosols feature blackish chernic surface horizon and with secondary carbonates.

3. During interstadials of the Late and Middle Pleistocene the latitudinal zonality was fairly well pronounced, two zones being distinguished within the considered region. Interglacial paleosols – Mikulino permitted to identify three latitudinal zones, the Kamenka and Inzhavino interglacial soils were also distributed over two latitudinal zones.

ACKNOWLEDGEMENTS

The study was funded in part by Russian Foundation for Basic Research to the research projects № 18-04-00145, 17-55-53035. Micromorphological studies of the Sebryakovo-Mikhailovka section were carried out in the framework of the State Task № 0148-2019-0005 (Registration Number 01201352491).

The author is thankful to Spasskaya I.I. for her help in language editing. The authors would like to thank the anonymous reviewers for their helpful suggestions.

REFERENCES

Agadjanian A.K. and Glushankova N.I. (2017). Quaternary stratigraphy and developmental history of the central Russian periglacial–loessal province. Stratigraphy and Geological Correlation, 25(4), pp. 445-462.

Bolikhovskaya N.S. and Molodkov A.N. (2006). East European loess–palaeosol sequences: Palynology, stratigraphy and correlation. Quaternary International, 149, pp. 24-36. doi: https://doi.org/10.1016/j.quaint.2005.11.015.

Bolikhovskaya N.S. (1995). The evolution of the loess-paleosol formation of the Northern Eurasia. Moscow: Moscow State University press. (in Russian).

Bronger A. and Heinkele T.H. (1989). Micromorphology and genesis of paleosols in the Luochuan Loess Section, China: pedostratigraphic and environmental implications. Geoderma, 45, pp. 123-143. doi: https://doi.org/10.1016/0016-7061(89)90046-3

Bronger A., Winter R. and Heinkele T. (1998). Pleistocene climatic history of East and Central Asia based on paleopedological indicators in loess–paleosol sequences. Catena, 34, pp. 1–17. doi: https://doi.org/10.1016/S0341-8162(98)00078-2

Bronnikova M.A. and Targulian V.O. (2005). Assemblage of cutans in texturally differentiated soils (case study for Albeluvisoils of the East European Plain). Moscow: PBMC «Akademkniga». (in Russian)

Chernova O.V. (2011). Vorony - Calcic CHERNOZEMS. In: Shoba S.A. (Ed.). National Soil Atlas of Russia. Moscow. Astrel. pp. 136-137. (in Russian)

Chizhikova N.P., Morozova T.D. and Panin P.G. (2007). Mineralogical composition of the clay fraction and micromorphology of the Middle and Late Pleistocene paleosols and loesses of the center part of the East European plain. Eurasian Soil Science, 40(12), pp. 1343-1354.

Costantini EAC. (2017). Paleosols and pedostratigraphy. Applied Soil Ecology, 123, pp. 597-600. doi: https://doi.org/10.1016/j.apsoil.2017.09.021

Urusevskaya I.S. (2011). Umbric ALBELUVISOLS. In: Shoba S.A. (Ed.). National Soil Atlas of Russia. Moscow. Astrel. pp. 106-107. (in Russian)

Urusevskaya I.S., Martynenko I.A. and Alyabina I.O. (2011). Soil map. In: Shoba S.A. (Ed.). National Soil Atlas of Russia. Moscow. Astrel. pp. 72-73. (in Russian)

Dlussky K.G. (2001). Middle Pleistocene soil formation of the center of the East European Plain. M.: Ph.D. Thesis in Geography. Moscow: Institute of Geography, Russian Academy of Science/ (in Russian)

Dlussky K.G. (2007). Likhvin interglacial polygenetic paleosol: A reconstruction on the Russian Plain. Quaternary International, 162–163, pp. 141-157. doi: https://doi.org/10.1016/j.quaint.2006.10.029

Dodonov A.E. and Velichko A.A. (Eds.). (2003). Loess and Paleoenvironment. Abstracts and Field Excursion Guidebook. Moscow: GEOS. (in Russian)

FAO. (2006). Guidelines for Soil Description. fourth ed. Rome.

Fedoroff N., Courty M.-A. and Guo Z. (2010). Palaeosoils and Relict Soils. In: Stoops G., Marcelino V., Mees F., editors. Interpretation of micromorphological features of soils and regoliths. pp. 623-662.

Gerasimova M.I., Gubin S.V. and Shoba S.A. (1992). Micromorphological features of the USSR zonal soils. Information and reference materials. Pushchino. (in Russian)

Gerasimova M.I., Kovda I.V., Lebedeva M.P. and Tursina T.V. (2011). Micromorphological terms: The state of the art in soil microfabric research. Eurasian Soil Science 44(7), pp. 739–752.

Glushankova N.I. and Agadjanian A.K. (2015). Reconstruction of paleogeographic events in Pleistocene history of Don, Volga and Kama basins. Proceedings of the Russian Geographical Society 47(2), pp. 38-56. (in Russian with English abstract and references)

Glushankova N.I. (2008). Paleopedogenesis and past environments of Eastern Europe during the Pleistocene. Moscow-Smolensk. (in Russian)

Glushankova N.I. (2012). Structure, composition, and depositional environments of recent sediments in the Upper Don River basin inferred from the Korostelevo section. Lithology and Mineral Resources, 47(3), pp. 204–216.

Haase D., Fink J., Haase G., Ruske R., Pécsi M., Richter H., Altermann M. and Jäger K.D. (2007). Loess in Europe - its spatial distribution based on a European Loess Map, scale 1:2,500,000. Quaternary Science Reviews, 26, pp. 1301–1312. doi: https://doi.org/10.1016/j.quascirev.2007.02.003

IUSS Working Group WRB. (2015). World Reference Base for Soil Resources 2014, update 2015 International soil classification system for naming soils and creating legends for soil maps. World Soil Resources Reports No. 106. FAO, Rome.

Kemp R.A. (1999). Micromorphology of loess–paleosol sequences: a record of paleoenvironmental change. Catena 35(2–4), pp. 179-196. doi: https://doi.org/10.1016/S0341-8162(98)00099-X

Kemp R.A. (2013). Paleosols and wind-blown sediments. Soil Micromorphology. In: Elias S.A., editor-in-chief. Reference Module in Earth Systems and Environmental Sciences. Encyclopedia of Quaternary Science (Second Edition). Elsevier, pp. 381-391.

Kovda I.V., Morgun E.G., Lebedeva M.P., Oleinik S.A. and Shishkov V.A. (2016). Identification of carbonate pedofeatures of different ages in modern chernozems. Eurasian Soil Science 49(7), pp. 807-823.

Kubiena W. (1938). Micropedology. Ames IA: Collegiate Press.

Lazukov G.I. and Chebatoreva N.S. (Eds.). (1977). Sections of the glacial deposits of the Center of the Russian Plain. Moscow: Moscow State University. (in Russian)

Lindbo D.L., Stolt M.H. and Vepraskas M.J. (2010). Redoximorphic Features. In: Stoops G., Marcelino V., Mees F., editors. Interpretation of micromorphological features of soils and regoliths. Amsterdam: Elsevier. pp. 129-147.

Markov K.K. (Ed.). (1977). Sections of glacial deposits in the center of the Russian Plain. Moscow: Moscow State University press. (in Russian)

Little E.C., Lian O.B., Velichko A.A., Morozova T.D., Nechaev V.P., Dlussky K.G. and Rutter N.W. (2002). Quaternary stratigraphy and optical dating of loess from the East European Plain (Russia). Quaternary Science Reviews, 21, pp. 1745–1762. doi: https://doi.org/10.1016/S0277-3791(01)00151-2

Matvishina J.N. (1982). Micromorphology of Pleistocene Soils of the Ukraine. Kiev. Sci. dumka. (in Russian)

Mehra O.P. and Jackson M.L. (1960). Iron oxide removal from soils and clays by a dithionite citrate system buffered with sodium bicarbonate. Clays and Clay Minerals, 7, pp. 317-327.

Minashina N.G. and Shishov L.L. (2002). Gypsum-containing soils: their distribution, genesis, and classification. Eurasian Soil Science, 35(3), pp. 240-247.

Morozova T.D. (1965). Micromorphological characteristics of pale yellow permafrost soils of Central Yakoutia in relation to cryogenesis. Sov. Soil Science, 7, pp. 1333.

Morozova T.D. (1981). The development of the soil cover of Europe in the Late Pleistocene. Moscow: Nauka. (in Russian)

Morozova T.D. (1995). Identification of paleosol types and their applicability for paleoclimatic reconstructions. GeoJournal, 36(2-3), pp. 199-205.

Nettleton W.D., Olson C.G. and Wysocki D.A. (2000). Paleosol classification: Problems and solutions. Catena, 41(1–3), pp. 61–92. doi: https://doi.org/10.1016/S0341-8162(00)00109-0

Novenko E.Yu., Zuganova I.S. and Koslov D.N. (2008). Evolution of Vegetation Cover in Late Pleistocene within the Central State Reserve Region. Izvestiya RAN Seriya Geograficheskaya, 1, pp. 87-99. (in Russian)

Panin P.G. (2007). Specificity of the morphology of interglacial and interstadial paleosol complexes of the middle and late Pleistocene in the center of the East European Plain. Eurasian Soil Science, 40(2), pp. 126-139.

Panin P.G. (2015). Paleosoils as an Indicator of Climate Change in the Late and Middle Pleistocene of the Center of the East European Plain. Izvestiya RAN Seriya Geograficheskaya, 5, pp. 69-82. (in Russian)

Panin P.G., Timireva S.N., Morozova T.D., Kononov Yu.M., and Velichko A.A. (2018). Morphology and micromorphology of the loess-paleosol sequences in the south of the East European plain (MIS 1–MIS 17). Catena, 168, pp. 79-101. doi: https://doi.org/10.1016/j.catena.2018.01.032

Poch R.M., Artieda O., Herrero J. and Lebedeva-Verba M. (2010). Gypsic Features In: Stoops G., Marcelino V., Mees F., editors. Interpretation of micromorphological features of soils and regoliths. pp. 195-216.

Rastvorova O.G., Andreev D.P., Gagarina E.I., Kasatkina G.A. and Fedorova N.N. (1995). Chemical analysis of soils. St. Petersburg: University. (in Russian)

Rozanov B.G. (2004). Soil Morphology. Moscow: Akademicheskii Proekt. (in Russian)

Rusakov A.V. and Korkka M.A. (2004). The Bryansk fossil soil of the extraglacial zone of the Valday glaciations as an indicator of landscape and soil forming processes in the center of the Russian Plain. Revista Mexicana De Ciencias Geologicas, 21(1), pp. 94-100.

Ryskov Ya.G., Velichko A.A., Nikolaev V.I., Oleinik S.A., Timireva S.N., Nechaev V.P., Panin P.G. and Morozova T.D. (2008). Eurasian Soil Science, 41(9), pp. 937-945.

Sedov S., Rusakov A., Sheinkman V. and Korkka M. (2016). MIS3 paleosols in the center-north of Eastern Europe and Western Siberia: Reductomorphic pedogenesis conditioned by permafrost? Catena, 146, pp. 38–47. doi: https://doi.org/10.1016/j.catena.2016.03.022

Stoops G. (2003). Guidelines for Analysis and Description of Soil and Regolith Thin Sections. Soil Science Society of America. Madison. Wisconsin.

Świtoniak M., Charzyński P., (Eds). (2014). Soil Sequences Atlas. Nicolaus Copernicus University press.

Sycheva S. and Khokhlova O. (2016). Genesis, 14C age, and duration of development of the Bryansk paleosol on the Central Russian Upland based on dating of different materials. Quaternary International, 399, pp. 111–121. doi: https://doi.org/10.1016/j.quaint.2015.08.055

Sycheva S.A., Sedov S.N., Bronnikova M.A., Targulian V.O. and Solleiro-Rebolledo E. (2017). Genesis, evolution, and catastrophic burying of the ryshkovo paleosol of the mikulino interglacial (mis 5e). Eurasian Soil Science, 9, pp. 1027-1046.

Sycheva S.A. and Sedov S.N. (2012). Paleopedogenesis during the Mikulino interglacial (MIS 5e) in the East-European plain: buried toposequence of the key-section «Alexandrov quarry». Boletin de la Sociedad Geologica Mexicana, 64(2), pp.189-197.

Sycheva S.A. (1998). New Data on the Composition and Evolution of the Mezin Loess-Paleosol Complex in the Russian Plain. Eurasian Soil Science, 31(10), pp. 1177-1189.

Tabor N.J., Myers T.S. and Michel L.A. (2017). Sedimentologist's guide for recognition, description, and classification of paleosols. In: Zeigler K.E., Parker W.G., editors. Terrestrial Depositional Systems. Deciphering complexities through multiple stratigraphic methods. p. 165–208.

Tamm O. (1922). Eine Methode zur Bestimmung der anorganischen Komponenten des Gelkomplexes im Boden. Medd. Statens skogsforsoksanstalt 19, pp. 385-404.

Todisco D. and Bhiry N. (2008). Micromorphology of periglacial sediments from the Tayara site, Qikirtaq Island, Nunavik (Canada). Catena, 76, pp. 1–21. doi: https://doi.org/10.1016/j.catena.2008.08.002

Van Vliet-Lanoë B. (1998). Frost and soils: implications for palaeosols, palaeo-climates and stratigraphy. Catena, 34, pp. 157-183.

Van Vliet-Lanoë B. (2010). Frost Action. In: Stoops G., Marcelino V., Mees F., editors. Interpretation of micromorphological features of soils and regoliths. Amsterdam: Elsevier. pp. 81-108.

Velichko A.A., Borisova O.K., Zakharov A.L., Kononov Yu.M., Konstantinov E.A., Kurbanov R.N., Morozova T.D., Panin P.G. and Timireva S.N. (2017a). Landscape changes in the Southern Russian Plain in the Late Pleistocene a case study of the loess-soil sequence in the Azov Sea Region. Izvestiya RAN Seriya Geograficheskaya, 1, pp. 74-83. (in Russian)

Velichko A.A., Faustova M.A., Pisareva V.V., Gribchenko Yu.N., Sudakova N.G., and Lavrentiev N.V. (2011). Chapter 26 - Glaciations of the East European Plain: Distribution and Chronology. In: Ehlers J., Gibbard P.L., Hughes P.D., editors. Developments in Quaternary Sciences, 15, pp. 337-359. doi: 10.1016/B978-0-444-53447-7.00026-X ISSN: 1571-0866, # 2011 Elsevier B.V.

Velichko A.A., Gribchenko Y.N., Drenova A.N., Morozova T.D. and Timireva S.N. (1997). Soil section Gunki. In: Velichko A.A., editor. Loess-soil formation East-European plain. Paleogeography and stratigraphy. Moscow: Institute of Geography, Russian Academy of Science, pp. 60-79. (in Russian)

Velichko A.A. and Khalcheva T.A. (1982). Late Pleistocene loesses and their spatial distribution (map 3 - Loess cover during Valdai ice age). In: Velichko A.A., Gerasimov I.P., editors. Paleogeography of Europe during the last hundred thousand years (atlas-monograph) Moscow: Nauka. pp. 70-74. (in Russian)

Velichko A.A., Morozova T.D., Nechaev V.P. and Porozhnyakova O.M. (1996). Paleocryogenesis, soil cover and agriculture. Moscow: Nauka. (in Russian)

Velichko A.A., Morozova T.D. and Panin P.G. (2007). Soil polygenetic complexes as a systematic phenomenon of Pleistocene macrocycles. Izvestiya RAN Seriya Geograficheskaya, 2, pp. 44-54. (in Russian)

Velichko A.A., Morozova T.D. and Udartsev V.P. (1985). General and regional properties of the Middle and Late Pleistocene loess strata of the Russian Plain. In: The theory of cyclicity of loesses in the practice of engineering and geological surveys. Moscow: Nauka. pp. 90-98. (in Russian)

Velichko A.A. and Morozova T.D. (1963). Mikulino paleosol, its features and stratigraphic significance. In: Neustadt M.I., editor. Anthropogen of the Russian Plain and its stratigraphic components. Moscow: USSR Academy of Sciences Press. pp. 100-146. (in Russian)

Velichko A.A. and Morozova T.D. (1972). The main horizons of loess and fossil soils of the Russian Plain. In: Velichko A.A., editor. Loesses, paleosols and cryogenic phenomena on the Russian Plain. Moscow: Nauka. pp. 5-25. (in Russian)

Velichko A.A. and Morozova T.D. (2010). Basic features of Late Pleistocene soil formation in the East European Plain and their paleogeographic interpretation. Eurasian Soil Science, 43(13), pp. 1535-1546.

Velichko A.A. and Morozova T.D. (2015). Main features of soil formation within the Pleistocene on the East European Plane and their paleogeographical. In: Kudeyarov V.N., Ivanov I.V., editors. Evolution of soil and soil cover. Theory, diversity of natural evolution and antropogenic transformations of soil. Moscow: GEOS. pp. 321-337. (in Russian)

Velichko A.A., Semenov V.V., Pospelova G.A., Morozova T.D., Nechaev V.P., Gribchenko Y.N., Dlussky K.G., Rutter N.W., Catto N.R. and Little E.C. (2006). Matuyama–Brunhes boundary in key sections of the loess–paleosol–glacial formations on the East European Plain. Quaternary International, 152–153, pp. 94–102. doi: https://doi.org/10.1016/j.quaint.2005.12.018

Velichko A.A., Timireva S.N. and Khalcheva T.A. (1994). Late Pleistocene loessts of periglacial areas of the western Russian Plain. In: Velichko A.A., Starkel L., editors. Paleogeographic basis of the modern landscapes. Moscow: Nauka. pp. 63-69. (in Russian)

Velichko A.A., Yang T., Alekseev A.O., Borisova O.K., Kalinin P.I., Konishchev V.N., Kononov Yu.M., Konstantinov E.A., Kurbanov R.N., Panin P.G., Rogov V.V., Sarana V.A., Timireva S.N. and Chubarov I.G. (2017b). A comparative analysis of changing sedimentation conditions during the last interglacial-glacial macrocycle in the loess areas of the southern East European Plain (the Azov Sea region) and Central China (Loess Plateau). Geomorphology, 1, pp. 3-18. (in Russian)

Velichko A.A., Zelikson E.M., Borisova O.K., Gribchenko Y.N., Morozova T.D. and Nechaev V.P. (2004). Quantitative climate reconstructions of East-European plain for the last 450 thousand years. Izvestiya RAN Seriya Geograficheskaya, 1, pp. 7-25. (in Russian with English abstract)

Velichko A.A. (Ed.). (2002). Dynamics of terrestrial landscape components and inner marine basins of Northern Eurasia during the last 130000 years. Atlas-monography «Evolution of landscapes and climates of Northern Eurasia. Late Pleistocene – Holocene – elements of prognosis. II. General paleogeography». Moscow: GEOS. (in Russian)

Villagran X.S., Schaefer C.E.G.R. and Ligouis B. (2013). Living in the cold: Geoarchaeology of sealing sites from Byers Peninsula (Livingston Island, Antarctica). Quaternary International, 27, pp. 184–199. doi: https://doi.org/10.1016/j.quaint.2013.07.001

Virina E.I., Heller F., Faustov S.S., Bolikhovskaya N.S., Krasnenkov R.V., Gendler T., Hailwood E.A. and Hus J. (2000). Palaeoclimatic record in the loess–palaeosol sequence of the Strelitsa type section (Don glaciation area, Russia) deduced from rock magnetic and palynological data. Journal of Quaternary Science, 15(5), pp. 487-499.

Yakimenko E.Y. (1995). Pleistocene paleosols in the loess and loess-like sediments of the Central part of the Russian Plain. Quaternary Science Reviews, 14, pp. 747-753. doi: https://doi.org/10.1016/0277-3791(95)00049-6

Zaidel'man F.R. and Nikiforova A.S. (2010). Ferromanganese concretionary neoformations: A review. Eurasian Soil Science, 43(3), pp. 248-258.

Zykin V.S. and Zykina V.S. (2015). The Middle and Late Pleistocene loess-soil record in the Iskitim area of Novosibirsk Priobie, south-eastern West Siberia. Quaternary International, 365, pp. 15-25.

Received on July 11th, 2018 Accepted on November 15th, 2018

Elena Berezina[1*], Konstantin Moiseenko[1], Andrey Skorokhod[1], Nikolay Elansky[1], Igor Belikov[1], Natalia Pankratova[1]
[1] A.M. Obukhov Institute of Atmospheric Physics, Russian Academy of Sciences, Moscow, Russia
***Corresponding author:** e_berezina_83@mail.ru

ISOPRENE AND MONOTERPENES OVER RUSSIA AND THEIR IMPACTS IN TROPOSPHERIC OZONE FORMATION

ABSTRACT. Ground-based levels of important biogenic volatile organic compounds (BVOCs), isoprene and monoterpenes, as well as NO_x and O_3 measured simultaneously along the Trans-Siberian railway on a mobile railway laboratory in TROICA-12 campaign in summer 2008 are analyzed. It was shown that the highest isoprene (≥2.5 ppb) concentration was observed in the daytime in the Far East region where several favorable factors for its emissions occurred: a large amount of deciduous forests, high temperatures (>28°C) and light conditions. Maximum levels of monoterpenes (up to 3-9 ppb) along the Trans-Siberian railway were observed during the nighttime in the Ural region and in Central Siberia where coniferous vegetation is located. To evaluate the relative importance of isoprene and monoterpenes in ground-level ozone formation in Russian cities along the Trans-Siberian railway, where high NO_x concentration leads to tropospheric ozone generation, daytime ozone-forming potential (OFP) was calculated. The chemical losses of the studied BVOCs during their transport from sources to the measurement point were taken into account. Calculated OFPs due to isoprene (OFP_{iso}) and monoterpenes (OFP_{mono}) along the Trans-Siberian railway are in average 15±13 and 18±25 ppbv of ozone, respectively. The highest OFP_{iso} (up to 40 ppbv) were estimated in Central Siberia and in the Far East. OFPmono was the highest in the regions of coniferous vegetation, Ural and Central Siberia, and reached 80 ppbv. In the most cities along the Trans-Siberian railway, where high NO_x concentration (10-20 ppbv) along with high daytime temperatures (>25°C) were observed, monoterpenes made a main contribution to tropospheric ozone formation. Only in the Far East cities, where the largest deciduous vegetation area of the Trans-Siberian railway is located, isoprene played the main role in tropospheric ozone generation. It was also noted that OFP_{iso} increases with the population-size of the cities. It can be either due to the greater proportion of deciduous vegetation in the large cities along the Trans-Siberian railway or due to the impact of anthropogenic isoprene source. OFP_{mono} was the lowest in the medium cities and the highest in the small ones.

KEY WORDS: isoprene, monoterpenes, tropospheric ozone, biogenic volatile organic, ozone-forming potential, Trans-Siberian railway, mobile laboratory, TROICA

CITATION: Elena Berezina, Konstantin Moiseenko, Andrey Skorokhod, Nikolay Elansky, Igor Belikov, Natalia Pankratova (2019) Isoprene and monoterpenes over Russia and their impacts in tropospheric ozone formation. Geography, Environment, Sustainability, Vol.12, No 1, p. 63-74
DOI-10.24057/2071-9388-2017-24

INTRODUCTION

One of the important consequences of human activity on the atmosphere is an increase in tropospheric ozone level. Environmental changes, higher temperature, in combination with higher concentrations of specific anthropogenic pollutants lead to higher tropospheric ozone concentration. The highest ozone levels are often observed in urban environment, which is not only characterised by higher temperatures (heat islands), but also by higher levels of ozone precursors, nitrogen oxides (NOx), carbon monoxide (CO), methane (CH_4) and volatile organic compounds (VOCs). CO, CH_4 and VOCs are mainly oxidized in the troposphere by OH radicals, and at high air temperature and solar radiation in NO_x-polluted conditions can cause the formation of high ozone levels which pose a threat to human health (Sillman 1999). Thus, the proper estimates of ozone precursors impact on its ground-based production are very important for the diagnostics of the atmospheric photochemical system (APS) state and for extreme ecological situations forecasting. Atmospheric oxidation of CH_4 and CO is significantly slower (atmospheric lifetimes for CH_4 and CO are about 10 years and 1-2 month, respectively), and can cause mainly global and regional ozone increase. However, the oxidation of many VOCs occurs in the daytime and causes ozone increase near their local pollution sources as it takes place in urban environment.

Biogenic volatile organic compounds (BVOCs) constitute approximately 90% of global volatile organic compound (VOC) emissions, with the isoprene (C_5H_8) and monoterpenes ($C_{10}H_{16}$) being the most abundant (Guenther et al. 2012), and have significant effects on atmospheric chemistry and physics. Due to high reactivity of BVOCs, they are rapidly oxidized by OH radicals (Fan and Zhang 2004; Bowman and Seinfeld 1994; Sillman 1999; Wagner and Kuttler 2013), thus significantly influencing the oxidizing capacity of the atmosphere and thereby impacting the residence time of air pollutants and the most reactive greenhouse gases. The simulations of chemical-transport models showed that the impact of biogenic VOCs on tropospheric ozone formation can vary from 40 to 70% of the impact of all nonmethane hydrocarbons (NMHCs), with isoprene (C_5H_8) playing the major role (Guenther et al. 2000). As BVOC emissions increase with ambient light and temperature (Penuelas and Staudt 2010), the expected progression of climate change may affect BVOC emissions and contribute to regional changes of atmospheric composition. The atmospheric composition measurements over Russia along the Trans-Siberian railway in the unique TROICA (TRanscontinental Observations Into the Chemistry of the Atmosphere) experiments on a mobile laboratory in summer 2008 allowed the detailed analysis of the main BVOCs levels, isoprene and monoterpenes, over Russia and the estimation of their impact in tropospheric ozone formation.

Monitoring of the most important ozone precursors is carried out on the Global Atmospheric Watch (WMO GAW) network stations. In Russia, the ozone precursors are measured occasionally at the stations of the State air pollution control network existing only in large cities with population of over 100 thousand people. The transcontinental measurements of atmospheric composition on a mobile laboratory carried out in the international experiments TROICA in 1995-2010 are filled the deficit of the information on ozone levels in the atmosphere over continental Russia significantly (Elansky et al. 2009). In particular, a tendency to an increase of ozone formation in urban air was revealed especially in stagnant air conditions.

Along the Trans-Siberian railway, 87 cities are located, which are different in urbanization and anthropogenic load intensity. The measurements of BVOCs by PTR-MS method simultaneously with other atmospheric compounds along the Trans-Siberian railway in summer 2008 (TROICA-12) allowed the detailed analysis of the contribution of the main tropospheric ozone precursors to its production in differently populated Russian cities.

MATERIALS AND METHODS

TROICA experiments

TROICA experiments over Russia on a mobile laboratory were carried out regularly from 1995 to 2014 (Elansky et al. 2009). About 10 inorganic compounds as well as aerosols and meteorological parameters were measured continuously and simultaneously by a specially constructed automated system. The system was built on a railway carriage with air inlets at the height of about 4 m above the ground. VOC concentrations have been measured routinely since 2008. The TROICA carriage–laboratory is equipped in accordance with the measurement requirements of the Global Atmospheric Watch (WMO), and is located just after the electric locomotive to minimize various effects of near-surface air perturbations due to moving train (Skorokhod et al. 2017). The possible impact of oncoming trains as well as human activities in the train (all conveniences were placed at the end part of the train) on the measurements is expected to be generally non-significant as demonstrated previously in Crutzen et al. (1996), Elansky et al. (2000) and Panin et al. (2001).

This paper is a continuation one from Skorokhod et al. (2017), where benzene and toluene were investigated. Thus, it describes the data from the same experimental period and setup.

In present study, the data from the summer campaign TROICA-12 (21.07.2008 – 04.08.2008) along the Trans-Siberian railway (Fig. 1) are analyzed. The train covers the total length of the route from Moscow to Vladivostok (~ 9288 km) for approximately 6 days, so the total duration of a single campaign is about two weeks. (Henceforth, we denote forward path from Moscow to Vladivostok, and return path from Vladivostok to Moscow, as east and west segments of the whole route, correspondingly).

Undoubtedly, the results of the observations at each particular location performed from the moving carriage are strongly influenced by specific weather conditions (synoptic patterns), as well as by complex interplay of local pollution sources and atmospheric transport by turbulent eddies on a variety of scales, the latter being considered as a source of random noise in the measurement data. Generally, straightforward quantification of the effects of atmospheric dilution and absolute strength of the associated nearby emission sources is inhibited in data analyses. Yet, the passage of each location twice (in the forward and return paths of the TROICA campaign) allows for some qualitative assessment of the impact of weather conditions, since the time between the two subsequent measurements is of the order of one week, which is comparable to the characteristic time of the boundary layer ventilation in mid-latitudes (Skorokhod et al. 2017).

Various types of meteorological conditions along the railroad can be generalized into three distinctive weather patterns when traversing mountain area adjacent to Baikal Lake (~110° E) in east and west segments. There was clear and warm (>20° C at noon) weather on the route from Moscow to Baikal, hot weather (>24° C at noon) between Baikal Lake area and Vladivostok (east and west segments), and cool (daytime temperatures of 15 – 20° C) and rainy weather between Baikal Lake and Moscow on the return west segment of the route. Nighttime surface temperature inversions and stagnant air conditions were common for the east segment, although light winds were typical for the both east and west segments of TROICA. This feature is clearly seen in Fig.1 where 2-day back trajectories along the TROICA route calculated with the use of NOAA HIGHSPLIT model (Stein et al. 2015; Rolph 2016) based on 3D wind fields are shown as averages of corresponding ensembles of trajectories originated within a height range from 0 – 400 m a.g.l. According to Fig.1, the characteristic distances of transport within a planetary boundary layer does not exceed 500 – 600 km in the two days preceding measurement time, so the measured chemical composition of the respective air masses can be considered as representative of the cumulative impact of pollutant sources at local to regional scales. The exception is the Far East Region where regional advection by southerly winds may contribute to measured pollutant concentrations from highly urbanized areas of the north-east China.

In the whole, in TROICA-12 experiment meteorological conditions was favorable to study chemical composition of fresh air masses from regional sources and ozone production from the emitted precursors due to high daytime surface air temperatures and solar radiation.

VOC measurements

Isoprene and monoterpenes concentrations were measured by a Compact Proton Transfer Reaction Mass Spectrometer (Compact PTR-MS) from Ionicon Analytik GmbH (Austria). Errors in instrument's calibration by the proper gas standard (Ionicon Analytic GmbH, Innsbruck, containing 17 VOCs) did not exceed 15%. For PTR-MS instrumental parameters (in particular, drift tube voltage, temperature and pressure) factory settings were used.

The Compact PTR-MS measurement range depends on the substances measured, integration time and system set-up. Its detection limits for the investigated VOCs are in order of pptv. Isoprene and monoterpenes were detected by the instrument at masses M69 and M137, and M81, respectively. In case of isoprene, other aldehydes and ketones are known to be detectable at this mass. However, isoprene has been found to be the dominant species at M69 within various kinds of air masses (de Gouw and Warneke 2007). Monoterpenes were analyzed as the sum of the M137 and M81 signals as total monoterpenes.

Other components and meteorology

NO and NO_2 concentrations were measured at different times with a TE42C-TL instrument (Thermo Electron Corp., USA) and with a M200AU instrument produced by Teledyne Corp. (USA). These instruments apply the chemiluminescent method. The minimum NO and NO_2 concentrations detectable with these instruments are equal to 0.05 ppb, which makes it possible to measure the so-called background con-

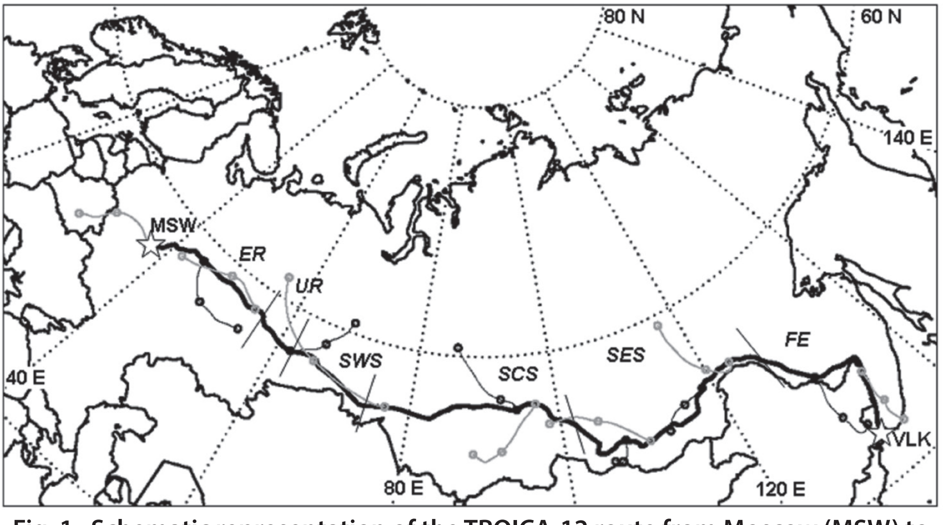

Fig. 1. Schematic representation of the TROICA-12 route from Moscow (MSW) to Vladivostok (VLK). Thin solid lines across the route represent approximate boundaries of various geographic regions: European Russia (ER), Ural mountain region (UR), southern parts of West (SWS), Central (SCS), and East (SES) Siberia, and Far East (FE). Back 2-day trajectories with endpoints at Trans-Siberian Railroad at local noon of each successive day of carriage movement are shown for East (black solid) and West (gray solid) routs of the campaign. Open circles mark air particles positions at 0, 24, and 48 hours along the each trajectory

centrations not influenced by the pollution sources. NO_x concentration is the sum of NO and NO_2 concentrations (Skorokhod et al. 2017).

Ozone concentration was measured with Dasibi 1008RS and 1008AH gas analyzers. These instruments are based on the photometric method (Skorokhod et al. 2017). They allow measuring the ozone concentration in the range from 1 to 1000 ppb with a total error of ±1 ppbv. These instruments undergo scheduled calibrations against the secondary standard, the O3-41M No. 1294 instrument, which undergoes in its turn annual calibrations against the SRP No. 38 standard owned by the Mendeleev Research Metrology Institute (Russia).

For measuring of atmospheric pressure, air temperature, relative air humidity, as well as wind speed and direction, the device of type ACAT-3M produced by "SPA Typhoon" (Russia) was used. This device included a sonic anemometer and proper pressure, temperature and relative humidity sensors. Additionally, air temperature and relative humidity were measured by HMP-233 device, and atmospheric pressure were measured by PTA-427 device. Both devices produced by Vaisala (Finland).

RESULTS AND DISCUSSION

Isoprene and monoterpenes along the Trans-Siberian railway

The areas adjacent to the Trans-Siberian railway are markedly different in amount of urbanization and anthropogenic load. Eighty-seven towns are located immediately on the railway, sixty-eight towns are in the Ural mountain region and West Siberia with the remaining ones located in the East Siberia and the Far East. Yet, it is in the area of first tens to hundreds of kilometers from the Trans-Siberian railway where the most significant regional anthropogenic sources are commonly located in all the regions considered. As mentioned above, the meteorological conditions during the most of the TROICA campaign were favorable for both studying chemical composition of fresh air masses contaminated by regional sources and for ozone production from the emitted precursors due to high daytime surface air temperatures and solar radiation.

The major problem of the TROICA data analyses is a correct elimination of screening effects (relative to regional scale pollution sources) produced by local pollution sources along the railroad. Except for small areas of biomass burning and smoldering in the vicinity of railway, such sources are mainly of anthropogenic origin and characterized by highly limited spatial extents (and, hence, an impact upon a chemical composition), so they can be effectively filtered out by applying some objective criteria based on the NO/NO_2 ratio to the original 10-second dataset as described in detail in Vasileva et. al. (2011) and in Skorokhod et al. (2016). The filtered data (~75% of the dataset) were used to calculate 10-min averaged dataset, which is analyzed hereafter.

The most important parameters of tropospheric ozone formation are VOCs and NO_x (NO_x =NO+NO_2) concentrations, temperature and solar radiation. For TROICA-12 measurements, NO_x–sensitive regime (NMHC/NO_x > 20, where NMHC is a sum of nonmethane hydrocarbons) was typical. Fig. 2 shows a subset ([O_3]≥24 ppbv) of 1-hour averages for O3 and NO_x(=NO+NO_2) along with the corresponding regression curve, which were measured under clear sky, high air temperature (>25°C), clear sky conditions favorable for rapid photochemical ozone production during the course of the day. According to Fig.2a, the ozone mixing ratio increases nonlinearly with NO_x, with the measured ozone and NO_x are broadly satisfying the dependence

$$\left[O_3\right]=\left[O_3\right]_b+\alpha\left[NO_x\right]^{\beta} \tag{1}$$

The large scatter of measurement points on the plot is due to different degree of photochemical processing of the measured air samples and variations in local vertical mixing conditions affecting near-surface ozone and NO_x abundances. We can also see that the discrepancy between the measurements and the fitted curve has a tendency to increase with $[NO_x]$ which may be explained by a high dependence of the O_3 production rate, $P(O_3)$, on NO_x and VOC abundances so that $P(O_3) \propto ([NO_x]^2/[VOC])^2$ (Kleinman et al. 2001).

The data shown on Fig. 2a may be viewed in a more systematic way by considering $[O_3]/[NO_x]$ as a proxy for the ratio of local ozone photochemical production, $P(O_3)$, to $[NO_x]$ by assuming a proportionality between the measured ozone concentrations and the rate of ozone production, $P(O_3)$, in the sampled air parcel en route to a measurement point. Then, $P(O_3) = c_1 \cdot [O_3]$, where a constant c_1 is a function of measured $[NO_x]$, air mass history, and meteorological conditions affecting boundary layer chemistry. We then obtain a non-linear fit $[O_3]/[NO_x] = \bar{\alpha}[NO_x]$, $\bar{\alpha}$ =29.08, $\bar{\beta}$ =0.87 (Fig.2b) which represents a uniformly valid approximation for a $[O_3]/[NO_x]$ ($[NO_x]$) dependence in the sampled air mass. The above relation can be rearranged to $d\ln[O_3]/d\ln[NO_x] = 1-\bar{\beta}$, where the left hand side of the expression gives the relative sensitivity of O_3 production rate to $[NO_x]$ averaged over the whole set of measurements performed in the photochemically processed urban air masses encountered in the TROICA. Kleinmann et al. (1997, 2001) use the conservation equation for free hydrogen radicals (OH, HO_2, and organic peroxides RO_2):

$$Q = L_R + L_N \tag{2}$$

where Q is the radical production rate, and L_R and L_N are the loss rates due to radical-radical reactions and reactions of radicals with NO_x, to propose a functional relationship between $d\ln[O_3]/d\ln[NO]$ and L_N/Q:

$$dIn[O_3]/dIn[NO_x] = (1-\frac{3}{2}L_N/Q)/(1-\frac{1}{2}L_N/Q) \tag{3}$$

which is valid over a wide range of pollution levels. Using (3), one can obtain a regional average day time ratio for L_N/Q from the corresponding slope of the regression line shown on Fig.2b given the best-fit value for the $\bar{\beta}$ exponent: $L_N/Q = 2\bar{\beta}/(2+\bar{\beta})$ =0.6 ($\bar{\beta}$=0.87). The derived value for L_N/Q is slightly above the theoretically predicted threshold value of 0.5 separating between NO_x and VOC sensitive regimes of ozone production (see Fig. 1b from Kleinmann et al. (1997)). The final conclusion is that the average day-time conditions in the urban air masses measured in the TROICA campaign are somewhere in the transition from NO_x to VOC sensitive regimes so that the both anthropogenic emissions of NO_x along with the predominant biogenic VOC emissions play equally important role in controlling day-time ozone levels in the towns along the Trans-Siberian Railroad during the weather conditions favorable for intence ozone photochemistry.

Fig. 3 shows isoprene and monoterpenes derived from the filtered 10-second dataset for the east and west segments of the TROICA-12 experiment. Simultaneous measurements of O_3, NO_x, meteorological parameters and altitude a.s.l. along the Trans-Siberian railway are also shown in the figure. To clarify the time of day, the times

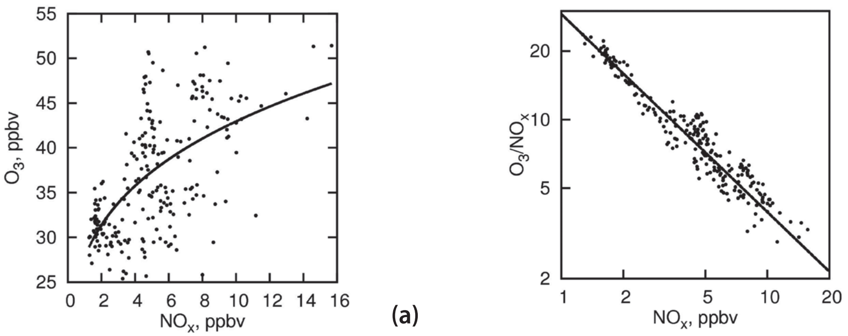

Fig. 2. Day-time (10:00–17:00 local time) correlations of O_3 and NO_x along with the fitting curves for $[O_3]$≥25 ppbv: $[O_3] = [O_3]_b + \alpha[NO_x]^{\beta}$, $[O_3]_b$ =24 ppbv, α =4.4 ppbv, and β =0.62 (a) and $[O_3]/[NO_x] = \bar{\alpha}[NO_x]^{-}$, $\bar{\alpha}$ =29.08, $\bar{\beta}$ =0.87 (b)

of local noon (12:00 LT) are presented by white circles in Fig. 3. The whole path from Moscow to Vladivostok is divided into 6 lengthy segments according to climatological conditions and anthropogenic load intensity: European Russia (ER), Ural mountain region (UR), southern parts of West (SWS), Central (SCS), and East (SES) Siberia, and Far East (FE).

Maximum levels of NO_x (> 20 ppb), were observed in large cities (with population size of 0.25 – 1 million people: Perm, Ekaterinburg, Tumen, Omsk, Krasnoyarsk, Irkutsk, Ulan-Ude, Chita, Khabarovsk) along the Trans-Siberian railway (see Fig. 3). It was shown in Skorokhod et al., 2017 that motor vehicle exhausts were the most significant anthropogenic source of air pollution in the cities along the Trans-Siberian railway, even though in some cities (Khabarovsk, Birobidzhan, Skovorodino, Tulun, Tajshet, and Tyumen) the contribution from other sources (including industrial emissions, coal burning and gasoline evaporation) was also important. Ozone had a pronounced daily cycle, with a maximum concentration being observed in the daytime (see Fig. 3). The absence of clearly defined peaks in ozone distribution points to the essential role of horizontal advection and regional photochemical processes in its spatial distribution in the developed ABL conditions.

Isoprene and monoterpenes depended significantly on temperature and solar radiation during the experiment (Fig. 3). In this regard, the highest isoprene (≥2.5 ppb) concentration was observed in the daytime (10:00-19:00 LT) in the FE region where several favorable factors for their emissions occurred: a large amount of deciduous forests, high temperatures (>28°C) and light conditions (see Fig. 3). Monoterpenes can emit from coniferous vegetation both during the day and at night with their night concentration increasing due to accumulation of monoterpenes in a stable atmosphere. Maximum levels of monoterpenes along the Trans-Siberian railway (up to 3-9 ppb) were observed during the nighttime (19:00 – 02:00 LT) in UR region, in SCS and ECS where coniferous vegetation is located.

Estimation of ozone forming potential in Russian cities

To evaluate the relative importance of VOCs in ground-level ozone formation, in

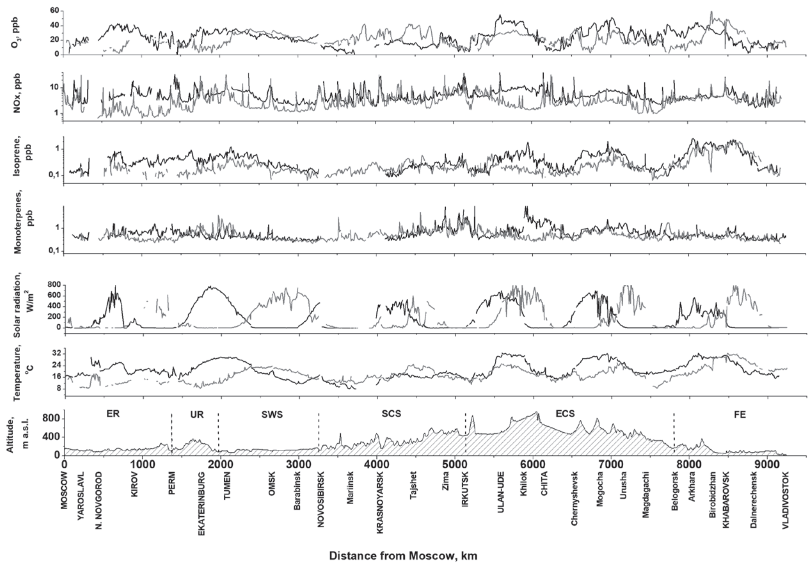

Fig. 3. 10-minute isoprene and monoterpene concentrations derived from the filtered 10-sec dataset for the east (black line) and west (gray line) segments of the TROICA-12 experiment. Simultaneous measurements of O_3, NO_x, meteorological parameters and altitude a.s.l. along the Trans-Siberian railway are also shown

numerous studies (Xie et al. 2008; Wagner et al. 2014) ozone-forming potential (OFP) is employed. OFP is defined as:

$$OFP_{VOC}\left[\mu g / m^3\right] = C_{VOC} \times MIR_{VOC} \qquad (4)$$

where C_{VOC} is a VOC concentration having the dimension of μg/m^3, MIR_{VOC} is a maximum incremental reactivity (Carter 1994). The latter is a dimensionless quantity defined as gram of O^3 produced per gram of the VOC, which defines the maximum ozone concentration formed from chemical destruction of the given VOC.

We used this method to evaluate the contribution of the studied ozone precursors to its production in the Russian cities along the Trans-Siberian railway. Taking into account the fact that all VOCs studied, especially reactive isoprene, can have significant chemical losses during the time before the train will pass the mixed air mass in the measurement point, we calculated their initial concentrations preliminary.

Initial isoprene concentrations was derived from simultaneous measurements of its products, MVK and MACR, and isoprene concentration following Xie et al. (2008). The calculations are based on isoprene reaction with OH radicals, which is the main photochemical loss for isoprene in the atmosphere (Stroud et al. 2001). Since this method is valid in the daytime, only daytime measurements (10:00 – 19:00 LT) were used for calculations of initial isoprene concentrations in this study.

For monoterpenes, atmospheric oxidation by ozone and nitrate radical (NO_3) is also very important (Perakyla et al. 2014). However, monoterpene loss due to the reactions with NO_3 is more important during the night. The evaluations based on ozone oxidation is a problem at this stage of the study and expected to be taken into account in future work. Thus, we estimated initial daytime concentration of monoterpenes basing only on their reaction with OH radicals following the method of Wiedinmyer et al. (2001).

The derived initial concentrations of isoprene and monoterpenes are 4 and less than 1.5 times higher on average, respectively, than the measured ones. The OFPs were calculated from the initial concentrations of isoprene and monoterpenes for differently populated Russian cities along the Trans-Siberian railway during the daytime (10 – 19 LT (local time)). This period is characterized by the most active photochemical ozone formation due to VOCs reactions with OH radicals.

Contribution of isoprene and monoterpenes to ozone formation in Russian cities

Calculated OFP_{iso} and OFP_{mono} along the Trans-Siberian railway are in average 15±13 and 18±25 ppbv of ozone, respectively. The highest OFPs due to isoprene (up to 40 ppbv) were estimated in Central Siberia and in the Far East. OFPs due to monoterpenes were the highest in the regions of coniferous vegetation, Ural and Central Siberia, and reached 80 ppbv. Significant OFPs due to BVOCs (16±12 and 28±34 ppbv of ozone due to isoprene and monoterpenes, respectively) were obtained in the cities along the Trans-Siberian railway, where high NO_x concentration (10-20 ppbv) along with high daytime temperatures (>25°C) were observed. Fig.4 shows that monoterpenes mainly contribute to tropospheric ozone formation in most Trans-Siberian cities. Only in the Far East cities, where a large deciduous vegetation area of the Trans-Siberian railway is located, isoprene plays the main role in tropospheric ozone generation (see Fig. 4).

Table 1 shows that OFPiso increases with the population-size of the cities. It can be due to either the greater proportion of deciduous vegetation in the large cities along the Trans-Siberian railway or the impact of anthropogenic isoprene sources (transport exhausts, power plants etc.), which can fluctuate in summer urban air between 10-50% (Borbon et al. 2001; Starn et al. 1998). An impact of monoterpenes on ozone formation is generally the lowest in the medium-sized cities and the highest in the small-sized ones.

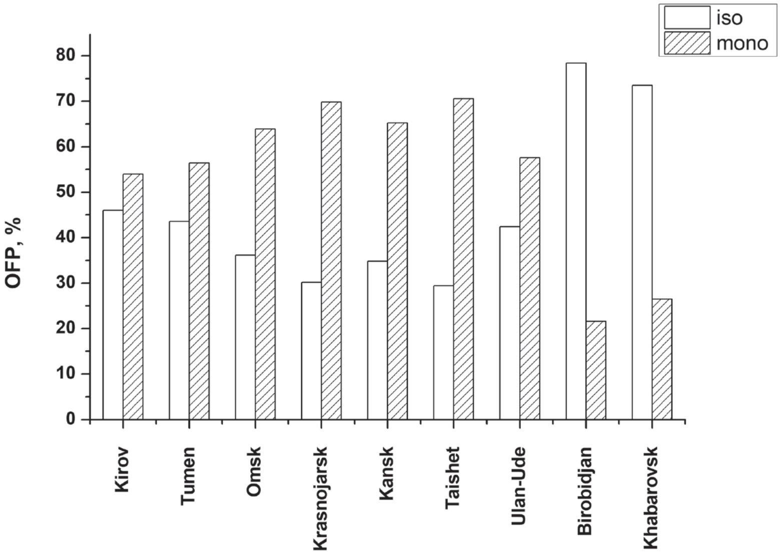

Fig. 4. Contribution of isoprene and monoterpenes to ozone formation potential (OFP) in the cities along the Trans-Siberian railway (OFP_{iso} + OFP_{mono} in each city gives 100%)

Table 1. The percentiles of OFPs and NO_x (P_{10} - P_{90} (P_{50})) in all cities along the Trans-Siberian railway (in ppb)

Population, thous. (number of cities crossed in daytime)	OFP_{iso}	OFP_{mono}	NO_x
<50 (2)	5.65-17.35 (9.67)	6.32-54.45 (18.99)	1.99-10.74 (5.12)
50-250 (4)	7.19-37.65 (11.02)	4.45-23.19 (10.53)	2.48-13.61 (4.89)
>250 (5)	5.43-54.02 (24.49)	6.89-40.35 (16.19)	2.65-16.29 (9.71)

CONCLUSION

Due to a lack of information about the impact of the most important ozone precursors on its production in Russian cities, ground-based levels of important BVOCs, isoprene and monoterpenes, as well as NO_x and O_3 measured simultaneously along the Trans-Siberian railway on a mobile railway laboratory in TROICA-12 campaign in summer 2008 were analyzed. Meteorological conditions during the most of the TROICA campaign were favorable for both studying chemical composition of fresh air masses contaminated by regional sources as well as for ozone production from the emitted precursors due to high daytime surface air temperatures and solar radiation.

It was shown that the highest isoprene (≥2.5 ppb) concentration was observed in the daytime in the FE region where several favorable factors for their emissions occurred: a large amount of deciduous forests, high temperatures (>28°C) and light conditions. Monoterpenes also emitted from coniferous vegetation during the night with their concentration increasing due to accumulation in a stable atmosphere. Maximum levels of monoterpenes along the Trans-Siberian railway were observed during the nighttime measurements (up to 3-9 ppb) in UR region, in SCS and ECS where coniferous vegetation is located. Thus, biogenic ozone precursors are dependable on the parameters of atmospheric boundary layer (ABL).

Maximum levels of NO_x (> 20 ppb), were observed in large cities (with population size of 0.25 – 1 million people: Perm, Ekaterinburg, Tumen, Omsk, Krasnoyarsk, Irkutsk, Ulan-Ude, Chita, Khabarovsk) along the Trans-Siberian railway. To evaluate the relative importance of BVOCs in ground-level ozone formation in Russian cities along the Trans-Siberian railway, daytime ozone-forming potential (OFP) was calculated. Taking into account that all VOCs studied can have significant chemical losses during their transport from sources to the measurement point, calculated initial concentrations of isoprene and monoterpenes were used for OFPs evaluation. Initial concentrations of isoprene and monoterpenes is about 4 and up to 1.5 times higher than the measured concentrations.

Calculated OFP_{iso} and OFP_{mono} along the Trans-Siberian railway are in average 15±13 and 18±25 ppbv of ozone, respectively. The highest OFP_{iso} (up to 40 ppbv) was estimated in Central Siberia and in the Far East. OFP_{mono} was the highest in the regions of coniferous vegetation, Ural and Central Siberia, and reached 80 ppbv. In the most cities along the Trans-Siberian railway, where high NO_x concentration (10-20 ppbv) along with high daytime temperatures (>25°C) were observed, monoterpenes made a main contribution to tropospheric ozone formation. Only in the Far East cities, where the largest deciduous vegetation area of the Trans-Siberian railway is located, isoprene played the main role in tropospheric ozone generation. It was also noted that OFP_{iso} increased with the population-size of the cities. It can be either due to the greater proportion of deciduous vegetation in the large cities along the Trans-Siberian railway or due to the possible impact of anthropogenic isoprene source. OFP_{mono} was the lowest in the medium cities and the highest in the small ones.

ACKNOWLEDGEMENTS

This study was supported by the Russian Foundation for Basic Research (grants no. 16-35-00158, 17-29-05102 and 18-35-20031).

REFERENCES

Borbon A., Fontaine H., Veillerot M., Locoge N., Galloo J. C., and Guillermo R. (2001). An investigation into the traffic-related fraction of isoprene at an urban location. Atmos. Environ., 35, 3749–3760.

Bowman F. M. and J. H. Seinfeld (1994). Ozone productivity of atmospheric organics. Journal of Geophysical Research Atmospheres 99(D3):5309-5324.

Carter W. P. L. (1994). Development of ozone reactivity scales for volatile organic compounds. J. Air Waste Manage. Assoc., 44, 881–899.

Carter W. P. L. (2010). Updated Maximum Incremental Reactivity Scale and hydrocarbon reactivities for regulatory applications. California Air Resources Board Contract 07-339, January 28, 2010.

Crutzen P.J., Elansky N.F., Hahn M., Golitsyn G.S., Brenninkmeijer C.A.M., Scharffe D., Belikov I.B., Maiss M., Bergamaschi P., Rockmann T., Grisenko A.M., and Sevastyanov V.V. (1996). Trace gas measurements between Moscow and Vladivostok using the Trans-Siberian Railroad. J. Atm. Chemistry, No 29, 179–194.

de Gouw J. and Warneke C. (2007). Measurements of volatile organic compounds in the Earth's atmosphere using proton-transferreaction mass spectrometry. Mass Spectrom. Rev., 26, 223–257. doi:10.1002/mas.20119

Duan J.C., Tan J.H., Yang L., Wu S.X., and Hao J.M. (2008). Concentration, Sources and Ozone Formation Potential of Volatile Organic Compounds (VOCs) during Ozone Episode in Beijing. Atmos. Res. 88: 25–35.

Elansky N.F., Belikov I.B., Berezina E.V. (2009). Atmospheric composition observations over Northern Eurasia using the mobile laboratory: TROICA experiments, edited by N.F. Elansky, Moscow, 73 p.

Elansky N.F., Golitsyn G.S., Vlasenko T.S., and Volokh A.A. (2000). Volatile organic compounds observed in the atmospheric surface layer along the Trans-Siberian Railroad. Dokl. Akad. Nauk, V. 373, No 6, 816–821.

Fan J. and Zhang R. (2004). Atmospheric oxidation mechanism of isoprene. Environ. Chem. 2004, 1, 140–149. doi:10.1071/EN04045

Guenther A., Geron C., Pierce T., Lamb B., Harley P., Fall R. (2000). Atmospheric Environment, 34, pp. 2205–2230.

Kleinman L.I., Daum P.H., Lee J.H., Lee Y.-N., Nunnermacker L.J., Springston S.R., Newman L., Weiristein-Lloyd J.b., Sillman S. (1997). Dependence of ozone production on NO and hydrocarbons in the troposphere. GRL. 24:2299–2302.

Kleinman L.I., Daum P.H., Lee Y.-N., Nunnermacker L.J., Springston S.R., Weinstein-Lloyd J., Rudolph J. (2001). Sensitivity of ozone production rate to ozone precursors. Geophysical Research Letters 28, 2903–2906.

Panin L.V., Elansky N.F., Belikov I.B., Granberg I.G., Andronova A.V., Obvintsev Yu.I., Bogdanov V.M., Grisenko A.M., and Mozgrin V.S. (2001). Estimation of Reliability of the Data on Pollutant Content Measured in the Atmospheric Surface Layer in the TROICA Experiments. Izvestiya, Atmospheric and Oceanic Physics, V. 37, Suppl. 1, 81-91.

Penuelas J. and Staudt M. (2010). BVOCs and global change. Trends Plant Sci., 15, 133–144. doi:10.1016/j.tplants.2009.12.005

Peräkylä O., Vogt M., Tikkanen O-P., Laurila T., Kajos M.K., Rantala P.A., Patokoski J., Aalto J., Yli-Juuti T., Ehn M., Sipila M., Paasonen P., Rissanen M., Nieminen T., Taipale R., Keronen P., Lappalainen H.K., Ruuskanen T. M., Rinne J., Kerminen V-M., Kulmala M., Back J. and Petaja T. (2014). Monoterpenes' oxidation capacity and rate over a boreal forest. Boreal Environment Research, 19, suppl. B, pp. 293-310.

Sillman S. (1999). The relation between ozone, NOx and hydrocarbons in urban and polluted rural environments. Atmos. Environ., 33, 1821–1845. doi:10.1016/S1352-2310(98)00345-8

Skorokhod A.I., Berezina E.V., Moiseenko K.B., Elansky N.F., Belikov I.B. (2017). Benzene and Toluene in the surface air of North Eurasia from TROICA-12 campaign along the Trans-Siberian railway. Atmos. Chem. Phys., 17, 5501-5514. doi: 10.5194/acp-17-5501-2017

Starn T.K., Shepson P.B., Bertman S.B., White J.S., Splawn B.G., Riemer D.D., Zika R.G., and Olszyna K. (1998). Observations of isoprene chemistry and its role in ozone production at a semirural site during the 1995 Southern Oxidants Study. J. Geophys. Res., pp. 103, 22, 425-22, 435.

Stroud C.A., Roberts J.M., Goldan P.D., Kuster W.C., Murphy P.C., Williams E. J., Hereid D., Parrish D., Sueper D., Trainer M., Fehsenfeld F.C., Apel E.C., Riemer D., Wert B., Henry B., Fried A., MartinezHarder M., Harder H., Brune W.H., Li G., Xie H., and Young V.L. (2001). Isoprene and its oxidation products, methacrolein and methylvinyl ketone, at an urban forested site during the 1999 Southern Oxidants Study. J. Geophys. Res.: Atmos. 106 (D8), 8035–8046.

Vasileva A.V., Moiseenko K.B., Mayer J.-C., Jurgens N., Panov A., Heimann M., Andreae M.O. (2011). Assessment of the regional atmospheric impact of wildfire emissions based on CO observations at the ZOTTO tall tower station in central Siberia. J.Geophys. Res., 116, D07301. doi:10.1029/2010JD014571

Wagner P. and Kuttler W. (2014). Biogenic and anthropogenic isoprene in the near-surface urban atmosphere–A case study in Essen, Germany. Sci. Total Environ., 475, 104–115. doi:10.1016/j.scitotenv.2013.12.026

Wiedinmyer C., Friedfeld S., Baugh W., Greenberg J., Guenther A., Fraser M., Allen D. (2001). Measurement and analysis of atmospheric concentrations of isoprene and its reaction products in central Texas. Atmospheric Environment 35 (6), 1001–1013.

Xie X., Shao M., Liu Y., Lu S., Chang C.C., and Chen Z.M. (2008). Estimate of initial isoprene contributions to ozone formation potential in Beijing, China. Atmos. Environ., 42, 6000–6010.

Received on November 11th, 2017 Accepted on November 15th, 2018

Quang Khanh Nguyen[1], Le Hung Trinh[2*], Khanh Hoai Dao[2], Nhu Duan Dang[3]
[1] Hanoi University of Mining and Geology, North Tuliem District, Hanoi, Vietnam
[2] Le Quy Don Technical University, Hoang Quoc Viet Street, Hanoi, Vietnam
[3] Vietnam Institute of Geodesy and Cartography, Hoang Quoc Viet Street, Hanoi, Vietnam
***Corresponding author:** trinhlehung125@gmail.com

LAND SURFACE TEMPERATURE DYNAMICS IN DRY SEASON 2015-2016 ACCORDING TO LANDSAT 8 DATA IN THE SOUTH-EAST REGION OF VIETNAM

ABSTRACT. Located in Southeast Asia, Vietnam is one of the most severely affected countries by climate change and faces to series of challenges related to climate change, in which droughts are one of the most serious natural disasters. Land surface temperature (LST) is important factor in evaluating soil moisture and drought phenomenon. Remote sensing technique with many advantages, compared with traditional methods, can be used effectively for retrieving LST. This article presents study on the application of LANDSAT 8 multi – temporal data for monitoring LST changes in dry season 2015 – 2016 in Loc Ninh district, Binh Phuoc province in Southeast region of Vietnam. LST was derived using Split-Window (SW) algorithm. The results showed that the LST at the end of 2015 – 2016 dry seasons (in February and March) is much higher than at the early of dry season. The area with LST higher than 309 K increases very fast in dry season 2015 – 2016, from less than 1% of the total study area in November and December to 19.59% in February and 30.74% in March. The results obtained in this study can be used to create the LST distribution map and to monitor drought phenomenon.

KEY WORDS: remote sensing, LST, drought, thermal infrared, LANDSAT, Vietnam

CITATION: Quang Khanh Nguyen, Le Hung Trinh, Khanh Hoai Dao, Nhu Duan Dang (2018) Land Surface Temperature Dynamics In Dry Season 2015-2016 According To Landsat 8 Data In The South-East Region Of Vietnam. Geography, Environment, Sustainability, Vol.12, No 1, p. 75-87
DOI-10.24057/2071-9388-2018-06

INTRODUCTION

Vietnam is likely to be one of the several countries most adversely affected by climate change. During the last 50 years, Vietnam's annual average surface temperature has increased by approximately 0.5 – 0.7 0C (Vietnam assessment report on climate change). LST is important factor in global change studies, in estimating radiation budgets in heat balance studies and as a control for climate models. LST can provide important information about the surface physical properties and climate which plays a role in many environmental processes (Mallick et al. 2008; Mira 2007). The estimation of LST pays important role in numerical modeling especially in physical based hydrological models where water balance/budgeting of the catchment is an important component (Thakur and Gosavi 2018).

Many researchers have used remote sensing data to determine and monitor LST distribution. Retrieval of LST using thermal infrared bands of satellite images is the most effective way to derive energy balance and evapotranspiration (ET) on regional basis (Pariada et al. 2008). Since the last of 20th century, satellite-derived surface temperature data have been utilized for regional climate analyses on different scale (Carnahan and Larson 1990). Beginning with Landsat 4, Landsat satellite series provides the data for retrieval of LST for longer period of time. Landsat 5 TM and Landsat 7 ETM+ data were used to estimate LST in urban area (Alipour et al. 2007; Mallick et al. 2008; Kurma et al. 2012; Balling and Brazel 1988; Grishchenko 2012; Marchokov and Trinh 2013; Tran et al. 2009; Trinh 2014). The results of these studies have demonstrated that in the big cities, urban heat island effect is becoming a problem due to increasing coverage of land with asphalt pavements.

The relationship between LST and vegetated areas has been documented in the many studies. Cueto et al. (2007) found correlation between surface temperature in Mexicali (Mexico) and land use by using remote sensing data. Hyung Moo Kim et al. (2005) proposed algorithm to estimate the statistical correlation between LST and vegetation index. A study by Cai et al. (2017) analyzed the relationship between LST and land cover changes in Zhengzhou city (Huabei Plain) using multi-temporal satellite data. They examined the usefulness of Landsat 5 TM imagery for classifying land cover/land use and using thermal infrared band (band 6) to produce a thermal map of Zhengzhou city.

LST is also one of the most important factors in studying drought phenomenon, as well as input parameters for climate models (Alshaikh 2015). Many studies have proven that a combination of surface temperature and normalized difference vegetation index (NDVI) can provide information about surface soil moisture. A study by Lambin and Ehrlich (1996) reviewed extensively the drivers between normalized difference vegetation index (NDVI) and brightness temperature (BT), and described a general spatial pattern of relationships between NDVI and BT, related to land cover. They concluded that BT/NDVI slope could be used to classify land cover, and monitor land cover changes over time when associated to seasonality information, retrieved from NDVI annual variations alone (Julien and Sobrino 2009). Sandholt et al. (2002) proposed a drought index called Temperature Vegetation Dryness Index (TVDI), which is calculated from satellite derived vegetation index (NDVI) and surface temperature. This drought index is also used in many other studies to assess soil moisture and drought status (Zverev and Trinh 2015; Chen et al. 2011; Shang et al. 2017).

A number of algorithms have been used to estimate the LST using remote sensing thermal infrared (TIR) data as it is capable to decipher the thermal characteristic of the land surface. These algorithms are namely mono-window (MW), split-window (SW), dual-angle (DA), single-channel (SC)… (Galve et al. 2008; Rongali et al. 2018). The studies carried out in different areas, such as the northern Negev Desert, Israel (Du et al. 2014; Rozenstein et al. 2014) and the Beas River basin, India (Rongali et al., 2018) show that the split-window algorithm can be adjusted for estimating LST from Landsat 8 data to get better accuracy. The objective of our paper is to evaluate the dynamics of LST in Loc Ninh district, Binh Phuoc province of Southeast region of Vietnam during 2015 – 2016 dry season using Landsat 8 multi-temporal data. SW algorithm was used to calculate LST from Landsat 8 data in this case study.

STUDY AREA AND MATERIALS

Loc Ninh is a mountainous district in the northwestern border of Binh Phuoc province, with a borderline of over 100 kilometers. It is bordered by Kratie and Cong Pong Cham provinces (Cambodia). The area is bounded between latitude 11^{0}39’6.09”N to

12^{0}05’50.7”N and longitude 106^{0}24’39.5”E to 106^{0}59’19.3”E (Fig. 1) (locninh.binhphuoc.gov.vn, 2018). The district covers an area of 853.95 km^2 and had a population of 115268 people (locninh.binhphuoc.gov.vn, 2018). Loc Ninh district has a high terrain in the north and low terrain in the south. It located in tropical monsoon region; the climate is divided into two seasons: the rainy season from May until October and the dry season from November to April, while March and April are the warmest and driest months. This is the largest pepper growing area of Binh Phuoc province and also is one of the most regions severely affected by drought in Southeast region of Vietnam.
In this study, five multispectral cloud – free LANDSAT 8 OLI - TIRS images (path 124, row 52) with a spatial resolution of 30x30 meters were acquired from November 24, 2015, December 26, 2015, January 11, 2016, February 28, 2016 and March 31, 2016 (Fig. 2). The LANDSAT 8 data was the standard terrain correction products (L1T), downloaded from United States Geological Survey (USGS – http://glovis.usgs.gov) website. The data used in this study was grouped into two categories (Table 1): the thermal infrared data (band 10) was used to calculate temperature, the red (band 4) and near infrared band (band 5) to calculate surface emissivity based on normalized difference vegetation index (NDVI).

The SW algorithm is based on the different atmospheric absorption behavior of two ra-

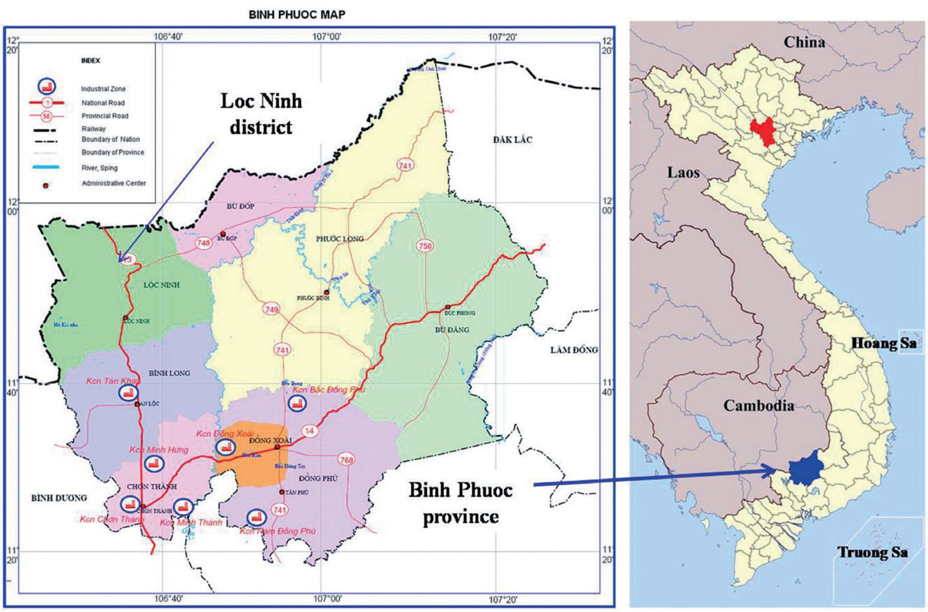

Fig. 1. The study area, Loc Ninh district, Binh Phuoc province, Vietnam

Table 1. Overview of the satellite scenes applied in this study

No.	Data type	Band used for temperature	Band used for NDVI	Time of data acquisition
1	LANDSAT 8	10	4, 5	24 November 2015
2	LANDSAT 8	10	4, 5	26 December 2015
3	LANDSAT 8	10	4, 5	11 January 2016
4	LANDSAT 8	10	4, 5	28 February 2016
5	LANDSAT 8	10	4, 5	31 March 2016

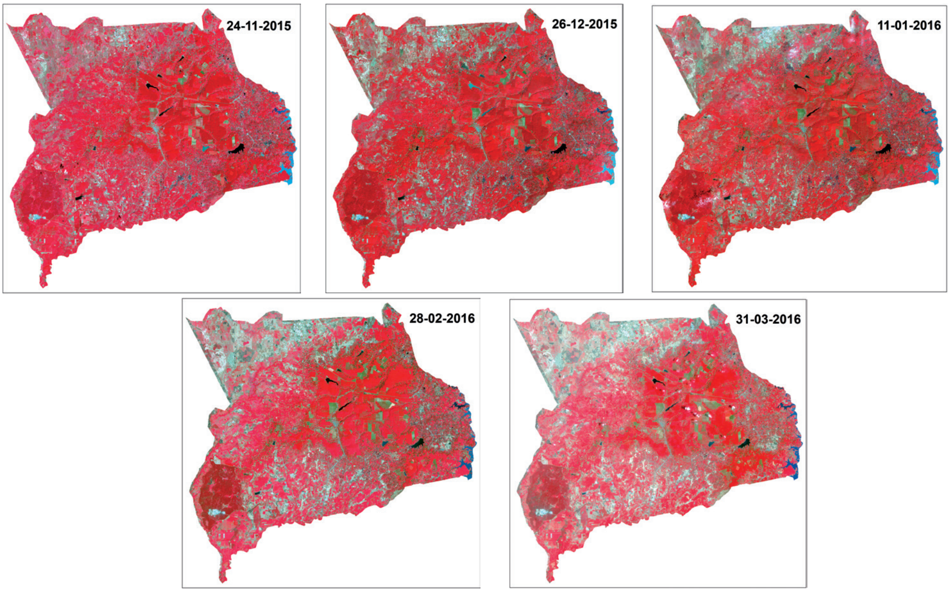

Fig. 2. LANDSAT 8 multispectral images in Loc Ninh district, RGB:543

Methodology

Table 2. SW coefficient values for TIRS band of Landsat 8 imagery

No.	Constants	Value
1	C_0	-0.268
2	C_1	1.378
3	C_2	0.183
4	C_3	54.300
5	C_4	-2.238
6	C_5	-129.200
7	C_6	16.400

diometric channels within the 10 – 12.5µm window region (Rongali et al. 2018). The basis of the SW algorithm is the radiance attenuation for atmospheric absorption, which is proportional to the radiance difference of simultaneous measurements at two different wavelengths, each of them being subject to varying amounts of atmospheric absorption (McMillin 1975; Rongali et al. 2018). According to this algorithm, LST can be determined by the following formula (Jiménez-Muñoz et al. 2014):

Where:

$$T_s = T_{B10} + c_1(T_{B10} - T_{B11}) + c_2(T_{B10} - T_{B11})^2 + \dots$$
$$\dots + c_0 + (c_3 + c_4 w)(1 - \varepsilon) + (c_5 + c_6 w)\Delta\varepsilon \quad (1)$$

T_s – land surface temperature;
T_{B10}, T_{B11} – brightness temperature of band 10 and 11 of Landsat 8 imagery;
W – atmospheric water vapor content (g/cm^2). The value of atmospheric water vapor content is calculated using formula proposed by Huazhong (Huazhong et al. 2014);
ε – mean emissivity;
Δε – emissivity difference;
C_0 to C_6 – SW coefficients values. The values of SW coefficients are given in Table 2 (Sobrino et al. 2006; Skokovic et al. 2014).

The flowchart of SW algorithm utilized in the present study for the estimation of LST is shown in Fig. 3.

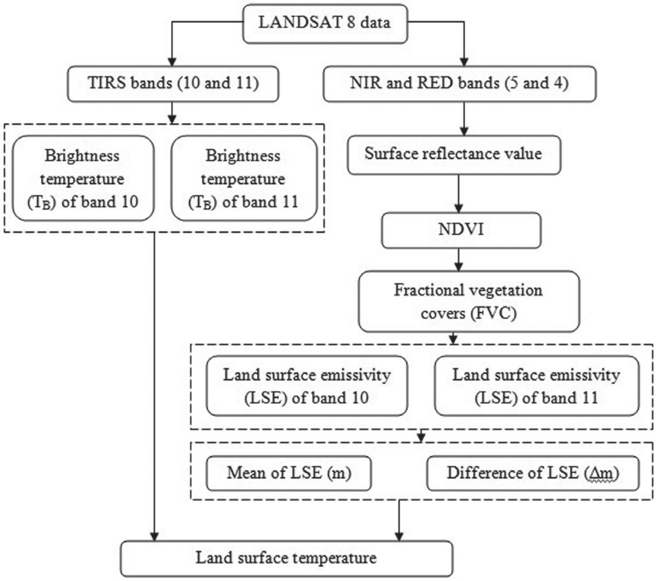

Fig. 3. Split-Window algorithm for LST retrieval

In first step, OLI and TIRS band data must be converted to TOA spectral radiance using the radiance rescaling factors provided in the metadata file (Landsat.usgs.gov, 2018):

$$L_\lambda = M_L \cdot Q_{cal} + A_L \qquad (2)$$

where:
L_λ - TOA spectral radiance (Watts/(m^2 * srad * µm)),
M_L - Band-specific multiplicative rescaling factor from the metadata (RADIANCE_MULT_BAND_x, where x is the band number) (Landsat.usgs.gov, 2018),
A_L - Band-specific additive rescaling factor from the metadata (RADIANCE_ADD_BAND_x, where x is the band number) (Landsat.usgs.gov, 2018),
Q_{cal} - Quantized and calibrated standard product pixel values (DN).

Table 3. LANDSAT 8 TIRS spectral radiance ML, AL dynamic ranges

No.	Data type	Band	M_L	A_L
1	LANDSAT 8 TIRS	10	3.3420×10^{-4}	0.10000

In second step, the LANDSAT thermal band data (band 10 and band 11) can be converted form spectral radiance to brightness temperature using following equation (Landsat.usgs.gov, 2018):

$$T_B = \frac{K_2}{In(\frac{K_1}{L_\lambda}+1)} \qquad (3)$$

where:
T_B – At satellite brightness temperature (K),
K_1 – Calibration constant 1 (W/(m^2.sr.µm)),
K_2 – Calibration constant 2 (K) (Landsat.usgs.gov, 2018).

For determining LST from LANDSAT data, values of land surface emissivity are needed. In this paper, the surface emissivity is

Table 4. LANDSAT 8 thermal band calibration constants

No.	Data type	Band	K_1 (W/(m^2.sr.µm))	K_2 (Kelvin)
1	LANDSAT 8	10	774.89	1321.08
2	LANDSAT 8	11	480.89	1201.14

determined by using method based on NDVI image, which proposed by Valor and Caselles (1996) by following equation (Valor and Caselles 1996):

$$\varepsilon = \varepsilon_v \cdot P_v + \varepsilon_s (1 - P_v) \tag{4}$$

where:
ε – Surface emissivity,
ε_v, ε^s – Emissivity of pure vegetation covers and pure soil areas, respectively.
P_v - The percentage of vegetation in one pixel, which calculated by equation (Vlassova et al. 2014):

$$Pc = \left(\frac{NDVI - NDVI_{soil}}{NDVI_{veg} - NDVI_{soil}} \right)^2 \tag{5}$$

where:
NDVI – normalized difference vegetation index, which can be calculated by equation (Rouse et al. 1973):

$$NDVI = \frac{NIR - RED}{NIR + RED} \tag{6}$$

RED and NIR – the spectral reflectance in red and near – infrared band, respectively. NDVIveg. and NDVIsoil - the NDVI values of vegetation and open soil, which are determined experimentally using a series of test area for vegetation and open soil.

For calculating NDVI index, the digital number of red and near infrared band was converted to surface reflectance value. In this study, one very advance atmospheric approach (FLAASH) has been applied on the Landsat 8 multispectral image, and then, the NDVI is calculated according to Eq. 7.

The land surface emissivity images of bands 10 and 11 are used to calculate mean and difference emissivity:

$$\varepsilon = \frac{\varepsilon_{10} + \varepsilon_{11}}{2} \tag{7}$$

$$\Delta\varepsilon = \varepsilon_{10} - \varepsilon_{11} \tag{8}$$

In last step, LST can be calculated by following equation (1).

RESULTS AND DISCUSSION

The reflectance values for red and near infrared channels of LANDSAT 8 data was used to calculate normalized difference vegetation index (NDVI). For determining surface emissivity by this methodology, values of soil and vegetation emissivity are needed. The emissivities of pure soil and pure vegetation cover were calculated from the MODIS UCSB emissivity library using method proposed by Tang (Tang et al. 2011). Soil and vegetation emissivities for Landsat 8 TIRS bands are listed in Table 5 (Yu et al. 2014).

Basing on the emissivities values of soil and vegetation, emissivity image was prepared using method of Valor and Caselles by using formula (5).

From brightness temperature and land surface emissivity images, the LST image was obtained by using Spatial Modeler of ERDAS Imagine 2014 program. Fig. 4 shows the spatial distribution of LST in Loc Ninh district, Binh Phuoc province (Southeast region of Vietnam) in dry season 2015 – 2016.

The LST ranged from 296.85 to 316.04 K in November 24, 2015; 292.52 to 311.17 K in December 26, 2015; 298.85 to 313.92 K in January 11, 2016; 298.42 to 321.27 K in February 28, 2016 and 300.20 to 321.53 K in March 31, 2016. Thus, it can be seen that the minimum and maximum LST in the early months of the dry season 2015 – 2016 (November and December) is much lower than in February and March (the end of dry season). The average LST in dry season 2015 – 2016 in Loc Ninh district, Binh Phuoc province also increased significantly, corresponding to 301.02 K in

Table 5. Emissivities of soil and vegetation for Landsat 8 TIRS band 10 and 11

No.	Band	Soil	Vegetation
1	Band 10	0.9668	0.9863
2	Band 11	0.9747	0.9896

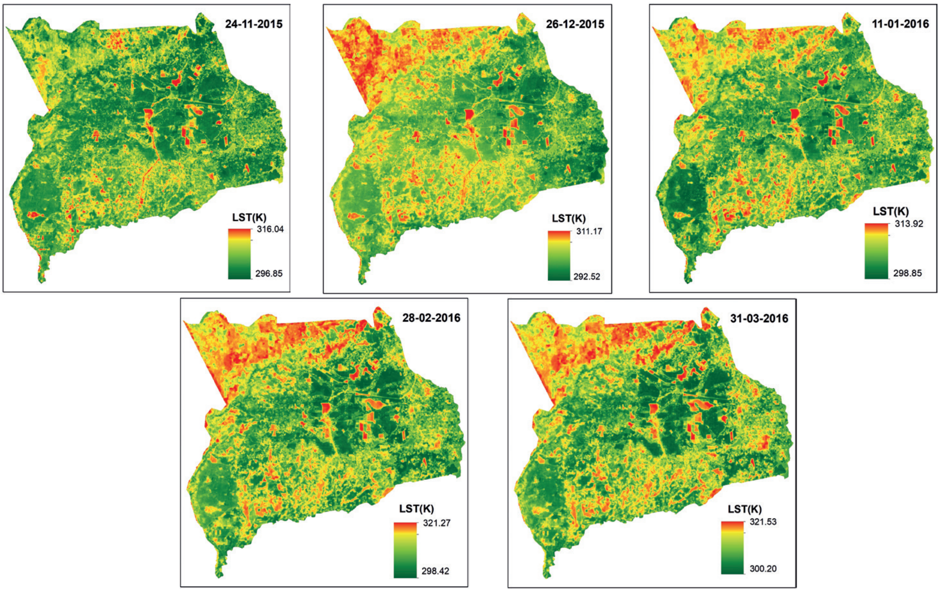

Fig. 4. LST over study area in dry season 2015 – 2016 retrieval from LANDSAT 8 data

November 24, 2015; 300.89 K in December 26, 2015; 303.82 K January 11, 2016; 305.18 K in February 28, 2016 and 308.42 K in March 31, 2016. According to obtained result, the northern area has highest LST in all months of dry season 2015 – 2016 (Fig. 4). These areas have sparse vegetation cover and uncultivable land. High LST are also recorded in agricultural land use and residential land in the center and southern part of the study area. Meanwhile the area with full vegetation coverage in center of study area has much lower LST.

LST data from 10 measurements points at February 28, 2016 (Fig. 5d) were used in the comparison with temperature calculated from Landsat 8 image, which acquired from same day. This in situ data were observed in the framework of the ministry-level project (Ministry of Natural Resources and Environment (Vietnam), No. 2015.08.10) and were collected from 10:00 am to 11:00 am local time in the day selected. Comparison between the LST at the measurement points and the results calculated from the Landsat 8 satellite image (February 28, 2016) based on SW and MW algorithms is presented in Table 6. It can be seen that LST at the measurements points is lower than the temperature calculated from the Landsat 8 image. The biggest difference between in situ data and LST calculated from the Landsat 8 image is 1,75 (K) degree. In addition, it can be seen that the LST value determined by SW and single-channel (SC) algorithms are highly similar. However, overall the LST value determined by used SW algorithm tends to be smaller than using the SC algorithm (Table 6). Thus, the difference between the LST values determined by used SW algorithm and the in situ data is lower than using the SC algorithm.

The LST distribution map of the study area displays the different zone of temperatures. The density sliced image shows seven temperature zones that represents greater than 310, 309 – 310, 307 – 309, 305 – 307, 303 – 305, 301 – 303 and less than 301 K respectively. LST distribution maps in Loc Ninh district, Binh Phuoc province in dry season 2015 – 2016 are shown in Fig. 4 and Table 7. Analysis of the results showed that, in the early of dry season, much of the study area has a lower LST (less than 301 K), corresponding to 57,12% and 58,11% of the total area on November 24 and December 26, 2015. Areas with temperatures between 301 and 303 K also occupy significant areas in the early dry season (33,57% and 22.20% of the total area on November 24 and December 26,

Table 6. Compare the LST at the measurement points and the results calculated from the Landsat 8 satellite image

No. of monitoring location	Coordinates	LST (K)			Difference (K)
		From remote sensing data		In situ data	
		SW algorithm	SC algorithm (band 10)		
1	11⁰ 49'24" N 106⁰ 35'48" E	308.45	309.31	307.50	0.95
2	11⁰ 50'59" N 106⁰ 35'27" E	310.34	310.45	309.10	1.24
3	11⁰ 50'24" N 106⁰ 31'20" E	311.27	311.94	310.20	1.07
4	11⁰ 51'14" N 106⁰ 36'07" E	302.68	302.93	301.40	1.28
5	11⁰ 50'49" N 106⁰ 35'36" E	310.65	310.80	308.90	1.75
6	11⁰ 50'28" N 106⁰ 34'47" E	309.29	309.48	308.30	0.99
7	11⁰ 51'24" N 106⁰ 36'17" E	300.78	300.90	299.50	1.28
8	11⁰ 51'34" N 106⁰ 35'57" E	300.47	300.75	299.20	1.27
9	11⁰ 50'26" N 106⁰ 36'07" E	303.88	303.97	303.10	0.78
10	11⁰ 52'10" N 106⁰ 39'16" N	313.74	313.81	312.50	1.24

2015). Areas with LST over 309 K occupy relatively small areas; especially areas with temperatures above 309 K are almost negligible (less than 0.1% of the total study area at the early of dry season).

Areas with LST less than 301 K strongly decreased at the mid-dry season (January 2016), which occupies only 5,41% of the total area of the district. Most of the study area at the mid-dry season has LST between 301 to 307 K (over 92% of the total area). Areas with LST over 307 K, although increased compared to the early of dry season, however, it accounts for over 2% of the total study area.

The LST increases rapidly at the end of the dry season, from the end of February 2016. Most of the study area at the end of dry season 2015 – 2016 has LST over 303 K, in that area with LST over 309 K a significant increase, corresponding to 20,46% and 31,20% of the total study area on February 28 and March 31, 2016. Thus, it can be noticed, LST of Loc Ninh district tend to increase significantly in dry season 2015 – 2016, in that March is considered to be the hottest month. This is also consistent with monitoring data at meteorological stations and in situ data of ministry-level project (Ministry of Natural Resources and Environment (Vietnam), No. 2015.08.10).

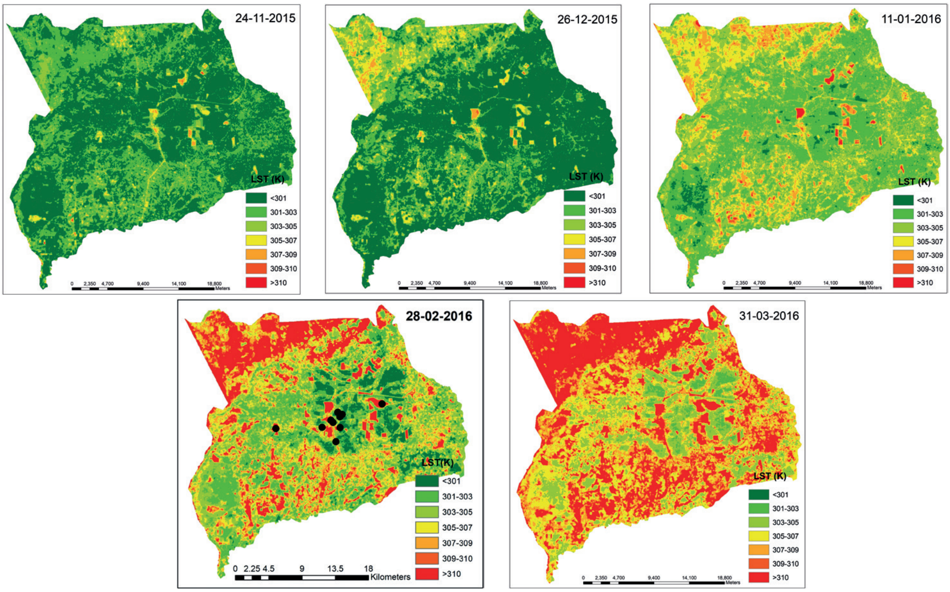

Fig. 5. Spatial distribution of LST over study area in dry season 2015 – 2016 using LANDSAT 8 data

Table 7. Temporal dynamics of LST in Loc Ninh district, Binh Phuoc province in dry season 2015 - 2016

No.	LST (K)	Area									
		November 24, 2015		December 26, 2015		January 11, 2016		February 28, 2016		March 31, 2016	
		ha	%	ha	%	ha	%	ha	%	ha	%
1	< 301	48580.56	57.12	49422.56	58.11	4601.21	5.41	5162.54	6.07	2423.93	2.85
2	301-303	28551.29	33.57	18881.1	22.2	30796.61	36.21	16780.37	19.73	13837.64	16.27
3	303-305	6259.68	7.36	10112.44	11.89	25276.86	29.72	19714.59	23.18	17988.08	21.15
4	305-307	1292.76	1.52	5307.12	6.24	15972.39	18.78	16559.24	19.47	17350.2	20.4
5	307-309	314.685	0.37	1233.23	1.45	6693.44	7.87	9432.05	11.09	6914.57	8.13
6	309-310	34.02	0.04	25.52	0.03	995.09	1.17	13276.31	15.61	22912.47	26.94
7	> 310	17.01	0.02	68.04	0.08	714.42	0.84	4124.93	4.85	3623.13	4.26

CONCLUSION

In this study, we applied SW algorithm to retrieve LST from Landsat 8 TIRS data for a case study of Southeast region of Vietnam in 2015 – 2016 dry season. Results obtained from the proposed SW algorithm have been compared with the results obtained from the SC algorithm (using only band 10) and in situ data of LST to assess the performance of the SW algorithm. It is observed that the LST obtained from SW and SC algorithms are having similar order of values, however, the SC algorithm estimates higher temperature values as compared with the SW algorithm.

The spatial distribution of LST obtained from SW algorithm showed that LST in Loc Ninh district, Binh Phuoc province (Southeast region of Vietnam) at the end of 2015 – 2016 dry season is a significant increase compared to the early dry season. This increase expressed in minimum, maximum and average LST, especially areas with temperatures higher than 309 K. The study reveals that the central part of Loc Ninh district with high canopy cover has lower LST, whereas in the northern part with barren lands and residential area have high LST values.

The results obtained in this study can be used to map and evaluate the dynamics of LST, and to provide the input information for drought assessment and monitoring models.

ACKNOWLEDGMENTS

The authors would like to express their sincere gratitude to the research team from the Hanoi University of Natural Resources and Environment for providing in situ data on this paper.

REFERENCES

Alipour T., Sarajian M.R., Esmaseily A. (2004). Land surface temperature estimation from thermal band of LANDSAT sensor, case study: Alashtar city. The International Archives of the Photogrammetry. Remote Sensing and Spatial Information Sciences, 38(4)/C7.

Alshaikh A.Y. (2015). Space application for drought assessment in Wadi-Dama (West Tabouk), KSA. The Egyptian Journal of Remote Sensing and Space Science, 18, 543 – 553.

Balling R.C., Brazel S.W. (1988). High – resolution surface temperature patterns in a complex urban Terrain. Photogrammetric engineering and Remote sensing, 54(9), 1289 – 1293.

Cai Q., Ki E., Jiang R. (2017). Analysis of the relationship between land surface temperature and land cover changes using multi-temporal satellite data. Nature Environment and Pollution Technology, 16(4), 1035 – 1042.

Carnahan W.H., Larson R.C. (1990). An analysis of an urban heat sink. Remote Sensing of Environment, 33(1), 65–71.

Chen J., Wang C., Jiang H., Mao L., Yu Z. (2011). Estimating soil moisture using temperature – vegetation dryness index (TVDI) in the Huang-huai-hai (HHH) plain. International Journal of Remote Sensing, 32, 1165 – 1177.

Cueto G., Jauregui Ostos E., Toudert D., Tejeda Martinez A. (2007). Detection of the urban heat island in Mexicali and its relationship with land use. Atmosfera, 20(2), 111 – 131.

Du C., Ren H., Qin Q., Meng J., Li J. (2014). Split-window algorithm for estimating land surface temperature from Landsat 8 TIRS data. International Geoscience Remote Sensing Symposium 3578–3581, https://doi.org/10.1109/IGARSS.2014.6947256

Galve J.M., Coll C., CasellesV., Valor E., Mira M. (2008). Comparison of split-window and single-chanel methods for land surface temperature retrieval from MODIS and ASTER data. International Geoscience Remote Sensing Symposium 3:294 – 297, https://doi.org/10.1109/IGARSS.2008.4779341

Grishchenko M.Y. (2012). ETM+ thermal infrared imagery application for Moscow urban heat island study. Current Problems in Remote Sensing of the Earth from Space, 9(4), 95-101 (In Russian).

Jiménez-Muñoz J.C, Sobrino J.A., Skoković D., Mattar C., Cristóbal J. (2014). LST retrieval methods from Landsat-8 thermal infrared sensor data. IEEE Geoscience and Remote Sensing Letters, Vol. 11, No. 10, 1840-1843, doi: 10.1109/LGRS.2014.2312032.

Julien Y., Sobrino J.A. (2009). The yearly land cover dynamics method: an analysis of global vegetation from NDVI and LST parameters. Remote Sensing of Environment, 113, 329 – 334.

Kumar K.S., Bhaskar P.U., Padmakumari K. (2012). Estimation of land surface temperature to study urban heat island effect using LANDSAT ETM+ image. International journal of Engineering Science and technology, 4(2), 771 – 778.

Huazhong R., Du C., Qin Q., Liu R. (2014). Atmospheric water vapor retrieval from Landsat 8 and its validation, IEEE International Geoscience and Remote Sensing Symposium, 3045 – 3048, doi: 10.1109/IGARSS.2014.6947119.

Hyung Moo Kim, Beob Kyun Kim, Kang Soo You (2005). A statistic correlation analysis algorithm between land surface temperature and vegetation index. International Journal of Information Processing Systems, 1(1), 102 – 106.

Lambin T.R., Ehrlich D. (1996). The surface temperature – vegetation index space for land cover and land cover change analysis. International Journal of Remote Sensing, 17(3), 163 – 187.

Landsat.usgs.gov, (2018). Landsat 8 (L8) data users handbook, Version 3.0. [online] Available at http://landsat.usgs.gov [Accessed 31 October 2018]

Li S., Jiang G. (2018). Land surface temperature retrieval from Landsat-8 data with the ggeneralized split-window aalgorithm. IEEE Access, Vol. 6, 18149-18162, doi: 10.1109/ACCESS.2018.2818741.

Lo C.P., Quattochi D.A., Luvall J.C. (1997). Application of high resolution thermal infrared remote sensing and GIS to assess the urban heat island effect. International Journal of Remote Sensing, 18, 287 – 304.

Locninh.binhphuoc.gov.vn, (2018). Locninh district Official Website. [online] Available at http://locninh.binhphuoc.gov.vn [Accessed 20 October 2018]

Mallick J., Kant Y., Bharath B.D. (2008). Estimation of land surface temperature over Delhi using LANDSAT 7 ETM+. Geophysics Union, 3, 131 – 140.

Marchukov V.S., Trinh L.H. (2013). Monitoring land surface temperature using LANDSAT thermal infrared image. Izvestiya Vuzov «Geodesy and Aerophotography», 6, 41 – 43 (In Russian).

McMillin L. (1975). Estimation of sea surface temperatures from two infrared window measurements with different absorption. Journal of Geophysical Research 80:5113–5117,

Mira M., Valor E., Boluda R., Caselles V., Coll C. (2007). Influence of the soil moisture effect on the thermal infrared emissivity. Tethes, 4, 3 – 9, doi: m10.3369/Tethys.2007.4.01.

Parida B.R., Oinam B., Patel N.R., Sharma N., Kandwal R., Hazarika M.K. (2008). Land surface temperature variation in relation to vegetation types using MODIS satellite data in Gujarat state of India. International Journal of Remote Sensing, 29(14), 4219 – 4235.

Rongali G., Keshari A.K., Gosain A.K., Khosa R. (2018). Split-window algorithm for retrieval of land surface temperature using Landsat 8 thermal infrared data. Journal of Geovisualization and Spatial Analysis, Published online 05 September 2018, Springer, 19 pp.

Rouse J.W., Hass R.H., Schell J.A., Deering D.W. (1973). Monitoring vegetation systems in the Great Plains with ERTS. In: Earth Resources Technology Satellite-1 Symposium, 3, Washington- DC, p. 309-317

Rozenstein O., Qin Z., Derimian Y., Karnieli A. (2014). Derivation of land surface temperature for landsat-8 TIRS using a split window algorithm. Sensors 14:5768–5780, https://doi.org/10.3390/s140405768

Sandholt I., Rasmussen K., Anderson J. (2002). A simple interpretation of the surface temperature/vegetation index space for assessment of the surface moisture status. Remote Sensing of Environment, 79, 213–224.

Shang Y., Hu Q., Liu G., Zhang H. (2017). Winter wheat drought monitoring and comprehensive risk assessment: case study of Xingtai administrative district in North China, Journal of Environmental Science and Engineering, A6, 135 – 143.

Sobrino J.A., Jimenez-Munoz J.C., Zarco-Tejada P.J., Guadalupe Sepulcre-Canto, Eduardo de Miguel (2006). Land surface temperature derived from airborne hyperspectral scanner thermal infrared data. Remote Sensing of Environment, 102, 99 – 115.

Skokovic D., Sobrino J.A., Jiménez Muñoz J.C., Soria G., Julien Y., Mattar C., Cristóbal J. (2014). Calibration and validation of land surface temperature for Landsat8- TIRS sensor TIRS Landsat-8 characteristics. Land Product Validation and Evolution ESA/ESRIN 27.

Tang B.H., Wu H., Li C., Li Z.H. (2011). Estimation of broadband surface emissivity from narrowband emissivities. Optical Express, 19, 185 – 192.

Thakur P., Gosavi V. (2018). Estimation of temporal land surface temperature using thermal remote sensing of Landsat 8 (OLI) and Landsat 7 (ETM+): A case study in Sainj river basin, Himachal Pradesh, India. Environment & We: International Journal of Science & Technology, Vol. 13, 29 – 45.

Tran T.V., Hoang T.L., Le V.T. (2009). Thermal remote sensing method in sudy on urban surface temperature distribution. Vietnam Journal of Earth Sciences, 31(2), 168 – 177.

Trinh L.H. (2014). Studies of land surface temperature distribution using LANDSAT multispectral image. Vietnam Journal of Earth Sciences, 36(1), 82 – 89.

Ulivieri C., Castronuovo M., Francioni R., Cardillo A. (1994). A split window algorithm for estimating land surface temperature from satellites. Advanced Space Research 14:59–65, https://doi.org/10.1016/0273-1177(94)90193-7

Valor E., Caselles V. (1996). Mapping land surface emissivity from NDVI. Application to European African and South American areas. Remote Sensing of Environment, 57, 167 – 184.

Van de Griend A.A., Owen M. (1993). On the relationship between thermal emissivity and the normalized difference vegetation index for natural surface. International Journal of Remote Sensing, 14, 1119 – 1131.

Vietnam assessment report on climate change (VARCC) (2009), Institute of strategy and policy on natural resources and environment. Hanoi, 127 pp.

Vlassova L., Perez-Cabello F., Nieto H., Martin P., Riaflo D., de la Riva J. (2014). Assessment of methods for land surface temperature retrieval from Landsat 5 TM images applicable to multiscale tree-grass ecosystem modeling, Remote Sensing, 6, 4345-4368; doi:10.3390/rs6054345.

Yu X., Guo X., Wu X. (2014). Land surface temperature retrieval from Landsat 8 TIRS – Comparison between radiative transfer equation based method, split window algorithm and single channel method, Remote Sensing, 6, 9829 – 9852, doi:10.3390/rs6109829.

Zverev A.T., Trinh L.H. (2015). Monitoring soil moisture using LANDSAT multispectral images. Issledovanie Zemli iz Kosmosa, 6, 62 – 67 (In Russian).

Received on February 22nd, 2018 Accepted on February 20th, 2019

Sergei P. Koshkin[1*] and Tatiana M. Krasovskaya[1]
[1] Faculty of Geography, Lomonosov Moscow State University, Moscow, Russia
***Corresponding author:** spkoshkin@gmail.com

WIND FARMS – COMBINING ENERGY AND ECOLOGICAL PERFORMANCE IN CRIMEA

ABSTRACT. Renewable energy use is spreading worldwide presenting the future of the power engineering – its renewable resources and low ecological impact characterize one of the best technologies to support permanently growing energy consumption and contribute to sustainable development. But its development is sometimes hampered by lack of suitable technologies and strong positions of the competing conventional energy production. Moreover, critics emphasize such problems of renewable energy use as unstable energy production, complicated connection to power lines, some ecological problems. To prove its efficiency renewable energy development needs support by relevant resource and ecological assessments. This paper presents our research concerning wind farm location issue regarding both production efficiency and minimal ecological impact. Our field research in Crimea was directed at on-site assessment of wind farm location efficiency as well as studies of public opinion concerning local wind farms and wind energy use in general. It was found out that Crimean wind farms have controversial location efficiency related to its power production. But their ecological impact was minimal proved by both on-site measurements and sociological survey results. It was also found that wind turbine noise impact had a very complicated character, but had no significant ecological impact.

KEY WORDS: wind energy, wind farm, placement, ecological impact, Crimea

CITATION: Sergei P. Koshkin and Tatiana M. Krasovskaya (2018) Wind Farms – Combining Energy And Ecological Performance In Crimea. Geography, Environment, Sustainability, Vol.12, No 1, p. 88-103
DOI-10.24057/2071-9388-2018-51

INTRODUCTION

Nowadays economic activities are promoted by power engineering development which ecological footprint may be clearly determined. Turn to renewable energy use may help to solve both problems. But renewable energy use also has a certain negative ecological impact, depending mainly on technological issues. Combining energy and ecological efficiency is a very complicated task. We tried to characterize wind farms at our study area in this respect using world experience in efficient work of wind farms and minimization of wind turbines environmental impact. We avoid discussion of financial aspects of wind farms construction and operation presenting quite different aspect of efficient wind energy use.

Background

The principle factor controlling wind farm energy generation and environmental impact at a local level of wind energy use is its location in the environment. .Efficiency of electricity generation is defined by two issues: wind power potential depending on meteorological parameters and interdependent work of wind turbines since each wind turbine (being a physical obstacle) produces a turbulent trace in the airflow. Such effect is noticeable at some distance from a wind turbine depending on a rotor diameter (UK Department of the Environment 2007; Samorani 2010; Meyers and Meneveau 2011).

Being at the top list of environment-friendly power production wind energy production still has some negative impact (Fig. 1) (Rabl and Spadaro 2005). Minimization of wind farm ecological impact requires detailed field studies of local landscapes, fauna, human health.

Environment impact also depends on a stage of wind farm project implementation. At the construction stage mechanical disturbances are typical and might be harmful for local land use (Brannstrom at al. 2017), while there is only contradictory visual impact at the operation stage (Filin 1997; NZWEA 2017). Impact on animals differs a lot: from physical contact (birds, bats, insects) (AWEA 2006; Baerwald at al. 2008; Dillo and Tronstad 2012) to low-frequency vibrations and noise (livestock in stalls, meadow and desert fauna) and ground vibration (soil meadow and desert fauna) (Mikolajczak at al. 2013; Lopucki and Perzanowski 2018). Human impact is connected with low-frequency vibrations and noise, but it should be a long-term impact to have any effect (Leventhall 2003). Noticeable impact on microclimate is possible only in case of large wind farms, where decreased annual wind speed leads to larger amplitudes of daily temperatures (Keith at al. 2004; Bettex 2012).

Study area

Our field research was conducted in September, 2017 in Crimea. This region was chosen as one of the best areas in Eastern Europe to develop wind energy use. Besides the Crimean Peninsula has sufficient wind (and solar) resources, this territory has already several wind (and solar) power stations (Fig. 2) which generated 25% of Crimean electricity in 2015 (MERF, 2015). But Crimean power production covered only 20% of local consumption (MERF, 2015). Considering this fact and problems with energy transport from other regions (RIA News Crimea 2015; Kommersant 2016; Regnum 2017; SM news 2017), the necessity of Crimean local power production is obvious. And this gives a chance to wind energy production development.

Nowadays seven wind farms (103.9 MW of total installed capacity) are being operated in different parts of the peninsula (Fig. 2). We have chosen three wind farms to study different models of wind turbines used for power production: Ostaninskaya, Presnovodnenskaya and Sakskaya (Mirnovsky site) wind farms (Table 1).

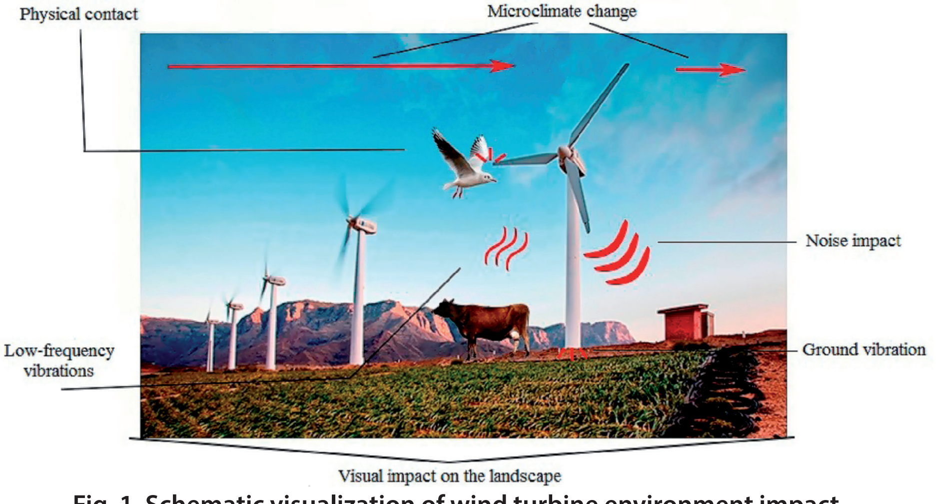

Fig. 1. Schematic visualization of wind turbine environment impact

Table 1. General characteristic of the studied wind farms

Wind farm	Location, operation period	The characteristic of installed wind turbines (SUE Crimean Generating Systems, 2017)				Total installed capacity
		Model	Capacity	Tower height/ Rotor diameter	Amount	
Ostaninskaya	25 km to the west from Kerch town, 1 km to the south-west from Stantsionnoe village: since year 2013	Furhlander FL2500/100	2,5 MW	98/100 m	10 turbines	25 MW
Presnovodnenskaya	25 km to the west from Kerch town, 2 km to the south from Stantsionnoe village: since year 2006	USW 56-100	107,5 kW	18/17 m	52 turbines	7,4 MW
		AN Bonus 600 kW	600 kW	50/44 m	3 turbines	
Sakskaya (Mirnovsky site)	21 km to the north-west from Evpatoria town, 2 km to the north from Krylovka village: since year 1998	USW 56-100	107,5 kW	18/17 m	155 turbines	18,46 MW
		Turbowinds T-600-48	600 kW	50/48 m	3 turbines	

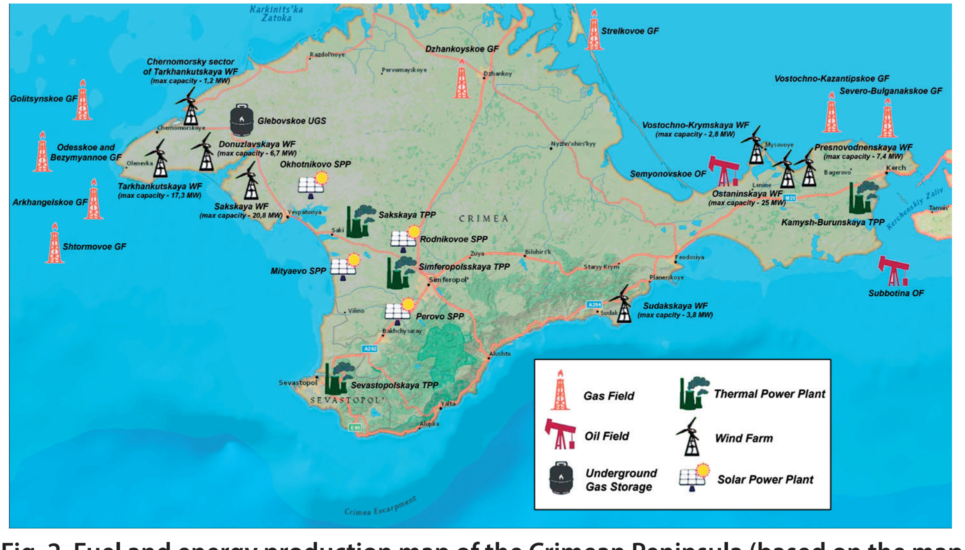

Fig. 2. Fuel and energy production map of the Crimean Peninsula (based on the map from Krymsky Telegraf 2013)

MATERIALS AND METHODS

To characterize the efficiency of electricity generation on the selected wind farms we assessed wind power potential at wind farms areas. The assessment data included Gismeteo meteorological data, relief (SRTM model) and land use pattern studies. The results were compared with projects data. Land use and wind farms schemes were received from IKONOS images (1m resolution). Wind power potential of wind farms areas was calculated using the following formulas (Elistratov, Kuznetsov, 2003):

U – wind speed at wind turbine height,

$$U = U_a \cdot K_h \qquad (1)$$

U_a – wind speed at anemometer height (10 m),

K_h – height adjustment factor, where

H – wind turbine height,

$$K_h = (H / h_a)^m \qquad (2)$$

h_a – anemometer height (10 m),

m – exponent which is taken depending on the wind speed at the height of anemometer

During the field research we visited the selected wind farms to measure noise and visual impact (loss of aesthetic landscape features) of wind farms and impact produced by specific wind turbine models. Noise measurement was provided by standard methods (SWL[1] type) using handheld SLM[2]. The received data was imposed on a land use map to define impact zones of wind farm. Visual impact of wind farms was characterized using aesthetical landscape science methods (Nikolaev 2005) and visual pollution methods (Filin 1997). We followed guidelines for visual impact assessment presented at Fig. 3.

At the same time, we conducted sociological survey asking local people about noise and visual impact of the neighboring wind farms and their general view on wind energy development in the region (Fig. 4).

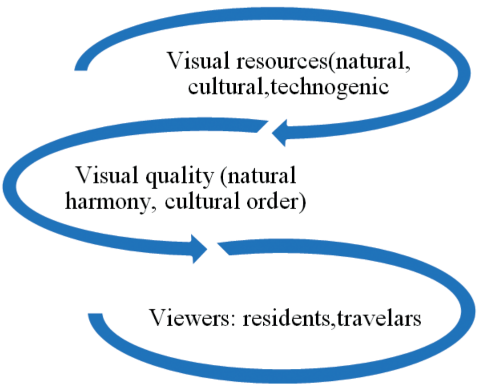

Fig. 3. Visual impact assessment process (Wilson 2002)

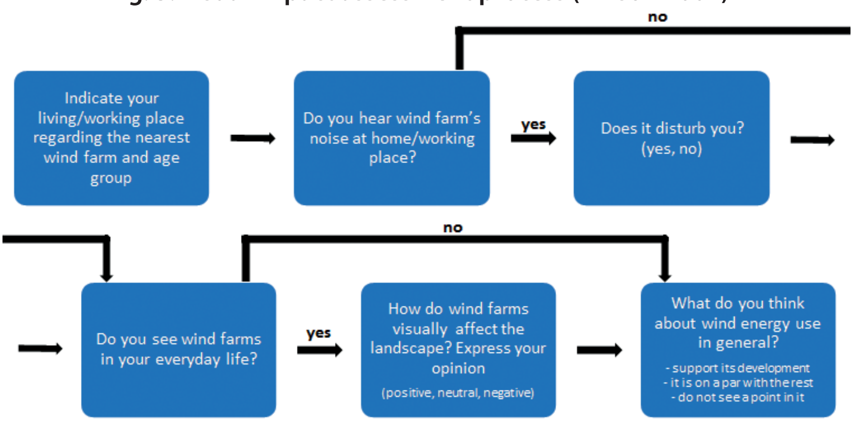

Fig. 4. The principal scheme of our sociological survey

RESULTS AND DISCUSSION

Each of the selected wind farms was characterized regarding their locations (affecting its energy production efficiency) and visual impact. Noise pollution was measured for each type of wind turbine models.

Location factors

Electricity generation efficiency of wind turbines highly depends on their location regarding wind power potential of a territory. Properly positioned modern wind turbines, being equipped by yaw system, may effectively and independently produce electricity permanently in case of strong enough winds of different directions.
But the situation changes when we deal with a wind farm consisting of two and more wind turbines. Every wind turbine causes air turbulence reducing wind power potential at some distance. That is why wind turbines should be placed to avoid negative affect on each other. If it is impossible, because of landscape factors or land space deficiency, the best variant is location directed to reduce negative effect from turbulent traces: to meet the maximal negative effect at the rarest wind direction minimizing it at the rest directions.

Current situation in wind energy development (which is confirmed in our research as well – see below) is controlled by wind turbine manufacturers trying to maximize sales while wind project developers try to receive maximal financial investments and minimize expenditures on rent/purchase of land sites (Mitchell 2014). As a result, the maximal possible number of wind turbines is placed at the minimal area rising economic efficiency of a project, but only at the stage of construction. A territory purchased by wind farm owners consists of wind turbine sites and linking roads. The rest belongs to municipal property (FSSRCCRF[3] 2018).

Receiving maximal economic efficiency at the construction stage, wind project developers reduce it in future as far as the installed wind turbines experience impact of turbulent traces and generate less electricity. Recent research (based on turbulent trace and land cost data) showed different data considering economically effective distances between wind turbines – from seven (Samorani 2010) to fifteen (Meyers and Meneveau 2011) rotor diameters of an installed wind turbine. In our research we used this range (seven to fifteen rotor diameters) and local wind roses to characterize selected wind farms layout and to assume the most optimal scheme considering land accessibility.

Sakskaya wind farm (Mirnovsky site). Mirnovsky site of Sakskaya wind farm is situated near Lake Donuzlav in the western flat part of the Crimean Peninsula. Wind farm territory and its surroundings consist of partly abandoned and flat fields with fragmentary tree rows, 5-10 m height which may cause turbulence affecting USW 56-100 wind turbines during western and southern winds (Fig. 5).

The distances between this wind farm turbines (Fig. 5), partially mismatch optimal – 119-225 m for USW 56-100 wind turbines and 336-720 m for T-600-48 wind turbines. General orientation of wind turbine rows is north-west/south-east – it is the rarest wind direction there. We supposed that the wind rose of the territory had been probably taken into account when designing Mirnovsky site, but there was obvious minimization of land use expenses. This caused losses in electricity generation by wind turbines – all of them were affected by turbulent traces from neighbor ones.

Ostaninskaya and Presnovodnenskaya wind farms.

Ostaninskaya and Presnovodnenskaya wind farms are located in the east and hilly part of the Crimean Peninsula near

[1] Sound Power Level
[2] Sound Level Meter)
[3] The Federal Service for State Registration, Cadastre and Cartography of Russian Federatio

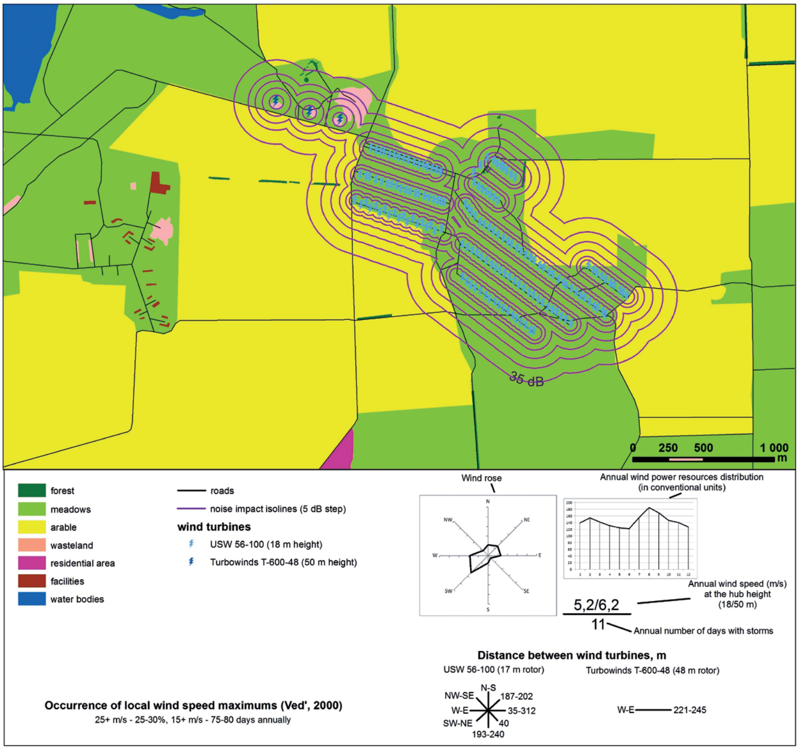

Fig. 5. Situational map at Mirnovsky site, Sakskaya wind farm

the Kazantip bay of the Sea of Azov (Fig. 6). While Ostaninskaya wind farm turbines were scattered over smooth meadows around Zelenoyarskoe water reservoir, Presnovodnenskaya wind farm stretched along the Kamenistyi Ridge at the southern border of the Kerch reservoir valley – the best place to locate wind farm in this area considering active recreational use of the nearby seacoast.

Distances between wind turbines of Ostaninskaya and Presnovodnenskaya wind farms (Fig. 6) (as well as for the previously discussed wind farm), did not match the following optimal distances – 119-255 m for US 56-100 wind turbines, 308-660 m for AN Bonus and 700-1500 m for FL2500/100 wind turbines. There might be different reasons for each case.

The row of Presnovodnenskaya wind farm turbines changed its direction from west/east to north-west/south-east. Winds of these directions were the rarest for the area (70 days per year for each direction). We consider this fact as coincidental, because the line of wind turbines was determined by the Kamenistyi Ridge. The top of the ridge was the most optimal position for wind turbines of Presnovodnenskaya wind farm, but the Kamenistyi Ridge length was much longer than the wind farm. We think that it was possible to prolongate the wind turbines row further to the east to reduce wake effect.

Arrangement of Ostaninskaya wind farm turbines was generally chaotic. Some wind turbines directed north-east/south-west or north/south experienced mutual trace effect It was particularly important as far as these directions were the most frequent for local winds. We suppose that local wind rose might have been analyzed during this wind farm project development, but developers probably considered turbulent traces shorter than they were if to regard the latest research data. (Samorani, 2010) (Meyers, Meneveau, 2011). Chaotic arrangement of Ostaninskaya wind farm may be as well the result of land use expenses minimization. We found out that insufficient research

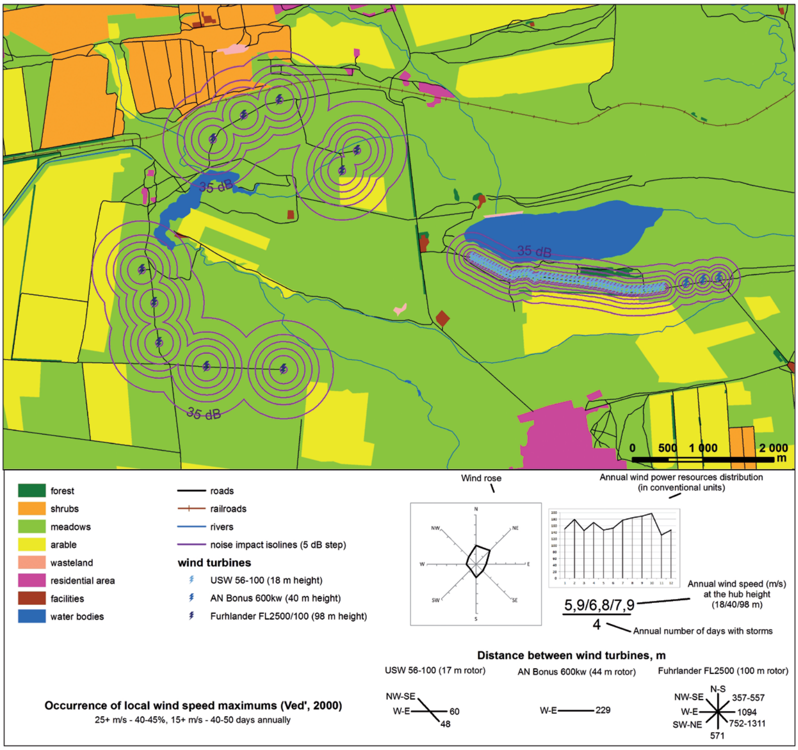

Fig. 6. Situational map of Ostaninskaya and Presnovodnenskaya wind farms

of technological features of wind farms operation (and sometimes even meteorological factors as well) were typical for the studied wind farms. Mirnovsky site of Sakskaya wind farm might be identified as an example of controlled arrangement while Presnovodnenskaya wind farm presents the result of favorable location choice. The arrangement of Ostaninskaya wind farm is the most debatable because of its random arrangement.

Noise impact

Our research demonstrated that noise impact of the studied wind farms did not influence the surrounding inhabited area (Fig. 5-6). Background noise in still weather was measured beyond the limits of the noise impact zone and it was about 28-30 dB. In case of wind turbine blades rotation following the blowing wind which produced noise itself, sometimes even muffling the noise from a wind turbine even at its base, we considered background noise as different from the above mentioned value: the blowing wind sound was more than 30-35 dB (up to 70-75 dB). So we regarded 35 dB as the minimal level of noise impact from wind turbines in our research (Fig. 5-6).

The highest noise was produced by 18 m height wind turbines USW 56-100 (70 dB at the turbine base). It might be explained by two factors – the nearest distance from the blades to our SLM and design features. While the major sound from the rest wind turbine models was the sound of air cutting produced by their blades, USW 56-100 wind turbines filled the air with the sound of rotary elements friction inside the turbine. It was detected on both Mirnovsky site and Presnovodnenskaya wind farm and may be explained by mechanisms worn as well. Meantime, the largest radius of noise impact was recorded from the 98 m height FL2500/100 turbine – about 700 meters. Probably this is explained by the largest size of blades (100 m diameter). The radius of noise impact from two other wind turbine models was about 300 meters.

We have detected some features of noise impact from wind turbines of different size. While noise from 18 m height USW 56-100 turbine decreased permanently with distance from its base, 50 m height AN Bonus 600 kW and T-600-48 turbines had 55 dB a sound 'plateau' at the distance of 50-60 m from the base; 98 m height FL2500/100 turbine produced the loudest sound at the distance of 50-75 m from the base (Fig. 7).

Such differences in noise patterns from turbine to turbine may be explained by their design and the main source of noise. 50 and 98 m height wind turbines produced the loudest sound by fast blades tips heightened from the base in case they moved downward provoking noise peaks right under them at the place of their location. Moreover, as far as different-origin sound had different frequency, noise spreading pattern was also different (Fig. 7).

Back to the fact that blowing wind was capable to muffle wind turbines noise it should be mentioned that the noise of air cutting from rotating blades was very similar to that of simultaneously blowing wind. Thus, we may suggest that noise impact from wind turbines at the site was not so much as diagrams showed because basic wind sound was not regarded.

We think it is possible to install wind turbines closer to residential areas than it is done now but in case of adequate assessment of on-site noise structure and distribution. As far as the rest Crimean wind farms are concerned, we extrapolated the received results of noise studies for their territories. In the result, it was found out that one of the rest wind farms had noise impact on inhabited area (Fig. 8). Considering noise sound from wind turbines - about 500-1000 Hz (Bolin at al., 2011), the permitted noise level for residential areas in the Crimean Republic according to local health standards (SCSES-RF[4], 1996) – 40 dB. Donuzlav wind farm violated them at the territory of Veterok dacha settlement, while it matched them for the adjacent industrial areas.

Donuzlav wind farm affected a part of Novoozyornoe urban settlement, including Rodniki and Veterok dacha settlements. All of them were used for temporary (summer) residences or working places of local agriculture.. We made a rough assessment based on remote sensing images and local statistics and found out that the number of the affected varied from 50 to 500 people depending on the season. Up to 30-40 people might be affected by illegally high noise at night.[5]

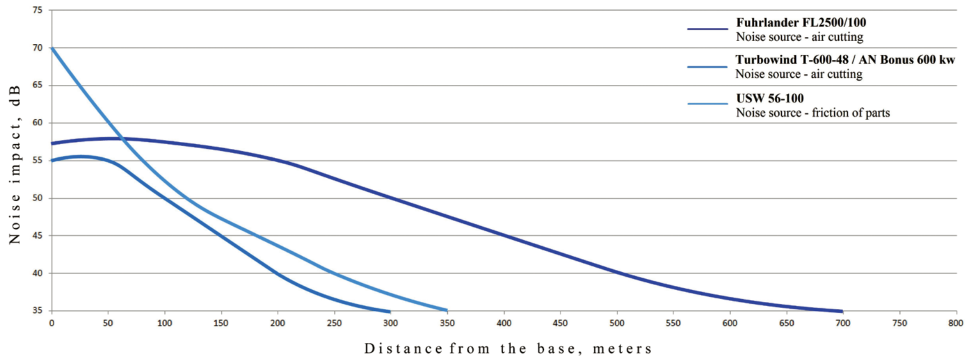

Fig. 7. Noise diagrams for the studied wind turbine models

[4] State Committee for Sanitary-Epidemiological Surveillance of the Russian Federation

[5] We would like to emphasize that described situation considers open-air residential areas. The situation with inner space of residential buildings is a bit different and cannot be assessed due to the differences in insulating characteristics of dacha walls.

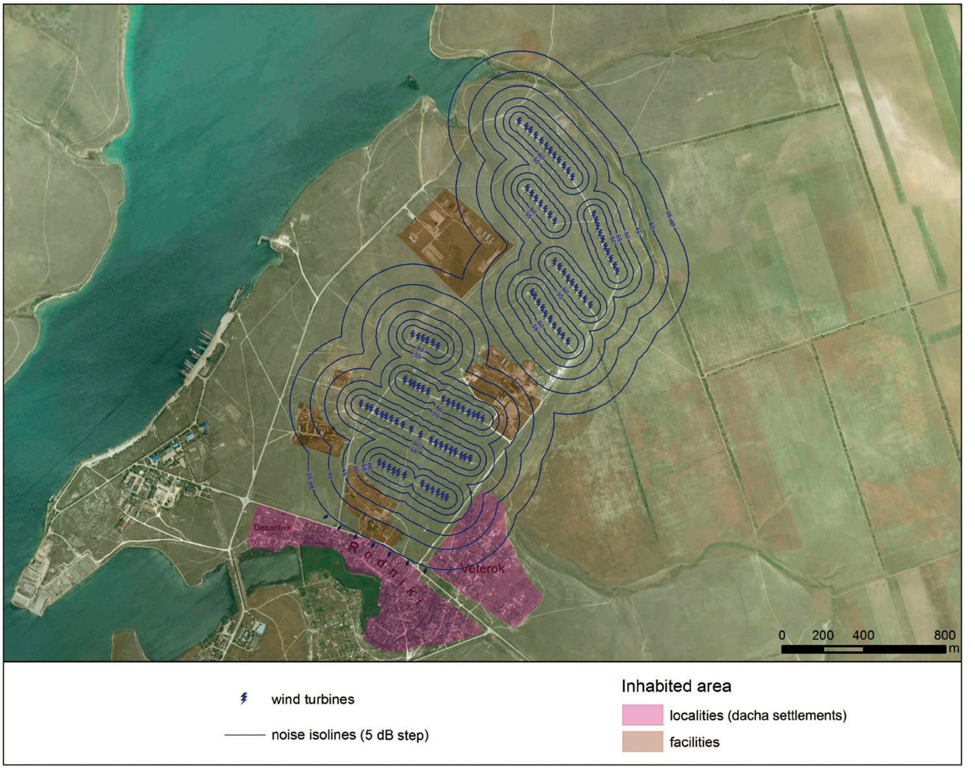

Fig. 8. Donuzlav wind farm noise impact on the surroundings

Visual impact

Visual impact means changes to the scenic attributes of a landscape connected with introduction of artificial visual elements. Visual impact assessment is of special importance for recreation and heritage territories presenting traditional cultural landscapes. This is the case of Crimea. Visual scenic harmony provides comfortable psychological environment for residents.

Visual impact of wind turbines depends on many aspects including size and design of wind turbines, their number and arrangement of wind farm scheme and surrounding landscape. Thereby overall visual impact varies from negative to positive. Though even a single wind turbine has a visual impact on surroundings, many local people characterized it as a neutral (see the results of our sociological survey below). Such attitude is explained by the fact that people grew up viewing wind farms, adapted to such visual landscape or simply ignored this issue.

Our research demonstrated that the most negative visual impact was registered from Mirnovsky site of Sakskaya wind farm (Fig. 9). It was explained by the design of USW 56-100 wind turbines which 'violated' the background by their wide blades and gray lattice towers. Then, of course, it was the number of wind turbines (155 units) and their compact arrangement in multi-rows. Mirnovsky site of Sakskaya wind farm visually polluted landscape by strengthening the visual effect of its natural monotony character. As we found out, it was better to use wind turbines with tubular towers and place them in one row and further from each other.

In some cases, USW 56-100 wind turbines had positive visual impact on the scenery. And this was the case of Presnovodnenskaya wind farm. Its wind turbines were stretched in a single row along the top of a ridge making it more vivid and improving visual image of scatted steppe hills (Fig. 10).

Fig. 9. View of Mirnovsky site of Sakskaya wind farm

Fig. 10. Outlining the relief – Presnovodnenskaya wind farm (vkerchi.com 2018)

We also marked a positive visual impact of Ostaninskaya wind farm. Its large and spread FL2500 wind turbines became focal objects for the scenery contributing diversity into monotonous steppe landscape (Fig. 11).

Finally, we may conclude the following: the majority of modern wind turbines looked in a standard way – both white tubular towers and elongated blades. This seems optimal for local landscapes visual image. Meanwhile, FL2500 wind turbines were various and the largest of them, tow-

Fig. 11. «Something to catch a glance» – Ostaninskaya wind farm (photo by Andrey Pletmentsev 2017)

ering up to 160 meters, were equipped by a wide lattice tower (Fig. 12). We think that their design violated landscape visual harmony.

The larger wind turbine is the more visual impact is observed. While 18 m height wind turbines were seen at a distance up to 21 km, modern 80 to 160 m height

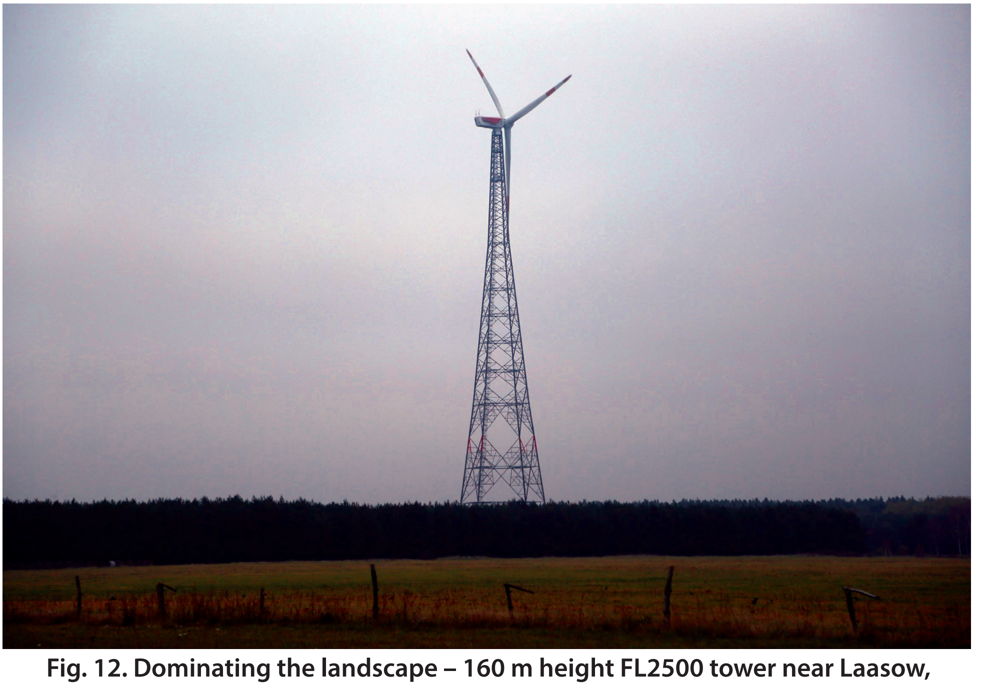

Fig. 12. Dominating the landscape – 160 m height FL2500 tower near Laasow, Germany (photo by Silvio Matysik 2014)

wind turbines changed the scenery at the distance up to 39 to 53 km[6] (Perelman 2010). Another problem was revealed – a new wind farm near the already existing one may damage the visual landscape image more than a single multi-row wind farm (see Fig. 9).

Sociological survey

Our sociological survey involved people from the vast part of the Crimean Peninsula as we moved from Sakskaya wind farm at the West to Ostaninskaya and Presnovodnenskaya wind farms at the East. We have questioned 106 people[7] aged 14-75, whose permanent residence was the Crimean Peninsula. During interviews we asked their opinion about noise and visual impact of wind farms and their general view on wind energy based on their personal experience. We tried to make our survey more representative by taking into account answers of respondents who appeared near wind farms regularly or live at the distance about 5 km from them.

Age structure of respondents was of special interest. Wind farms of the Crimean Peninsula were operating since 1990s. This time period enabled to consider three categories of local population: people 35+, born earlier than the construction of the Crimean wind farms; people from 18 to 35, who grew during construction and operation periods of local wind farms; and people under 18, born when the Crimean wind farms became routine elements of local landscape.

The results of our survey showed that the majority of local people had a positive view on wind farms in the region and did not feel negative effect from them (Fig. 13). Only 6% of respondents from surrounding localities heard noise from wind turbines and 1/3 of them found it disturbing.[8] This confirmed the results of our sound level measuring on Ostaninskaya, Presnovodnenskaya and Sakskaya wind farms. Then, more than 2/3 of local residents considered visual impact of wind farms as positive. They supported their development as well.

Comparing results from different age groups (graphs 2 and 3), we found out that the younger generation was more positive in their responses: the share of positive opinions and neutral+positive answers were 83, 77 and 62 % for people under 18, from 18 to 35 and 35+ age groups respectively. We noticed an interval in the "positivity share" between people under 35 and the elder group.

CONCLUSION

This research was based on original methods of environment features studies concerning wind energy development at a local level. The main results are the following:

Arrangement of the studied wind farms was not optimal. This was true for Ostaninskaya wind farm explained by inadequate turbulence or wind rose analysis

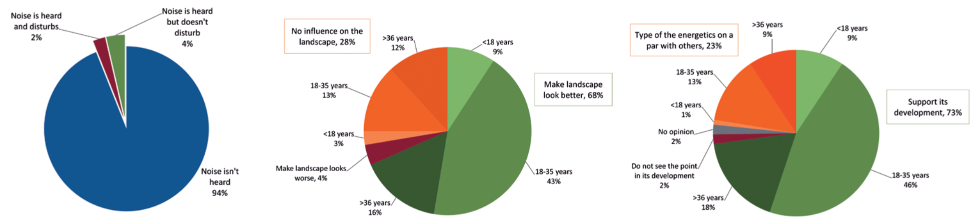

Graph 1. Noise from wind turbines Graph 2. Visual impact of wind farms Graph 3. General view on wind energy

Fig. 13. Local residents' perception of wind farms in Crimea

[6] Considering all assessments – situation with flat relief, clear weather and absence of any ground objects.

[7] Unfortunately, local people were far from willing to participate in the survey as they were inexperienced in this kind. Moreover, many of them were short-term recreational residents spending most of the time on the coastline.

and Mirnovsky site of Sakskaya wind farm and Presnovodnenskaya wind farm, where losses of generation efficiency were obvious following land use expenses minimization.

Noise impact of wind farms was minimal and did not spread on surroundings– this was confirmed by our field measurements and sociological survey. Nevertheless Donuzlav wind farm assessed virtually violated local health standards of noise impact on residential areas at night.

Visual impact of wind farms varied a lot and had both positive and negative effect in Crimea, but local people opinion was in general positive in this respect.

Local people demonstrated their support to wind energy development in general although they permanently experienced a certain ecological impact.

SUGGESTIONS

Such assessments may contribute to adequate wind energy use studies at local (wind farm) level. Back to Background section, we want to emphasize once more two aspects of wind farm projecting.

Wind power potential assessments are adequate nowadays but not enough as far as local studies are concerned. More studies of turbulence effect of wind turbines depending on wind turbine model, wind speed and landscape characteristics are necessary.

The least covered aspect of wind farm projecting is an ecological one. While wind energy is environment friendly in general, still it might have a negative effect on environment and local population. Ecological impact assessment should be added to the process of wind farm projecting. Dialogue with local residents, authorities and business might be useful for both economic effectivities of the wind farms and local economic and social development.

REFERENCES

American Wind Energy Association (2006). Wind Power Myths vs. Facts [online]. Available at: http://web.archive.org/web/20060131235323/http://www.awea.org/pubs/factsheets/050629_Myths_vs_Facts_Fact_Sheet.pdf (Accessed 24.01.2017).

Baerwald E.F., D'Amours G.H., Klug B.J., Barclay R.M.R. (2008). Barotrauma is a significant cause of bat fatalities at wind turbines. [online] University of Calgary. Available at: http://www.cell.com/current-biology/abstract/S0960-9822(08)00751-3?_returnURL=http%3A%2F%2Flinkinghub.elsevier.com%2Fretrieve%2Fpii%2FS0960982208007513%3Fshowall%3Dtrue&cc=y= (Accessed 21.03.2017).

Bettex M. (2012). Wind resistance. [online] Massachusetts Institute of Technology. Available at: http://news.mit.edu/2010/climate-wind-0312 (Accessed 30.06.2017).

Bolin K., Bluhm G., Eriksson G., Nilsson M.E. (2011). Infrasound and low frequency noise from wind turbines: exposure and health effects. Environmental Research Letters. – v. 6, no. 3.

Brannstrom C., Gorayeb A., de Sousa Mendes J., Loureiro C., de Andrade Meireles A.J., da Silva E.D., de Freitas A.L.R., de Oliveira R.F. (2017). Is Brazilian wind power development sustainable? Insights from a review of conflicts in Ceará state. Renewable and Sustainable Energy Reviews, v.67, p. 62-71.

climate-data.org (2017). Climate: Autonomous Republic of Crimea [online]. Available at: https://ru.climate-data.org/region/619/ (Accessed 07.09.2017).

Dillon M. and Tronstad L. (2012). Baseline Research for Long-term Effects of Wind Farms on Insects in Wyoming. [online] University of Wyoming. Available at: https://www.uwyo.edu/wyndd/_files/docs/reports/wynddreports/u13dil01wyus.pdf (Accessed 25.09.2016).

Elistratov V.V. and Kuznetsov M.V. (2003). Theoretical basis for unconventional and renewable energy. Saint-Petersburg: SPbSPU Publishing House (in Russian).

The Federal Service for State Registration, Cadastre and Cartography of Russian Federation (2017). Public cadastral map. [online] Rosreestr. Available at: https://pkk5.rosreestr.ru/ (Accessed 05.12.2017).

Filin V.A. (1997). Videoecology. Moscow: TASS-Reklama (in Russian).

Furhlander Windtechnology (2017). Kerchensky wind park (Ostaninskaya wind farm) [online]. Available at: http://fwt.com.ua/ветропарк-останинский/ (Accessed 02.09.2017) (in Russian).

Gismeteo (2017). Weather Diary [online]. Available at: https://www.gismeteo.ru/diary/ (Accessed 07.09.2017) (in Russian).

International Renewable Energy Agency (2018). Data and Statistics [online]. Available at: http://resourceirena.irena.org/gateway/dashboard/index.html (Accessed 01.03.2018).

Keith D.W., DeCarolis J.F., Denkenberger D.C., Lenschow D.H., Malyshev S.L., Pacala S., Rasch P.J. (2004). The influence of large-scale wind power on global climate. [online] Proceedings of the National Academy of Sciences of the United States of America. Available at: http://www.pnas.org/content/101/46/16115.full (Accessed 22.09.2016).

Kommersant (2016). Energy supply of Crimea has been reestablished [online]. Available at: https://www.kommersant.ru/doc/3106583 (Accessed 02.09.2017) (in Russian).

Krymsky Telegraf (2013). How much resources Crimea needs and what is its energy potential?. Krymsky Telegraf newspaper, v. 216 (in Russian).

Leventhall G. (2003). A Review of Published Research on Low Frequency Noise and its Effects. [online] U.K. Department for Environment, Food and Rural Affairs. Available at: http://archive.defra.gov.uk/environment/quality/noise/research/lowfrequency/documents/lowfreqnoise.pdf (Accessed 01.10.2016).

Lopucki P. and Perzanowski K. (2018). Effects of wind turbines on spatial distribution of the European hamster. Ecological Indicators, v. 84, p. 433-436.

Mikolajczak J., Borowski S., Marć-Pieńkowska J., Odrowaz-Sypniewska G., Bernacki Z., Siódmiak J., Szterk P. (2013). Preliminary studies on the reaction of growing geese (Anser anser f. domestica) to the proximity of wind turbines. Polish Journal of Veterinary Sciences, v. 16(4), p. 679-686.

Meyers J. and Meneveau C. (2012). Optimal turbine spacing in fully developed wind-farm boundary layers. [online] Wind Energy. Available at: https://people.mech.kuleuven.be/~jmeyers/resources/downloads/WE2012_15_305-preprint.pdf (Accessed 01.10.2016).

Ministry of Energy of Russian Federation (2017). Energy supply of Crimean Peninsula. [online] Available at: https://minenergo.gov.ru/sites/default/files/texts/Энергосистема%20Крыма_на%20сайт.pdf (Accessed 02.09.2017) (in Russian).

Mitchell P. (2014). Wind turbine separation distances matter. [online] Waubra Foundation. Available at: https://waubrafoundation.org.au/resources/mitchell-p-wind-turbine-separation-distances-matter/ (Accessed 04.02.2018).

New Zealand Wind Energy Association (2017). Visual Effects. [online] Available at: http://www.windenergy.org.nz/visual-effects (Accessed 04.02.2018).

Nikolaev V.A. (2005). Landscape science. Aesthetics and design. Moscow: Aspect Press (in Russian).

Perelman Y.I. (2010). Horizon. Entertaining geometry. Moscow: Rimis (in Russian).

Rabl A. and Spadaro J. (2005). Externalities of Energy: Extension of accounting framework and Policy Applications. [online] European Community, EESD Programme. Available at: http://www.externe.info/externe_2006/expoltec.pdf (Accessed 14.09.2016).

Regnum (2017). Energy supply of Crimea and Sevastopol has been reestablished [online]. Available at: https://regnum.ru/news/2307920.html (Accessed 02.09.2017) (in Russian).

RIA News Crimea (2015). The development of Crimean energy supply system [online]. Available at: http://crimea.ria.ru/infographics/20151215/1102118990.html (Accessed 02.09.2017) (in Russian).

Russian Association of Wind Industry (2018). The first wind farm in Russia was launched in Ulyanovsk. A new history of wind power in Russia [online]. Available at: https://rawi.ru/en/the-first-wind-farm-in-russia-was-launched-in-ulyanovsk-a-new-history-of-wind-power-in-russia/ (Accessed 01.03.2018).

Samorani M. (2010). The Wind Farm Layout Optimization Problem . [online] Leeds School of Business, University of Colorado. Available at: https://www.researchgate.net/publication/242580464_The_Wind_Farm_Layout_Optimization_Problem (Accessed 08.09.2017).

Semyonov V.G. (2014). Crimean energetics. What is to build? . [online] Energosovet Journal. Available at: http://www.energosovet.ru/bul_stat.php?idd=472 (Accessed 02.09.2017) (in Russian).

SM news (2017). Aksyonov gave 72 hours for energy supply reestablishment for Crimea [online]. Available at: https://sm-news.ru/news/energetika/aksenov-otvel-72-chasa-na-vosstanovlenie-elektrosnabzhenie-kryma/ (Accessed 02.09.2017) (in Russian).

State Committee of Sanitary-Epidemiological Surveillance of Russian Federation (2017). Health standards HS 2.2.4/2.1.8.562-96 "The noise at work, in the spaces of residential, public buildings and on residential areas" (established by Decree №36 at October, 31, 1996). Moscow: Morkniga (in Russian).

SUE Crimean Generating Systems (2017). Business units [online]. Available at: http://www.energysystem-crimea.ru/производство.html (Accessed 04.09.2017) (in Russian).

System Operator of United Power System (2018). 2017 Russian United Power System functioning report [online]. Available at: http://so-ups.ru/fileadmin/files/company/reports/disclosure/2018/ups_rep2017.pdf (Accessed 01.03.2018) (in Russian).

UK Department of the Environment (2007). Draft Planning Policy Statement 18: Renewable Energy [online]. Available at: http://www.planningni.gov.uk/index/policy/planning_statements_and_supplementary_planning_guidance/pps18-draft-renewable-energy.pdf (Accessed 08.09.2017).

Ved' I.P. (2000). Climatic atlas of Crimea. Simferopol : Tavriya-Plyus (in Russian).

Wilson S. (2002). Guidelines for Landscape & Visual Impact Assessment. London: Spon Press.

Received on September 21st, 2018 Accepted on February 20th, 201

Md Arafat Hassan[1*], Rehnuma Mahjabin[1], Md Rakibul Islam[1], Sakib Imtiaz[1]
[1] Department of Geography and Environment, University of Dhaka, Dhaka, Bangladesh
***Corresponding author:** mh20457@email.vccs.edu

LAND COVER CLASSIFICATION AND CHANGE DETECTION ANALYZING MULTI-TEMPORAL LANDSAT DATA: A CASE STUDY OF GAZIPUR SADAR, BANGLADESH BETWEEN 1973 AND 2017

ABSTRACT. This paper analyzed land cover changes in Gazipur Sadar – an important urban fringe of expanding Dhaka City, Bangladesh, by leveraging remotely sensed imageries between 1973 and 2017. Landsat images of1973, 1991, 2006, and 2017 were classified using widely-preferred supervised classification method. Compared against ground-truth data, the reported classification accuracy ranges from 85% to 89%. Our classified land cover maps reveal that built-up areas in Gazipur Sadar increased by 312.9%, mostly replacing vegetation cover. An overall 199.7% decrease of vegetative covers highlights on the degree of urbanization process and increasing population pressure faced by Gazipur Sadar over the past decades. The rapid decrease of vegetative cover only 57 sq. km remains out of 344 sq. km throughout the region, including the Sal *(Shorea robusta)* forest and other floral species – invaluable resources for biodiversity and ecosystem health, should be taken as 'alarming' situation by the local authority responsible for promoting and managing sustainable development goals. In that light, this study emphasizes on the need for a critical assessment of future development initiatives in the Gazipur Sadar area and suggests for maintaining acceptable tradeoffs between development and environmental protection.

KEY WORDS: land cover (LULC) classification, change detection, geographic information system, Gazipur Sadar (Bangladesh), urban, sustainability

CITATION: Md Arafat Hassan, Rehnuma Mahjabin, Md Rakibul Islam, Sakib Imtiaz (2019) Land Cover Classification and Change Detection Analyzing Multi-Temporal Landsat Data: A Case Study of Gazipur Sadar, Bangladesh between 1973 and 2017. Geography, Environment, Sustainability, Vol.12, No 1, p. 104-118
DOI-10.24057/2071-9388-2018-12

INTRODUCTION

Man is leaving his mark on every part of the Earth surface and altering the physical attributes at a rapid rate with his activities (Lambin et al. 1999). The changing ecosystem has been a matter of concern in the global studies (Dixon et al. 1994; Ojima et al. 1994), as harmful human activities are constantly changing the natural land cover, which in turn, affect the carbon cycle and disturb the balance of carbon dioxide (CO_2) in the atmosphere (Alves and Skole 1996). In the developing countries, urban growth, coupled with the industrial development and the transformation of agricultural land into built-up areas are some of the leading causes of vegetation loss (Shalaby and Tateishi 2007). Land cover is supposed to be the natural and manmade vegetation cover but at present, it includes human settlements, infrastructure, industries space without vegetation and water and other natural and anthropogenic features (Klimanova et al. 2017). Additionally, the rapid alteration of land cover have raised a huge number of issues such as the adverse effect on the relationship between biosphere and atmosphere, extinction of a diverse range of species and deteriorating soil condition (Meyer and Turner 1994). Conservation of the existing vegetation areas and regeneration of the lost vegetation cover is now essential for maintaining the ecological balance and improving the health of the environment (Xin et al. 2011). Conservation and regeneration initiatives require the accurate measurement and mapping of areas experiencing vegetation loss. Tropical regions are covered with large forest areas that contribute to the protection from climate change, by absorbing billions of tons of CO_2,and can play an important role in reducing the environmental externalities due to the degradation of forest areas (Canadell et al. 2008).

Bangladesh is a developing country and accommodates a huge population with in a very small geographic area. The connection between population and environment was not well understood until recent times. At present, the strong inter-relationship between the population and the natural environment is known to all. This issue came into attention especially after the RIO declaration in Brazil (1992) and 1994 Cairo conference on global population (World Bank 2017). Bangladesh has 162,951,560 people living in an area of 147,570 km^2 and with a population growth rate of 1.1% (World Bank Data 2016). This huge population has different needs and consumption behavior, which create excessive pressure on the environment. Requirements of food and housing facilities triggers deforestation (Rahman 1994). Moreover, rapid urbanization has caused a decrease in the forest area, agricultural land and water bodies (Giri et al. 1996). Many agricultural and vegetation covered areas are being transformed into built up and infrastructural constructs (Quasem 2011). Hasan et al suggested that the country has experienced a decrease of about 1.12 million ha of vegetation area, comprising agricultural and mangrove forest areas, from the year 1976 to 2010.However, the increase of non-agricultural land during this period was 1.22 million ha (Hasan et al. 2013). According to Food and Agriculture Organization, the annual deforestation rate of Bangladesh is 0.2%, one of the high deforestation rates in the developing countries (Fao 2015).

Gazipur district is located at the Northern part of Dhaka city and is one of the nearest districts from the capital city (Bangladesh Bureau of statistics 2011). In the past, the region was a part of a deep forest named as *Vawal Pargana*. The district has an area of 1806.36 sq. km with 17.53 sq. km of wetlands and 273.42 sq. km of forest area. Around 34,03,912 people live in this district, having a density of 1884 people per sq. km and a population growth rate of 5.2% (Bangladesh Bureau of Statistics 2011). The area is most suitable for agricultural work and the majority of the people are involved with agro-based economic activities. But with the increasing pressure of population and socioeconomic changes, the area can characterized of having sharp urbanization and industrialization rates (Islam 2013).

Sal forest (also known as *Madhupur* forest) is an asset of Bangladesh, which spreads across Dhaka and Gazipur districts. Gazipur disctrict contains around 86% of the Sal forest of the country. Human activities like land overuse, deforestation, urbanization, agricultural and industrial activities are creating a threat for this forest. Gazipur Sadar Sub-district used to contain 20% of this forest but the forest area is decreasing gradually (Fazal et al. 2015). Gazipur Sadar Sub-district is becoming the new industrial hub of the country due to its proximity to the capital city and the enhanced transport facilities. However, this development is having a negative impact on the forest area in this region. Industries are growing exponentially at the expense of forest land and are causing heavy pollutions with adverse environmental consequences (Dong et al. 1997).

As a developing country, the application of land use and other relevant geographic data is quite scarce in Bangladesh. For a developing country, remote sensing images can be the most reliable source of an updated land use or land cover data (Dong et al. 1997; Yang 2002). Updated and accurate data can help in many ways to compare scenarios at different temporal scales (seasonal, monthly or annually) and can also help devising plans and policies for the future development (Alpha 2003). Therefore, this paper employed remote sensing data for detecting the land cover change.

This paper aims to analyze the changing pattern of vegetation cover in Gazipur *Sadar Upazila*. This analysis attempts to give a clear picture of the present day vegetation condition and to help understand the rate and cause of the changing patterns.

STUDY AREA

Gazipur *Sadar Sub-district* is located between latitudes of 23°53′ and 24°11′ N and longitudes from 90°20′ to 92°30′ E (Fig. 1). The total area is about 446.38 sq. km, consisting a total population of 866,540 and a population density of about 1,941 people per sq. km. Gazipur *Sadar Sub-district* is administratively made up of eight unions: Bashan, Baria, Gachha, Kasimpur, Kaultia, Konabari, Mirzapur, Pubail (Bangladesh Bureau of Statistics 2011).

The Turag River flows past over the western part of the city and the Balu River flows along the eastern side. Other notable waterbodies are the Labandanga River, the Salda River, and the Tongi canal. The *Sub-districtis* surrounded by the Sreepur Sub-district in its north, Rupganj Sub-district from south to east and Savar Sub-district from south to west.

Gazipur *Sadar* is a part of *Madhupur* tract, which is a terrace having Dhaka in the south and Jamalpur and Mymensingh districts in the north. The total area of the terrace is about 4,244 sq. km and is slightly elevated than the nearby floodplains, the area is also subjected to occasional tectonic activities (Brammer 1996). There is a similarity between Gazipur alluvium and Brahmaputra floodplain alluvium but the clay is called *Madhupur* clay. The area has slopes and low-level circular ridges in different places (Rashid, 2008).Huge range of soils can be found in this area such as the Red-Laterite soil and Pleistocene clay. (FAO, 1988)

The climatic condition of the Gazipur districtis similar to a tropical climate. The area has a moderate temperature and rainfall of 25.8 °C and 2036 mm respectively. The highest temperature can be recorded in the month of May and the lowest temperature can be recorded in the month of January.

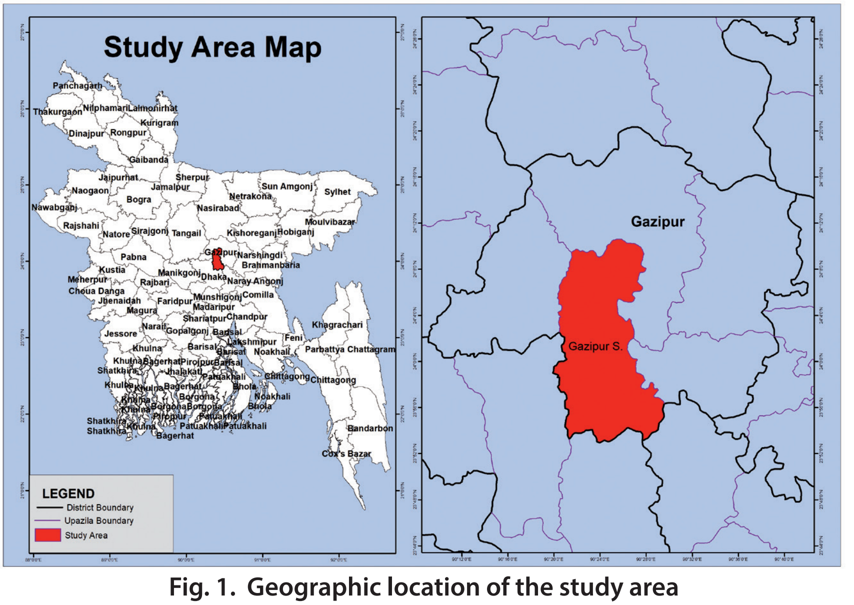

Fig. 1. Geographic location of the study area

DATA AND METHODOLOGY

Remote sensing data can give a perfect image of land use change in different sections of the land (Klimanova et al. 2017). This study used multi-temporal remotely sensed images from Landsat 5, 7, and 8, between the years 1973 and 2017. Last 40 years have been very crucial for the forest land of Gazipur, as from 1989 to 2009 about 20.29% forest area have decreased (Yesmin et al. 2014). We chose four years that can represent the past decadal variations of land cover in the area. The Landsat database made for this research was constructed by four sets of data, they are Landsat images from MSS (05 December 1973), Path/ Row: 147 / 043 for 1973, TM (26 November 1991) for 1991, ETM+ (21 December 2006) for 2006 and OLI (07 December 2017) for 2017. In the Landsat image selection process, 'less than 10% cloud' cover was a criterion for ensuring the accuracy of the classified images. Therefore, it was not possible to find the images of the same month for every year. In the Gazipur district, November to February is winter and less cloudy (Uddin and Gurung 2010). So, Landsat data were selected from November to February to minimize the seasonal and cloud cover influences on the acquired images. ERDAS Imagine (Leica Geosystems 2006) and ArcGIS (ESRI 2005) are both very important tools for land cover assessments and hence, for this paper both of the software were used for data processing and analysis. First of all, geometric correction was performed as the data needed to be properly coordinated to adjust for the tectonic movements. For executing geometric correction, we selected a reference image of Landsat TM for the year 2017. 80 ground control points were taken at random that were scattered over the study area for acquiring the perfect geometrically corrected image. The root means square error (RMSE) was very low from 0.25 to 0.45 pixel. All the data were resampled to 30 m pixel size, using the nearest neighbor method. The coordinate system of the image was set as the Bangladesh Transverse Mercator system (BTM). Different sources are tested to identify correct training area and to perform the accuracy assessment.

Atmospheric correction was also performed to reduce the atmospheric dust, solids, and liquids. Atmospheric correction was done following López-Serrano et al. (2016).

Image classification

The classification of image is partly affected by the method of Anderson Scheme Level 1. (Anderson et al. 1976). The image classification was based on broad categories of land cover and spatial resolution with a range of 30 m to 79 m. Classification was carried out based on the four broad land cover categories (shown in Table 1), vegetation cover, waterbody, built-up area and agricultural land.

A minimum of 70-80 samples were collected to train each of the classes and if the sample was big enough, about 200 to 400 pixels were taken. Every land use category consisted of about 15-20 subclasses to get the perfect accuracy. The training classes underwent several stages like merging, deletion or renaming. A model is built from the training data, which is then run to obtain the final classified image. Despite the caution taken while devising the model, errors could be found in the final output. Common errors of classification include the difficulties arising while distinguishing between the agricultural grasslands and healthy vegetation (Bolstad and Lillesand 1991).

The land cover change for each of the classes was calculated using the following formula (Islam et al. 2017):

Magnitude = magnitude of the new year - magnitude of the previous year

Percentage change of a particular class was calculated by dividing the change in area by the area in the base year (primary year), and multiplied by 100.
For calculating the rate of yearly change for every land cover class, the percentage change was divided by the number intervening years. Calculated data are shown in Fig. 8.

Table 1. Land cover classification scheme

Land use cover types	Description
Water body	River, permanent and temporary open water, reservoir.
Vegetation	Sal forest , deciduous forest, mixed forest,bamboo
Agricultural land	Crop, open field, fallow land, mixed forest lands
Built-up	Residential, commercial, industrial,road and streets

Table 2. Summary of land cover classification data between 1973 and 2017 (area in sq km)

Land cover types	1973 Area	1973 (in %)	1991 Area	1991 (in %)	2006 Area	2006 (in %)	2017 Area	2017 (in %)
Vegetation	145.63	46.93	84.85	37.32	24.15	6.99	57.76	16.72
Built-up area	0.0948	0.02	13.17	3.83	133.79	38.74	137.79	39.91
Water bodies	37.59	10.88	58.21	16.85	1.62	0.47	36.83	10.66
Agricultural land	162.03	42.17	189.13	42	185.81	53.8	112.99	32.71

Table 3. Classification accuracies in percent (Producers-Users accuracy)

Land cover class	1973 producer's	1973 user's	1991 producer's	1991 user's	2006 producer's	2006 user's	2017 producer's	2017 user's
Water bodies	88.5	85.5	98	77	93.5	100	84.3	100
Built-up area	90.3	100	75.4	98.5	87.5	87.4	90.5	98.5
Vegetation	82	72.3	95.5	92.3	85.5	88.5	87.5	82.3
Agricultural land	74.4	76.5	89.5	83.5	85.3	92.5	82.3	73.5

Accuracy Assessment

Mixed pixel or pixel with the same color always create a problem (Lu and Weng 2005). The sample for this training site has been demarcated by area of interest or AOI which also gives local knowledge. For validating the classified images with the real life features, different accuracy assessments were performed. To asses 1973, 1991 and 2006 data, a total 120 pixels were developed through stratified random sampling method. These pixels were used to compare with the features in a high-resolution topographic map of Gazipur district. For 2017, the reference data collected from the field were used. For this purpose, a total of 90 ground data pointes were collected and used to calculate the classification accuracy. Then, the accuracy of each classification was evaluated in terms of the overall and producers-users accuracy as well as the kappa coefficient.

RESULTS AND DISCUSSION

The pattern of land cover change during 1973 to 2017 is shown in Fig. 2. During this period, *Gazipur Sadar* has shown a rapid land use change. The changes in vegetation cover are illustrated in Fig. 4, 5, 6 and 7. In the year 1973, a noticeable amount of vegetation cover (145 sq. km) can be observed in the northern part of the *Sadar Sub-district*, which comprised of 47% of the total land cover and extended along the eastern border of the area. This year was during the period after independence when the industrial growth of the country was slow. Gazipur Sadar at that time was a fully agrarian society (Lesser 1888).

Fig. 2 shows that the agricultural land is covering the central part of the *Gazipur Sadar sub-district* and some patches of agricultural lands are visible in the northern part, inside the vast vegetation cover. The agricultural land covered an area of 162 sq. km in 1973, which was 42% of the total land cover. The waterbodies mainly covered the eastern and western borders of the area. After the independence of Bangladesh in 1971, most of the settlements in the area were observed to be small and negligible (only 0.02% of the land cover). The changes between 1973 and 1991 is quite evident as the amount of vegetation cover in the northwestern part had almost vanished completely (Fig. 5). It was the first sign of massive human activity in Gazipur. The northwestern part of the region has turned vegetation into agricultural land and thus, vegetation cover decreased from 47% to 37%. The scattered vegetation that can be seen in midst of the agricultural land was mainly planted by the humans. Rapid development leading to the uncontrolled expansion of the built up area has resulted in the filling up of rivers indifferent parts of the Turag and Balu river.

Fig. 2 shows that 38 % of the total areas was the built-up area in 2006. Scattered vegetation of the central part had been destroyed and infrastructure was developed in that area. The natural forest of the northeastern part was disturbed badly due to urban sprawl and other construction activities. Dhaka city would be expanding and developing towards the Gazipur and Narayangang (Dewan et al. 2009). Our results and findings support this prediction. A noticeable fact is that in the year 2006, a patch of the built-up area can be observed expanding from south to north in a linear pattern. This was actually the newly developed industrial territory in *Gazipur Sadar*. Fast-growing industries were the main reason behind the loss of agricultural land, wetlands, and vegetation in this area. The change was markedly rapid from 2004 to 2010. Another interesting fact is that the parts of the Turag River and Balu River were significantly filled up and turned to temporary agricultural land in 2006. By 2017, this newly developed agricultural land in 2006was destroyed by the built-up area. The river flows and the vegetation beside these areas, which together had formed an ecosystem itself, was totally removed and replaced by settlements. In 2017, the Institution of Human Rights and Peace for Bangladesh filled a petition against these encroachments that comprised of about 30 illegal structures along the coast of Turag River. According to the lawyers,

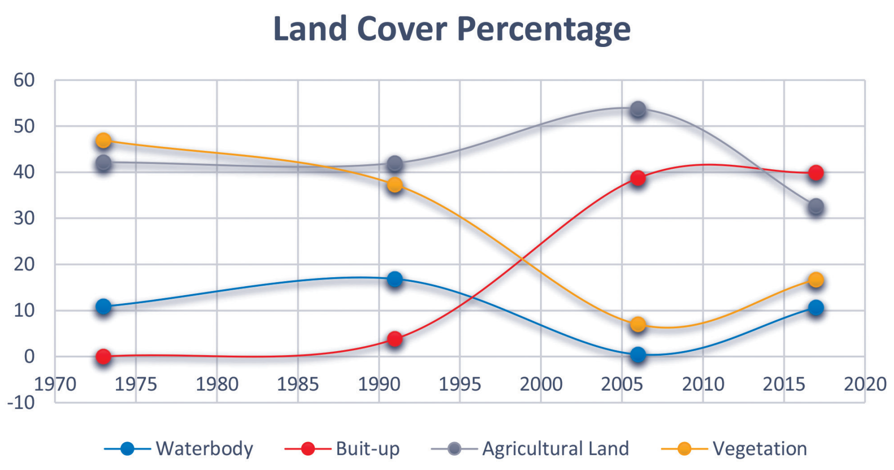

Fig. 2. Temporal comparison between the amount of vegetation coverage and other land cover classes

government agencies had built pillars and walkways near the banks of the river and the land grabbers took this opportunity to grab the surrounding land and build illegal structures (The Daily Star 2017).

In the late 1990s, the area started to develop industrially and thus, instigating a rapid change that had mainly focused on the economic development and not on the health of the environment. With the ever-increasing population, the built-up area began to rise. In Fig. 3, it is evident that the area covered by vegetation and waterbody classes have experienced a sharp declining pattern. According to Fig. 3, the amount of vegetation coverage was 145 sq. km in 1973, which with a decreasing rate of 72% was reduced to 84 sq. km in 1991. Similarly, further vegetation clearing was observed with a 250% decrease rate in the next 15 years, which reduced the figure to just 24.15 sq. km by 2006. These rates show that the diminishing of vegetation coverage had proliferated throughout the years and also increased progressively over the passing years.

People in this region had encroached illegally when there was no fixed demarcation of the forests (Rahman, 2016). The national forest policy was adopted by the government of Bangladesh in 1979 with an emphasis on forest protection. However, the policy had partially failed because of lack of prioritization on the participation of the local people. The present forest policy had been continuing from 1994, which is much broader and well-constructed than the previous one (Millat-e-Mustafa 2002). But the impact of this policy was evident after the year 2000.

At the same time, there was a Forestry sector project (1997-2004), which was implemented with the concept of protected forest area, buffer zones and participatory tree plantation (Salam et al. 2004). After the effective stage of vegetation conservation, it is evident that the vegetation coverage has increased by about 315% (Fig. 8) which resembles Salam's work

Population explosion and the expansion of the built-up area can be identified as the two of the main reason behind the diminishing vegetation coverage. From 1973 to 1991, lots of construction activities were carried out in the region, such as the garments industries. Built up area increased from 0.02 to 13 sq. km that was a drastic change but as mentioned earlier, there was no observable pattern in settlement and built up area. The houses of dwellers were scattered all over the region. Moreover, there was no strong base or foundation of these types of houses. These were mainly temporary *Jhupri* (shack) type of settlement structures. In 2006, the amount of built-up area had remained same (133 sq. km) as the rate of development or the growth of built-up area gets stability with stable population increase. In the succeeding years, the amount of built up area rose to 137 sq.km, which reiterate the fact that over the past 11 years the built-up area had reached a stable condition or is close to reaching the peak of its growth. During the initial stage,

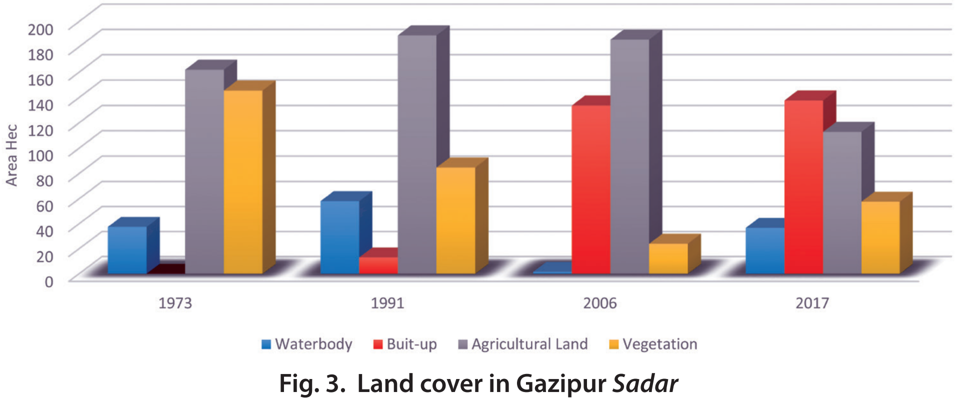

Fig. 3. Land cover in Gazipur *Sadar*

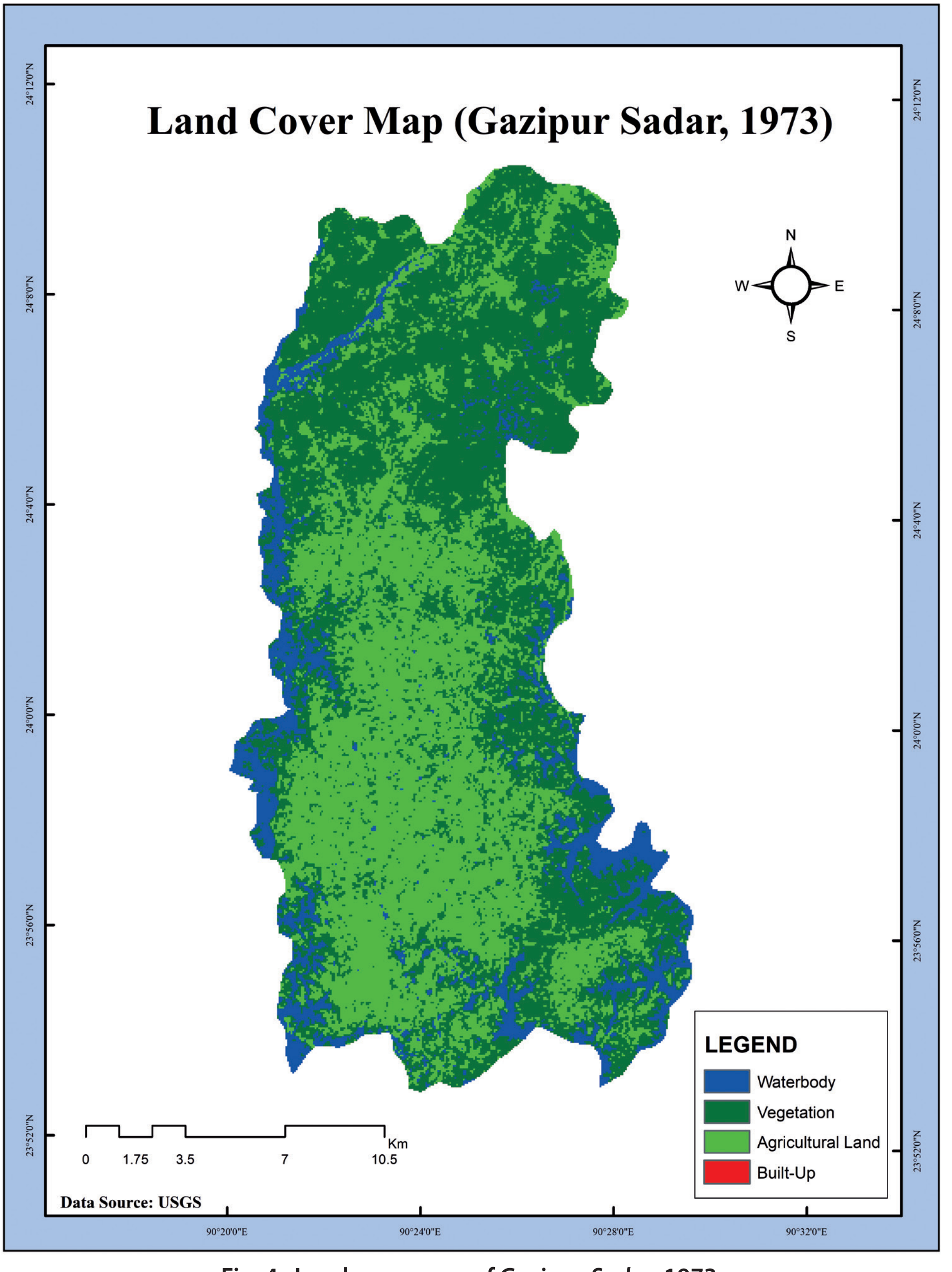

Fig. 4. Land cover map of Gazipur *Sadar*, 1973

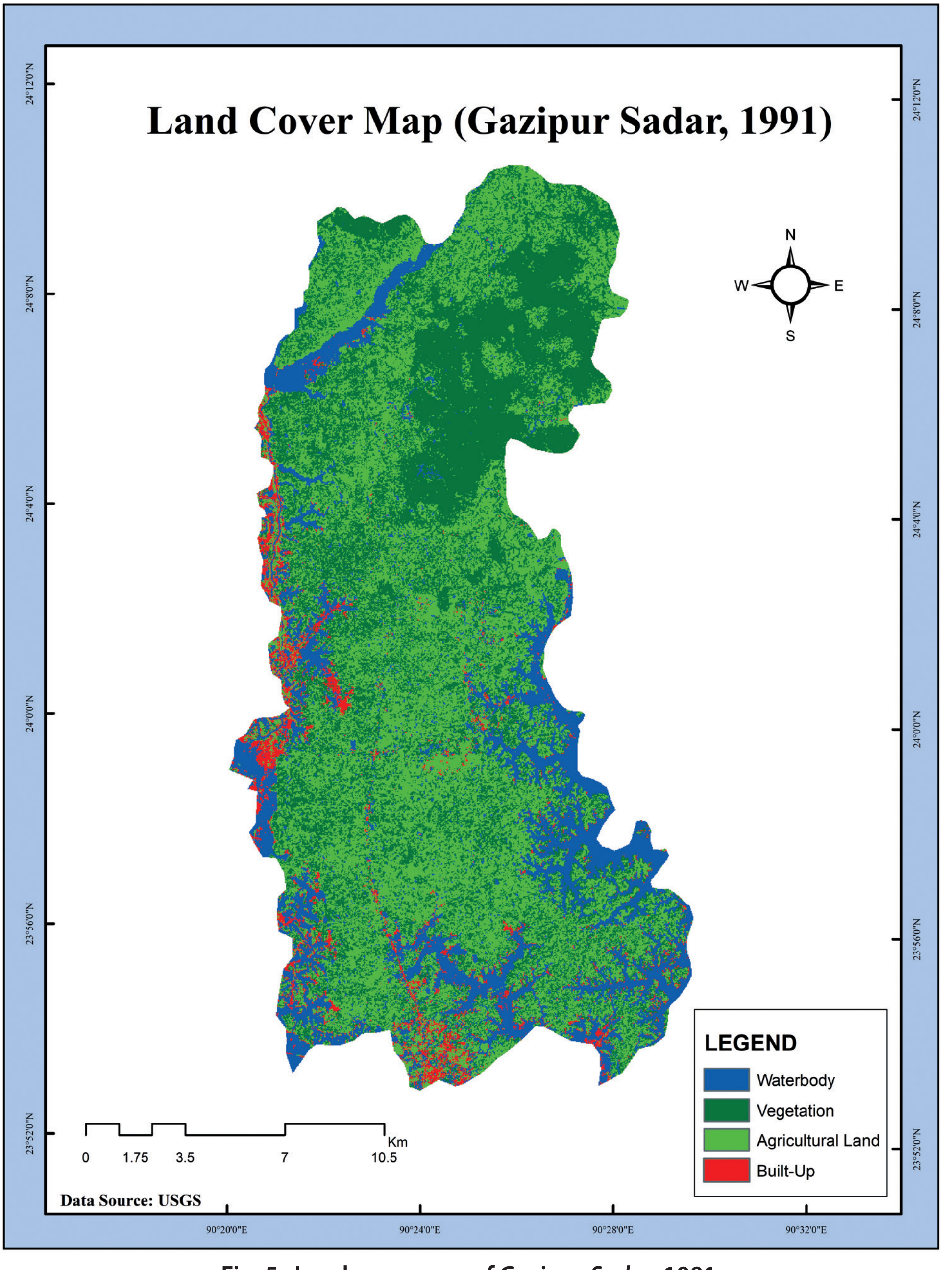

Fig. 5. Land cover map of Gazipur *Sadar*, 1991

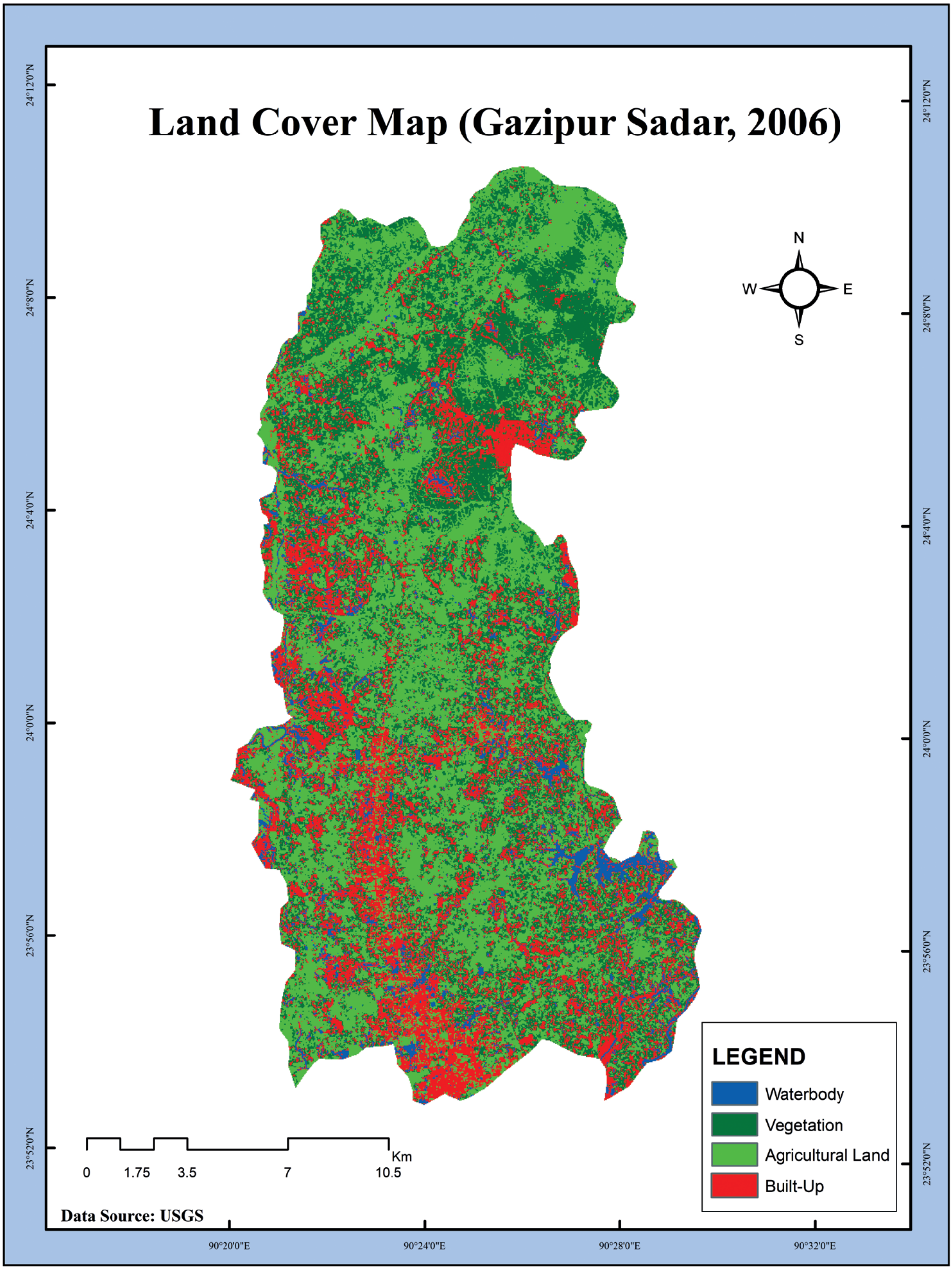

Fig. 6. Land cover map of Gazipur *Sadar*, 2006

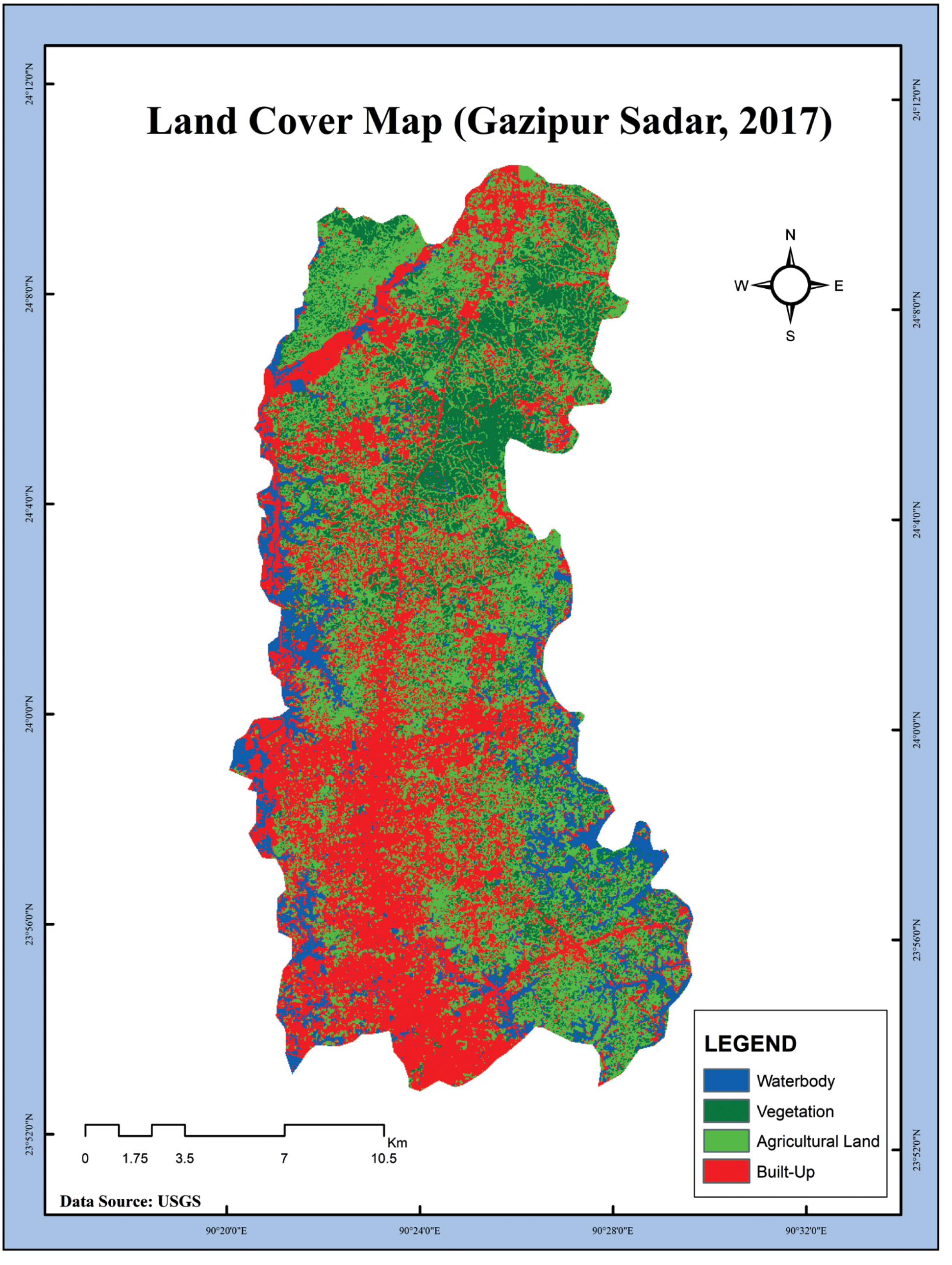

Fig. 7. Land cover map of Gazipur Sadar, 2017

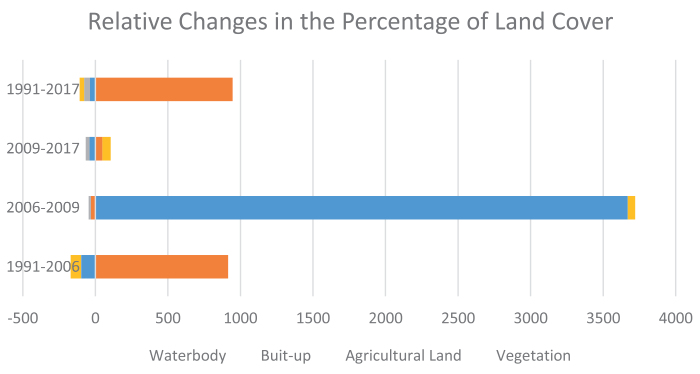

Fig. 8. Relative changes in land cover (%) in Gazipur *Sadar*

the increase of the agricultural land was a major reason behind the clearing of natural vegetation. This was because the region's economy was totally dependent on agriculture and therefore, a growth from 162 sq. km to 189sq. km in the agricultural land can be observed from 1973 to 1991.

However, with the gradual development of industries in Gazipur, the city has now become an important industrial hub of Bangladesh. BSIC (Bangladesh Small and Cottage Industries Corporation) area was developed that further promoted industrialization along the coast of the Turag River (Sultana et al. 2012). After the development of the industries, the agricultural growth had slowed down in the year 2006. The agricultural land comprised of 185sq km and was drastically reduced to 72 sq. km by 2017. Another reason for this drastic change is that the lands previously used for agriculture are now being used for fish cultivation, which is presently a very popular practice in this area. Adopting the concept of integrated farming, many farmers are using the agricultural lands for fish farming and are even destroying the vegetation coverage for the same purpose. Although, it is a profitable initiative for the economy of the region, sometimes poor maintenance poses a challenge for environmental sustainability (Ferdous et al. 2001).

CONCLUSION

This paper analyzed the changes in land cover in Gazipur *Sadar Sub-district* using Landsat data between 1973 and 2017. While historically Gazipur district has been well-known for its rich forest resources, significant LULC changes are taking places due to the rapid urbanization over the past few decades. The present trend in LULC change indicates the negative impact of human activities on the vegetation coverage. Over the past 44 years, vegetation coverage had diminished by 199.7% - an alarming issue for the environment of the area. Industrial pollution, growth of built-up areas, encroachment of rivers and waterbodies along with the exploitation of existing resources are having devastating consequences to the vegetation coverage. Considering the present condition, conservation of vegetation coverage is necessary and should be one of the key prioritizing issues. Rules and regulations must be strictly followed prior to the establishment of settlements or industrial projects. Implementation of existing policies pertaining to the reservation of forest is essential and appropriate policies for the conservation vegetation coverage and valuable land must be introduced by the concerned authorities. Moreover, it is the dweller's duty to maintain the natural environment and the intricate balance between economic growth and environmental health, for ensuring a sustainable development in the region. For this reason, participatory programs with a bottom up approach are highly recommended. The management of vegetation coverage and the efficacy of any conservation initiatives will depend on the overall role-play of the general people. More research and the collection of adequate data will help build the consciousness of the public. Remote sensing data aid in acquiring reliable images of the study area that can be used for further analysis, especially when there is a limited access to data or maps. Careful analysis can help maintaining the accuracies of classifications to over 85%. Hence, satellite images can be an effective data source for environmental analysis.

ACKNOWLEDGEMENTS

Authors wish to thank the unknown referees for their valuable suggestions, which improved the final form of this paper.

REFERENCES

Alphan H. (2003). Land use change and urbanization in Adana, Turkey. Land Degradationand Development, 14(6), 575–586.

Alves D.S. and Skole D.L. (1996). Characterizing land cover dynamics using multi-temporal imagery. International Journal of Remote Sensing, 17(4), 835–839.

Anderson R., Hardy E. E., Roach J.T., and Witmer R.E. (1976). A land use and land cover classification system for use with remote sensor data. USGS Professional Paper 964. Washington, DC.

Bangladesh Bureau of Statistics (BBS) and informatics division (SID) Ministry of planning government of the people's republic of Bangladesh (2011).

Bangladesh (1996). Int. J. Remote Sens., 17, 2749–2759.

Bolstad P.V. and Lillesand T.D. (1991). Rapid Maximum Likelihood classification. Photogrammetric Engineering & Remote Sensing, 57, 67–74.

Center for Urban Studies (CUS), National Institute of Population, Research and Training (NIPORT), & Measure Evaluation (2006). Slums in urban Bangladesh: Mapping and census, 2005. Dhaka, Bangladesh/Chappell Hill, USA.

Brammer H. (1996). The Geography of the Soils of Bangladesh, Dhaka Bangladesh, University Press: 1996.

Canadell J.G and Raupach M.R. (2008). Managing Forests for Climate Change Mitigation. Science, 5882(320), pp. 1456-1457.

Dewan A.M., Yamaguchi Y. (2009a). Using remote sensing and GIS to detect and monitor land use and land cover change in Dhaka Metropolitan of Bangladesh during 1960–2005. Environ. Monit. Assess., 150, 237–249, doi: http://dx.doi.org/10.1007/s10661-008-0226-5

Dewan A.M., Yamaguchi Y. (2009b). Land use and land cover change in Greater Dhaka, Bangladesh: using remote sensing to promote sustainable urbanization. Appl. Geogr. 29, 390–401, doi: http://dx.doi.org/10.1016/j.apgeog.2008.12.005

Hundreds of acres of forest, crop land, water bodies destroyed (August 6, 2013). Dhaka Mirror.
Dixon R.K., Brown S. Houghton R.A., Solomon A.M., Trexler M.C., and Wisniewski J. (1994). Carbon pools and flux of global forest ecosystems. Science, 263, pp. 185-190.

Dong Y., Forster B., and Ticehurst C. (1997). Radar backscatter analysis for urban environments. International Journal of Remote Sensing, 18(6), pp. 1351–1364.

Environmental System Research Institute (2005). Using ArcGIS. Redlands, USA: ESRI.

Fazal S.A., Bhuiyan M.A.H., Chowdhury M.A.I. and Kabir M.M. (2015). Effects of Industrial Agglomeration on Land-Use Patterns and Surface. Water Quality in Konabari, BSCIC area at Gazipur, Bangladesh. International Research Journal of Environment Sciences, ISSN 2319–1414, 4(11), pp. 1-10.

Ferdous A., Kenneth J.T. (2001). Current constraints and future possibilities for Bangladesh fisheries. Food Policy, 26, pp. 297–313.

Food and Agricultural Organization, Soil Portal (1988). World Reference Base.

Giri C., Shrestha S. (1996). Land cover mapping and monitoring from NOAA AVHRR data in Bangladesh. Int. J. Remote Sens., 17, 2749–2759.

Hasan M., Hossain M., Bari M., Islam M. (2013). Agricultural Land Availability in Bangladesh; SRDI, Ministry of Agriculture: Dhaka, Bangladesh, p. 42, ISBN 978-984-33-6141-7.

Haq S., Rahman A., Mallik D. (2017). Population and Environment in Bangladesh. World Development Indicators database, World Bank, 15 December 2017.

Islam K., Jashimuddin M., Nath B., Nath T.K. (2018). Land use classification and change detection by using multi-temporal remotely sensed imagery: The case of Chunati wildlife sanctuary, Bangladesh. The Egyptian Journal of Remote Sensing and Space Science, 21, 37–47. doi: https://doi.org/10.1016/j.ejrs.2016.12.005

Klimanova O., Naumov A., Greenfieldt Y., Prado R.B., Tretyachenko D. (2017). Regional trends of land use and land cover transformation in Brazil in 2001-2012. Geography, Environment, Sustainability, 10(4), 98-116, doi: https://doi.org/10.24057/2071-9388-2017-10-4-98-116

Lambin E.F., Baulies X., Bockstael N., Fischer G., Krug T., Leemans R., Moran E.F., Rindfuss R.R., Sato Y., Skole D., Turner B.L., Vogel C. (1999). Land-use and land-cover change (LUCC): Implementation strategy. IGBP Report No. 48, IHDP Report No. 10, Stockholm, Bonn.

Lawrence B. Lesser. «Economic Reconstruction after Independence». A Country Study: Bangladesh (James Heitzman and Robert Worden, editors).

Leica Geosystems (2006). Erdas Imagine Tour Guides. USA: Leica Geosystems Geospatial Imaging.

López-Sánchez C.A. (2016). Evaluation of radiometric and atmospheric correction algorithms for aboveground forest biomass estimation using Landsat 5 TM data. Remote Sens., 8, 1–19, doi: http://dx.doi.org/10.3390/rs8050369

López-Serrano P.M., López-Sánchez C.A., Díaz-Varela R.A., Corral-Rivas J.J., Solís-Moreno R., Vargas-Larreta B., Álvarez-González J.G. (2015). Estimating biomass of mixed and uneven-aged forests using spectral data and a hybrid model combining regression trees and linear models. iForest - Biogeosciences and Forestry 9, 226, doi: https://doi.org/10.3832/ifor1504-008

Meyer W.B. and Turner B.L. (1994). Changes in Land Use and Land Cover: A Global Perspective. Cambridge University Press, Cambridge, UK.

Millat-e-Mustafa M. (2002). A Review of Forest Policy Trends in Bangladesh -Bangladesh Forest Policy Trends. Policy Trend Report, 2002:114-121.

Ojima D.S., Galvin K.A., and Turner B.I. (1994). The global impact of land-use change. Bioscience 44, pp. 300-304.

Quasem M.A. (2011). Conversion of agricultural land to non-agricultural uses in Bangladesh: Extent and determinants. Bangladesh Dev. Stud., 34, pp. 59–85.

Rahman, A.A., Huq S., Haider R., Jansen E.G. (1994). Environment and Development in Bangladesh, The University Press Limited, Dhaka, Bangladesh.

Rahman L.M. (2000). The Sundarbans: a unique wilderness of the world. USDA Forest Service Proceedings RMRS-P-15-VOL-2, 143-148.

Rasheed S. (2008). Bangladesh Resource and Environmental Profile, AH Development Publishing House, Dhaka, Bangladesh.

Salam M.A., Noguchi T., and Koike M. (2005). Factors influencing the sustained participation of farmers in participatory forestry: a case study in central Sal forests in Bangladesh. Journal of Environmental Management, 74(1), 43-51.

Shalaby A. and Tateishi R. (2007). Remote sensing and GIS for mapping and monitoring land cover and land use changes in the Northwestern coastal zone of Egypt. Applied Geography, 27(1), 28–41.

Sultana M.S., Kulsum U., Shakila A. and Islam M.S. (2012). Toxic Metal Contamination on the River near Industrial Area of Dhaka. Universal Journal of Environmental research and Technology, 2(2), 56-64.

30 Structures Constructed Illegally along Turag River (2017, October 09). The Daily Star. https://www.thedailystar.net/country/30-structures-constructed-illegally-along-turag-river-gazipur-judicial-probe-report-1478797

Uddin K. and Gurung, D.R. (2010). Land cover change in Bangladesh – a knowledge based classification approach. In Proceedings of the 10th International Symposium on High Mountain Remote Sensing Cartography, ICIMOD, Kathmandu, Nepal, pp. 8-11.

Xin Z.B., Xu J.X., Zheng W. (2008b). Spatiotemporal variations of vegetation cover on the Chinese Loess Plateau (1981–2006): impacts of climate changes and human activities. Sci. China Ser. D: Earth Sci. 51 (1), 67–78.

Yang X. and Lo C.P. (2002). Using a time series of satellite imagery to detect land use and cover changes in the Atlanta, Georgia. International Journal of Remote Sensing, 23(9), 1775–1798.

Received on March 28th, 2018 Accepted on November 15th, 2018

Kassahun Gashu[1*] and Tegegne Gebre-Egziabher[2]
[1] Department of Geography and Environmental studies, University of Gondar, Ethiopia
[2] Department of Geography and Environmental Studies, Addis Ababa University, Ethiopia
***Corresponding author:** Kg19me@gmail.com

COMPARISON OF URBAN SUSTAINABILITY USING INDICATORS APPROACH IN THE CITIES OF BAHIR DAR AND HAWASSA (ETHIOPIA)

ABSTRACT. Measuring urban sustainability remains an arena of dispute for long time. The promotion and development of urban sustainability are important to maximize the benefits of urbanization and minimize the negative externalities in urban environment and livelihoods. Each city has its strength and weakness towards sustainable urban development from different perspectives of various indicators. It is understood that assessment of sustainable city is related to identification and selection of sustainable development indicators. Therefore, in this research, we tried to develop a set of indicators, and indices for sustainability assessment in Bahir Dar and Hawassa cities in Ethiopia. The study focuses on the principal indicators, and an indicator framework has developed. The main purposes of sustainability indicators are to understand sustainability, supporting decisions, directing, involving stakeholders and empowerment. Twenty-six indicators with four main dimensions (economic, socio-cultural, environmental and institutional) have been identified. The computation of urban sustainability has to take into account all four dimensions equally. In the calculation of indicators, this study chooses a standard method [0, 1] using the minimum and maximum values for each indicator as an objective indicator. The sustainability indices calculated are 0.53 and 0.52 for Bahir Dar and Hawassa respectively, indicating that both cities have a moderate performance towards the development of a sustainable city. Aggregated data demonstrates that environmental indicators are moving towards sustainability, while economic, socio-cultural and institutional dimensions are performing relatively low in both cities, suggesting that sustainability studies need to work on all of sustainability dimensions that tend to better inform concerned bodies for policy intervention.

KEY WORDS: Equal weighting; Indicator approach; Normalization; Urban Sustainability

CITATION: Kassahun Gashu and Tegegne Gebre-Egziabher (2018) Comparison Of Urban Sustainability Using Indicators Approach In The Cities Of Bahir Dar And Hawassa (Ethiopia). Geography, Environment, Sustainability, Vol.12, No 1, p. 119-136
DOI-10.24057/2071-9388-2018-39

INTRODUCTION

With 70% of the global GDP coming from urban areas, urbanization is a powerful force to bring economic growth and poverty reduction through agglomeration economies and productivity gains (World Bank 2018). On the other hand, urbanization if not properly managed, can lead to more informal settlement, poverty and greenhouse gas emissions (UN-Habitat 2016; UNDP 2016). Urbanization thus has to be sustainable in order to reap its benefits. The UN agenda 2030 of SDG number 11 clearly stated the new stand to make cities safe, inclusive, resilient, and sustainable (UN 2015). The new urban agenda (conference of Habitat III held in Quito, Ecuador) also aims at shaping cities to be sustainable and liveable (Caprotti et al. 2017; UN 2017). These goals of urban sustainability aim at improving the socio-cultural and economic conditions of an increasingly urbanized population by preserving life systems and maintaining the quality of the environment (Alberti and Susskind 1996; National Science Foundation 2000; Shen et al. 2011).

Baker (2006) pointed out that sustainable urbanization occurs when there is harmony between urbanization process and sustainable development principles. Sustainability should be understood in an integrated and holistic view (Sisay 2005; Huang et al. 2009). Its central element is the nexus among economic, social, environmental and institutional objectives (Ali-Toudert and Ji 2017). These are multi-dimensional perspectives of sustainability (Mayer 2008) and sustainability studies are mindful of these components (Van de Kerk and Manuel 2008).

Urban sustainability also involves the association of a particular kind of locality and urbanization processes (Mori and Christodoulou 2012). It focuses on urban localities and opportunities for achieving sustainable livelihoods. Urban sustainability entails examining urbanization within the context of dynamic and complex factors producing urban growth in sustainable ways (Arcadis 2015, 2016). The sustainability of urban environments is thus likely to be a major policy challenge of the near future (Mohammedameen et al. 2015).

Ethiopia is one of the least urbanized countries not only by the world's standard but also by African standard. Currently, about 20 % of its population lives in urban areas as compared to the African average of 36 % (MoUDHCo[1] and ECSU[2] 2015). However, because of high natural population growth rate (2.73 % per annum), high rate of in-migration to towns and cities, and increase in the number of urban centers, the rate of urbanization is increasing at an average rate of 5.6 % (Shlomo et al. 2013; MoUDH 2015). Furthermore, the country's urban population in future is expected to grow on average by 3.98 % and in 2050 about 42.1% of the total population is expected to live in urban areas (UN-Habitat 2007). It is evident that, in addition to the national capital Addis Ababa, regional capitals such as Bahir Dar, Hawassa, Mekele and Adama have experienced high population growth in the past two decades. While rapid urbanization is evident, Ethiopian cities are experiencing high levels of poverty, unemployment and environmental problems compromising their sustainability. For instance, according to the recent information, urban poverty stood at 14.8% in 2015/16 (NPC[3] 2017) and unemployment stood at 16.5% in 2013 (CSA 2013)

There is therefore, a need to assess the sustainability of Ethiopian cities using sound and applied technique. We believe that the approach presented in this study, focusing on urban sustainability in Ethiopian context has important implication for other African countries in a similar situation. Therefore, the main objective of this study was to assess the sustainability levels of the two fast growing cities in Ethiopia, using a set of environmental, economic, socio-cultural and institutional sustainability indicators. Specifically, the study has three distinct yet interrelated specific objectives. First, we briefly review the main components of urban sustainability in urban landscape of developing countries like Ethio-

[1] MoUDHCo- Ministry of Urban Development Housing and Construction
[2] ECSU- Ethiopian Civil Service University
[3] NPC- National Planning Commission

pia. Our second objective is to list down the major components and sub-components of sets of sustainability indicators. Based on this, our third objective is to analyze the sustainability indices of the two fast growing cities.

Theoretical framework of urban sustainability: Indicator Approach

In the contemporary debate, the concept of urban sustainability implies the vitality of urban areas as a complex system in terms of the quality of life of its citizens and the natural capacity to support activities (Basiago 1999; Ferris et al. 2001; Lafferty and Eckerberg 2013).

UN and EU have broadly endorsed an overarching goal of sustainable development to achieve greater environmental effectiveness through cost-effective policy integration that can be realized by employing different combinations of policy elements (Lafferty 2004). The OECD has also formulated the institutional challenges of sustainable development in order to achieve a better balance between the environmental, social and economic aspects of welfare provision (OECD 2002; Lafferty 2004). The general goals and the more specific objectives formulated by international and regional organizations (UN, EU, and OECD etc.) can be seen as a set of minimal external standards for adapting government practice to sustainable development (Lafferty 2004).

Urban sustainability rests on four conceptual dimensions: economic, socio-cultural, environmental and institutional (UNDPCSD 1996a and b; Spangenberg 2002). Economic dimension of sustainability is a concern with economic activities to consider natural, social and human capital (Labuschagne et al. 2005; Finkbeiner et al. 2010). It seeks to preserve the environment through economic growth and the alleviation of poverty (Shen et al. 2011). The economic component consists of the key elements of different modes of economic development and sustainable production through improved eco-efficiency and sustainable consumption lifestyles (Lafferty 2004).

The socio-cultural dimension of sustainability shows a less clear-cut definition (Martin 2001) because of the diversity of economic, social and cultural conditions in individual countries (Moldan et al. 2012). It is however characterized from a social perspective. For instance, Black (2004) defined socio-cultural sustainability as the extent to which social values, social identities, social relationships and social institutions of individual countries can continue into the future. Gilbert et al. (1996) perceived that the socio-cultural pillar of sustainability requires the cohesion of society and its ability to work towards common goals of health and well-being, nutrition, shelter, education and cultural expression. Lafferty (2004) also mentioned that the socio-cultural component of sustainable development to include equitable distributions of individual life chances to satisfy objectively defined basic needs such as national social equity, national generational equity, global social equity and global generational equity.

The environmental dimension of sustainable development is a concept based on the notion of ecosystem services of both renewable and non-renewable resources and waste absorptive capacity that provide benefits to humans and improve their welfare (Moldan et al. 2012). The OECD strategy for the 21st century (OECD 2001) defined four specific criteria for environmental sustainability: regeneration (renewable resources shall be used efficiently and their use shall not be permitted to exceed their long-term rates of natural regeneration), substitutability (non-renewable resources shall be used efficiently and their use should be limited to levels which can be offset by substitution with renewable resources or other forms of capital), assimilation (releases of hazardous or polluting substances into the environment shall not exceed their assimilative capacity) and avoiding irreversibility. Environmental sustainability involves ecosystem integrity, carrying capacity and biodiversity (Munda 2005). It requires that natural capital be maintained as a source of economic inputs and as a sink for wastes (Moldan et al. 2012). Lehtonen (2004) noted that on one hand, resources must be harvested no faster than they can be regenerated, on the other hand, wastes must be emitted no faster than they can be assimilated by the environment.

Environmental sustainability, unlike the economic or social spheres, seems to be open for developing and using targets that are firmly rooted in the bio-physical properties of the system (Moldan et al. 2012). Lafferty (2004) stated that environmental dimension of sustainability consists of nature conservation, environmental protection and ecological balance. The integration of environmental concerns into other policy areas has been diversely referred to as environmental policy integration (Lafferty 2004). An equally plausible and highly relevant case can however be made, that there are numerous very real conflicts of interests with respect to many environmental issues and non-environmental objectives. Any conflicts of interest between policy objectives of environmental issues and non-environmental objectives can be resolved by balanced means which has to be addressed to the satisfaction of all affected interests (Lafferty 2004). This implies that there will be at least some environmental objectives that should be balanced with either political or economic goals for life support systems. When environmental planners speak of urban sustainability; they mean the pursuit of urban form that synthesizes land development and nature preservation (Lozano and Huisingh 2011).

Institutional dimension of sustainability has stronger roots within the broader development literature (Bell and Morse 2008). Some studies (Keman and Pennings 1995; Spangenberg et al. 2002a) stated that institutions are broadly defined and analyzed by political science as the structure of rules for political decision-making and implementation. However, Spangenberg et al. (2002b) noted that social entities see it as actors as well as systems of rules shaping social behavior, including the mechanisms for rule enforcement. Political organizations perceive it as involving a combination of definitions given by political science and social entities: appearing as actors in political process and systems of rules structuring political behavior and facilitating societal views (UNDPCSD 1996a,b; Spangenberg et al. 2002b). Measuring institutional growth toward sustainability is vital in order to manage and improve its effectiveness. For these purposes institutional sustainability is taken as, the effectiveness of institutions through the implementation of their purposes for sustainable urban development.

In the analysis of urban sustainability measurement, the foregoing discussion implies these four dimensions of sustainability must be integrated and interlinked (Sikdar et al. 2017) in coordinated and comprehensive manner (Höjer et al. 2011).

The two common approaches used to measure urban sustainability are direct measurement and indicators approach (McCool and Stankey 2004). Direct measurement of urban sustainability is difficult in developing countries because of a paucity of comprehensive data set and technology. Hence, the most commonly used measurement approach of urban sustainability is indicator approach (Maclaren 1996; Turcu 2013). The core motivation behind the indicator based approach for measuring urban sustainable development lies in the ability of indicators to give a comprehensive, reliable, and easy-to-understand picture of the environmental, socio-cultural, economic and institutional trends in a concise form (Eurostat 2009; Mori and Yamashita 2015).

The first set of indicators was launched by the United Nations Commission on Sustainable Development in 1995 (UNESC 1995), followed by a number of countries adopting their own national sustainable development indicators. Since then, numerous global, national, and local scale indicator initiatives have been carried out in order to measure sustainable development. Sustainable development indicators have been produced for various purposes and by a wide spectrum of institutions (Munier 2011; Rametsteiner et al. 2011; Dahl 2012; Rinne et al. 2013; UN-Habitat 2016). Zilans and Abolina (2009) claimed that, it is crucial that cities are focusing on indicators to measure sustainability. The sustainability indicators implied the tight interconnectedness of economic, social and environmental components (Sustainable Cities International 2012). They can be either quantitative or qualitative measures (Camilla and Marc 2009; Sustainable Cities International 2012).

The main criticisms against them have to do with the subjectivity of the choice of variables and the weighting of the indicators (Mori and Christodoulou 2012). Bell and Morse (2008) also indicated although indicators are logical devices used to gauge progress towards attainment to sustainable development, there are a number of key questions related to their development and application including what indicators should be selected? who selects them? why are they selected? how are the indicators to be measured? how are the indicators to be interpreted, and by whom? how are the results to be communicated, to whom and for what purpose? how are the indicators to be used?. Therefore, with the limitations stated above, this study adopted indicator method to assess the cities sustainability in the study areas.

Selection of indicators

The framework of indicator approach is considered as the first step in the implementation and interpretation process of sustainability (Mascarenhas et al. 2010; Estoque and Murayama 2017). Indicators for each dimension of sustainability are distilled from the literature (see Annex 1 (available at https://ges.rgo.ru) for source, explanation and measurement of indicators). In total 26 indicators of which six for economic dimension, eight for socio-cultural dimension, six for environmental dimension and six for institutional dimension were chosen.

MATERIALS AND METHODS

Study areas

This study was conducted in the two fast growing cities of Ethiopia: Bahir Dar and Hawassa (Fig. 1). Bahir Dar is the capital of Amhara National Regional State. Its astronomical location is 11^0 36' North and 37^0 23' East and 565 km north of Addis Ababa. According to the municipality of Bahir Dar city (2015), the historical foundation of the city is associated with the establishment of KidaneMiheret Church in the present site of St. Giorgis church around the 14th century. Haregeweyn et al. (2012) elaborated that Bahir Dar was fast developed and transformed into a modern city during the Italian occupation period of 1928-1933. Haregeweyn et al. (2012) also mentioned that the name Bahir Dar which means the periphery of a water body is related to the city's proximity to two water bodies: Lake Tana and River Abay.

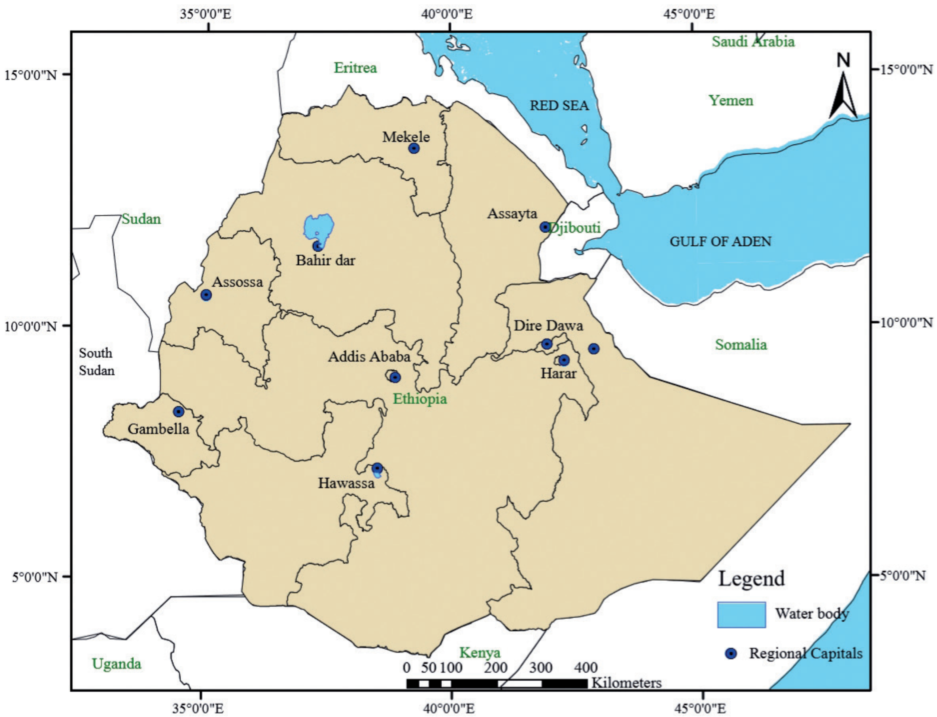

Fig. 1. Location map of study areas

The other study site, Hawassa city, is found in Southern Nations, Nationalities and Peoples National Regional State, at a distance of 275 km south of Addis Ababa. It is the regional capital and is bounded by Lake Hawassa on the west and north-west, Chelelaka swampy area to the east and south-east, TikurWuha river on the north and Alamura mountain on the south. Its astronomical location is at 07^0 03′ North and 38^0 28′ East.

According to the municipality of Hawassa city (2015) and as explained by elders, Hawassa was founded in 1968 by Ras Mangesha Seyoum under the permission of Emperor Haile Selassie. It was initially settled by pensioned soldiers and this was reckoned to have given an impetus to the growth and development of the city. Hawassa municipality was founded in 1970. The city got its name from Lake Hawassa. Most people choose it as a place of residence because of its relative nearness to the capital Addis Ababa and due to its suitable weather condition, natural attractions, business and job opportunity, investment potentials and friendly community.

DATA AND SAMPLING

This study used both qualitative and quantitative data collected from primary and secondary sources. Qualitative data were collected from two focus group discussion (one from each city) composed of six experts/practitioners (civil engineer, architecture, urban planner, surveyor, land administration and environmentalist) and face-to-face interviews with two focal persons (one from each city). The two focal persons for face-to-face interview were selected from the office responsible for the green infrastructure development, implementation, maintenance, preparation and status monitoring in each city. This helps for scrutinizing indicators at the local level. The quantitative data were collected from a cross sectional survey. Structured questionnaire was used to collect each of the economic, socio-cultural, environmental and institutional dimensions of indicators. A 5-point Likert scale was used to measure the level of each sub-indicator with scores of 0 (very low), 1 (low), 2 (average), 3(good) and 4 (very good). A full description of each indicator was provided in the questionnaire and each respondent was asked to rate the different dimensions of sustainability indicators in the city. All of the economic, socio-cultural, environmental, and institutional indicators were measured in nominal scale.

The survey was implemented in a two stage sampling. In the first stage, five sub-cities were purposively selected in each city on the basis of better availability of green infrastructure. The sub-cities selected in Bahir Dar were Facilo (with population number 26,349), Hidar-11 (with population number 33,950), Shume-abo (with population number 31,221), Gesh-abay (with population number 19,938) and Sefene-Selam (with population number 20,236). The sub-cities selected in Hawassa were Misrak (with population number 30,350), Menaheria (with population number 29,120), Tabor (with population number 25,125), Mehalketem (with population number 24,135) and Haik Dar (with population number 21,201).

In the second stage, a total of 430 respondents (215 from each city) were selected from sub-city sampling frame for survey questionnaire using a formula by Israel (1992) and substantiated by CRS[4] (2012). In each sub-city a proportional number of respondents were selected using the proportional sampling size method.

Data analysis

Descriptive statistics was used to summarize the socio-demographic data and the indicator method approach was used to compute the environmental, economic, socio-cultural and institutional dimensions of sustainability. The qualitative data were transcribed and analyzed using theme analysis techniques. Quantitative data were analyzed using normalization to make the decision whether or not urban sustainability in the study areas.

[4] Creative Research Systems

Mathematical calculation

In the calculation of indicators, this study chooses a standard method [0, 1] using the minimum and maximum values for each indicator as an objective indicator (Choon et al. 2011; Yang et al. 2017; Tanguay et al. 2010).
The value of indices fall between 0 and 1, where a value closer to 1 denotes better sustainability of urban development while a value closer to zero indicates poor sustainability of urban development. The actual ratings of individuals or actual values are transformed into values between 0 and 1 using the following equation 1:

$$Yi = Zi - a/e - a \tag{1}$$

Where, Yi: lies between 0 and 1, Zi: actual value; a: denotes minimum value of an indicator and e: denotes maximum value of an indicator.

The above indicators are normalized in order to allow comparisons between different dimensions of sustainability using the following equation 2:

$$Z = Yi(Avg) - \mu/\sigma \tag{2}$$

Where: Z: denotes the normalized value of each indicator in a given sustainability dimension, Yi (avg): the average value of each indicator for all respondents, μ: is the aggregated average value for each sustainability dimension, δ: denotes the standard deviation of each sustainability dimension

In order to examine each sustainability dimension index and overall sustainability index for Bahir Dar and Hawassa independently, we used an equal weighting method (Roldan and Valdes 2002; YCELP and CIESIN 2005, 2006). For the calculation of each sustainability dimension, standardized sub-indicators can be combined using the following formula (Wilson and Wu 2017).

$$\begin{aligned} INDEXnorm = (&Sub\_index1norm + \ldots \\ &+ Sub\_index2norm + \ldots\ldots.. \\ &+ Sub\_indexnnorm)/N \end{aligned} \tag{3}$$

Where: Sub-index$_1$norm,..., sub-index $_n$ norm is normalized values of each sub-indicator $_{1 \text{to } n}$; N is the total number of sub-indices.

To accomplish over all sustainability index, we generally selected economic, socio-cultural, environmental, and institutional sub-indicator sets, which are normalized and averaged. Therefore, over all sustainability index may take the following form using the technique formulated by Wilson and Wu (2017).

$$\begin{aligned} SI = (&Economic + Socio - cultural + \ldots \\ &+ Environmental + Insitutional)/N \end{aligned} \tag{4}$$

Where 'SI' represents over all sustainability indices, 'Economic' the normalized economic sub-index; 'Socio-cultural' the normalized socio-cultural sub-index; 'Environmental' the normalized environmental sub-index, 'and 'Institutional' the normalized institutional sub-index; N= 4.

In this study, we used a sustainable city classification system as presented in Table 1 adopted from OECD 2004; Choon et al. 2011; vanDijk and Mingshun 2005; Caprotti et al. 2017.

Table 1. Sustainable city classification

Score	Definition
≥ 0.75	strong sustainability
0.50 ≤ X< 0.75	moderate sustainability
0.25 ≤ X< 0.50	weak sustainability
<0.25	unsustainable

[5] Yale Center for Environmental Law & Policy
[6] Center for International Earth Science International

RESULTS

Socio-demographic background of respondents

The socio-demographic characteristics of the respondents are presented in Table 2. The average age of the respondents was almost similar in the two cities: 41 and 44 years old in Bahir Dar and Hawassa cities respectively. The educational status of the respondents in Bahir Dar shows that, just over two-third of the respondents (68.8%) have completed college or university degree and the remaining (23.2%) and (7.9%) have completed secondary and primary education respectively. In Hawassa, over half of them (57.2%) have completed college and university degree; the rest (18.6%) and (12.6%) have completed secondary and primary education respectively. Services are by far the most important sources of employment for respondents in both cities.

More than half of the respondents or 57.2% in Bahir Dar and 54.9% in Hawassa mentioned ownership of the house they occupy (Table 2). In both Bahir Dar and Hawassa,

Table 2. Socio-demographic characteristics of respondents (N=215 each city)

Variables		Bahir Dar	Hawassa
Age	Average	41years	44years
	Range	18-64years	18-64years
Sex	Female	38(18)	53(24.7)
	Male	177(82)	162(75.3)
Education	Primary education	17(7.9)	27(12.6)
	Secondary education	31(23.2)	40(18.6)
	College &University graduated	167(68.8)	148(68.8)
House Tenure	Owned the house unit currently occupied	123(57.2)	118(54.9)
	Renting (Private and Public)	92(42.8)	97(45.1)
Type of employment	Urban agriculture	9(4.2)	10(4.7)
	manufacturing	26(12.1)	29(13.5)
	Services	96(44.7)	78(36.3)
	Education	42(19.5)	40(18.6)
	Trade	39(18.1)	50(23.3)
	Unspecified	3(1.4)	8(3.7)
Awareness level of sustainability	Yes	175(81.4)	190(88.4)
	No	40(18.6)	25(11.6)
Can define meaning of sustainability	Yes	166(77.2)	185(86.0)
	No	49(22.8)	30(14.0)

**Numbers in parenthesis are percentage values, Source: Survey result* a very significant number of respondents (81.4% in Bahir Dar and 88.4% in Hawassa) are aware of the sustainability issues. Furthermore, 77% in Bahir Dar and 86% in Hawassa pointed out that they can explain the basic meaning of sustainability (Table 2).

Sustainability index analysis

Based on the concept presented in Table 1 and using equation 4, classification of urban sustainability at aggregate level, Bahir Dar and Hawassa scored 0.53 and 0.52 respectively which is almost equal to the mean index point of 0.52. However, neither of the two cities attained sustainability level of greater than or equal to 0.75, hence they are classified as moderately sustainable.

Economic dimension of sustainability index

The economic dimension is one of the main pillars of urban sustainability. The sub-indicators of economic dimension: transport infrastructure, economic growth, tourism and employment have shown a tendency towards sustainability, while this is not true for ease of doing business in both cities.

Fig. 2 shows the economic dimension of the sustainability index in Bahir Dar and Hawassa. Within this dimension, the transport indicator has the highest value with an average score of more than 0.6 and the smallest is ease of doing business with an average score of less than 0.5 in both cities. Transport, connectivity and employment achieved a higher score in Bahir Dar than Hawassa while economic growth, tourism and ease of doing business have a higher score in Hawassa. The overall economic sustainability indices using equation 3 are 0.52 and 0.53 in Bahir Dar and Hawassa respectively which according to the classification in Table 1 puts them at the moderate level of sustainability

Socio-cultural dimension of sustainability index

The sub-indicators of socio-cultural dimension: demographics, education, income inequality, housing, social and cultural network have values closer to one and hence reflect progress towards sustainability. Other indicators, however such as crime, should be standardized via adjustment

($Z^*= 1 - Z$), so that a value trending towards one indicates improved sustainability.

Fig. 3 presents the sustainability index of sub-indicators of socio-cultural dimension in Bahir Dar and Hawassa cities. Among the sub-indicators, demographics (0.67) in Bahir

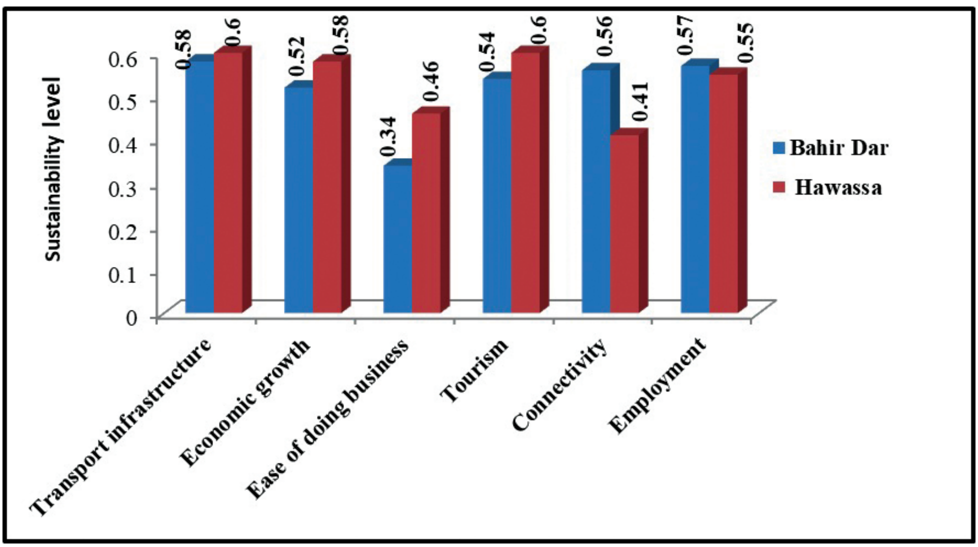

Fig. 2. Sustainability level of economic dimension indicators

Dar and education (0.67) in Hawassa have the highest values. In both cities, crime has highest values via adjustment mentioned implying that cities are safe and hence sustainable in this regard susceptibility of the cities for crime. Highly sustainable sub-indicators in Bahir Dar are demographics and education while education and housing have high sustainability in Hawassa.

Environmental dimension of sustainability index

Among the environmental sustainability sub-indicators, energy, land use/green spaces, greenhouse gas emission, and water availability are indicators with higher scores and hence reflect higher sustainability (Fig. 4). Like crime, which is one of socio-economic indicator mentioned above, environmental risks and greenhouse gas emission should be standardized via adjustment ($Z^* = 1 - Z$) so that, a value trending towards sustainability, one indicates improved sustainability. This shows, environmental risk indicator is not showing towards sustainability in both cities. Nevertheless, the score for waste management is low in both cities and this is an indication that there are no enough liquid and solid waste management practices. This leads to the disposal of waste in Lake Tana in Bahir Dar and Lake Hawassa in Hawassa.

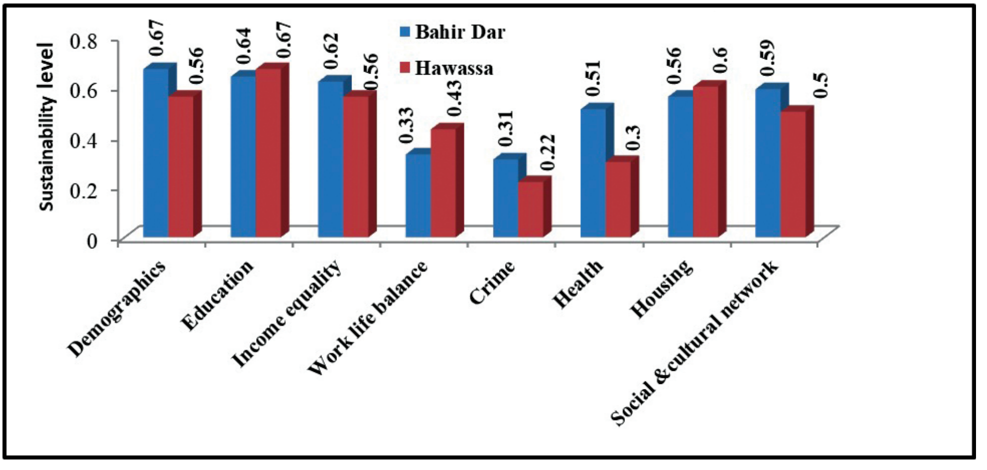

Fig. 3. Sustainability level of socio-cultural dimension indicators

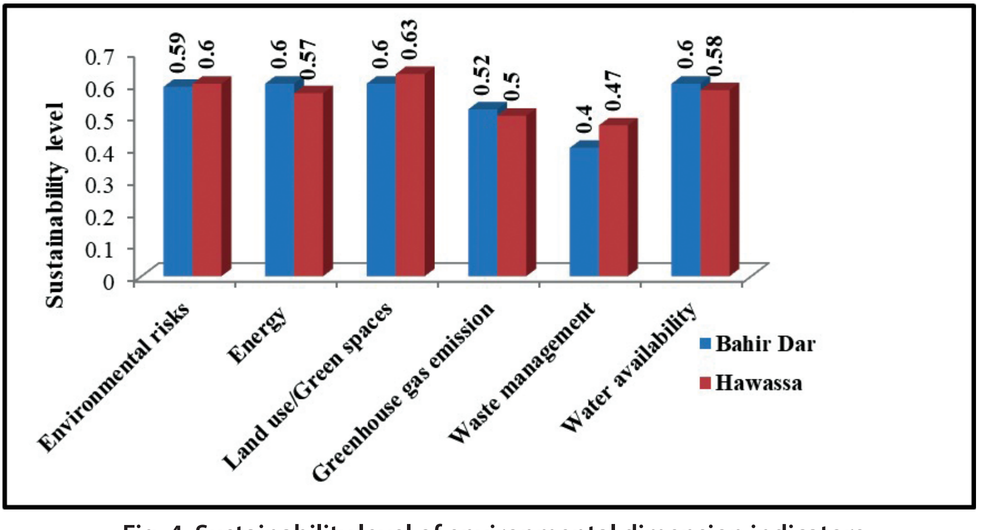

Fig. 4. Sustainability level of environmental dimension indicators

The sub-indicators with the highest sustainability score in Bahir Dar and Hawassa are energy consumption, land use/green space, and water availability (Fig. 4). The overall score for environmental sustainability in Bahir Dar is 0.55 and it is 0.56 in Hawassa. The results show that both cities are found at the moderate level of sustainability.

Institutional dimension of sustainability index

Fig. 5 depicts that among the institutional sustainability sub-indicators, institutional capacity, institutional framework, local community participation, and gender mainstreaming are those with higher scores in both cities. On the other hand, local authority services indicator has low score in both cities. In Hawassa, the institutional sub-indicaror with the highest score is institutional capacity with an average score of 0.59 while in Bahir Dar the sub-indicator with the highest score is local community partnership with an average score of 0.57 (Fig. 5). The average rating for institutional sustainability using equation 3 is 0.52 for Bahir Dar and 0.50 for Hawassa.

Overall urban sustainability indices

Fig. 6 and 7 provide the results of sustainability in terms of the four dimensions. It can clearly be seen that the three dimensions of sustainability in both cities fall in the category of moderate sustainability classification (0.50 ≤ X < 0.75) except socio-cultural dimension in Hawassa. Hawassa seems to have relatively a better performance in the economic and environmental dimensions. The economic sustainability score of Hawaasa (0.53) is higher than that of Bahir Dar (0.52) which could be due to the investment pooling potential of Hawassa since the city is relatively closer to the capital, Addis Ababa. Similarly the better performance of Hawassa in environmental dimension reveals that the attention the city has provided to this issue is better than Bahir Dar. Hawassa however lags behind Bahir Dar in terms of the socio-cultural and institutional dimensions of sustainability. The overall result of sustainability in Bahir Dar (0.53) is higher than that of Hawassa (0.52) reflects the values of the socio-cultural and institutional dimensions which are better for Bahir Dar city (Fig. 6 and 7).

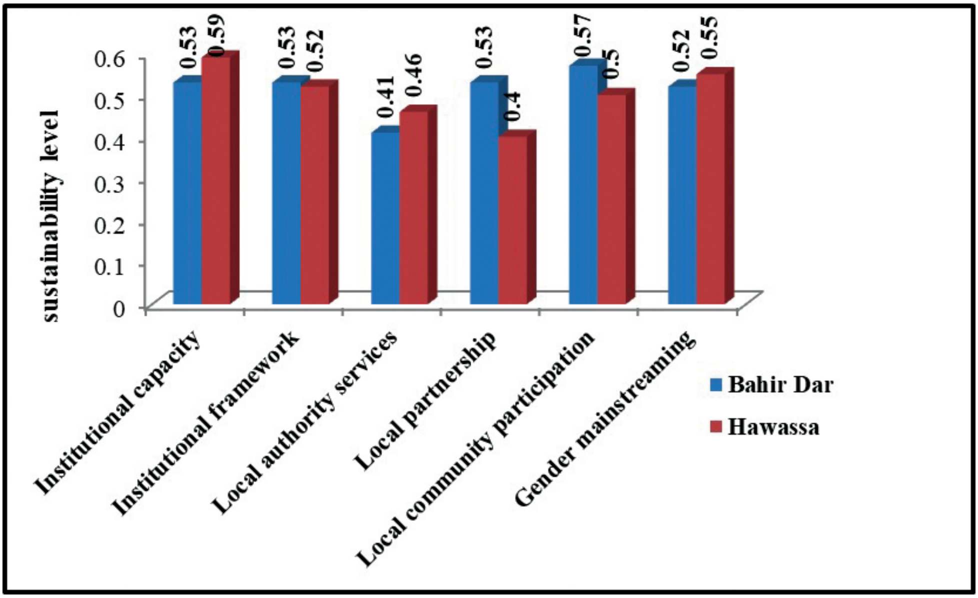

Fig. 5. Sustainability level of institutional dimension indicators

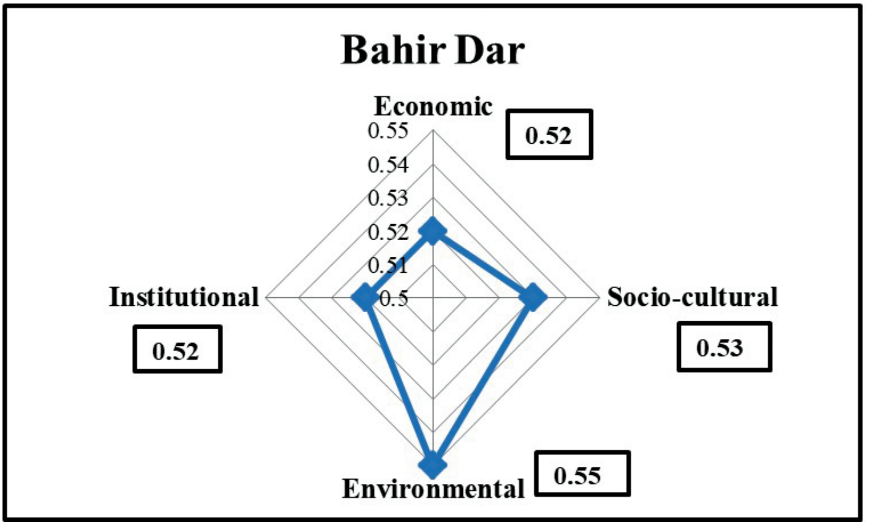

Fig. 6. Spider diagram of dimensions of sustainability for Bahir Dar

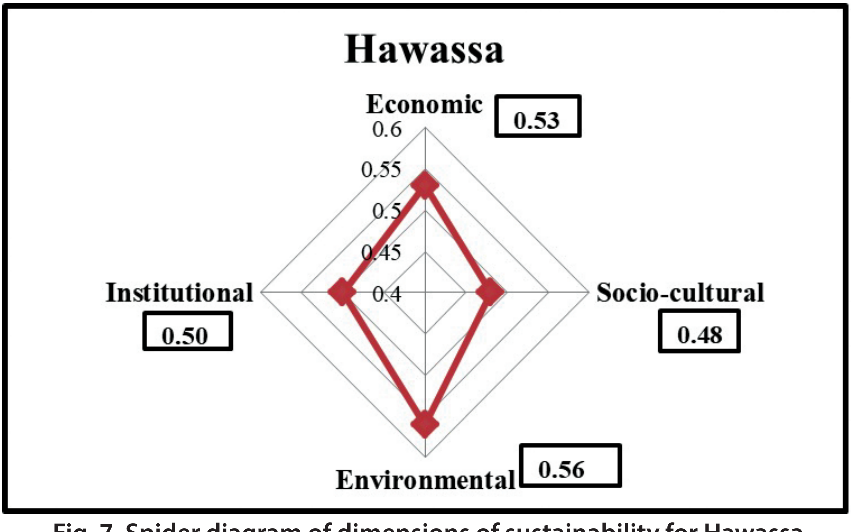

Fig. 7. Spider diagram of dimensions of sustainability for Hawassa

DISCUSSION

Recently, sustainability is given a high profile and it requires that decision makers should have information about the environmental, socio-cultural, economic, and institutional implications of development (Lyth and de Chastel 2007). In the same way sustainable, urban development requires major changes in managing the social, environmental and spatial effects of urban development (Roberts and Kanaley 2007). Sustainability however has to be understood correctly and this necessitates the use of techniques of selecting and using appropriate indicators for each of the dimensions of sustainability. Our exercise in constructing the sustainability index has helped us to examine the extent to which the two cities have managed their environmental, economic, institutional and socio-cultural aspects of urban development in a comparative perspective.

The computation of urban sustainability has to take in to account the four main dimensions equally. Urban sustainability is multidimensional optimization process by its very nature and cannot have one clear optimal solution. Therefore, sustainability assessment must be based on multi indicators analysis. The result showed that both cities have attained a moderate level of sustainability and there is little difference in the overall sustainability among the cities. The components of sustainability show slight variations between the two cities. In relation to economic dimension (Fig. 6 and 7), Hawassa has relatively higher index than Bahir Dar while Bahir Dar has relatively higher socio-cultural index than Hawassa. However, in both cities, the socio-cultural dimension of urban sustainability is at the lower range of sustainability classification. This shows that both cities have to work more in addressing housing, education, health needs, reducing crime and strengthening the social and cultural networks in their respective jurisdictions. In relation to environmental dimension, both cities show relatively higher index. This implies that most of the activities of the cities are focused on environmental issues. As a result environmental sustainability in the form of minimizing environmental risks, providing renewable energy consumption, reducing greenhouse gas emission and providing clean water has received a better attention in the cities.

The urban development policy in the country supports urban sustainability and strives to make cities the sources of the industrial value chain, centers of innovation and employment opportunity (MoUDH 2015). The findings of the result showed that priority is given to environmental dimension followed by economic dimensions. The socio-cultural and institutional dimensions have received less attention though they are equally important and incorporating them increases the possibility of broadening the coverage of sustainability.

CONCLUSION

The indicator-based approach provides a basis for identifying different indicators to urban sustainability in a comprehensive manner. It combines indicators-based interpretation of urban sustainability with the recognition of different indicators. An assessment of sustainability using the four main dimensions is necessary to determine if cities are able to consider the economic, socio-cultural, environmental, and institutional dimensions of sustainability simultaneously.

In this study, it is implied that one index is insufficient to understand fully the sustainability of a city, and therefore utilization of composite indices is required. According to the classification of a sustainability index, neither of our case study cities has yet achieved strong sustainability. Socio-cultural and institutional dimensions of sustainability are found to be low in Hawassa and Bahir Dar respectively as compared to the other dimensions. On the other hand, both cities have attained strong sustainability level in terms of environmental dimension. Each city has its strengths and weaknesses towards sustainable urban development. The sustainability indicators of these two cities in Ethiopia can be used as a framework and a guideline for urban managers and planners towards attaining sustainable urban development in other cities and towns in the country.

ACKNOWLEDGEMENT

Financial support is given by Addis Ababa University and University of Gondar for the first author. We thank also the data collectors and sample respondents and two reviewers for their comments.

REFERENCES

Alberti M., and Susskind L. (1996). Managing urban sustainability: Special issue. Environmental Impact Assessment Review, Vol, 16, pp, 213-221

Ali-Toudert F., and Ji, L. (2017). Modeling and measuring urban sustainability in multi-criteria based systems- A challenging issue. Ecological Indicators, Vol, 73, pp, 597–611

Arcadis (2015). Sustainable Cities Index 2015: Balancing the economic, social and environmental needs of the world's leading cities of city sustainability.

Arcadis (2016). Sustainable Cities Index 2016: Putting people at the heart of city sustainability. www.arcadis.com/SCI2016 [Accessed 19 Feb 2016]

Baker S. (2006). Sustainable development. Rutledge, Madison Avenue, New York.

Basiago A.D. (1999). Economic, social and environmental sustainability in development theory and urban planning practice. The Environmentalist, Vol, 19, pp,145-161

Bell S., and Morse S. (2008). Sustainability Indicators: Measuring the Immeasurable? 2nd edition Earth scan, London

Black A. (2004). The quest for sustainable, healthy communities, presented to Effective sustainability education conference. NSW Council on Environmental Education, UNSW, Sydney, 18–20 February, 2004.

Camilla A., and Marc P. (2009). Sustainable Development Indicators: An Overview of relevant Framework Programme funded research and identification of further needs in view of EU and international activities, European Communities, Brussels, Switzerland.

Caprotti F., Cowley R., Datta A., Broto V.C., Gao E., Georgeson L., Herrick C., Odendaal N., and Joss S. (2017). The new urban agenda: key opportunities and challenges for policy and practice. Urban Research & Practice, Vol, 10(3), pp, 367-378

Choon S.W., Siwar C., Pereira J., Jemain A., Hashim S.H., and Hadi A.S. (2011). A sustainable city index for Malaysia. International Journal of Sustainable Development & World Ecology, Vpl, 18(1), pp, 28-35.

Creative Research Systems (2012). Sample size formula for sample size calculator. Retrieved from http://www.surveysystem.com/sample-size-formula.htm [Accessed on 21May 2016]

CSA (2013). Statistical abstract, Addis Ababa, Ethiopia

Dahl A. L. (2012). Achievements and gaps in indicators for sustainability. Ecological Indicators Vol.17, pp, 14–19

Estoque R. C. and Murayama Y. (2017). A worldwide country-based assessment of social-ecological status (c. 2010) using the social-ecological status index. Ecological Indicators Vol.72, pp, 605–614

Eurostat (2009). Sustainable development in the European Union. 2009 monitoring report of the EU sustainable development strategy. Office for Official Publications of the European Communities.

Ferris J., Norman C., and Sempik J. (2001). People, land and sustainability: Community gardens and the social dimension of sustainable development. Social Policy & Administration, Vol, 35(5), pp, 559-568.

Finkbeiner M., Schau E. M., Lehmann A., and Traverso M. (2010). Towards life cycle sustainability assessment. Sustainability,Vol, 2(10), pp,3309-3322.

Gilbert R. (1996). Making cities work. In: The Role of Local Authorities in the Urban Environment. Earth scan, London.

Haregeweyn N., Fikadu G., Tsunekawa A., Tsubo M., and Tsegaye D.M. (2012). The dynamics of urban expansion and its impacts on land use/land cover change and small-scale farmers living near the urban fringe: A case study of Bahir Dar, Ethiopia. Landscape & Urban Planning Vol, 106, pp, 149– 157

Höjer M., Gullberg A. and Pettersson R. (2011). Images of the future city: Time and space for sustainable development. Springer Science+Business Media B.V.

Huang S-L.,Yeh C-T., Budd W.W., and Chen L-L. (2009). A Sensitivity Model (SM) approach to analyze urban development in Taiwan based on sustainability indicators. Environmental Impact Assessment Review Vol, 29, pp, 116–125.

Israel G. (1992). Determining Sample Size. IFAS, University of Florida, PEOD-6.

Keman H., and Pennings P. (1995). Managing political and societal conflict in democracies: do consensus and corporatism matter? British Journal of Political Science, Vol, 25(2), pp, 271-281.

Labuschagne C., Brent A. C., and Van Erck R. P. (2005). Assessing the sustainability performances of industries. Journal of cleaner production, Vol, 13(4), pp, 373-385.

Lafferty W. M., and Eckerberg K. (Eds.). (2013). From the Earth Summit to Local Agenda 21: working towards sustainable development (Vol. 12). Rutledge.

Lafferty, W.M. (2004). From environmental protection to sustainable development: the challenge of decoupling through sectoral integration in Lafferty, W.M. (edition) "Governance for sustainable development: The challenge of adapting Form to function". Edward Elgar, Cheltenhan, UK

Lehtonen M.(2004). The environmental–social interface of sustainable development: capabilities, social capital, institutions. Ecological economics, Vol, 49(2), pp, 199-214

Lozano R., and Huisingh, D. (2011). Inter-linking issues and dimensions in sustainability reporting. Journal of cleaner production, Vol, 19(2),pp, 99-107.

Lyth A. and de Chastel L. (2007). Shifting towards sustainability. Australian Planner, Vol, 44(3), pp, 12-14.

Maclaren V.W. (1996). Urban sustainability reporting. Journal of the American Planning Association, Vol, 62 (2), pp, 184-202

Martin J.P. (2001). The social dimensions of sustainable development speech delivered to the conference on the European social agenda and EUˇs international partners. Brussels, 20–21 November 2001.

Mascarenhas A., Coelho P., Subtil E., and Ramos T.B. (2010). The role of common local indicators in regional sustainability assessment. Ecological Indicators Vol, 10, pp, 646–656

Mayer A.L. (2008). Strengths and weaknesses of common sustainability indices for multidimensional systems. Environment International, Vol,34, pp, 277–291

McCool S.F., and Stankey G.H. (2004). Indicators of Sustainability: Challenges and Opportunities at the Interface of Science and Policy. Environmental Management, Vol, 33(3), pp,294–305

MohammedAmeen, R.F., Mourshed, M., and Li, H. (2015). A critical review of environmental assessment tools for sustainable urban design. Environmental Impact Assessment Review Vol, 55, pp, 110–125

Moldan B. Janouskova S., and Hak T. (2012). "How to understand and measure environmental sustainability: Indicators and targets". Ecological Indicators, Vol, 17,pp, 4–13

Mori K., and Christodoulou A. (2012). Review of sustainability indices and indicators: Towards a new City Sustainability Index (CSI). Environmental Impact Assessment Review, Vol, 32, pp, 94–106

Mori K., and Yamashita T. (2015). Methodological framework of sustainability assessment in city sustainability index (CSI): A concept of constraint and maximization indicators. Habitat International,Vol, 45,pp,10-14

MoUDH. (2015). Ethiopia National Urban Green Infrastructure Standard. Addis Ababa, Ethiopia

MoUDHCo and ECSU. (2015). State of Ethiopian Cities Report. Addis Ababa, Ethiopia

Munda G. (2005). Measuring sustainability a multi-criterion framework. Environment Development Sustainability, Vol, 7, pp, 117–134,

Municipality of Bahir Dar city. (2015). Annual Report. Bahir Dar, Ethiopia

Municipality of Hawassa city (2015). Annual report, Hawassa, Ethiopia.

Munier N. (2011). Methodology to select a set of urban sustainability indicators to measure the state of the city, and performance assessment. Ecological Indicators, Vol, 1, pp, 1020–1026

National Science Foundation. (2000). Towards a Comprehensive Geographical Perspective on Urban Sustainability. Final Report of the 1998 Workshop on Urban Sustainability, Center For Urban Policy Research, Rutgers, The State University of New Jersey

NPC (2017). Growth and transformation plan II. NPC, Addis Ababa, Ethiopia.

OECD (2001). OECD environmental strategy for the first decade of the 21st century. OECD, Paris, France.

OECD (2004). Measuring Sustainable Development: Integrated Economic, Environmental and Social Frameworks. OECD, Paris, France.

Rametsteiner E., Pülzl H., Alkan-Olsson J., and Frederiksen P. (2011). Sustainability indicator development - Science or political negotiation? Ecological Indicators,Vol, 11, pp, 61–71.

Rinne J. Lyytimaki J., and Kautto P. (2013). From sustainability to well-being: Lessons learned from the use of sustainable development indicators at national and EU Level. Ecological Indicators,Vol, 35,pp,35– 42

Roberts B., and Kanaley T. (2007). Sustainable urban development in Asia. Australian Planner, 44(1), pp, 18-21.

Roldan A.B., and Valdes A.S. (2002). Proposal and application of a sustainable development index. Ecological Indicators, Vol, 2, pp, 251–256.

Shen L. Y., Ochoa J. J., Shah M. N., and Zhang X. (2011). The application of urban sustainability indicators-A comparison between various practices. Habitat International, Vol, 35(1), pp, 17-29.

Shlomo A., David de G., Richard M., Yohannes F., Tsigereda T., and Patrick L. (2013). The Ethiopian urban expansion initiative: Interim report 2, NYU STERN, Urbanization Project

Sikdar S.K., Sengupta, D., and Mukherjee R. (2017). Measuring progress towards sustainability: A treatise for engineers. Springer International Publishing, Switzerland

Sisay A. (2005). The Economics of Sustainable Development W.E. Upjohn Institute for Employment Research, Michigan USA.

Spangenberg J. H. (2002). Environmental space and the prism of sustainability: frameworks for indicators measuring sustainable development. Ecological indicators, Vol,2(3),pp,295-3 09.

Spangenberg J.H., Pfahl S., and Deller K. (2002a). Towards indicators for institutional sustainability: lessons from an analysis of Agenda 21. Ecological indicators, Vol, 2(1-2), pp, 61-77.

Spangenberg J.H., Omann I., and Hinterberger F. (2002b). Sustainable growth criteria: Minimum benchmarks and scenarios for employment and the environment. Ecological Economics, Vol, 42(3),pp, 429-443.

Sustainable Cities International. (2012). Indicators for sustainability: How cities are monitoring and evaluating their success, 210-128 West Hastings Street, Vancouver, BC V6B 1G8 Canada, www.sustainablecities.net [Accessed on12 Apr 2017]

Tanguay G.A., Rajaonson J. Lefebvre J-F and Lanoie P. (2010). Measuring the sustainability of cities: An analysis of the use of local indicators. Ecological Indicators,Vol,10,pp,407–418

Turcu C. (2013). Re-thinking sustainability indicators: local perspectives of urban sustainability. Journal of Environmental Planning and Management, Vol, 56(5),pp, 695-719.

UN (2015). Transforming our world: The 2030 agenda for sustainable development A/RES/70/1.<https://sustainabledevelopment.un.org/content/documents/7891TRANSFORMING%20OUR%20WORLD.pdf> [Accessed on 21,Sep. 2018]

UN. (2017). New urban agenda: Habitat III conference, Quito, 17-20 October, 2016.

UNDP (2016). Sustainable urbanization strategy UNDP's support to sustainable inclusive and resilient cities in the developing world. New York, USA.

UNDPCSD (UN Division for Policy Co-ordination and Sustainable Development) (1996a). Measuring changes in consumption and production patterns. Consultation papers and questionnaires, New York.

UNDPCSD (UN Division for Sustainable Development. Department of Policy Co-ordination and Sustainable Development) (1996b). Indicators of sustainable development, framework and methodologies. United Nations, New York.

UNESC (1995). Indicators of sustainable development. commission on sustainable development United Nations Economic and Social Council. 3rd Session, New York, April 11–28.

UN-Habitat. (2007). State of the World Cities 2010/2011: Bridging the Urban Divide. United Nations Human Settlements Programme, Nairobi, Kenya.

UN-Habitat. (2016). World Cities Report 2016 Urbanization and Development: Emerging Futures. Nairobi, Kenya.

Van de Kerk G., and Manuel A.R. (2008). A comprehensive index for a sustainable society: The SSI -the Sustainable Society Index. Ecological Economics, Vol, 66, pp, 228-242

VanDijk M.P., and Mingshun Z. (2005). Sustainability indices as a tool for urban managers, evidence from four medium-sized Chinese cities. Environmental Impact Assessment Review,Vol, 25,pp,667–688.

Wilson M.C. and Wu J. (2017). The problems of weak sustainability and associated indicators". International Journal of Sustainable Development & World Ecology, 24:1, 44-51

Yang B., Xu T., and Shi L. (2017). Analysis on sustainable urban development levels and trends in China's cities. Journal of Cleaner Production,Vol, 141,pp, 868-880

YCELP and CIESIN [Yale Center for Environmental Law & Policy and Center for International Earth Science] (2005). Environmental sustainability index: benchmarking national environmental stewardship. New Haven (CT), Yale Center for Environmental Law & Policy and Center for International Earth Science Information Network.

YCELP and CIESIN [Yale Center for Environmental Law and Policy and Center for International Earth Science] (2006). Pilot 2006 environmental performance index. new haven (CT)". Yale Center for Environmental Law and Policy and Center for International Earth Science.

Zilans A., and Abolina K. (2009). A methodology for assessing urban sustainability: Aalborg commitments baseline review for Riga, Latvia. Environment, Development and Sustainability,Vol,11, pp, 85–114.

Received on August 1st, 2018 Accepted on February 20th, 2019

Vyacheslav V. Dolotov*[1] and Andrey V. Dolotov[1]
[1]Marine Hydrophysical Institute, Sevastopol, Russia
***Corresponding author:** vyadol@gmail.com

PERSPECTIVES OF POPULARIZATION OF OCEANOGRAPHIC INFORMATION SYSTEMS BASED ON INTERNET

ABSTRACT. The Internet version of the interactive geoinformation system names as «Crimea Sea Coast» based on javascript programming language and the modern open library «leaflet» is described. Development of a product supposed to use of the modern vector graphics technologies, such as D3, Flot and other superstructures over javascript. The main attention is paid to operational representation of full-scale results observations with assessment of Crimea coastal zone dynamics in general. Options of such approach are already realized with use of data on measurement of coast line position of the northwest coast now. In addition, the system reserves the special section described the basis and results of the implementation of the previously developed cadastral assessment of the Crimea beaches, including their recreational areas, economic assessment of recreational resources, as well as the results of comprehensive interdisciplinary monitoring of Sevastopol Bay environmental condition for the period from 1998 to the present, including a cartographic representation of the geographical elements of the region as a whole. The results of monitoring allow to realize visualization of spatial distributions of hydrological, hydrochemical and hydrobiological characteristics of the bay sea environment in the digital format defined by user, to perform the construction of vertical distributions, and also to calculate some ecological indexes. The final version of the system is expected to be posted on the official website of Marine Hydrophysical Institute.

KEY WORDS: Coastal zone, GIS, Internet, leaflet

CITATION: Vyacheslav V. Dolotov, Andrey V. Dolotov (2018) Perspectives Of Popularization Of Oceanographic Information Systems Based On Internet. Geography, Environment, Sustainability, Vol.12, No 1, p. 137-145
DOI-10.24057/2071-9388-2018-43

INTRODUCTION

The global implementation of geographic information systems both into the practice of scientific research and cartographic data representation allows more naturally to perceive of the spatial distribution of different fields and objects on the earth's surface and even in sea depths. Detailed overview of the specifics of oceanographic GIS-tools is presented by CRCPress (2002) and Davey Jones' Locker (2018). However, it is difficult to imagine a single information system for the whole of the world's oceans and therefore they are most often developed in the form of regional structures. Thus a few GIS for Black Sea region have been developed in Marine Hydrophysical Institute (Zhuk 2016; Konovalov 2013).

Increased interest in GIS creates the prospects of geoinformation data dissemination not only among specialists, but also among management structures and even for open access. In this regard, it's appears the need of provision for possibility of geoinformation data presentation without prior acquaintance with costly GIS tools and the acquisition of the necessary expensive licenses (ESRI 2018a; MapInfo 2018; Golden et al. 2018). Additionally, using of these professional GIS requires prior training and education.

In this regard, completely new horizons are opening with the implementation of GIS-tools through the Internet (Web-GIS) which, unlike the usual desktop-analogues are either fully or conditionally accessible and do not require to send of finished projects to users. (OIAS et al. 2018), which, unlike the usual desktop-analogues are either fully or conditionally accessible and do not require to send of finished projects to users.

One of the solutions in this direction is the newly developed leaflet library (Leaflet 2018) to the popular programming language javascript. The main leaflet advantage is the ability to represent a vector graphics in the network with use of online map services like MapBox, OpenStreetMap, Google Maps, Yandex Maps, etc. This is a very important fact allows to exclude from developing of GIS tools the process of base map creating and to focused on the data representation.

Marine Hydrophysical Institute, over the long years has accumulated a huge arrays of oceanographic observations data, collected in a single internal database (DB), access to which, however, is limited even for the employees of the MHI and, in addition, is implemented in outdated formats that do not facilitate its use in operational analysis.
At the same time, due to the objective loss of all research vessels in the 1990s, the role of coastal observations has increased, the number of which is increasing too, along with the growing importance of these data for the economic development of the Crimea. In view of these circumstances, the institute has developed a strategy of popularization of coastal observation data in order to support decision-making on the management of the sea coastal zone, aimed at ensuring the environmental sustainability of the territories for the development of recreational and economic factors. First and foremost, these decisions are aimed at counteracting both the sharply aggravated beaches degradation process and pollution of coastal areas. In this regard, the work on the formation of public media products that characterize the main trends in the state of the coastal zones has become quite popular (Konovalov et al. 2013; Dolotov 2007). However, of these, only the first work was framed in the form of freely distributed and updated information system, implemented, however, only in the form of personal computer application. At present, the above-mentioned technologies allow to prepare all the received materials in the form of Internet-oriented information systems, access to which does not require prior training. At the same time, unlimited Internet resources allow to saturate such systems not only with measurement data, but also with more general information about the coastal zone, which have an educational significance too.

MATERIALS

The work used the modern open library leaflet in conjunction with ESRI leaflet (2018b). The main page of the site is quite traditional (Fig. 1) and includes 6 information sections (Table 1).

The first and last sections is implemented using the traditional HTML language, and includes information on climate, cyclonic activity, storm surges and waves, atmospheric precipitation, changes in sea level and coastline position, anthropogenic impacts and coast types. As examples the Fig. 2 describes the coast types (a) and storm surge features (b).

The other sections in contrast include cartographic material with maximum use of interactive tools. So, three data sources are proposed for the cartographic representation of the base map in this implementation: MapBox, OSM and Yandex Map, the list of which can be later increased. It is important to note that, since the Internet base maps are represented by bitmaps, the diversity of their thematic options is realized by a map simple redrawing. For example, the well-known ser-

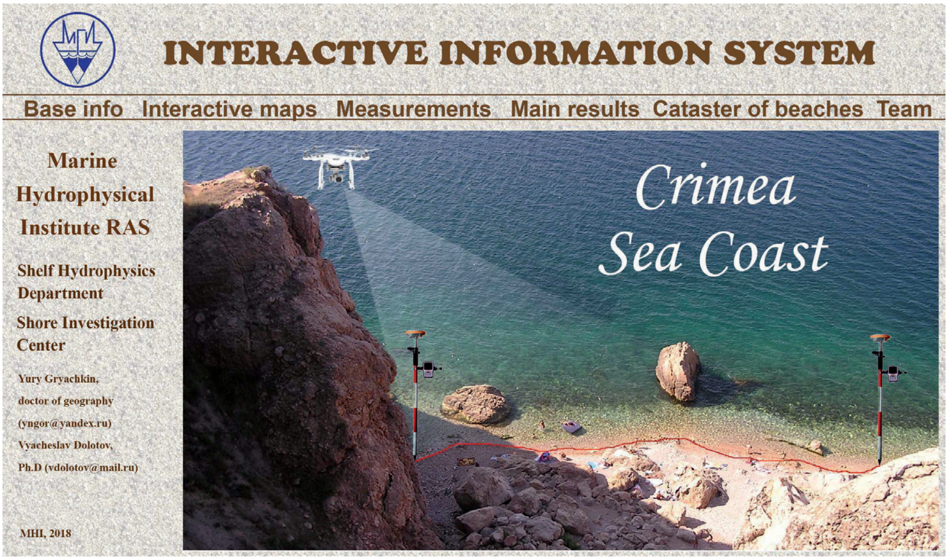

Fig. 1. The main page of interactive system

Table 1. List of potential system's features

Base info	Hydro meteorological information and shore structure
Interactive maps	Detailed description of individual sections of the coastal zone
Measurements	Operational results of surveys and measurements
Results	Modern and historical results of the coastal zone study
Cadaster of beaches	The concept and the pilot implementation of the results of Crimean beaches cadastral assessment
Team	Personality and contacts

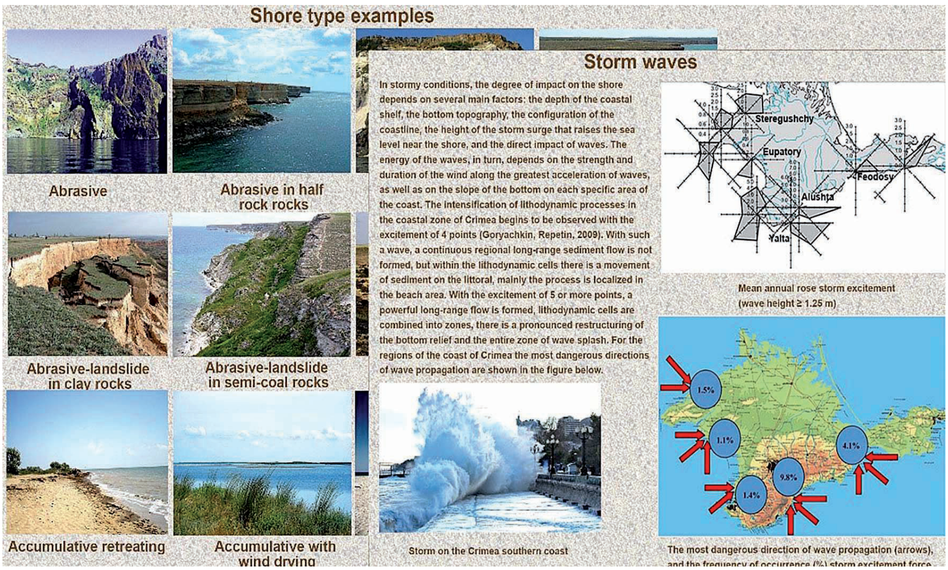

Fig. 2. Traditional visualization of HTML page format

vice ESRI offers the following set of thematic maps: navigation, topographic, geographic, monochrome and satellite. Additionally, we use additionally MapBox_light and MapBox_dark, extremely convenient for focusing the user's attention on the represented data. Moreover, the Internet providers offer up-to-date maps on some indicators, such as air temperature, humidity, directions and speed of the wind, which can even be animated.

METHODS

Recently, Marine Hydrophysical Institute released a monograph in the form of an Atlas of the Crimea sea coast current state, published, unfortunately, in a very small edition. Atlas consists of detailed description of 170 coast points belong all the shore. The first task of the work was to compare the complexity, quality and options for the convert of all Atlas materials into the new Internet format. The first positive decision was obtained at the beginning of the project development and was associated with the possibility of map zooming. This allowed to combine separate shore fragments of the printed Atlas into a single combined map. In addition, it is quite simple to implement additional mapping tools, such as coordinate grid, measuring ruler and some others.

Another important task was to check the spatial coincidence of the available data measured in the coastal zone with the Crimea coastline of the map services on maximum zoom levels. For this purpose, these maps were overlaid with a digitized image of the contour of the Crimea for July 2014 in the ESRI shape format. Fig. 3 presents the quite satisfactory results of the comparison. In this regard, it should be noted that the Internet maps are constantly updated, and some discrepancies are noticeable in the Fig. 3 on the right can be caused by natural changes in comparison with the test contour 2014. Confirmation of this conclusion is the exact match of fixed objects such as concrete piers. In the implementation of the online version of the Atlas, used a relatively small number of leaflet tools, allowing, however, to evaluate the prospects for the development of the system as a whole. So, the Atlas abounds with photos showing the current state of individual sections of the coastal zone, as well as historical photos in comparison with modern ones.

All these photos are geographically linked to points on the map, and the information output is easily implemented using standard leaflet markers and popups (Fig. 4).

Fig. 5 shows a more informative design options of interactive page implementation. Moving the mouse over the elements displays the length of the lines, the area of the polygons and some other characteristic information.

At the same time there is a zoom to the element spatial extent. The greatest attention in the work is supposed to be paid to the options of interactive presentation of the results of field observations. Thus, the interactive map shown in Fig. 6 at the left presents the results of measurements of the coastline position in the area of the North-Western Crimea near the Bakal lake.

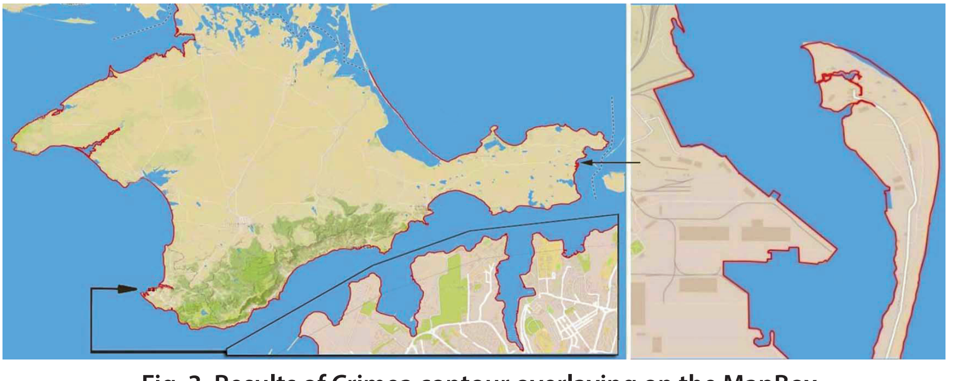

Fig. 3. Results of Crimea contour overlaying on the MapBox

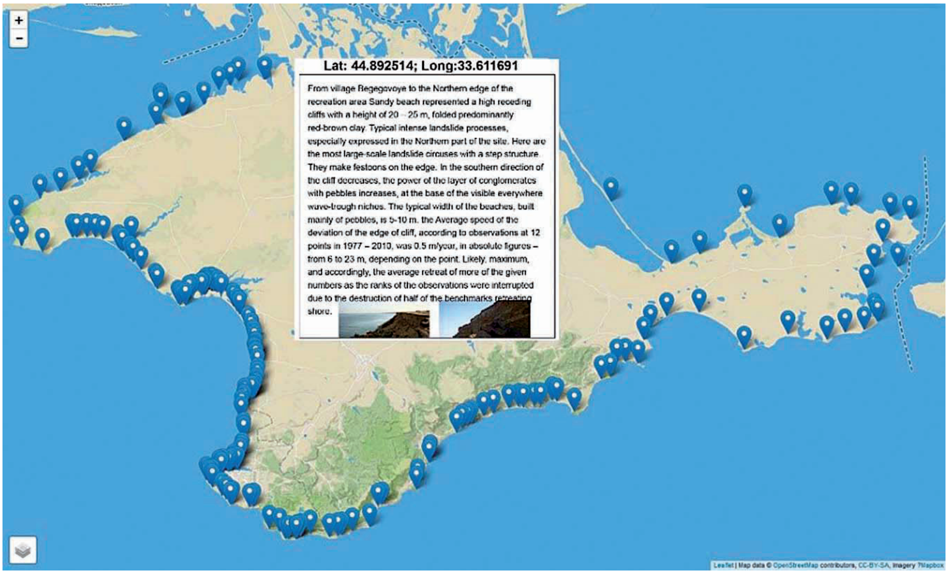

Fig. 4. The simple implementation of leaflet technology

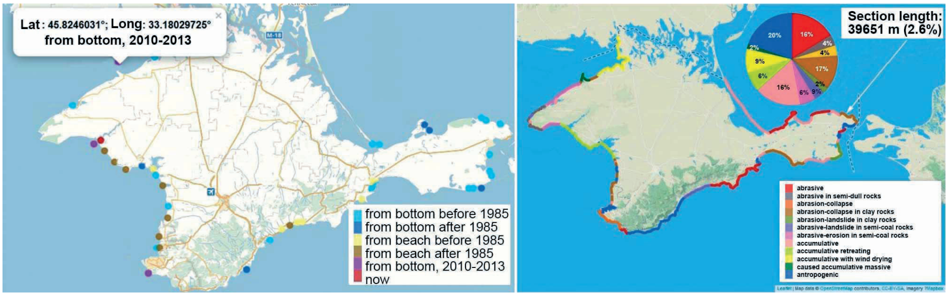

Fig. 5. The simple example of popup windows based on leaflet markers

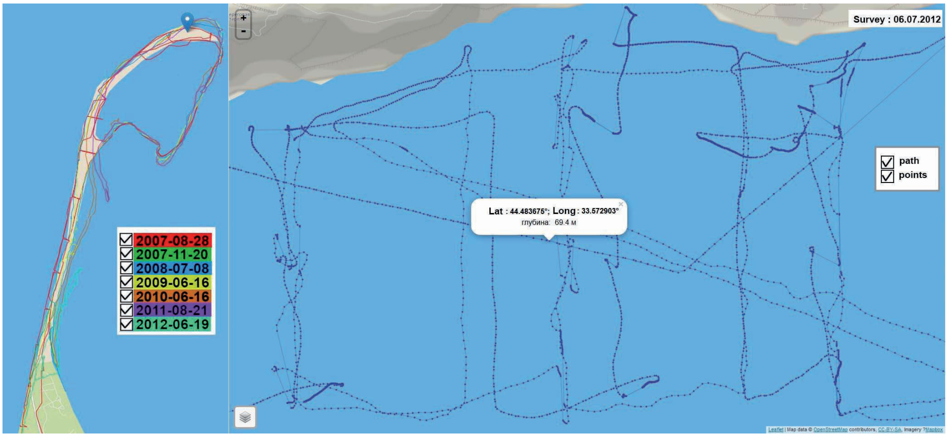

Fig. 6. Results of shoreline location (left) and depth measurements (right) as an interactive map

At the same time, the user can toggle the list of the presented data, as well as information about the characteristics of objects (length for lines and area for polygons). On the right, the results of depth measurements in the form of points and interpolated contours are presented in a similar way. A special switch allows you to select the type of data displayed. In comparison with coastal measurements, marine surveys are performed with high vertical resolution for analyze the vertical profiles of the distribution of individual elements (Fig. 7).

The grid format (Golden 2018) is most suitable for detailed investigation of numerous surveys of the Sevastopol Bay, which is a long-term system for monitoring its environmental condition. In this regard, the most interesting is the European system of environmental status indices with the assessment of indicators in certain areas of the Bay. Spatial distributions can be represented in three ways: a traditional gradient, a "traffic light" or a more familiar one – in the form of contours (Fig. 8).

The Table 1 shows that the system reserved a special Section for cadaster of Crimea beaches. The Crimea government have been trying to create it since 2004, but it is still in the state of the project. This may be due to either a lack of understanding of the cadaster concept or the importance of the project. In spite of the fact that MHI repeatedly represented the technique of beaches cadastral assessment developed by it the product still is absent. The inclusion of existing best practices, tools and proposals in the structure of the information system can serve the starting point to the beginning of the implementation of a systematic cadastral beach area studies, which, however, are performed by MHI since 2005. In contrast to the materials presented above, the content of cadaster of the beaches involves the calculation of a significant number of calculated indicators, which are usually formed the special cadastral database.

The main task of cadaster visualization is a cartographic representation of a complex cadastral structure (Fig. 9), including their recreational areas, as well as a variety of comparative and chronological charts of changes in individual cadastral indicators. The last task, which usually requires additional comments, is supposed to be implemented using spe-

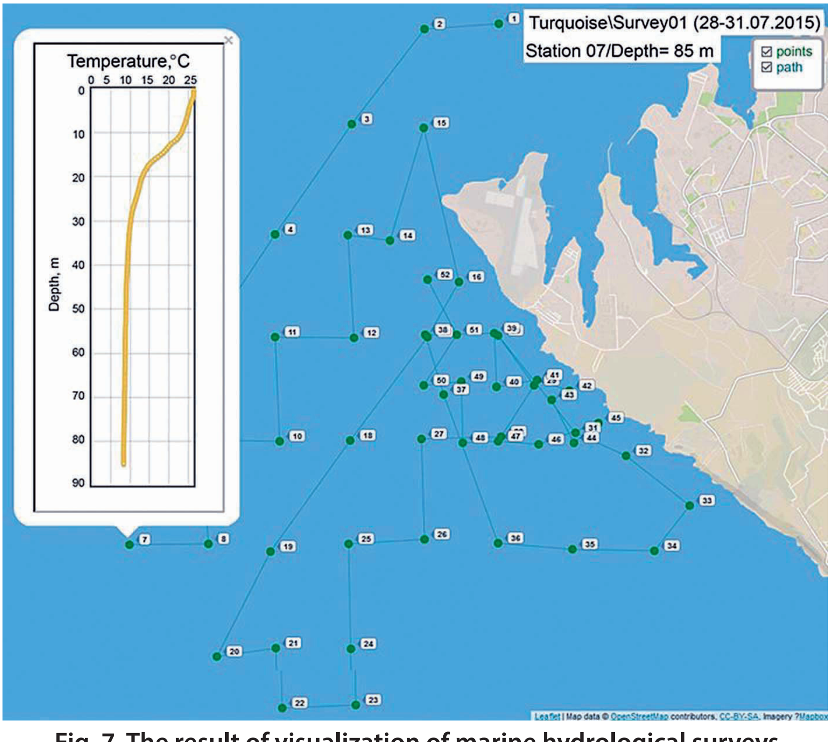

Fig. 7. The result of visualization of marine hydrological surveys

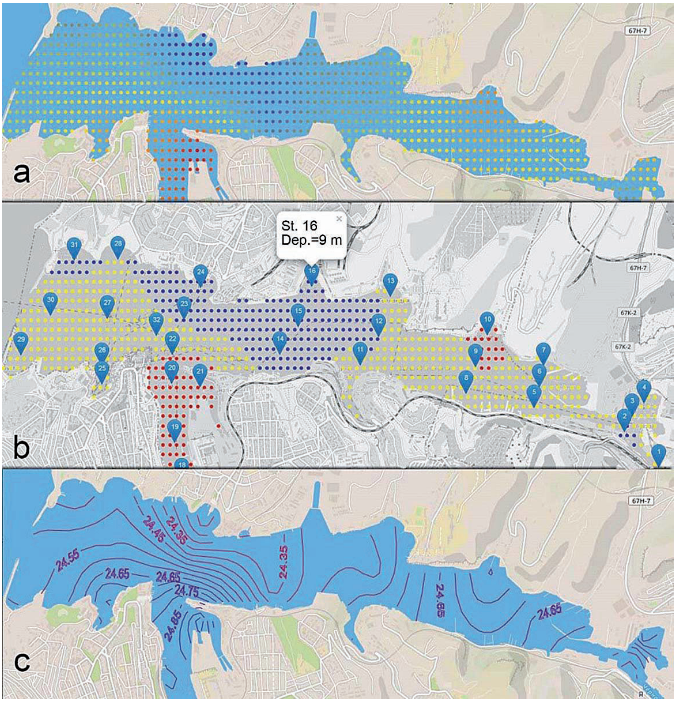

Fig. 8. Different kinds of spatial distribution of temperature: gradient (a), traffic light (b) and contours (c)

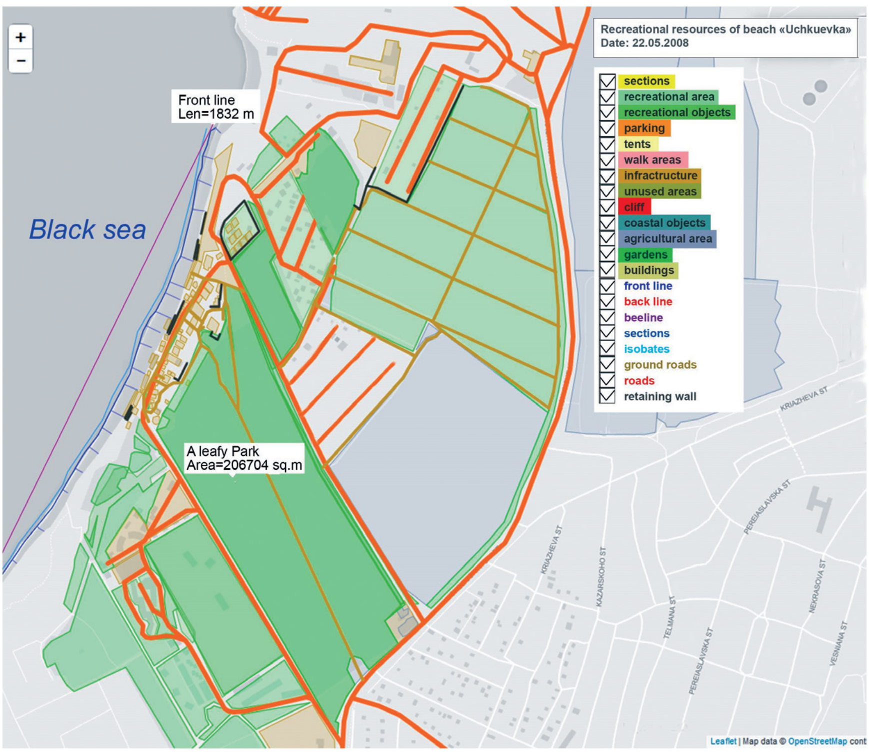

Fig. 9. The main cartographic cadastral visualization

cialized technologies C3-D3 (C3 2018), providing excellent interaction between digital data and graphics.

An additional advantage is the ability to use GIS on any platform, including tablets and smartphones.

CONCLUSION

Comparative variants of different GIS implementation allow us to assert that Internet products using modern open technologies can significantly speed up the work and the capabilities of such products often exceed the capabilities of traditional programming methods. In this regard, it should be noted that there is no need for careful preparation of the base map and zooming technologies.

ACKNOWLEDGEMENTS

The work was carried out within the framework of the state task on the topic № 0827-2014-0010 "Complex interdisciplinary studies of Oceanological processes that determine the functioning and evolution of the ecosystems of the Black and Azov seas on the basis of modern methods of monitoring the state of the marine environment and grid-technologies"

REFERENCES

C3.js (2018). D3-based reusable chart library. [online] Available at: http://c3js.org/examples.html Leaflet (2018) A JavaScript library for interactive maps. [Accessed 01 Aug. 2018]

CRCPress (2002). Geographic Information Systems in Oceanography and Fisheries. [online] Available at: https://www.crcpress.com/Geographic-Information-Systems-in-Oceanography-and-Fisheries/Valavanis/p/book/9780415284639 [Accessed 03 Dec. 2018]

Davey Jones' Locker (2018). Seafloor Mapping/Marine and Coastal GIS. [online] Available at: https://marinecoastalgis.net/soft [Accessed 03 Dec 2018]

Dolotov V., Ivanov V. (2007). Cadastral Assessment of Crimean Beaches as an Instrument for Sustainable Coastal Development. Geography, Environment, Sustainability, 2, 98-119.

ESRI (2018a). [online] Available at: http://www.esri.com [Accessed 03 Dec. 2018]

ESRI (2018b). A lightweight set of tools for using ArcGIS services with Leaflet. [online] Available at: http://esri.github.io/esri-leaflet/ [Accessed 01 Aug 2018]

Golden (2018). Surfer 7 Binary Grid File Format. [online] Available at: http://surferhelp.goldensoftware.com/surfer.htm#t=topics%2Fsurfer_7_grid_
[Accessed 01 Aug 2018]

Konovalov S., Vladymyrov V., Dolotov V., Sergeyeva O., Goryachkin Yu., Alyomov S. Moiseenko O., Orekhova N., Zharova L. (2013). Environmental Assessment Tools in the PEGASO Case - Sevastopol Bay. Proceedings of the Global Congress on ICM: Lessons Learned to Address New Challenges, Marmaris, Turkey, 30 Oct – 03 Nov 2013, 59-70.

Leaflet (2018). An open-source JavaScript library for mobile-friendly interactive maps. [online] Available at: https://leafletjs.com [Accessed 01 Aug 2018]

MapInfo (2018). MapInfo Pro Desktop GIS. [online] Available at: https://www.pitneybowes.com/us/location-intelligence/geographic-information-systems/mapinfo-pro.html [Accessed 03 Dec. 2018]

OIAS (2018). Oceanological information and analytical system. [online] Available at: http://oias.poi.dvo.ru/ [Accessed 01 Aug 2018]

Zhuk E., Khaliulin A., Zodiatis G., Nikolaidis A., Isaeva E. (2016). Black Sea GIS developed in MHI. Proc. SPIE 9688, Fourth International Conference on Remote Sensing and Geoinformation of the Environment (RSCy2016). 2016, 9688, p. 96881-96888.

Received on August 21st, 2018 Accepted on February 20th, 2019

AUTHOR GUIDELINES

1. Authors are encouraged to submit high-quality, original work: scientific papers according to the scope of the Journal. reviews (only solicited) and brief articles.

2. Papers are accepted in English. Either British or American English spelling and punctuation may be used.

3. All authors of an article are asked to indicate their names (with one forename in full for each author, other forenames being given as initials followed by the surname) and the name and full postal address (including postal code) of the affiliation where the work was done. If there is more than one institution involved in the work, authors' names should be linked to the appropriate institutions by the use of 1, 2, 3 etc superscript. Telephone and fax numbers and e-mail addresses of the authors could be published as well. One author should be identified as a Corresponding Author. The e-mail address of the corresponding author will be published, unless requested otherwise.

EXAMPLE:

Ivan I. Ivanov[1], Anton A. Petrov[1*], David H. Smith[2]
[1]University/Organization name, Street, City, ZIP-code, Country
[2]University/Organization name, Street, City, ZIP-code, Country
*** Corresponding author:** example@example.com

4. Article structure should contain further sections:
   - Abstract.
   - Keywords (Immediately after the abstract, provide a maximum of 6 keywords, avoiding general and plural terms and multiple concepts (avoid, for example, 'and', 'of'). Be sparing with abbreviations: only abbreviations firmly established in the field may be eligible. These keywords will be used for indexing purposes.).
   - Introduction (State the objectives of the work and provide an adequate background, avoiding a detailed literature survey or a summary of the results.).
   - Material and methods (Provide sufficient details to allow the work to be reproduced by an independent researcher. Methods that are already published should be summarized, and indicated by a reference. If quoting directly from a previously published method, use quotation marks and also cite the source. Any modifications to existing methods should also be described.
   - Results (Results should be clear and concise.).
   - Discussion (This should explore the significance of the results of the work, not repeat them. A combined Results and Discussion section is often appropriate. Avoid extensive citations and discussion of published literature.).
   - Conclusions (The main conclusions of the study may be presented in a short Conclusions section, which may stand alone or form a subsection of a Discussion or Results and Discussion section.).
   - Acknowledgements (List here those individuals who provided help during the research and funds which provided financial support of your research.).
   - References (Make a list of references according to guidance provided below).
   - Appendices (If there is more than one appendix, they should be identified as A, B, etc. Formulae and equations in appendices should be given separate numbering: Eq. (A.1), Eq. (A.2), etc.; in a subsequent appendix, Eq. (B.1) and so on. Similarly for tables and figures: Table A.1; Fig. A.1, etc.).

5. Sections and sub-sections shouldn't be numbered, but divided into sub-levels. If you would like to refer to a particular section, name it without any numbers (for example: see "Materials and methods")

6. Math equations should be submitted as editable text and not as images (use appropriate tool in text editor). Present simple formulae in line with normal text where possible and use the solidus (/) instead of a horizontal line for small fractional terms, e.g., X/Y. In principle, variables are to be presented in italics. Number consecutively any equations that have to be displayed separately from the text (if referred to explicitly in the text).

7. Figures and figure captions. Number the illustrations according to their sequence in the text. Regardless of the application used, when your figure is finalized, please 'save as' or convert the images to one of the following formats: TIFF, JPG. Supply files that are optimized for screen use. **The resolution should be at least 300 dpi**. Besides inserting figures into your manuscript, you must also upload appropriate files during paper submission. Ensure that each illustration has a caption. A caption should comprise a brief title (not on the figure itself) and a description of the illustration beginning from "Fig. 1…" (note: no any dots in the end of the capture!). Keep text in the illustrations themselves to a minimum but explain all symbols and abbreviations used.

Example of referring to the figure in text: (Fig. 1)
Example of figure caption: Fig. 1. The distribution of the family Monimiaceae

8. Tables. Please submit tables as editable text and not as images. Tables can be placed either next to the relevant text in the article, or on separate page(s) at the end. Number tables consecutively in accordance with their appearance in the text, place table caption above the table body and place any table notes below the body. Be sparing in the use of tables and ensure that the data presented in them do not duplicate results described elsewhere in the article. Please avoid using vertical rules and shading in table cells.

Example of table caption: Table 1. Case studies and used methods

9. The optimum size of a manuscript is about 3,000–5,000 words. Under the decision (or request) of the Editorial Board methodological and problem articles or reviews up to 8,000–10,000 words long can be accepted.

10. To facilitate the editorial assessment and reviewing process authors should submit "full" electronic version of their manuscript with embedded figures of "screen" quality as a **PDF or DOC file.**

11. We encourage authors to list three potential expert reviewers in their field. The Editorial Board will view these names as suggestions only.

12. Original reviews of submitted manuscripts remain deposited for 3 years.

SCIENTIFIC AND PRACTICAL PEER-REVIEWED JOURNAL "GEOGRAPHY, ENVIRONMENT, SUSTAINABILITY"

No. 01 (v. 12) 2019

FOUNDERS OF THE MAGAZINE: Russian Geographical Society, Faculty of Geography, Lomonosov Moscow State University and Institute of Geography of the Russian Academy of Sciences

The magazine is published with financial support of the Russian Geographical Society.

The magazine is registered in Federal service on supervision of observance of the legislation in sphere of mass communications and protection of a cultural heritage. The certificate of registration: ПИ № ФС77-67752, 2016, December 21.

PUBLISHER
Russian Geographical Society
Moscow, 109012 Russia
Novaya ploshchad, 10, korp. 2
Phone 8-800-700-18-45
E-mail: press@rgo.ru
www.rgo.ru/en

EDITORIAL OFFICE
Lomonosov Moscow State University
Moscow 119991 Russia
Leninskie Gory,
Faculty of Geography, 1806a
Phone 7-495-9391552
Fax 7-495-9391552
E-mail: ges-journal@geogr.msu.ru
www.ges.rgo.ru

DESIGN & PRINTING
Agency «CONNECT»
Moscow, 117452,
Artekovskaya str., 9, korp. 1
Phone: +7 (495) 955-91-53
E-mail: info@connect-adv.ru

Sent into print 25.03.2019
Order N gi119

Format 70 ½ 100 cm/16
11,4 p. sh.
Digital print
Circulation 20 ex.